AN INVESTIGATION INTO THE CONTROLS OF GRANITE PLUTONISM IN THE SIERRA DA FREITA REGION, NORTHERN PORTUGAL

Reginald John Reavy

A Thesis Submitted for the Degree of PhD
at the
University of St. Andrews

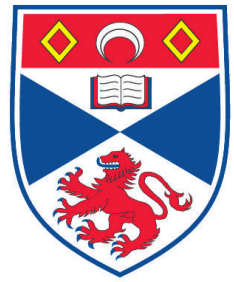

1988

AN INVESTIGATION INTO THE CONTROLS OF GRANITE PLUTONISM IN THE SERRA DA FREITA REGION NORTHERN PORTUGAL

Thesis presented in partial fulfilment for the
Degree of Doctor of Philosophy,
Geology Department, University of St Andrews

November 1987

VOLUME CONTAINS CLEAR OVERLAYS

CERTIFICATE

I, REGINALD JOHN REAVY, hereby certify that this thesis has been composed by myself, that it is a record of my own work and that it has not been accepted in partial or complete fulfilment of any other degree or professional qualification.

I was admitted to the Faculty of Science of the University of St Andrews under Ordinance General No 12 in October 1983 and as a candidate for the Degree of Ph.D. in March 1984.

Signed  Date 28/10/87

I hereby certify that the candidate has fulfilled the conditions of the Resolution and Regulations appropriate to the Degree of Ph.D.

Signed 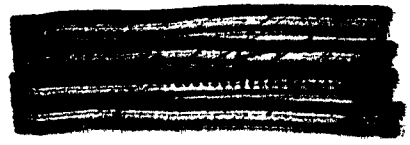 Date 28/10/87

ABSTRACT

The Serra da Freita region of north central Portugal was chosen for study as it displays the complex relationships between regional structure, plutonism, regional and contact metamorphism typical of this part of Iberia. The region was mapped on a scale of 1:10000.

The Serra da Freita pluton, which intrudes the core of the Porto-Viseu metamorphic belt developed in the late Pre-Cambrian - Cambrian Beira Schists, is shown to lie in a sinistral transpressive shear zone, the Serra da Freita shear zone. Early structures are progressively modified over a protracted period by shear zone deformation, during which time metamorphism reached a peak and the granite was emplaced. Mapping of the intrusive contacts of the granite show that following initial intrusion of a steeply inclined sheet of magma into the zone of highest strain, magmas were injected into a region of progressively lower strain where the magma was accommodated as a nearly flat sheet. The distal end of this mass ballooned upwards to form the small intrusion of Castanheira which has abundant biotite nodules which acted as near perfect strain markers.

The main pluton is shown to intrude obliquely the core of a narrow metamorphic belt characterized by parageneses of biotite, andalusite/staurolite, sillimanite, which maps distinctly from a younger cordierite sillimanite contact aureole around an adjacent quartz diorite body.

Several facies of granite within the pluton have been recognized; petrographical and structural studies allow the interpreted emplacement mechanism of these units to be integrated within a more general model for

the evolution of the shear zone.

Geochemical analyses of major and trace elements show that certain compositional trends within these facies cannot be simply related as part of a fractionation sequence. A model is put forward in which repeated melting of a heterogeneous source is followed by sequential emplacement of discrete batches of magma as sheets and wedges within the active shear zone. A Rb-Sr whole rock isochron age of 324 Ma was obtained and this dates not only the emplacement age of the syn-tectonic granite, but also constrains the time of movement along the shear zone.

Radiogenic and stable isotope data strongly point to the local high grade Beira Schists as being suitable source rocks for generation of magmas with marked S-type characteristics which now form the Serra da Freita pluton. 18O values for the granites of 10.64 ± 0.24 - 13.00 ± 0.12 overlap those of the schists which lie in the range 12.38 ± 0.24 - 14.15 ± 0.4. The whole rock Rb-Sr isochron for the granite has an initial ratio of 0.7136 ± 0.0008 (MSWD = 3.2).

A regional and tectonothermal model is put forward in which end-Palaeozoic oblique strike slip collision took place in the Ibero-Armorican Arc. The resulting peturbation in continental heat flow, coupled with the possible effects of shear heating, fluid concentration and local high ductility contrasts in the heterogeneous metasediments, are invoked as being responsible for causing anatexis of the Beira Schists at a depth of 10-12 km, and the generation of granitic melts. Emplacement of these bodies gave rise to the Porto-Viseu metamorphic belt, into which later smaller higher-level melts were injected. It is argued that some of these later magmas which reached higher levels are now exposed as the

constituent facies of the Serra da Freita pluton. The Serra da Freita shear zone, active throughout metamorphism, anatexis and magma emplacement was a dominant feature of the geological history of the region.

CONTENTS

FIGURES

TABLES

PLATES

ACKNOWLEDGEMENTS

I would like to express my sincere appreciation to many friends in St Andrews, Liverpool, and Portugal who have all played their part along the way. First thanks go to Ed Stephens for his constant advice, guidance and patience over the last four years, and to Prof. M.M. Godhino of the University of Coimbra who introduced us to the spectacular geology of northern Portugal. The project would not have been possible without his expert local knowledge and the logistical facilities of his department which he constantly made available to us. He and his family made visits to Coimbra very memorable social occas: ions which will not be forgotten.

During fieldwork the welcome from the staff of the Hotel Residencial S. Pedro, and from the people of Arouca and the Serra da Freita was greatly appreciated.

I have gained much from discussions with Tony Fallick, Alex Halliday, Tony Harris, Bob Hunter, Colin Grant, Judith Kinnaird and Grahame Oliver. Their ideas have always been stimulating and sometimes even helpful! In particular Donny Hutton's advice and time were invaluable during the 1985 campaign.

In St Andrews, the technical assistance of Andy Mackie, Donald Herd, Angus Calder, Richard Batchelor, and Alistair Reid was greatly appreciated, Jim Allan did a great job with the photographs. In East Kilbride, the help of Fiona Mclaren, Ted Donnelly and John Hutchinson was invaluable. Thank you all.

I would also like to thank my fellow post-grads for their companionship on many an adventure between Etna and Eriboll, namely Pete Holden, Richard

Greenwood, Lesley Evans, Martin Gillespie (the E-team lives!), Charles Morrison, Richard Curry and Alasdair Robertson, and all those undergraduates who made the trips to Ullapool, Mull and Scourie so memorable.

In Liverpool, Karen Muse and Phyllis Kon helped with typing tables and figure captions while Maureen Dodd brought me cake and toast in the mornings and told me my job. Special thanks go to Joe Lynch for his superb drafting of the diagrams which saved me weeks in the drawing office, and to Hilary Davies whose patient proof reading found the mistakes I was past seeing. At the eleventh hour, John Gibson saved the day with regards to a printing problem. Terry Boniface, Pete Briggs and a host of others have kept pushing me on towards the end... of the thesis that is! To all of you who have helped in any way, sincere thanks.

This work was carried out during the tenure of a post-graduate research studentship from the Department of Education for Northern Ireland in the Geology Department of the University of St Andrews, and as Demonstator in the Department of Earth Sciences of the University of Liverpool.

The Scottish Universities Research and Reactor Centre at East Kilbride is supported jointly by the NERC and by the Scottish Universities.

This thesis is dedicated to the people of the Republic of Portugal.

PART I -- INTRODUCTION

CHAPTER I -- THE REGIONAL SETTING AND AIMS OF THE PROJECT

1.1 - Background

Portugal occupies about one-fifth of the Iberian peninsula (Figure 1.1 inset), and is a country of very varied landscape. Coastal lowlands in the south and west contrast with much of the northern interior which is a region of densely populated valleys and steep-sided mountains, often thickly forested. The summits of these mountain ranges or "Serras" are typically bare rock-strewn plateaux, often over 1000 m in altitude. The Serra da Freita, the subject of this study, is one such plateau. These contrasts in geomorphology are a direct consequence of the diverse geology of the country which is briefly reviewed below.

The geology of Portugal can be divided into three great structural units (Figure 1.1): (i) the Iberian Massif or tableland which extends north and east into Spain, with metamorphic and igneous rocks and Palaeozoic formations; (ii) a western Mesozoic/Cainozoic border between the coast and the Iberian Massif, and (iii) a southern Mesozoic/Cainozoic border in Algarve extending east into Spain. The study area in north central Portugal lies within the Iberian Massif which occupies three-quarters of the country. A line of section from north of Aveiro to north of Viseu runs across the regional strike and encounters all the geological lithologies and formations present in the region (Figure 1.2).

Figure 1.1 - Location map

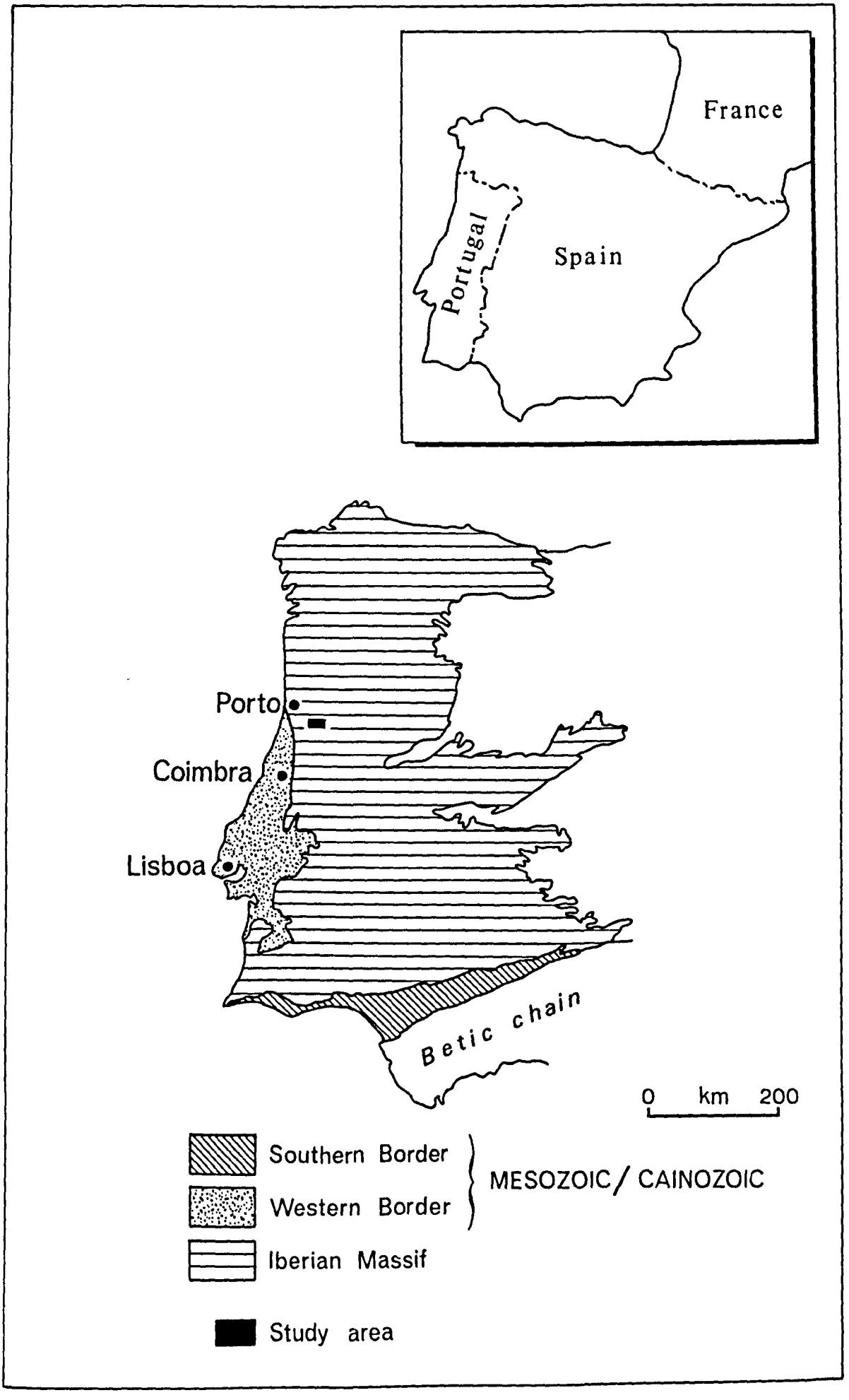

Figure 1.2 - The geology of
north central Portugal

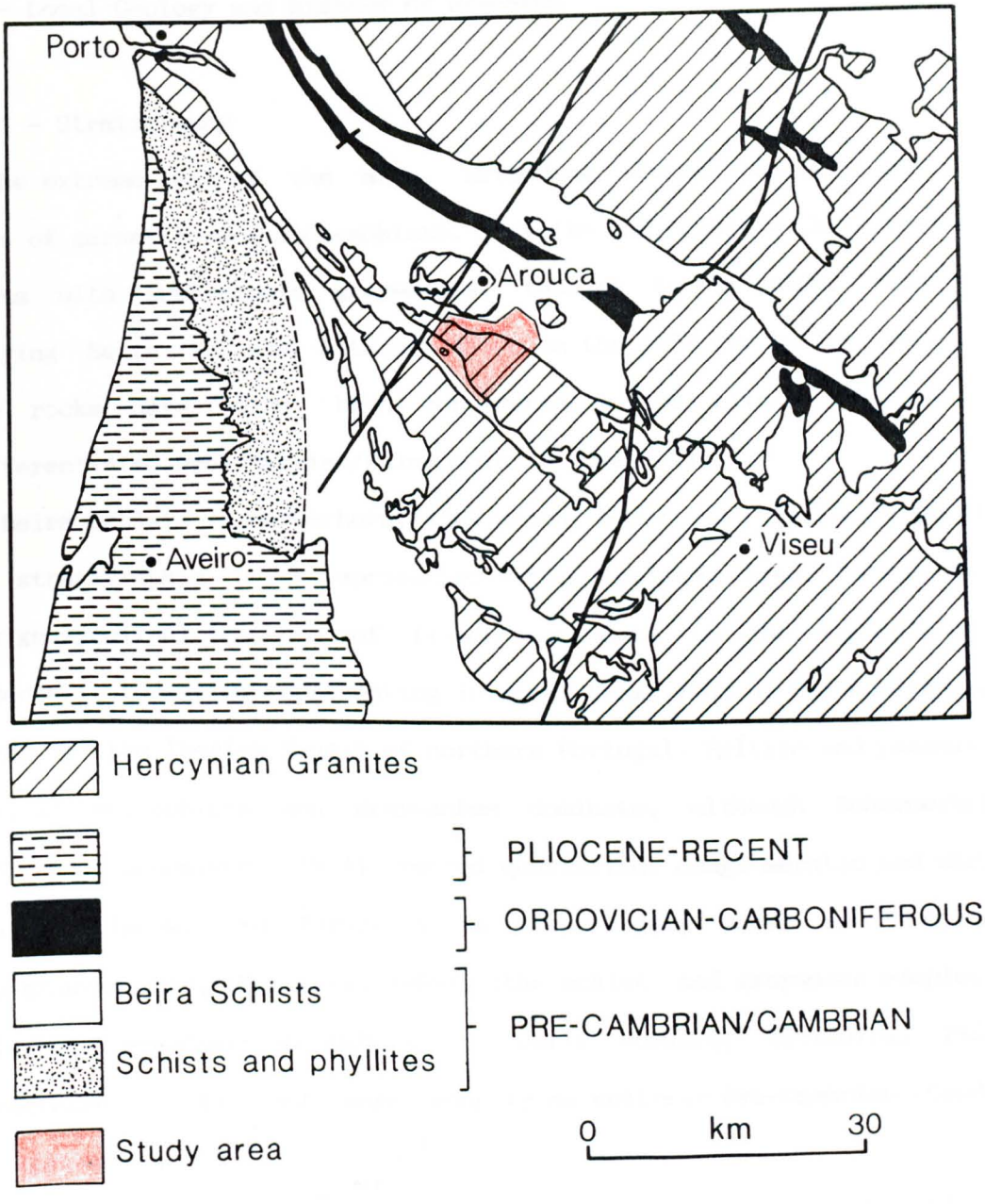

1.2 - Local Geology and History of Research

1.2.1 - Stratigraphy

In the extreme west of the area, extending almost to the coast is a series of garnetiferous mica-schists, sericite and chlorite phyllites, and schists with subordinate greywackes, thought to be older than the overlying Beira Schists. Although shown on the 1972 map as Pre-Cambrian, these rocks have also been considered to be either Cambrian or undifferentiated Pre-Cambrian/Palaeozoic (Figure 1.2).

The Beira Schists (Schermerhorn,1956) which occur to the east are the only stratigraphic units represented within the study area. Indeed, this thick geosynclinal sequence of flysch sediments is the region's main sedimentary formation representing in areal terms >90% of the non-igneous geology in the Iberian Massif of northern Portugal. Pelitic and psammitic rocks, slates, schists and greywackes dominate, although Schermerhorn (1956) and Goncalves (1974) record quartzitic, conglomeratic and marly units in places. The formation is also widely known as "Complexo xisto-grauvaquico", (Teixeira, 1955), (the schist and greywacke complex), considered Pre-Cambrian/Cambrian by early workers, (Teixeira, 1955; Schermerhorn, 1956), but more recently as entirely Pre-Cambrian (Conde, 1971; Goncalves, 1974).

The complex must be pre-Ordovician, as it is overlain unconformably by Arenig, Llanvirnian, Llandeilian and Caradoc quartzites and slates in the Porto-Satao syncline (Oen, 1970) which strikes NW-SE parallel with the main structural trends in the Beira Schists. Silurian, Devonian and Carboniferous sediments also occur, and in the axial zone they are of

Stephanian B-C age. These rest unconformably on both the Ordovician and on the Beira Schists.

1.2.2 - Granites

Exposed granites comprise a large proportion of northern Portugal (Figures 1.2, 1.3); these are generally accepted to have been emplaced during the Hercynian Orogeny (Fleury, 1922; Ribeiro, 1974; Schermerhorn, 1981). Within the Aveiro-Viseu traverse described, granite-gneisses and granites with an associated migmatite zone believed to be pre-Hercynian are confined to the western area, whereas Hercynian granitoids are much more abundant and widespread. Pinto (1979) assigned these rocks to 5 groups or belts (Figure 1.4) which form a convenient classification:

(1) gneisses and migmatites in the west associated with the Porto - Albergaria-A-Velha metamorphic belt, in particular the Oliveira de Azemeis granite gneiss;

(2) the Junqueira belt which also has a spatially associated migmatite zone;

(3) the S.Pedro do Sul belt;

(4) the central belt, in which lie the Arouca, Regoufe, and Castro Daire plutons;

(5) the north-eastern belt.

Ages of Granites

The age of Portuguese granites have long been problematical. Accurate dates are of prime importance as they help to clarify the tectono-stratigraphic development of the Iberian Hercynides.

Figure 1.3 - Hercynian granites of northern Portugal

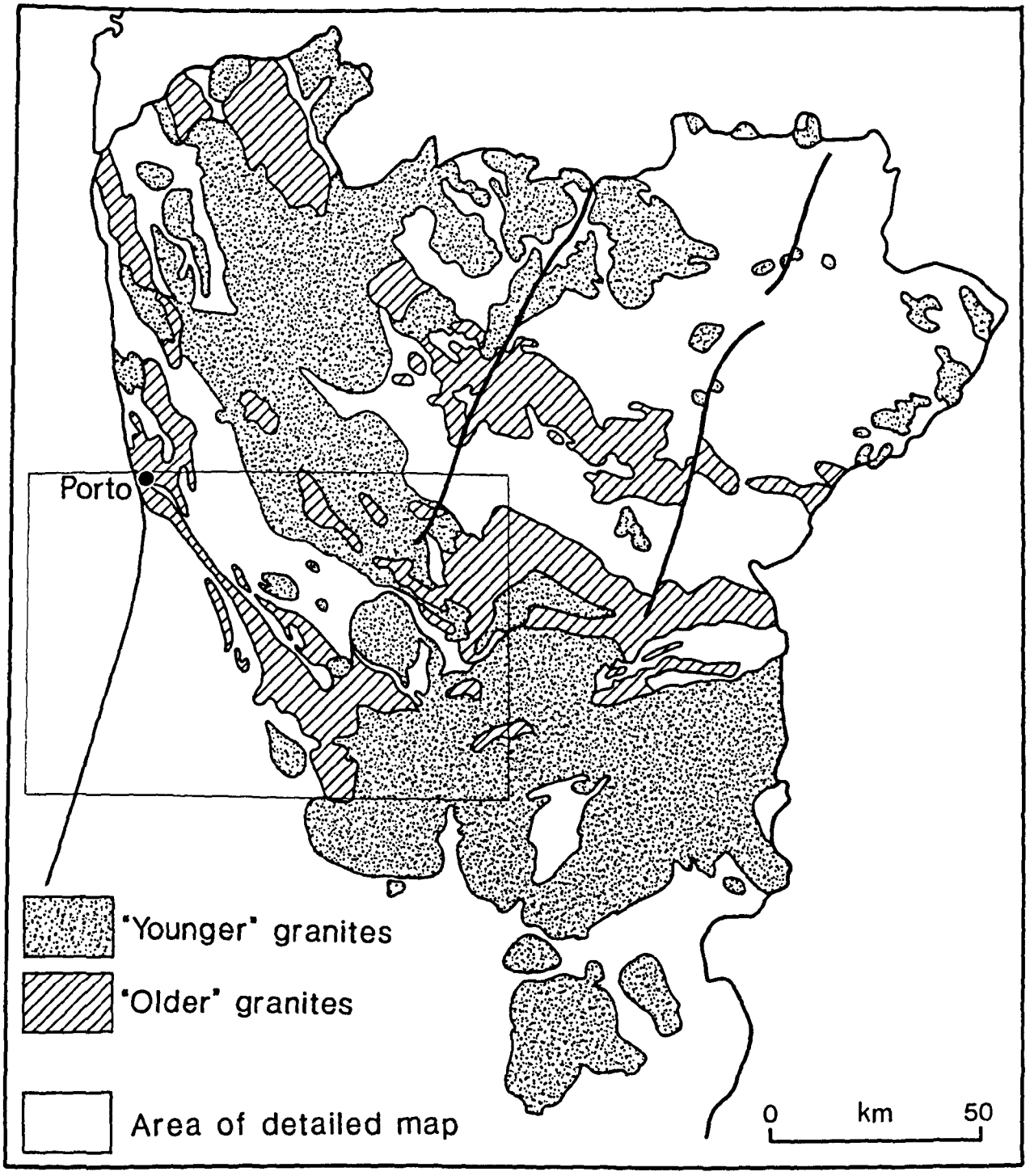

Figure 1.4 - Geology of the Oliviera de Azemeis-Satao region

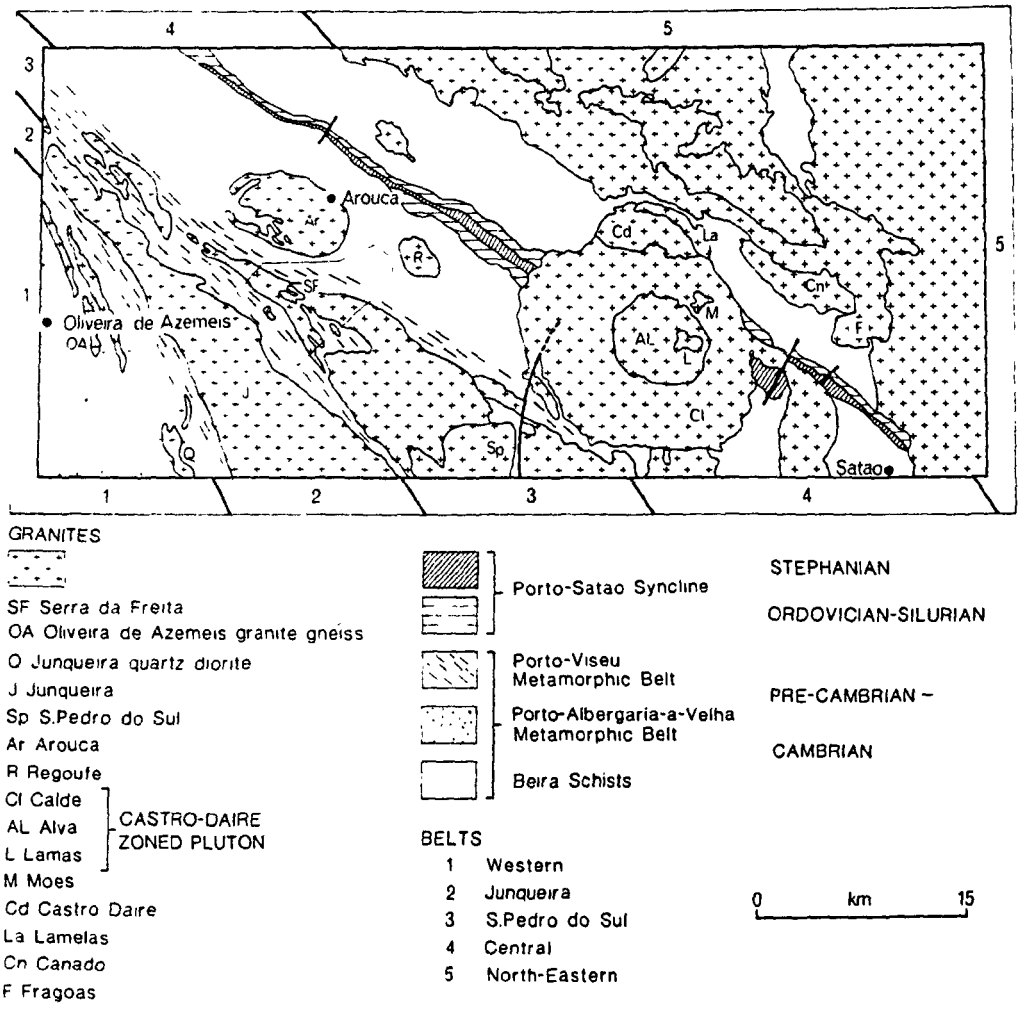

Dutch geologists responsible for much early mapping in the region (Schermerhorn, 1956; Oen, 1958; Sluijk, 1963; de Boorder, 1965) made a major field division of the granitoids into "Older" and "Younger" (Figure 1.3). They also recognized the relationship with the Hercynian Orogeny, the Older Granites being early to middle Hercynian, the Younger group considered late Hercynian, probably Permian. Teixeira (1947, 1970) however has maintained that gneisses and granites in the Porto - Albergaria-A-Velha metamorphic belt are pre-Hercynian (Figure 1.4).

As early as 1967, Mendes produced Rb/Sr biotite ages of 280, 290, 305 and 329 Ma for granites over a wide area in northern Portugal. These were later strongly criticized in terms of techniques employed and interpretation of results.

Priem et al. (1970) obtained a Rb/Sr isochron for each field division, giving ages of 298±10 Ma for an Older Granite and 280±11 Ma for a Younger Granite. ($Rb/Sr = 1.47 \times 10^{-11}$). Using the revised decay constant of 1.42×10^{-11} (Steiger & Jager, 1977) these recalculate at 309±10 Ma and 290±11 Ma. Oen (1970) extended these ages to all Older and Younger Granites, assuming all Portuguese granites fell within these two age ranges.

However it is now apparent that granites in northern Portugal were intruded over a much longer period than could be represented simply by these two time periods. Pinto (1979) reviewed all previous geochronological work and presented new Rb/Sr age data for granites in the structurally diverse traverse across the five belts described above (Table 1.1); some of these values coincided with the values obtained by Mendes (1967). The Serra da Freita pluton which forms the north-western extension of the S.Pedro do Sul belt was not included in Pinto's study. An age of

CHRONOLOGY OF PLUTONISM IN THE AVEIRO-VISEU REGION, N. PORTUGAL

	Pluton	Age	initial ratio				
							Early Permian
YOUNGER	Regoufe	280 ± 9	.7222 ± .0080	280 ± 10	NEWER	280 ± 5	
290 ± 11	Calde	282 ± 5	.7093 ± .0011				
*(280 ± 11)	Lamas	291 ± 10	.7075 + .0013	290 ± 11	YOUNGER	290 ± 5	286 Stephanian 296
	Alva	304 ± 7	.7061 ± .0012				
	Castro Daire	305 ± 6	.7077 ± .0005	308 ± 10	OLDER	305 ± 10	Westphalian
	Arouca	305 ± 8	.7058 ± .0003				
Older							315
	Fragoas	320 ± 10	.7069 ± .0006				
309 ± 10	Lamelas	322 ± 15	.7063 ± .0002	322 ± 15	PRE-OLDER	322 ± 10	Namurian
*(298 ± 10)	Canado	324 ± 11	.7110 ± .0024			345 ± 5	333 Visean 352
	O.Azemeis granite gneiss	379 ± 12	.7036 ± .0009	379 ± 12		379 ± 12	Devonian
*(Rb/Sr decay constant 1.47×10^{-11})				OLDEST			
	Quartz diorite west of Junqueira	512 ± 19	.7036 ± .0004	512 ± 19			Cambrian
		Pinto, 1979				Pinto, 1983, 1985	

Carboniferous

Priem et al. (1970)
Oen, 1970

All dates calculated using 1.42×10^{-11} as the decay constant, except those marked *.

Table 1.1

324±4 Ma has been found in the present study completing the radiometric dating of granites of this area.

Pinto (1983, 1985) proposed a new classification for the granites. Although this is a much more useful classification than the long-established Older/Younger division, the latter is still referred to as it has dominated discussion about the ages of Portuguese granites for the last decade. He collected data from many sources and interpreted them within the context of the Phanerozoic time scale of Harland et al. (1982). Dates tended to cluster in distinct periods, possibly reflecting discrete episodic plutonism (Table 1.1).

Geochemical Studies of Granites

Much analytical work has shown that the Older Granites are predominantly alkalic, whilst the Younger Granites have a calc-alkaline character: (Neiva, J., 1943, 1953, 1955; Neiva, J. and Faria, 1952; Pereira, 1959; Oen, 1970; Fernandes, 1970; Albuquerque, 1971; Neiva, A., 1973; Goncalves, 1974; Godhino, 1974). Trace element analyses have been published by Oliveira (1970), Albuquerque (1971), Costa et al. (1971), Neiva, A. (1973), Godhino & Silva (1974), though they have not yet been used to model the petrogenesis of Portuguese granitoids.

1.3 - Aims and Objectives

The main aims of the project were to consider important problems such as: (i) the petrogenesis of S-type granitic magma as exemplified in Iberia; (ii) the development of high temperature-low pressure metamorphic belts and their associated plutonism, common throughout Iberia, and (iii) the evolution of intra-continental shear zones and their common association with S-type granites, a major structural element in Iberian tectonics.

The Serra da Freita was selected for this study for several reasons. From the above account it is apparent that much detailed regional background knowledge was already available in terms of stratigraphy, lithologies present, and age and type of igneous intrusions. However the actual Serra da Freita pluton and the surrounding metasediments had not been studied except in the most general terms; the Serra da Freita granite was not dated in Pinto's (1979) regional traverse and no geochemical analyses were available. As the project aims to combine detailed geochemical and isotopic studies with structural analysis to gain a more complete understanding of a pluton's history than is normally possible, the Serra da Freita was recognized as suitable for such an approach. It soon became apparent that the tectonothermal setting of the area which involved intrusion of an S-type granite into a metamorphic belt lying within a major shear zone, combined with excellent exposure, afforded an opportunity, probably unique in the Portuguese Hercynides, to consider together the problems outlined as (i) to (iii) above.

1.3.1 - Petrogenesis of S-type Granites

The concept of S- and I-type granites (Chappell & White, 1974) is useful in that it reflects fundamental differences in source region. I-type granites derived from an igneous parent are distinct from S-types which are derived by partially melting rocks which have been through a weathering cycle, ie. in S-types, chemical fractionation during sedimentary processes will tend to produce a relative decrease in Na, Ca, and the ferric/ferrous ratio, with a corresponding increase in Al and K. S-types thus tend to be peraluminous.

The classification of S- and I-type granites was devised for the Lachlan Fold Belt in SE Australia, however it has proved useful within a global framework. The original classification has been refined and extended with the recognition of A- and M-types and two categories of I-type. These five divisions can be related to specific geological environments; S-types characterize continental collision zones and also encratonic, ductile shear belts where, in both cases, the crust is sufficiently tectonically thickened to cause the temperature at depth to rise and so promote crustal remelting (Pitcher, 1982).

A distinction needs to be made between "S-type" and "peraluminous" granite. S-types are generally peraluminous, however several authors advise caution in interpreting all peraluminous granites as S-types. Chappell & White (1974) initially restricted the S-type designation to granites thought to be derived from a mature strongly weathered pelitic source. Peraluminous granites, having normative corundum and A/CNK > 1 (Al/Ca+Na+K), crystallize assemblages including one or more of muscovite, Al-rich biotite, garnet, cordierite, andalusite and sillimanite (Clarke,

1981) and are commonly considered to be genetically linked to metapelites (thus designated S-types) owing to their chemical and mineralogical similarities to these sediments. However Clarke (1981) points out that a peraluminous composition can be reached by a variety of pathways, namely (i) a direct link to peraluminous source rocks, (ii) the result of reaction with host rocks (assimilation), (iii) fractional crystallization from metaluminous magmas, (iv) the result of interaction between late-stage magmas and hydrothermal fluids.

Miller (1985) defined strongly peraluminous compositions (Ps) as those which require the presence of a phase more aluminous than biotite, and concludes the following: "(i) very few Ps rocks are derived entirely from pelitic sources; (ii) a majority are derived largely from intermediate to felsic crustal sources, including both immature sedimentary rocks (e.g., metagreywackes) and metaigneous rocks; and (iii) some are the products of partial melting of metaluminous mafic (crustal or subcrustal) sources - Ps compositions of such magmas may be a primary feature or the result of fractional crystallization".

A Ps granite derived entirely from pelitic sources would therefore appear to be rare, however the Serra da Freita granite, part of a voluminous group of biotite/muscovite granites which comprise the most characteristic rock type of the Iberian Hercynian (Pitcher, 1982), is strongly peraluminous and intrudes a belt of high-grade pelitic schists. The possibility that these schists could give rise to such a peraluminous anatectic melt is one of the main hypotheses of this thesis.

1.3.2 - High Temperature, Low Pressure Metamorphic Belts

The Serra da Freita pluton intrudes the high grade core of the linear Porto-Viseu metamorphic belt (Figure 1.5b), characterized by a high temperature low pressure paragenesis of biotite, andalusite/staurolite and sillimanite zones in the Beira Schists. Both this granite and associated plutons to the NW intrude the sillimanite zone and the contacts are almost parallel to the isograds which they cut obliquely. The term "plutonometamorphism" has been widely used, e.g. (Westerfeld et al., 1956; Sluijk, 1963; Oen, 1970; Ferreira, 1972). Oen described this belt as "a lower pressure facies series of the non-almandinous Abukuma or Buchan type of regional metamorphism" with "almandine and kyanite absent or extremely rare." Godhino (1974) suggests a geothermal gradient of 49±6 °C/km for a similar situation to the south, and predicts anatexis at a depth of 12-15 km.

This thermal regime is not unique to the region, indeed many workers e.g. Gil Ilbarguchi & Martinez (1982) reported the same environment in north central Spain. Julivert et al.(1980) in a general summary of metamorphism in the Iberian massif, described metamorphic zonation in broadly symmetrical belts relative to a thermal axis, across strike from which the grade quickly decreases reaching unmetamorphosed rocks within a few kilometres. These thermal axes are "almost without exception outlined by granite plutons of alkaline tendency (2-mica granites)". The metamorphic climax is generally D2 and coincides with the generation of syn-tectonic anatectic melts. Wickham & Oxburgh (1985) reported a high-T, low-P environment in the Pyrenees which produces anatectic leucogranite, and propose a model of continental rifting. Although the tectonic setting in

Figure 1.5a - The structural setting of the Serra da Freita region

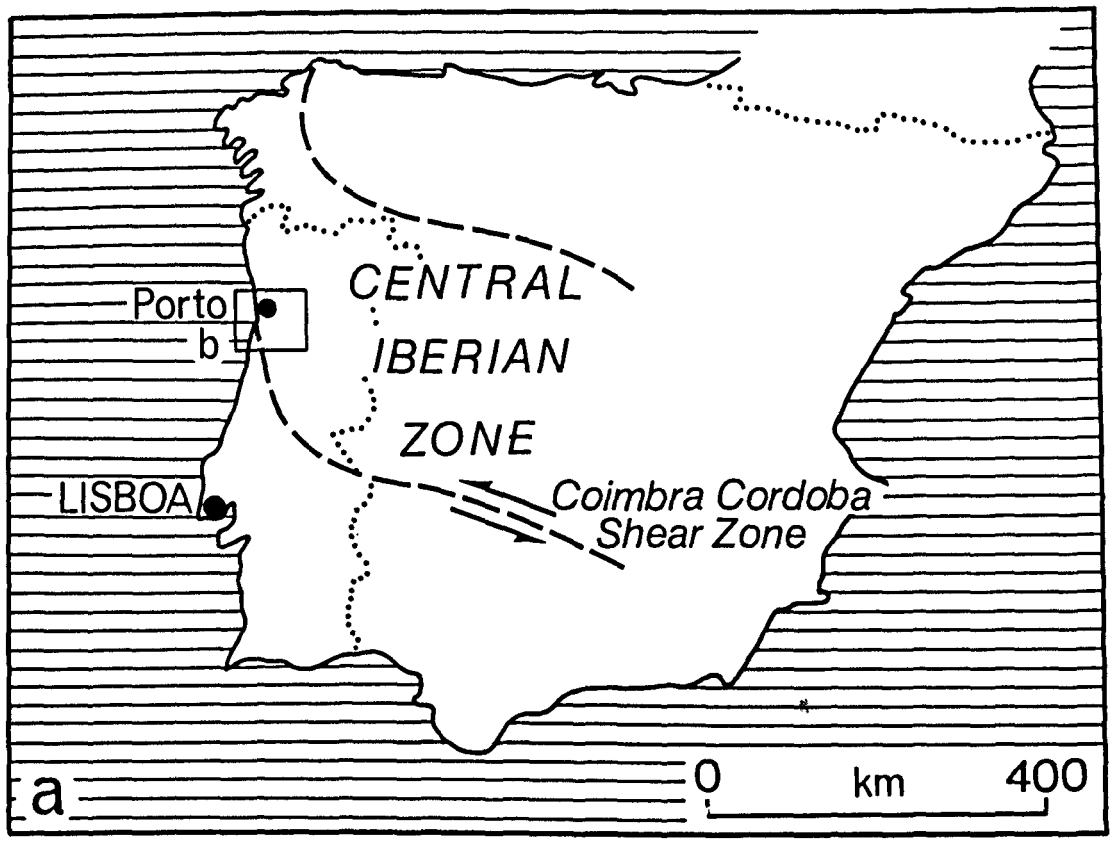

Figure 1.5b - The structural, metamorphic and plutonic components of the area

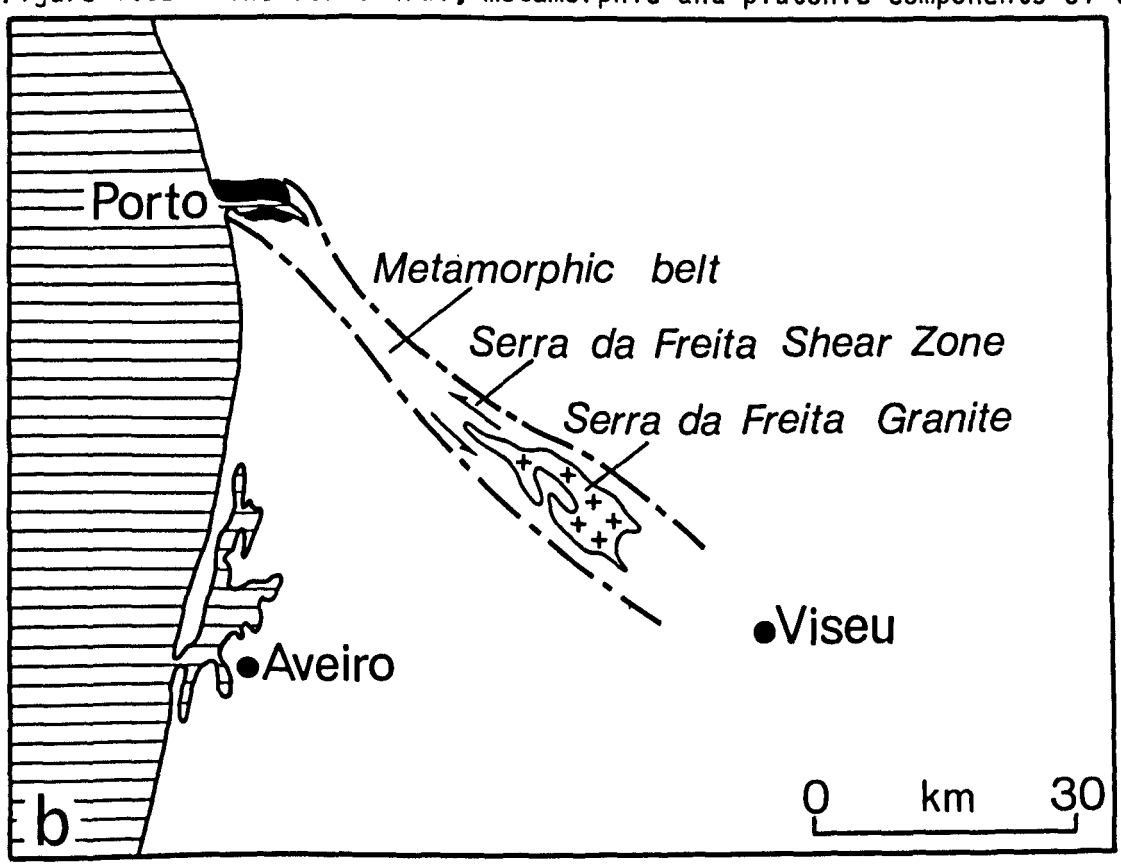

the Pyrenees is probably not comparable with northern Portugal, the metamorphic sequence and thermal gradient is similar; the Wickham & Oxburgh model predicts that almost total melting would occur at depths of > 14 km, comparable to the estimate of Godhino (1974). In conclusion, Wickham and Oxburgh (1985) suggested that a continental rift zone setting could explain all high temperature, low pressure belts and their associated steep geotherms. It is clear that: (i) the development of such belts is a general feature in the Iberian Hercynian, and (ii) their tectono-thermal significance is not well understood.

Excellent exposure in the Serra da Freita region allows detailed sampling of the metamorphic gradient from chlorite to sillimanite grade, and may shed light on the development of the Porto-Viseu metamorphic belt. Although the general absence of garnet precludes P/T calibration, the possibility of local anatexis to produce a peraluminous magma can be rigorously studied geochemically within a typical Iberian metamorphic dome.

1.3.3 - Shear Zones

Finally the relationships of these metamorphic zones and their associated peraluminous granites can be related both to local structure and regional tectonic considerations. The Iberian Arc and the Armorican Massif constitute the Ibero-Armorican Arc, interpreted in terms of a continental collision in the upper Palaeozoic (Matte & Ribeiro, 1975). Two great shear zones delimit this arc (Figure 1.6a): the dextral South Armorican (Berthe et al., 1979) and the sinistral Coimbra-Cordoba (Burg et al., 1981). Within this context, Iberia is divided into several tectonic zones (Figure

Figure 1.6 - Iberian tectonics

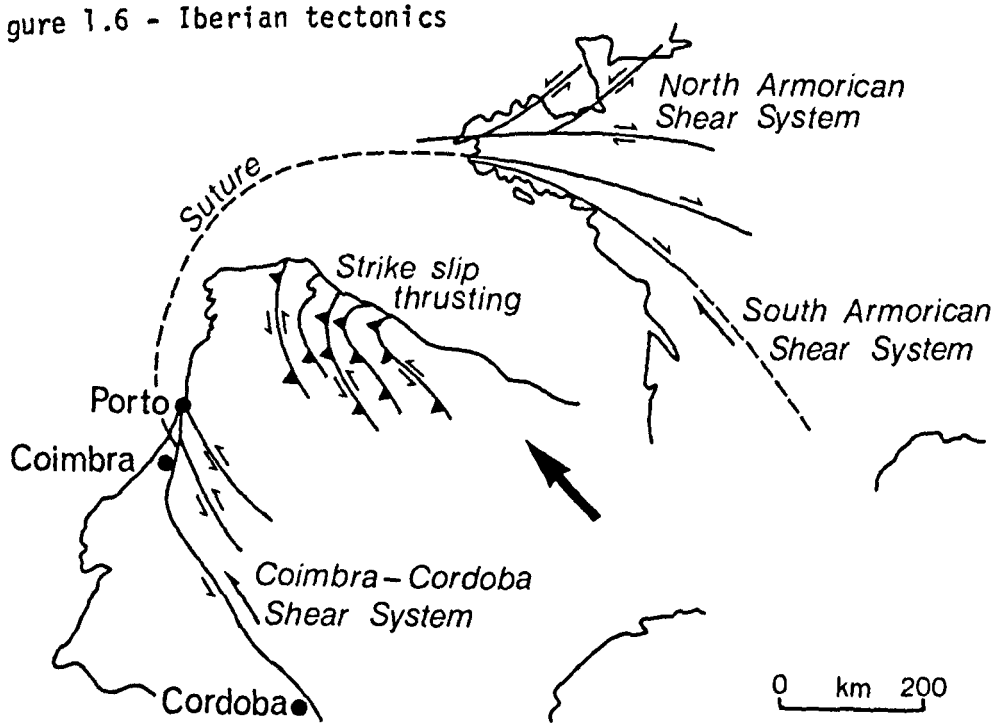

a The Ibero-Armorican Arc

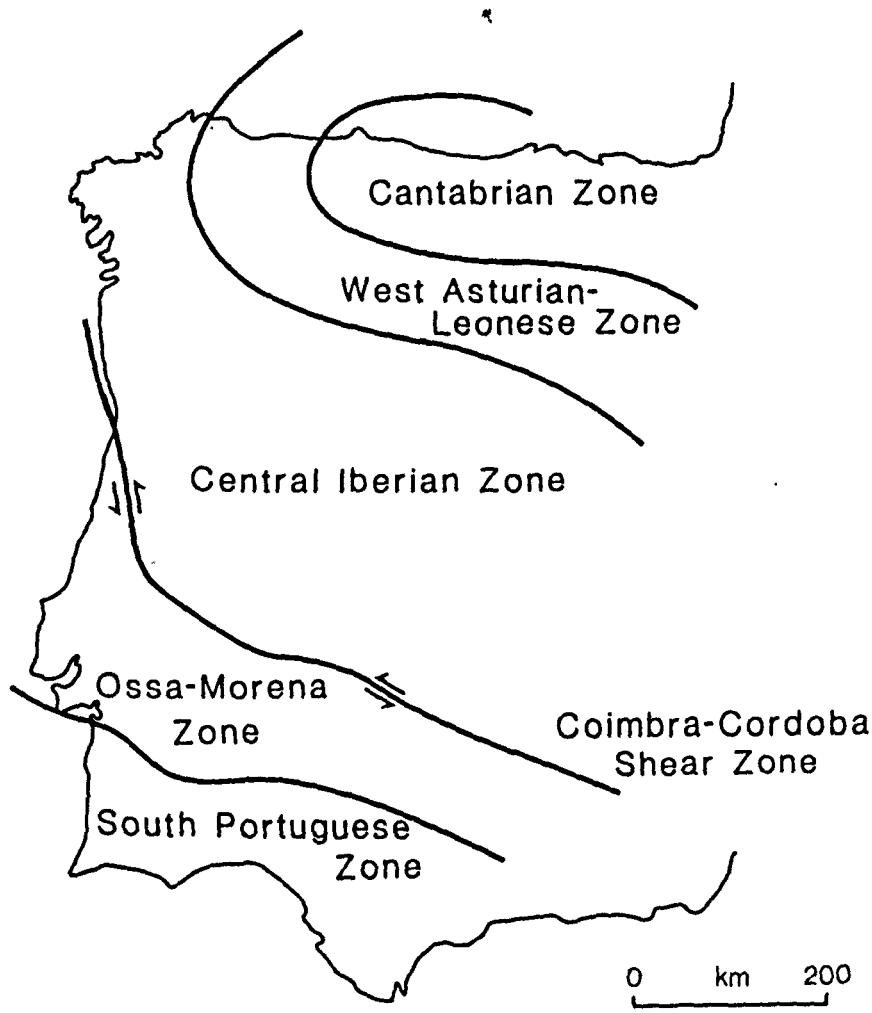

b Structural Zonation of Iberia
(Julivert et al.)

1.6b), (Julivert et al., 1972, 1980). In the interior of the arc, i.e. the Central Iberian Zone (CIZ) northwards, work in Galicia (Iglesias & Choukroune, 1980) and Extremadura (Castro, 1985) shows that almost identical structural associations exist over large areas, representing a distinct regional pattern of tectonic style, summarized by: (i) a clear correspondence between deformation in granitoids and the D2 peak; (ii) in these zones of intense deformation a C-S fabric (Lister & Snoke, 1984) is developed, which indicate strong components of non-coaxial flow. Detailed structural analysis of the Serra da Freita region shows it to be coincident with an unrecognized shear zone of this type, here named the Serra da Freita shear zone (Figure 1.5b).

Considerable controversy exists as to the nature of the association between granites and shear belts. It has been suggested that shear heating could raise temperatures sufficiently to cause partial melting (Nicholas et al., 1977). Strong & Hanmer (1981) discussed leucogranites in the South Armorican shear zone in Brittany and argued that such a close spatial and temporal occurrence of plutonism and shearing implied a genetic relationship. They proposed frictional melting in fault zones, by either frictional heating or lowering the solidus by fluid fluxing. In a discussion of the coastal batholith of Peru, Pitcher (1979) maintained that "large faults acting at depth would have imposed special P and T conditions in their vicinity, especially a decrease in pressure, favouring the formation and migration of anatectic melts. These melts rose and were emplaced at high crustal levels under the structural control imposed by the same deep-seated shearing event which helped produce the melts in the first place". A converse argument is that ascending plutons would localize

a shear zone by thermal softening and explain the association more readily (Poirier et al., 1979), but this does not explain the origin of the magmas.

1.4 - Methods of Analysis

A wide range of techniques was applied to gain insight into these problems:

(i) field mapping including detailed structural analysis;

(ii) petrographic studies of thin sections;

(iii) consideration of major and trace element whole rock data (XRF);

(iv) radiogenic (Rb/Sr) and stable (O2) isotope geochemistry of both whole rock and mineral separates.

Data obtained from this multidisciplinary approach allowed a study of the inter-relationships between regional metamorphism, deformation and plutonism in a small, well exposed area dominated by shear zone tectonics. However, as has been shown in this section, the associations represented here characterize Hercynian orogenic activity throughout much of the Ibero-Armorican arc, and the study therefore makes a contribution towards the interpretation of the geological evolution of Iberia.

PART II -- FIELD GEOLOGY

CHAPTER II -- BACKGROUND

2.1 - Introduction

The Serra da Freita lies between 40° 50' and 40° 54' N and between 8° 11' and 8° 19' W in north central Portugal and is a barren plateau approximately 1000 m above sea level. Several distinct summits are recognized in this area - S.Pedro Velho (1077 m), Serlei (1092 m), Vidoeiro (1097 m), and Malhada (1102 m) (Figure 2.1). Despite its elevation, access to the plateau is easy via several mountain roads and forest tracks; the best road leads from the nearest town, Arouca, 5 km from Malhada and this provided a convenient base during fieldwork (Plates 1 & 2). Detailed mapping and sampling were possible as exposure of the granite on the surface of the plateau varies from excellent (>70% exposure) to almost total (Plates 3-6). To the north and south the edges of the Serra da Freita fall steeply, occasionally sheer to the valleys below, these slopes are densely forested and of general poor accessibility (Plates 7 & 8).

The area is covered by the Carta Militar de Portugal, Servico Cartografico do Exercito Sheet 155 (Arouca) on the scale of 1:25000 (from which Figure 2.1 is taken). This topographic map proved excellent for basic mapping and was suitable for enlargement to 1:10000. The only geological map of the region is the 1:50000 scale Sheet 13-D (Oliveira de Azemeis) published by Servicos Geologicos de Portugal with an accompanying memoir (Pereira et al., 1980).

Figure 2.1 - Topographic map of the Serra de Freita

Plate 1 - The Serra da Freita viewed from the north with the town of Arouca in the foreground

Plate 2 - The view north from Detrelo de Malhada where the Arouca road reaches the summit of the plateau

Plate 3 - Typical Serra da Freita landscape looking NNW from Monte Calvo. At the extreme left, Albergaria das Cabras is seen beneath the prominent summit of S. Pedro Velho

Plate 4 - A continuation eastward from Plate 3, this shows the central part of the Serra da Freita with the Junqueiro road crossing the granite

Plate 5 - Looking south from Vidoeiro

Plate 6 - The Serra da Freita from Detrelo de Malhada, Serlei is the prominent summit right of centre

Plate 7 - The Mizarela Falls plunge drammatically from the southern edge of the plateau. S. Pedro Velho is the peak on the horizon. The well exposed plateau contrasts drammatically with the densely forested lower slopes. This view is from south of Castanheira

Plate 8 - The Caima River viewed from near Mizarela showing the nature of the southern slopes of the Serra da Freita

2.2 - Fieldwork Aims

Approximately 40 km^2 of the Serra da Freita were chosen for study, this incorporated the NW part of the Serra da Freita pluton, the Castanheira pluton and the Beira Schists exposed to the north and south before reaching the edge of the plateau. To the east the Ribeiro de Abundancia provided a convenient limit (Figure 2.2). Outside this specified area samples were collected on several regional traverses to the north and west, however mapping was confined to the Serra da Freita plateau.

Two periods of 8 weeks were spent in the area in the springs of 1984 and 1985; fieldwork in 1984 was directed in several areas: (i) production of a lithological map firstly on 1:25000 scale, this proved inadequate for detailed mapping and 1:10000 scale was eventually used for the whole area, resulting in the production of the most detailed map available for this part of Portugal; (ii) collection of 218 samples of plutonic rocks, minor intrusives and metasediments for laboratory study; these were in most cases of adequate size and freshness for geochemical analysis. In 1985, the thrust of the work was a detailed structural analysis of both granite and metasediments which led to the establishment of a deformation sequence for the region and an emplacement model for the pluton within the Serra da Freita shear zone.

Figure 2.2 - Place names and localities in the S. Pedro du Sul belt mentioned in the text.

(Serra da Freita shaded red).

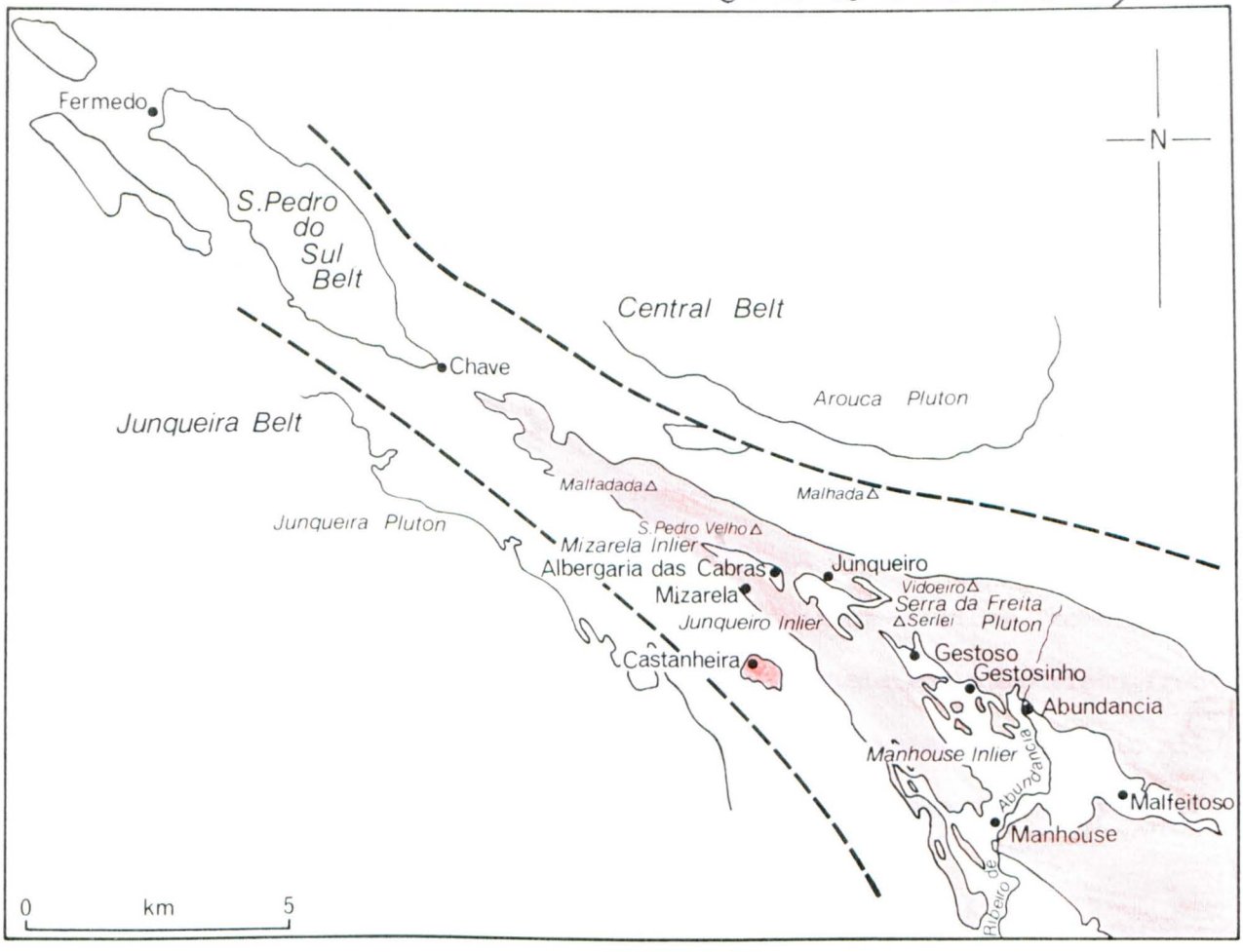

2.3 - Regional Setting

The Serra da Freita and Castanheira plutons form the north-western part of the NW - SE trending S.Pedro do Sul belt (Pinto, 1979) (Figures 1.4 & 2.2). Structural, petrographic, and geochemical evidence will be presented which shows that the two plutons are part of the same body. The Junqueiro pluton to the south lies in the belt to which it gives its name (Figures 1.4 & 2.2); the Arouca and Regoufe plutons to the immediate north are in the Central belt, so the S.Pedro do Sul belt in the Serra da Freita region is less than 5 km wide. Coincident with the S.Pedro do Sul belt is the axial region of the Porto-Viseu metamorphic belt and the maximum development of the Serra da Freita shear zone (Figure 1.5b). The study is confined to the complexities of the S.Pedro do Sul belt in the Serra da Freita area, although some regional sampling of the metasediments was undertaken and one granite sample was obtained from further to the NW along strike so that an analysis would be available for comparison from adjacent areas. The country rocks around the granites studied are in all cases the Beira Schists, ranging from chlorite grade shales and greywackes to sillimanite-bearing pelitic schists.

2.3.1 - The Serra da Freita Pluton

The granite exposed in the Serra da Freita is part of a pluton which extends some 20 km from S.Pedro do Sul to Chave, beyond which several smaller units crop out over a further 12 km in the Mansores/Fermedo region, in total comprising over half the distance from S. Pedro do Sul to Porto (Figure 2.2).

The pluton is markedly linear, approximately 6 km across at its widest point. Large areas of sillimanite bearing schist show complex sinuous contacts with the southern margin. Of the few which are actually enclosed within the granite, those west and east of Albergaria das Cabras lie within the study area and are shown as roof pendants on the cross-section on Sheet 13-D (Figure 2.3), and are here designated the Mizarela and Junqueiro inliers respectively. A large tract of schist north and east of Manhouse (the Manhouse inlier) causes the granite to bifurcate into two limbs, of which the southern displays the more complex contacts with the country rocks. The northern limb has much simpler relationships with its envelope and is generally 2-2.5 km wide north of the villages of Malfeitoso, Abundancia and Gestosinho. Gestoso lies at the end of the Manhouse inlier and beyond this the two limbs merge at Serlei. The pluton narrows considerably moving north-west, ranging between 1.5 and 2 km wide in the vicinity of the Mizarela and Junqueiro inliers. Beyond Alto da Malfadada the Serra da Freita drops steeply and the narrow granite sheet terminates south-east of Chave.

Figure 2.3 - Cross-section of the Serra de Freita pluton taken from the 1:50,000 scale 13-D (Oliviera de Azemeis) sheet published by Servicos Geologicos de Portugal (1980)

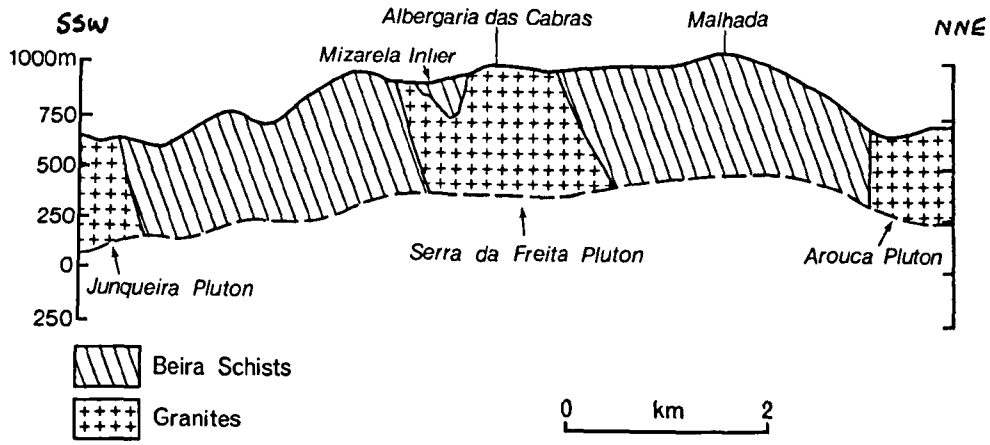

CHAPTER III -- STRUCTURE AND DEFORMATION SEQUENCE

Generally excellent exposure enabled detailed structural analysis to be carried out allowing a correlation between folding, cleavage, shear zone development and plutonism. The distinction of separate "deformation events" (i.e. D1, D2 ... etc) within this area tends to be misleading as too rigourous adherence to such a scheme conceals the essential fact that one is dealing with a continuum of deformation, in this case associated with the development of a shear zone over a protracted period of time.

3.1 - Early Structures

In the Beira Schists west of Rio de Frades, Portuguese Survey workers and Sluijk (1963) recognized regional gently SE plunging upright or slightly overturned folds (F1) with an associated axial planar slaty cleavage (S1) (Figures 3.1 & 3.2). In this area, regional metamorphism is of chlorite-biotite grade and sedimentary structures are clearly seen; younging evidence such as flame structures indicate F1 wavelengths of 1-1.5 km.

In zones of higher grade than biotite primary features are generally obscured by porphyroblast growth and penetrative later cleavages which overprint S1. However one distinctive unit can be easily mapped along the northern ridges of the Serra da Freita, within which staurolite porphyroblasts reach a size of 10 cm. The outcrop pattern of this bed suggests a fold closure near the radar station (GR 617260) (Figure 3.3).

The F1 fold style has a strong influence on the form of the Serra da Freita granite body, as discussed in Section 4.3.

Figure 3.1 - Geological sketch map of the Serra da Freita showing the relationship between the granite and its envelope with the main structures discussed in the text

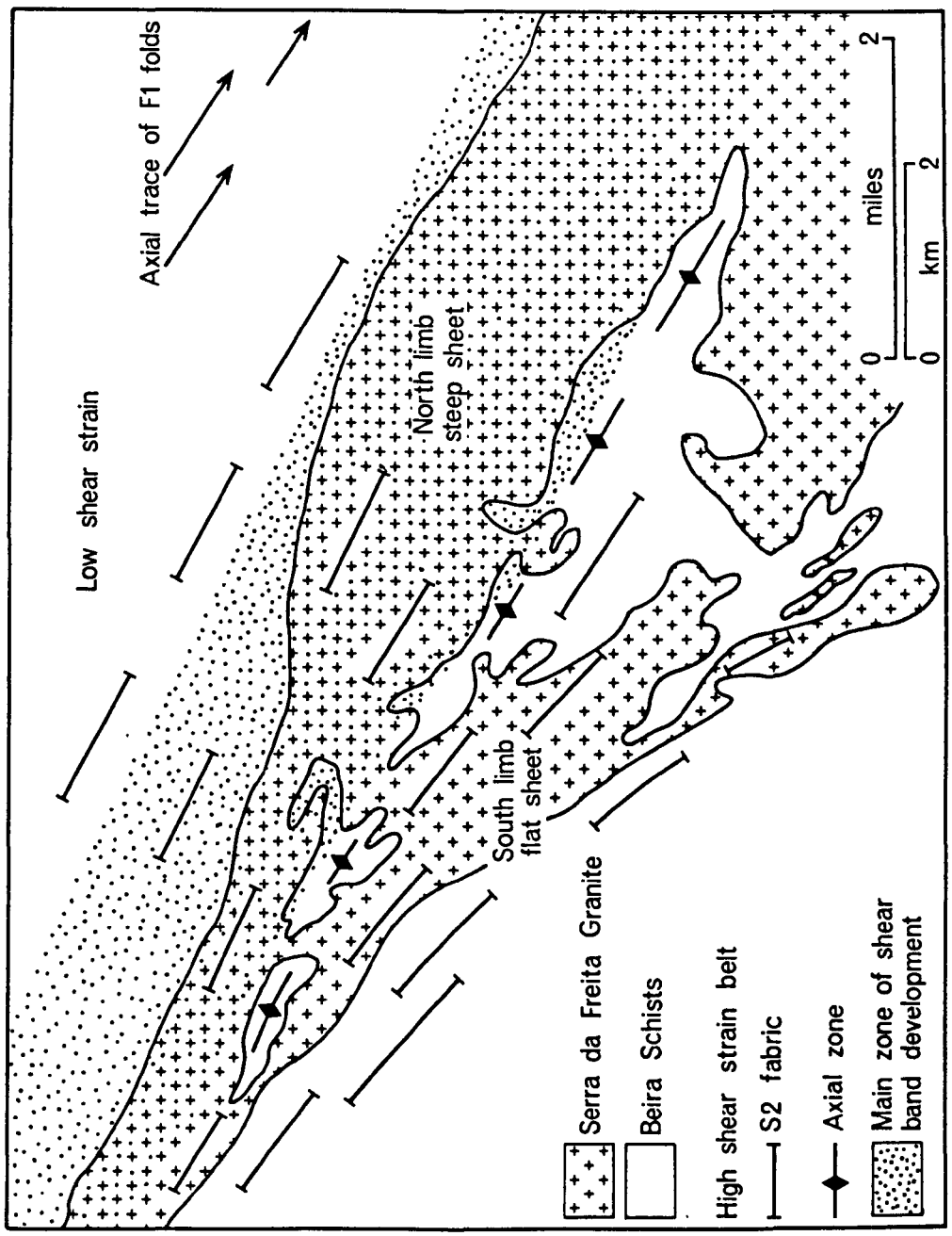

Figure 3.2 - F1 fold style

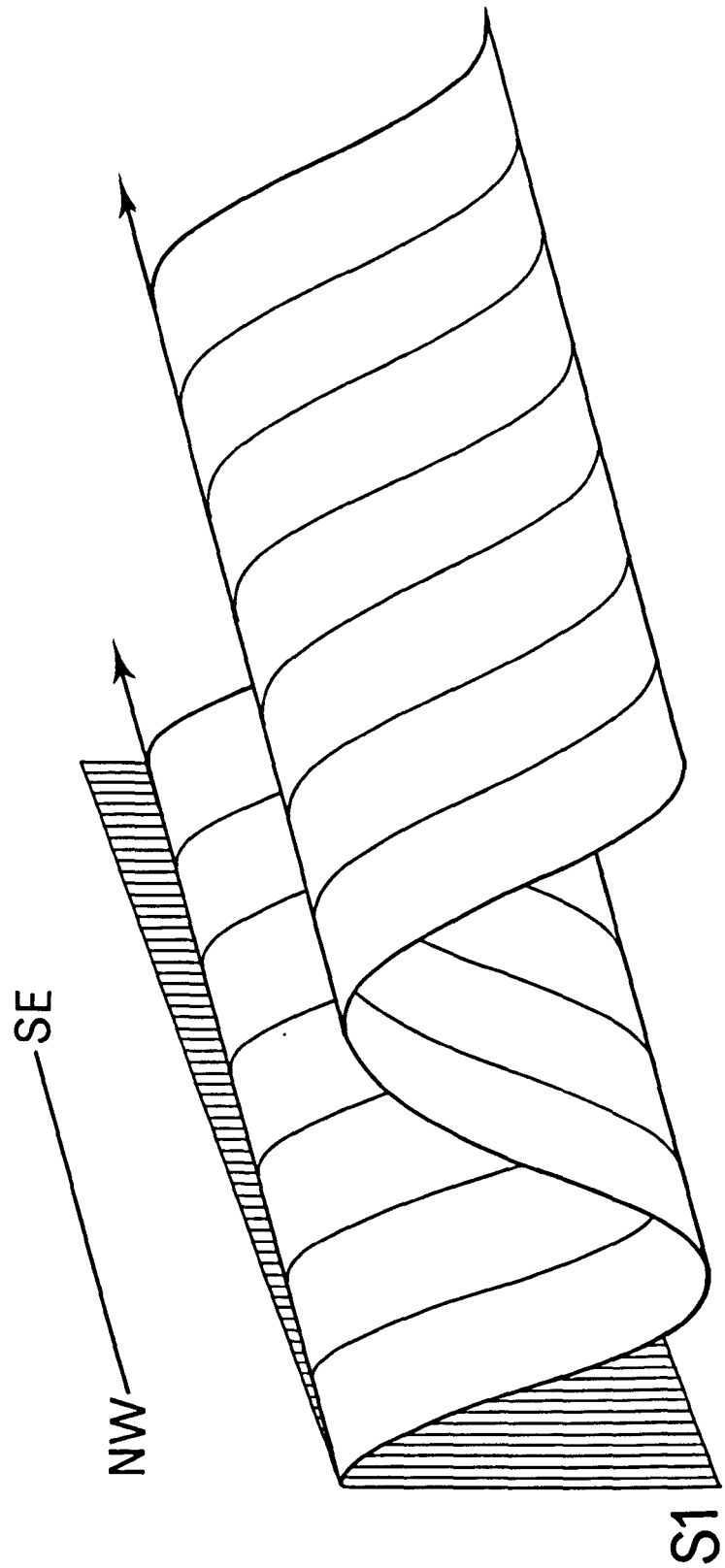

Figure 3.3 - Map of a possible F1 fold closure as defined by a unit rich in large staurolite porphyroblasts

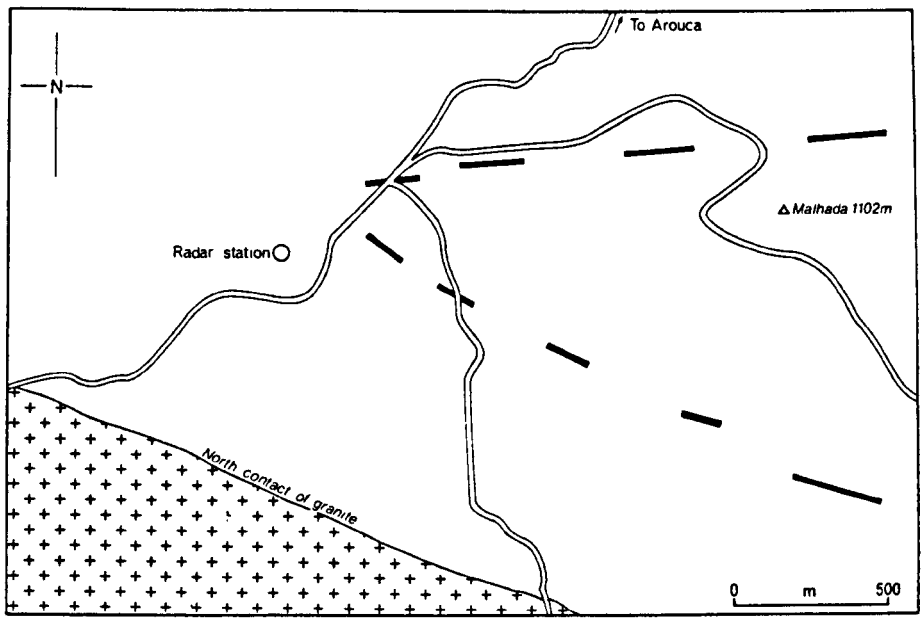

3.2 - Shear Zone Structures - Introduction

Structures formed during the main period of sinistral transcurrent movements are present throughout the area, however an approximate field boundary can be traced along the regional strike south of which strain greatly intensifies (Figure 3.1). This zone of high strain is coincident with the location of the Serra da Freita pluton and is interpreted as being the focus of movement in the Serra da Freita shear zone.

3.2.1 - Low Strain

The structures produced at low strain are confined to the northern-most ridges of the Serra da Freita: the Coto de Boi, Pena Amarela and the spur west of Rio de Frades. Here F2 folds are moderately to steeply plunging, have a sinistral sense of vergence, and a moderately to steeply inclined axial planar schistosity, S2 (Plates 9-13 and Figure 3.4). Most are close with ILA (inter-limb angle) c.60°-70°, although some of the larger folds are more open with ILA of 70°-75°. The short limbs of the latter may be 50-60 m across although 5-10 m is more common. Refraction across lithologies of varying competence is common due to the heterolithic nature of the shales and greywackes (Plate 14). Changes of S2 facing directions across strike indicate the crossing of F1 hinges.

3.2.2 - High Strain

This belt extends across strike for approximately 6 km; within which are found the axial zone of the metamorphic belt and the outcrop of the Serra da Freita pluton (Figure 3.1). It continues to the southern edge of the Serra da Freita where lack of exposure and precipitous slopes prevent a

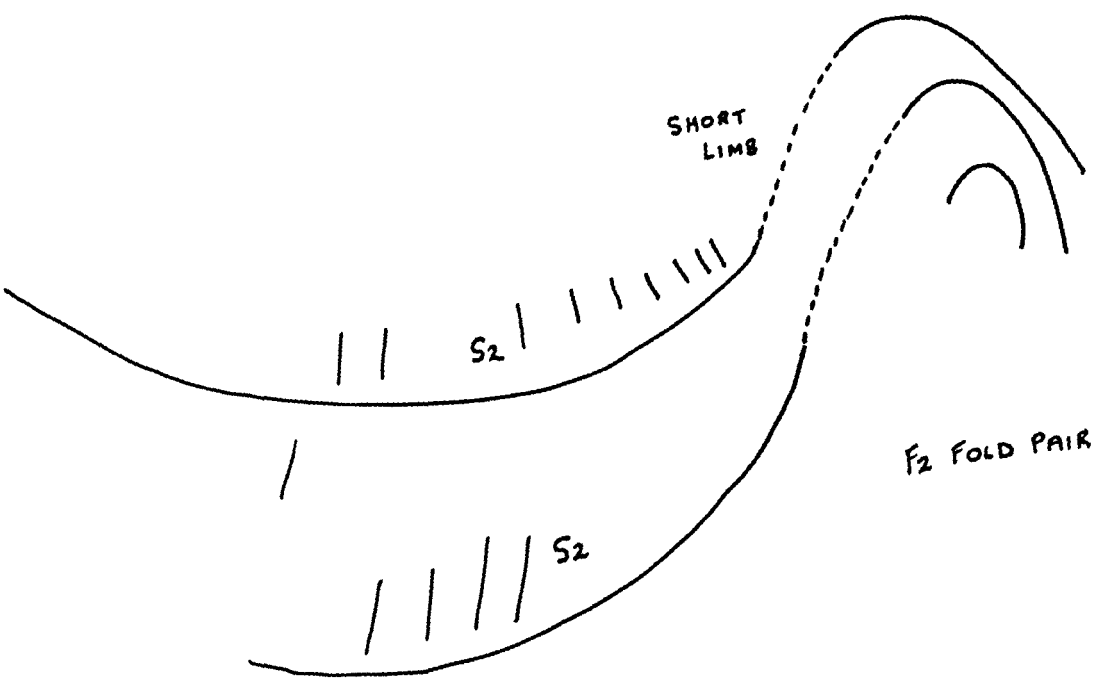
SHORT
LIMB
S2
S2
F2 FOLD PAIR

Plate 9 - The Pena Amarela ridge, scenery typical of the northern ridges of the Serra da Freita

Plate 10 - Looking obliquely down-plunge of a large F2 showing sinistral vergence. The short limb is poorly exposed to the right of centre

Plate 9 - The Pena Amarela ridge, scenery typical of the northern ridges of the Serra da Freita

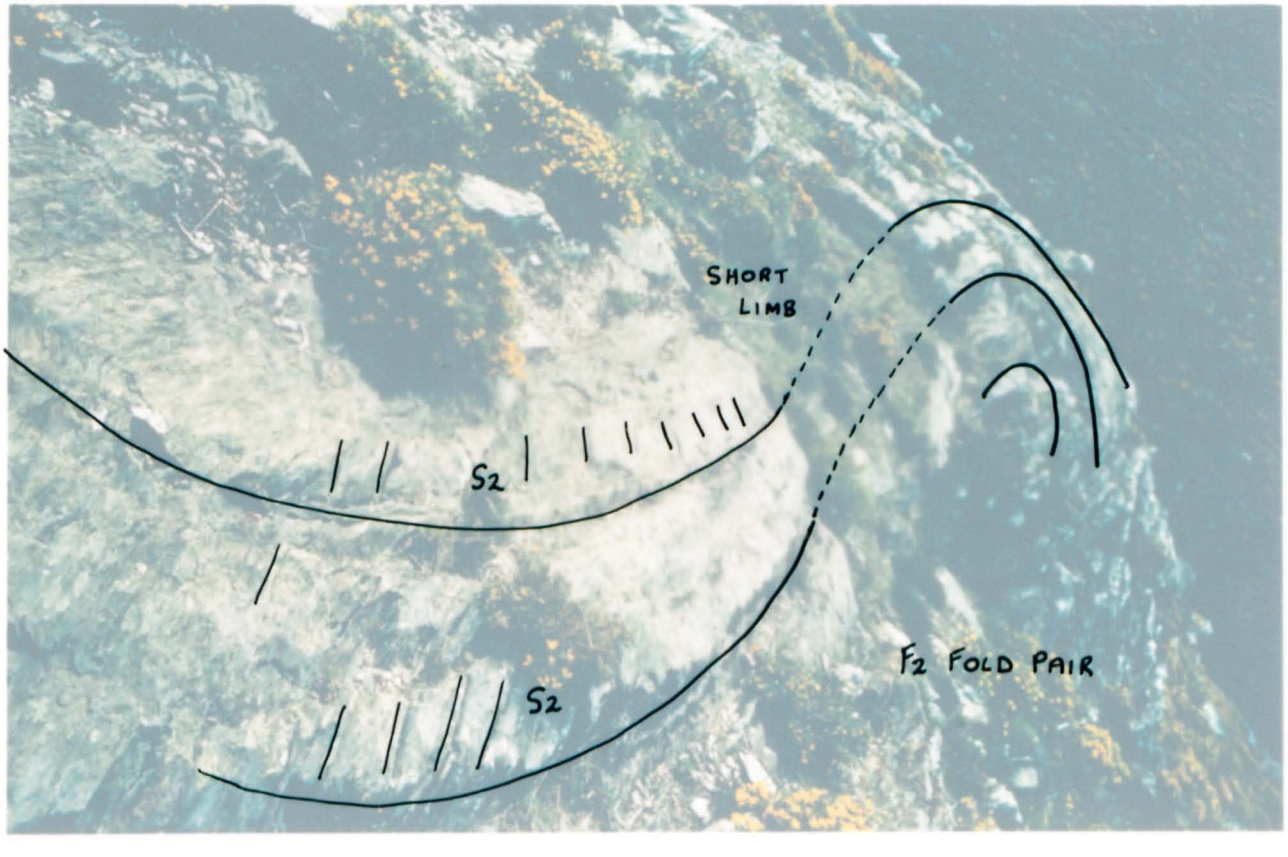

Plate 10 - Looking obliquely down-plunge of a large F2 showing sinistral vergence. The short limb is poorly exposed to the right of centre

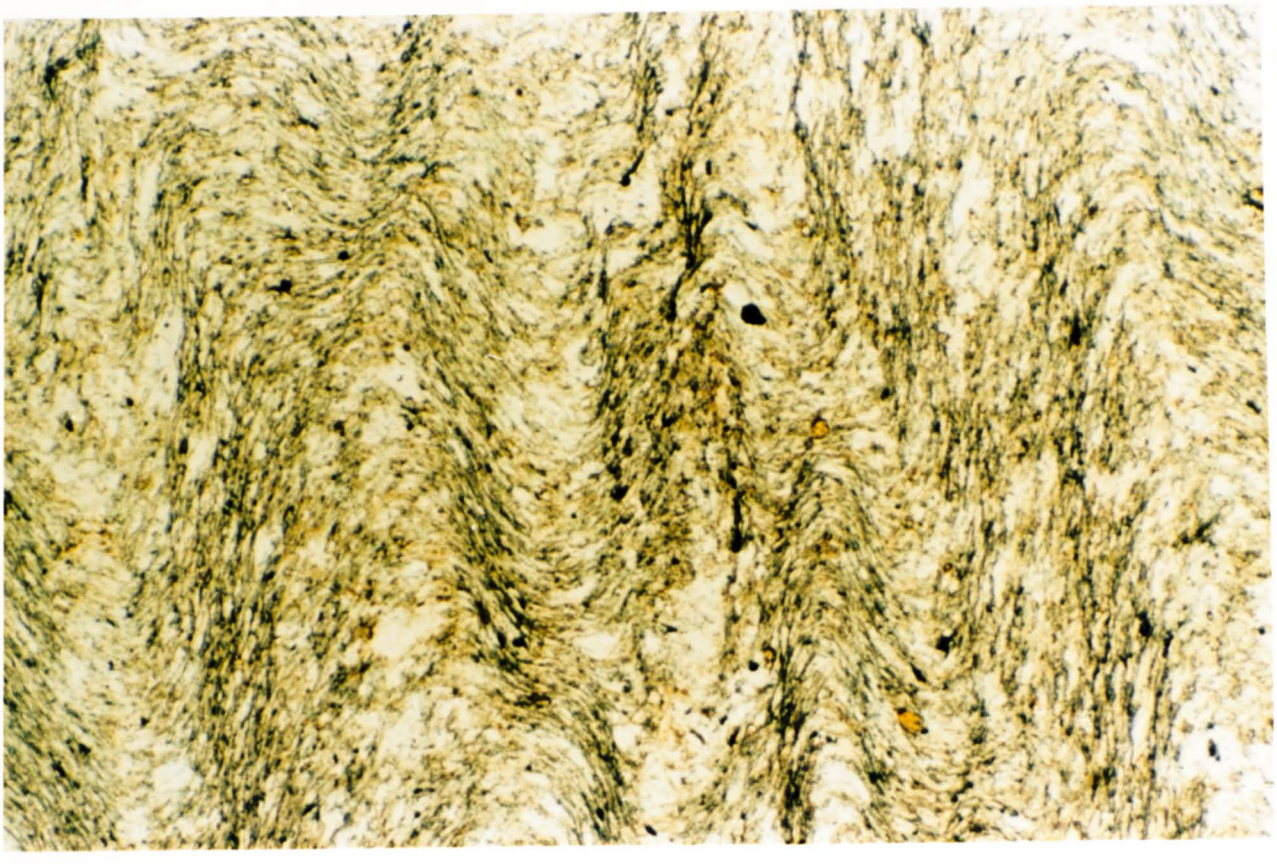

Plate 11 - A zonal cleavage S2 crenulates S0/S1 (F459S, GR 6744 2628, PPL, x 25)

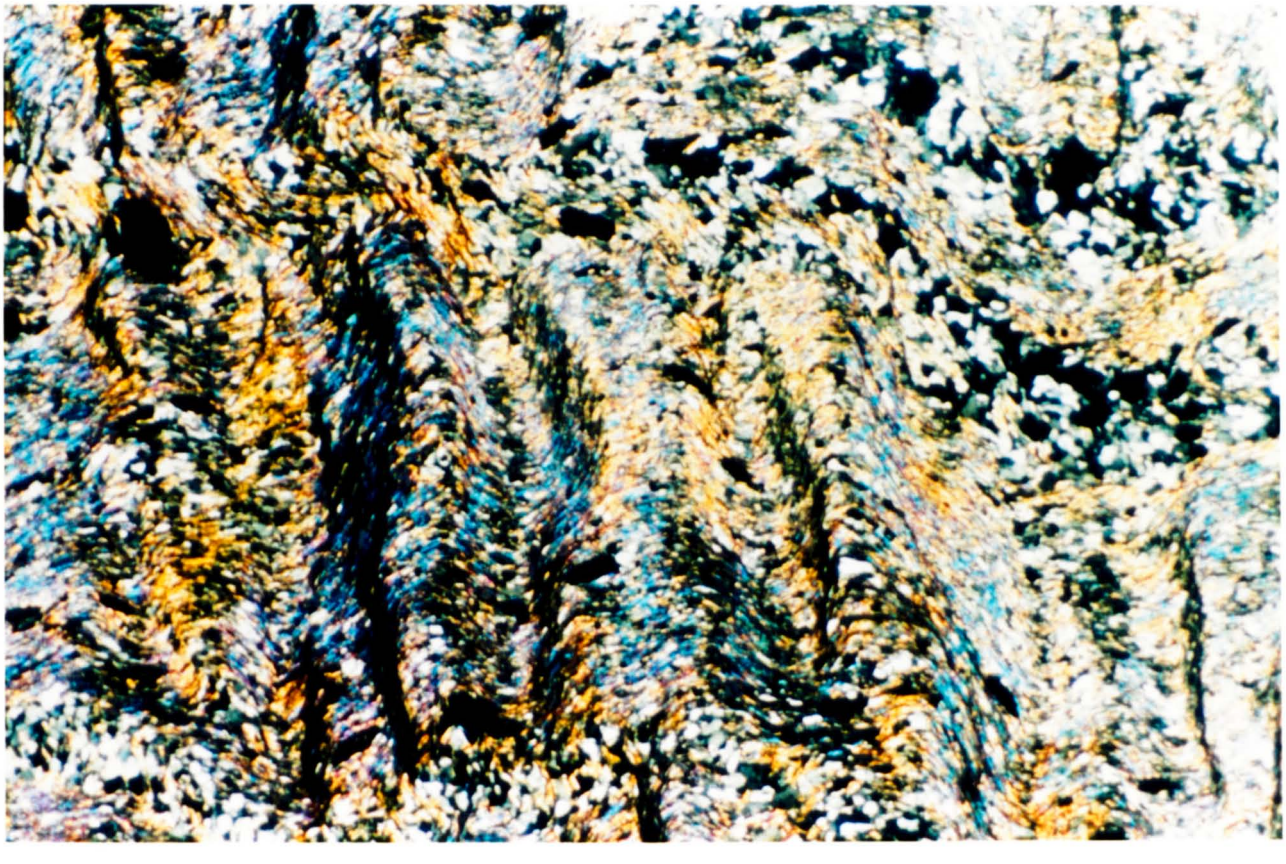

Plate 12 - Similar to Plate 11, quartz-rich bands define S0/S1, which is crenulated by S2 (F463S, GR 6689 2590, XPL, x 25)

Plate 13 - The S1/S0 fabric, defined by colour banding, is clearly crenulated by a steeply inclined cleavage, S2, Rio de Frades ridge

Plate 14 - Refraction of S2 cleavage between contrasting lithologies, Pena Amarela ridge

Figure 3.4 - F2 fold style formed at low strain

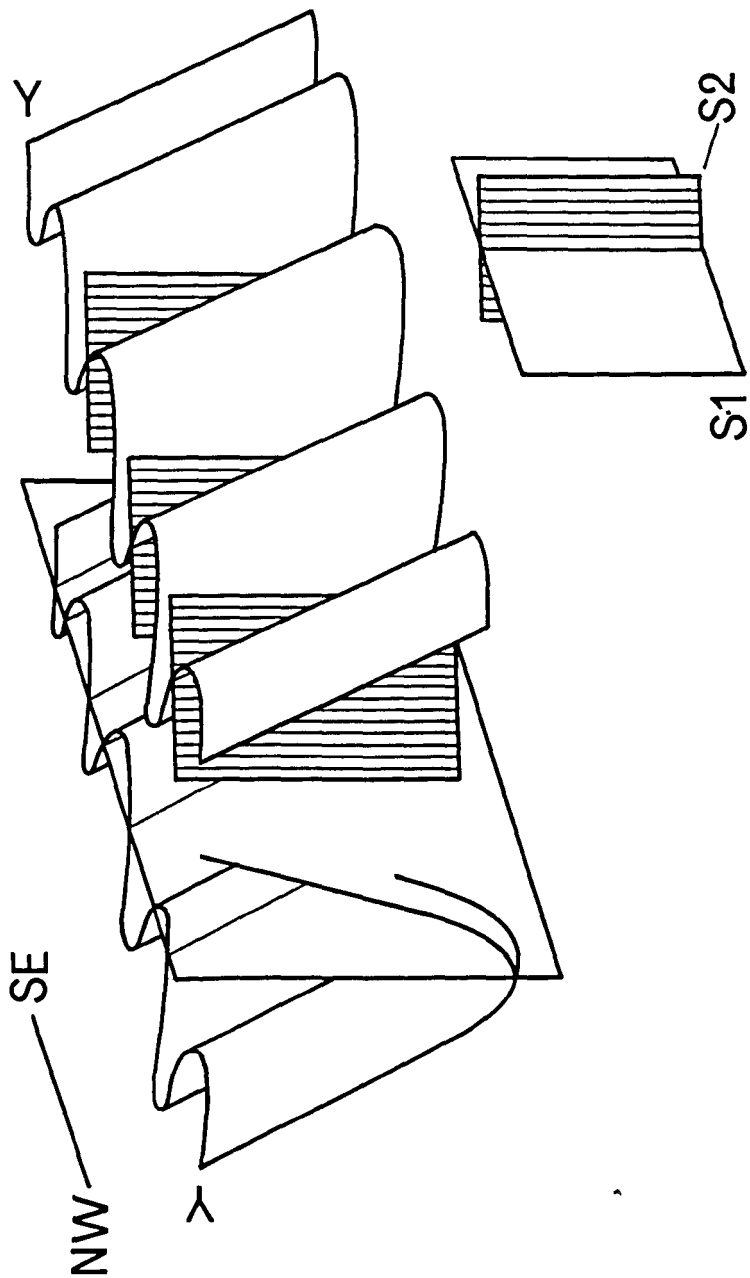

precise limit being established. S2 in the schists is now sub-vertical to vertical (Figure 3.5) and this coarse fabric which overprints bedding and S1 is easily exploited by weathering where a combination of excellent exposure and only minor changes in orientation of strike over many kilometres produce a dramatic outcrop pattern (Plates 15 & 16). This constancy of strike within the shear zone contrasts with more variable orientations in the low strain belt to the north, explained by tightening and rotation of F2 and intensification and steepening of S2 within the Serra da Freita shear zone, similar to the situation around the Main Donegal Granite in northern Eire (Hutton, 1982). In this environment, F2 hinges are obscured as the ILA approaches zero. This penetrative S2 is synchronous with the peak of regional metamorphism, ranging from andalusite/staurolite grade schists to those of sillimanite grade into which the pluton was intruded. It is represented in the southern limb of the granite as a primary magmatic foliation defined by preferred orientations of phyllosilicates and feldspars. An associated stretching lineation (Figure 3.6) plunges gently to the NW and implies transcurrent motion with a component of transpression. Evidence from tension gashes, boudinage and porphyroblast rotation implies a sinistral direction of translation in the shear zone (Plates 17 & 18).

Within this high strain zone the strain gradient decreases moving southwards across strike. Although the schists on the southern side of the granite still show a penetrative S2, the inclination is more variable and around the Castanheira granite evidence of reorientation produced by ballooning is observed. Such modification would have been hindered if the strain had been as high as on the northern side.

Figure 3.5 - Equal area projection of poles to S2

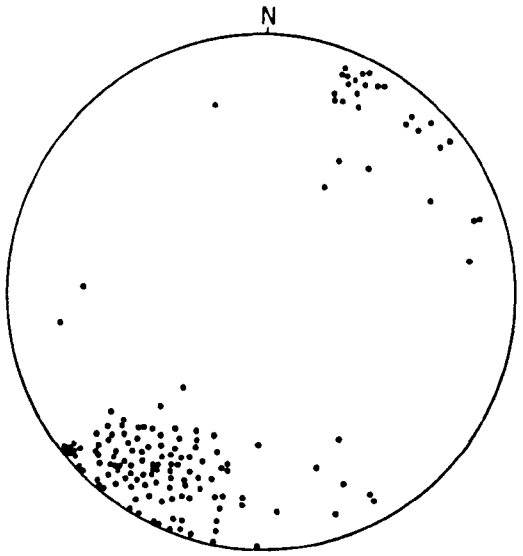

Figure 3.6 - Equal area projection of stretching lineation

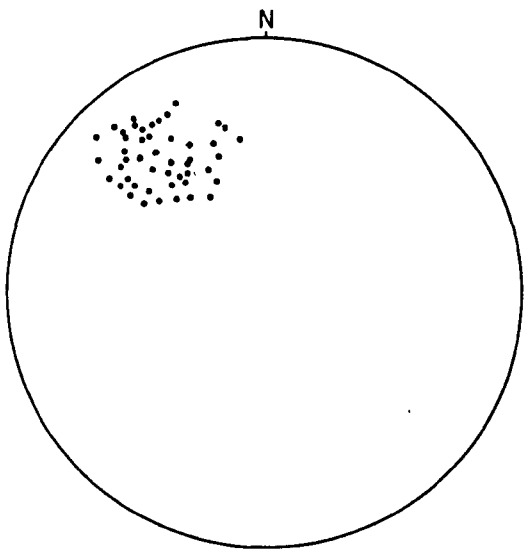

Plates 15 & 16 - These views, taken at the roadside west of Mizarela, show the drammatic outcrop pattern of the Beira Schists, controlled by the vertical S2 fabric within the high strain zone

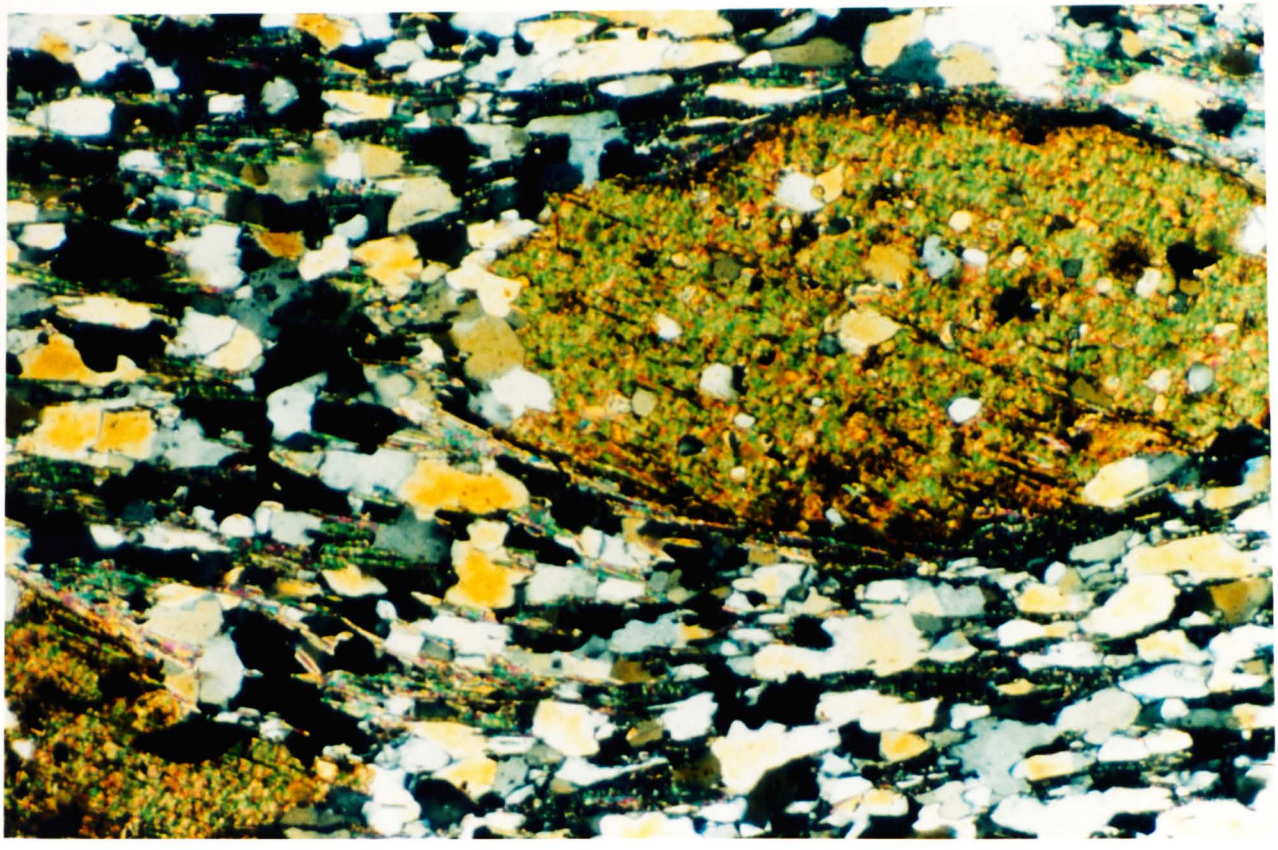

Plate 17 - Rotated biotite porphyroblast indicates sinistral sense of shear (F433S, GR 6190 2635, XPL, x 62.5)

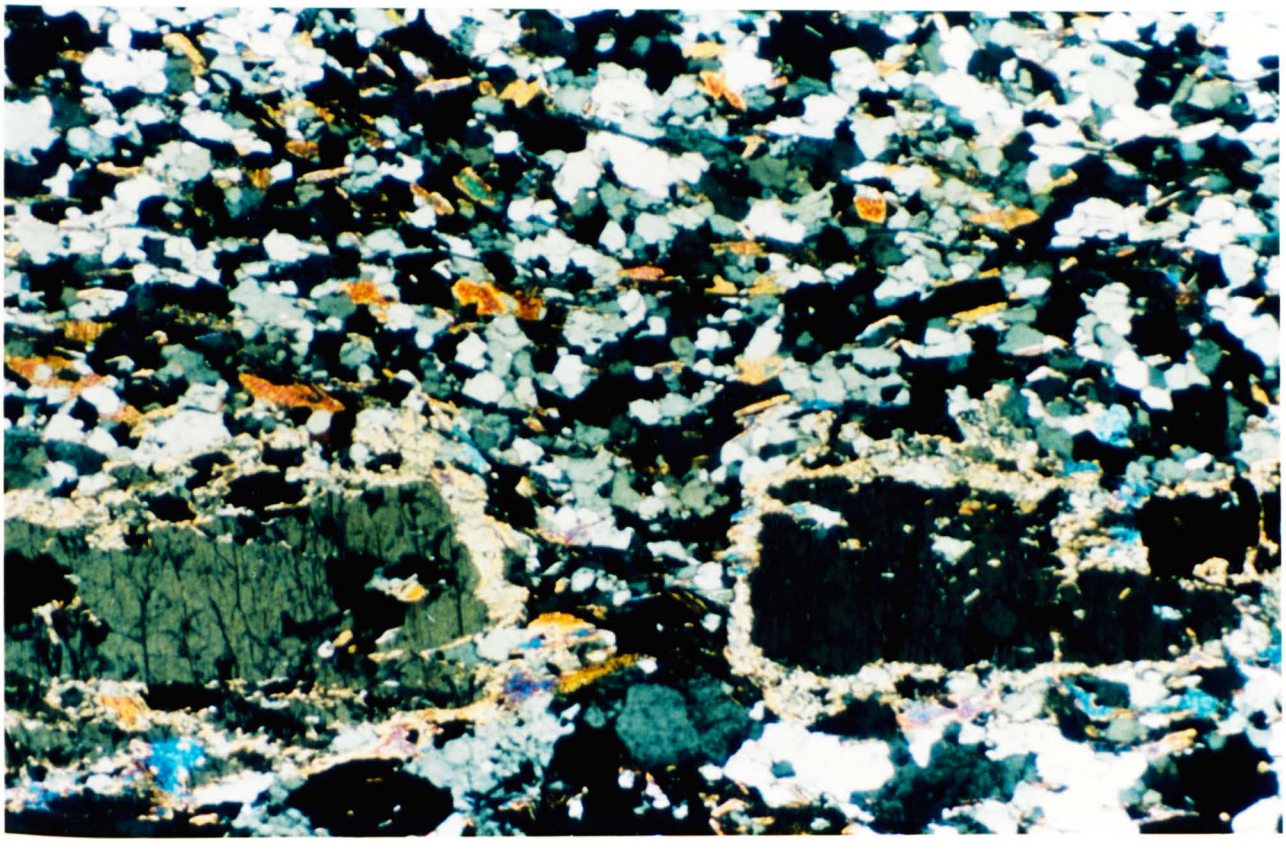

Plate 18 - Boudinage of andalusite porphyroblasts (F339S, GR 6210 2545, XPL, x 31.25)

In summary, it is possible to distinguish two zones, a region of low strain in the extreme north of the study area outwith the shear zone limits, and a high strain belt coincident with the location of the shear zone, within which the strain gradient decreases southwards (Figure 3.7). Problems of relief and exposure do not permit a southern limit to be recognized.

3.2.3 - Development of Ductile Shear Bands - C-S Fabric

Progressive deformation is marked by the appearance of ductile shear bands which increasingly affect the earlier S2 foliation. These structures occur in a 3-km wide belt (Figure 3.1) which involves the northern limb of the granite and the schists beyond it (Plates 19-22). These C surfaces are small scale parallel ductile shear bands recognized in the field as an extensional crenulation cleavage S2a (Figure 3.8). These shear bands are generally anticlockwise or synthetic to the main S2 fabric and show a sinistral sense of displacement. However in rare examples a second clockwise or antithetic set are developed with dextral offsets. S2a dips steeply NW or SE (Figure 3.9) with steep intersections with S2 (Figure 3.10). Its effects become less marked to the south, however a southern limit cannot be precisely defined. Generally, shear band development is rare south of the axial zone.

The idea of 2 sets of planar structures developing in tectonites has been reviewed by Lister and Snoke (1984). Berthe et al. (1979) applied these ideas to the South Armorican granites, and Castro (1985) to the central Extremadura batholith in Spain. Berthe et al. argued that C-S fabrics develop simultaneously, but Lister and Snoke maintain that a well

Figure 3.7 - Diagrammatic sketch illustrating the modification of existing structures by increasing shear strain

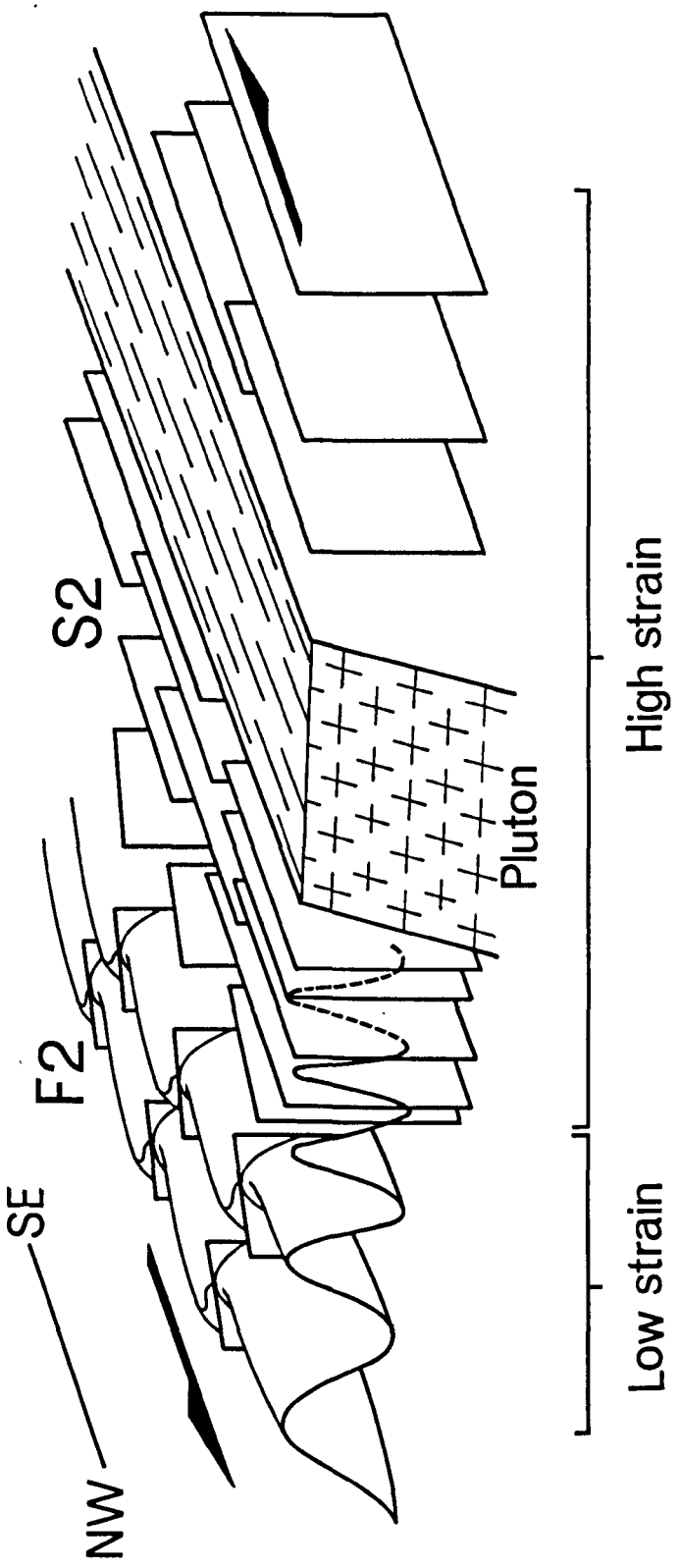

Plate 19 - Sinistral shear bands from sheared granite, at Vidoeiro summit

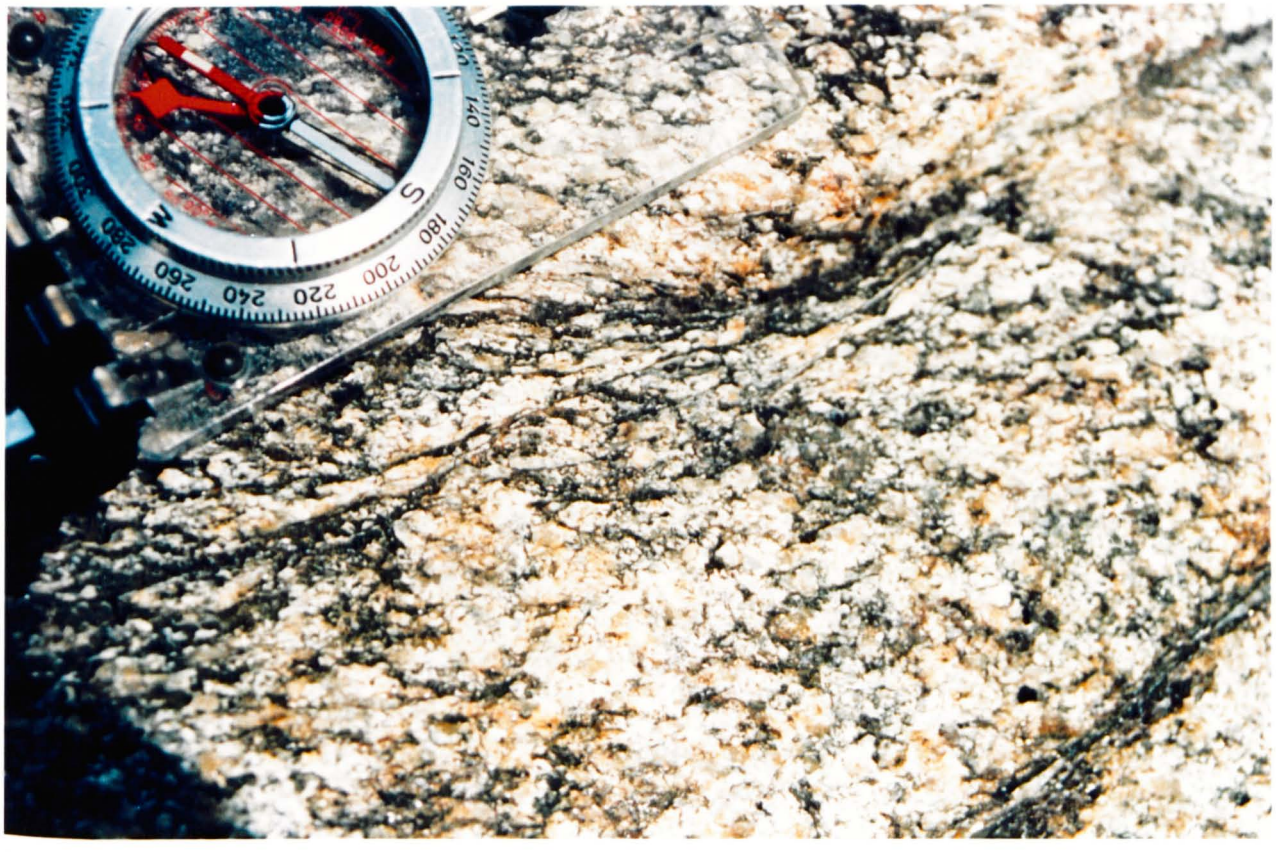

Plate 20 - Sinistral shear zone in main granite, 2 m south of S. Pedro Velho summit

Plates21 & 22 - Sinistral shear bands in the Beira Schists (Plate 21 - GR 6210 2585, Plate 22 - GR 6165 2580). In both photographs, the pen is parallel to S2 (S plane) and in Plate 21, the edge of the clinometer defines S2a (C plane). S2a in Plate 22 is more obvious

Figure 3.8 - Development of ductile shear bands - C-S fabric

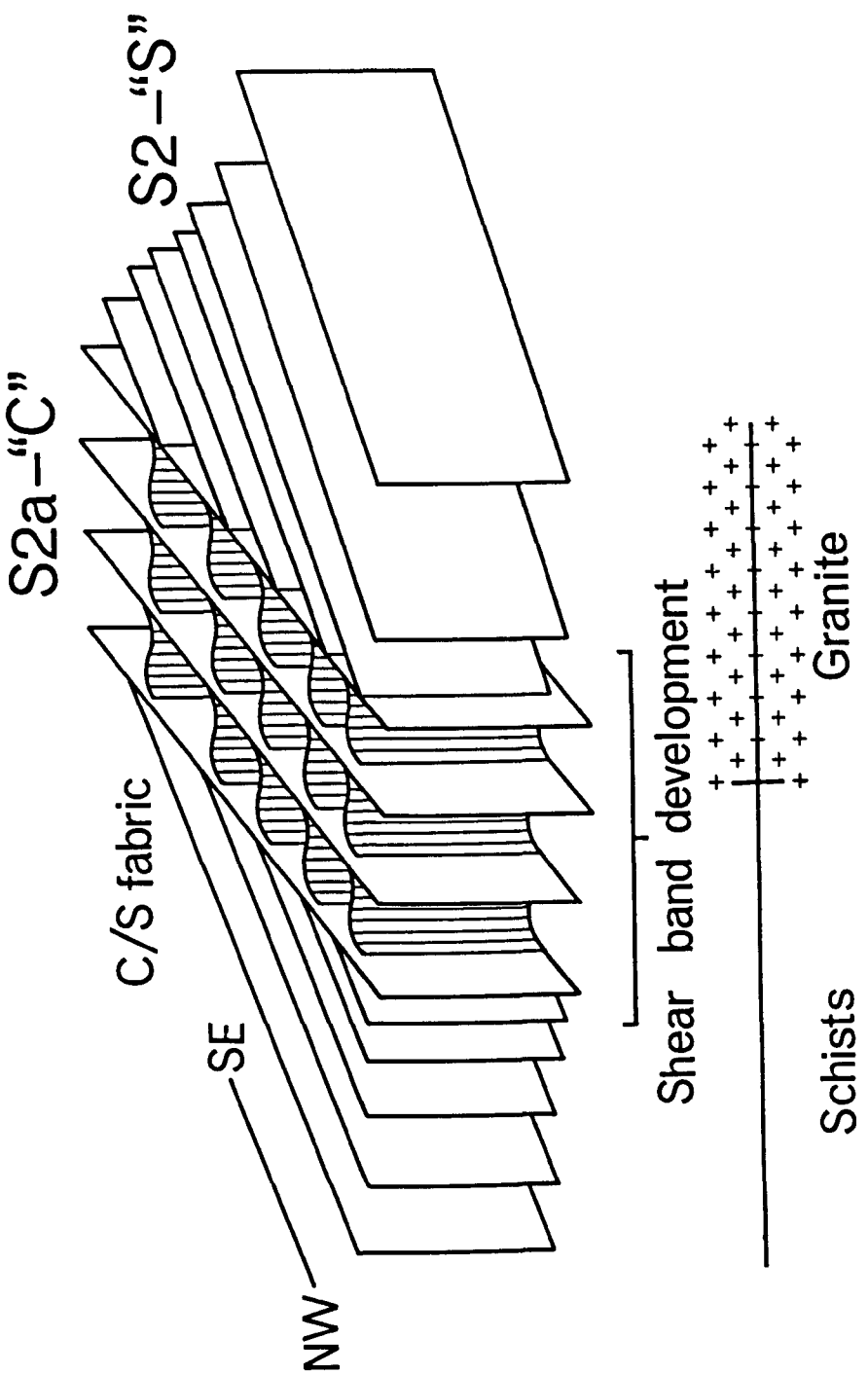

Figure 3.9 - Equal area projection of poles to S2a

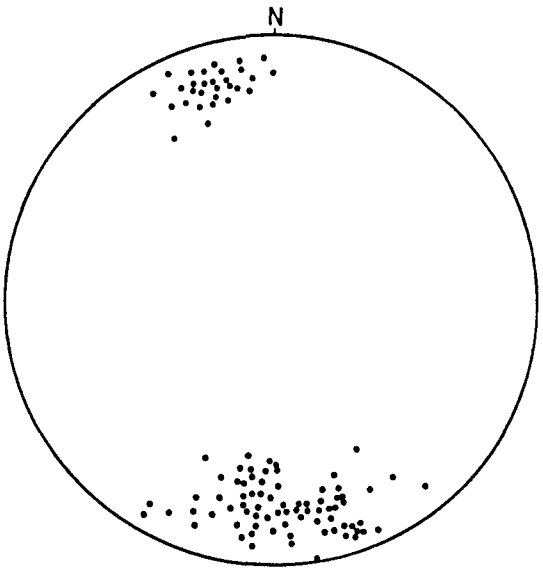

Figure 3.10 - Equal area projection of S2/S2a intersections

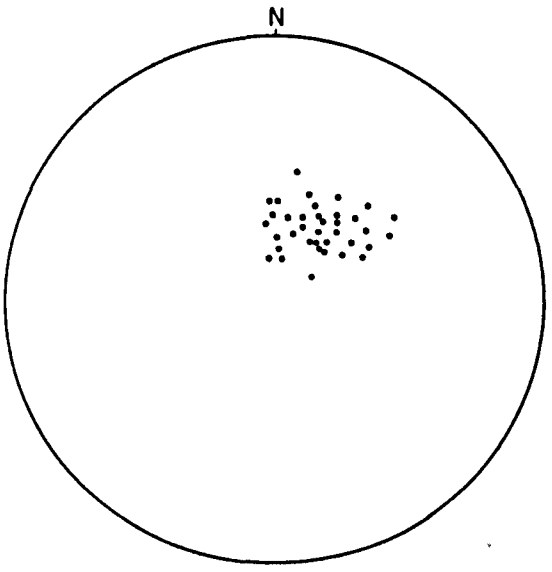

developed foliation can form first (S-surfaces) before localized yield and plastic deformation cause the formation of shear bands (C-surfaces). In the Serra da Freita, S2 corresponds to the S surfaces and S2a to the C surfaces.

During this phase of the evolution of the shear zone, sinistral transcurrent movements continued but in a more restricted zone adjacent to the northern limb of the granite.

3.3.3 - Late Structures

Tight folds recorded in the schists to the north and south of the granite have axial planar crenulation cleavages (S3) which clearly overprint S2. On the northern side of the granite S3 dips steeply NE or SE. South of the granite, between Monte Calve and Laceiras, a reverse crenulation is inclined to the NW (Figures 3.11 & 3.12). These structures are interpreted as a conjugate set of crenulations produced by late brittle movements, possibly the final movements in the shear zone (Figure 3.13).

Figure 3.11 - Equal area projection of F3 plunges

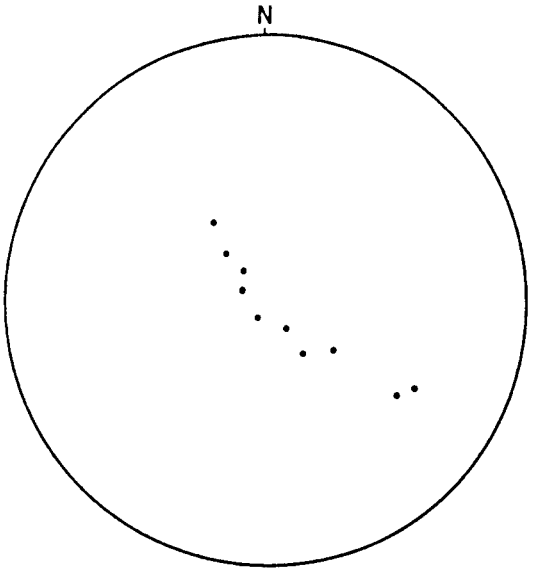

Figure 3.12 - Equal area projection of poles to S3

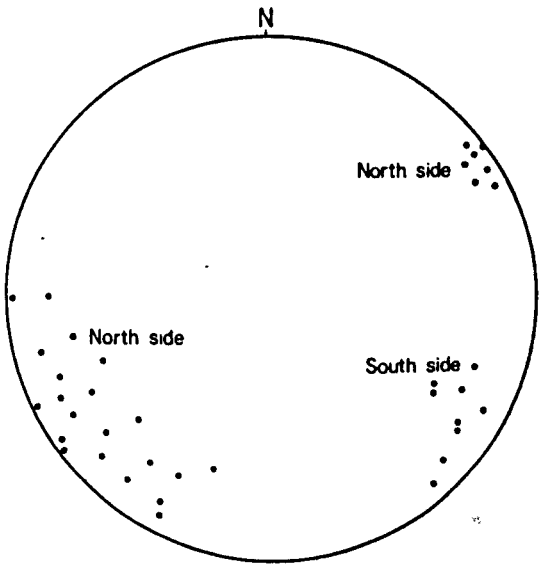

Figure 3.13 - Late brittle structures recorded as a conjugate set of crenulations north and south of the granite

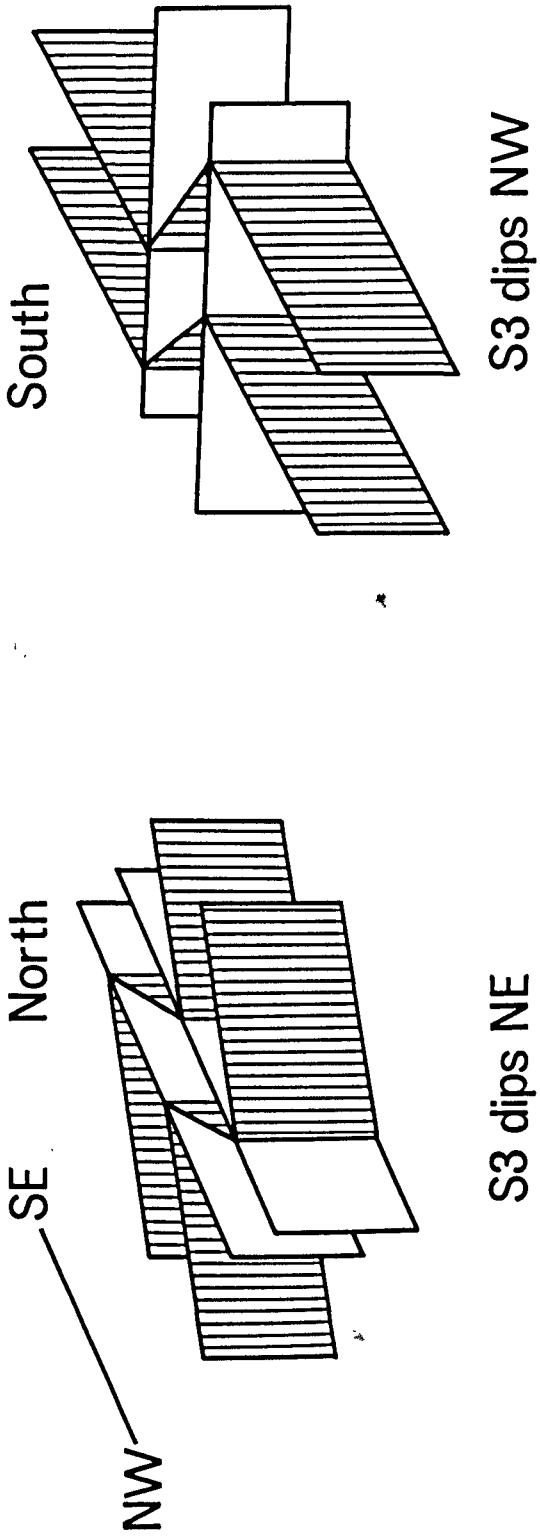

CHAPTER IV -- THE STRUCTURE AND EMPLACEMENT OF THE SERRA DA FREITA GRANITE

4.1 - Introduction

The cross-section on Sheet 13-D (Figure 2.3) Page 26 portrays the Serra da Freita granite as a steeply inclined sheet with the Mizarela and Junqueiro inliers as roof pendants; this interpretation suggests that the Manhouse inlier is in-situ country rock almost surrounded by the pluton with steep contacts. Detailed mapping shows that an alternative interpretation is required, and the emplacement model can be integrated within the framework of the deformation sequence associated with shear zone development outlined above.

4.2 - Pluton Structure

Measurements of the contacts between the granite and its envelope enable an overall picture of the pluton's geometry to be established. The outer contacts are relatively simple, and although some sheeting occurs parallel to the northern contact, they are in all cases sharp with no migmatites present (Plates 23 & 24). The strike is generally parallel to S2; i.e. 60°-$80^{\circ} \rightarrow 030^{\circ}$ in the north, the southern margin is steeper, usually sub-vertical to vertical and sheeting is very rare. The shape of the intrusion shows an apparent symmetry about a strike-parallel axis (Figure 3.1) extending from Albergaria das Cabras to beyond Malfeitoso. Such a line defines the maximum lateral extent of the Manhouse inlier and effectively divides the granite into its northern and southern limbs. Along this zone the granite overlies the Beira Schists, the inclination of the contact ranging from less than 10° to 70°. Immediately east of

Plate 23 - Looking W along the northern contact from GR 6370 2500 towards S. Pedro Velho

Plate 24 - Looking NW along the southern contact from GR 6218 2240

Albergaria das Cabras the contact is well exposed along a track and is almost horizontal. A sketch map of this locality is shown in Figure 4.1. In the schists beneath the granite, quartz veining is abundant and the gently NW plunging stretching lineation is locally very intense with mullions and quartz rods developed (Plates 25-32). In the valleys which converge on Gestoso on either side of Serlei the base of the granite follows the contours, implying a horizontal junction. The field evidence therefore points to a thin sheet with a much more complex geometry than was previously envisaged. Within this model, the northern limb of the granite comprises a steeply inclined sheet which becomes less steeply inclined southwards into the more diffuse southern limb, the granite of which shows complex sinuous contacts with the schists beneath (Figure 4.2). A model involving a root zone in the north where shearing was strongest and persisted longer than in the south, explains the regularity of shape of the northern limb, whilst the lobate nature of the southern limb and its apophyses can be readily explained as a cross-section through the base of an undulating but essentially flat-lying sheet. The latter was intruded into the region where shear strain was less intense.

4.3 - Tectonic Controls on Emplacement

The granite is inferred to have been intruded into a regime of nearly upright gently plunging folds within which a sinistral transpressive shear zone had developed. Any emplacement model envisaged must take account of these two tectonic controls.

There is considerable evidence for the influence of these early folds on the overall geometry of the granite. The shape of the Manhouse and

Figure 4.1 - Map of the Albergaria das Cabras Area

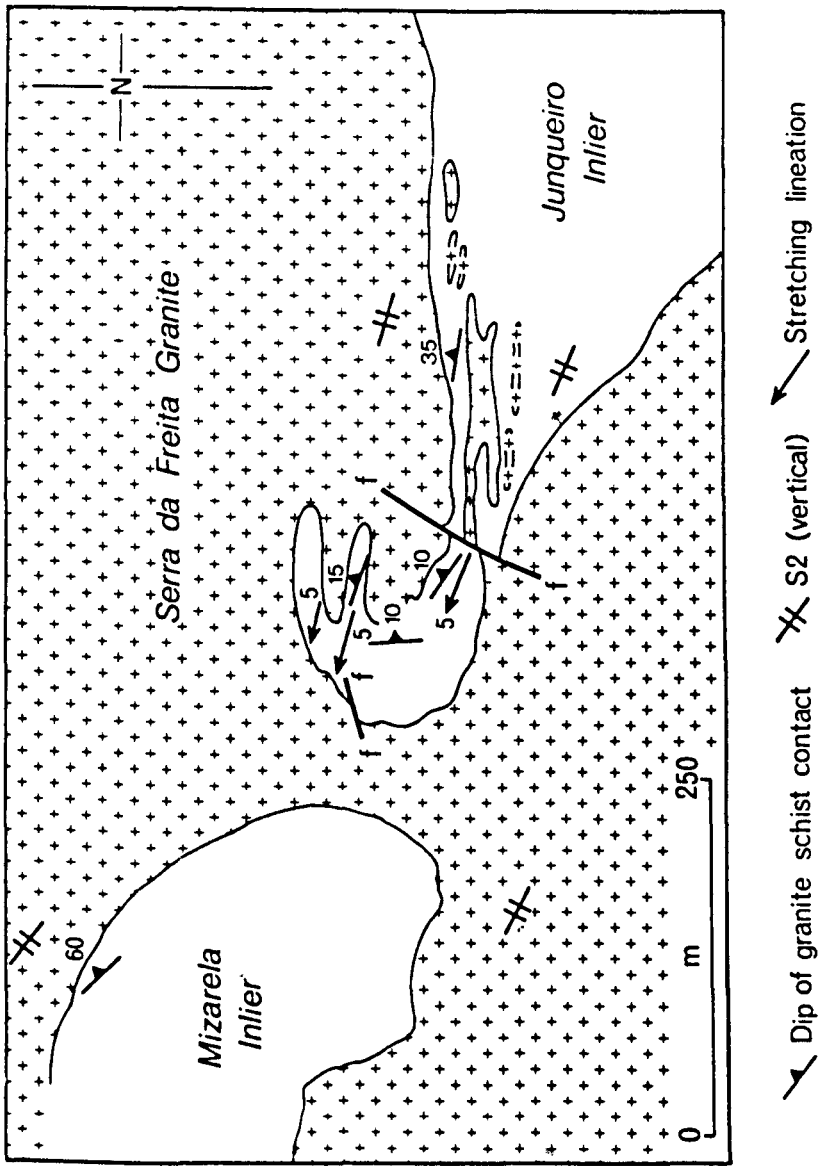

(Plates 25-32 - refer to Figure 4.1). Plate 25 - Looking NNE along the fault shown on the map (granite to the left of the photograph)

Plate 26 - Looking SSW along the fault (granite to the right of the photograph)

Plates 27 & 28 - Gently inclined (10^{o}) contact of granite overlying the schists at the localities shown on Figure 4.1

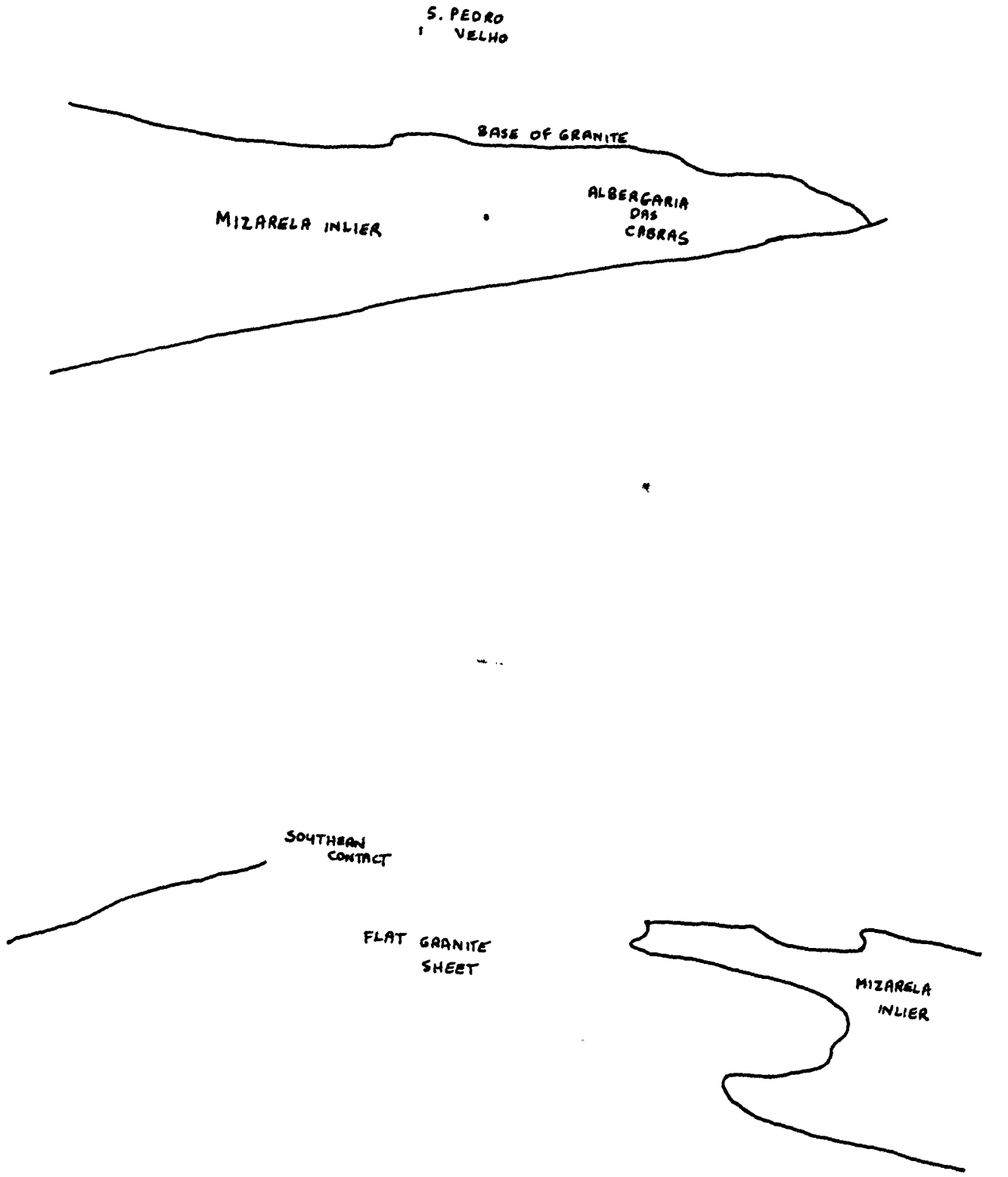
S. PEDRO
VELHO
BASE OF GRANITE
ALBERGARIA
DAS
CABRAS
MIZARELA INLIER
SOUTHERN
CONTACT
FLAT GRANITE
SHEET
MIZARELA
INLIER

Plates 29 & 30 - The Mizarela inlier viewed from GR 6140 2430. The inlier of schists is well defined by the green fields surrounding Albergaria das Cabras. The suggested lower contact of the granite sheet is outlined

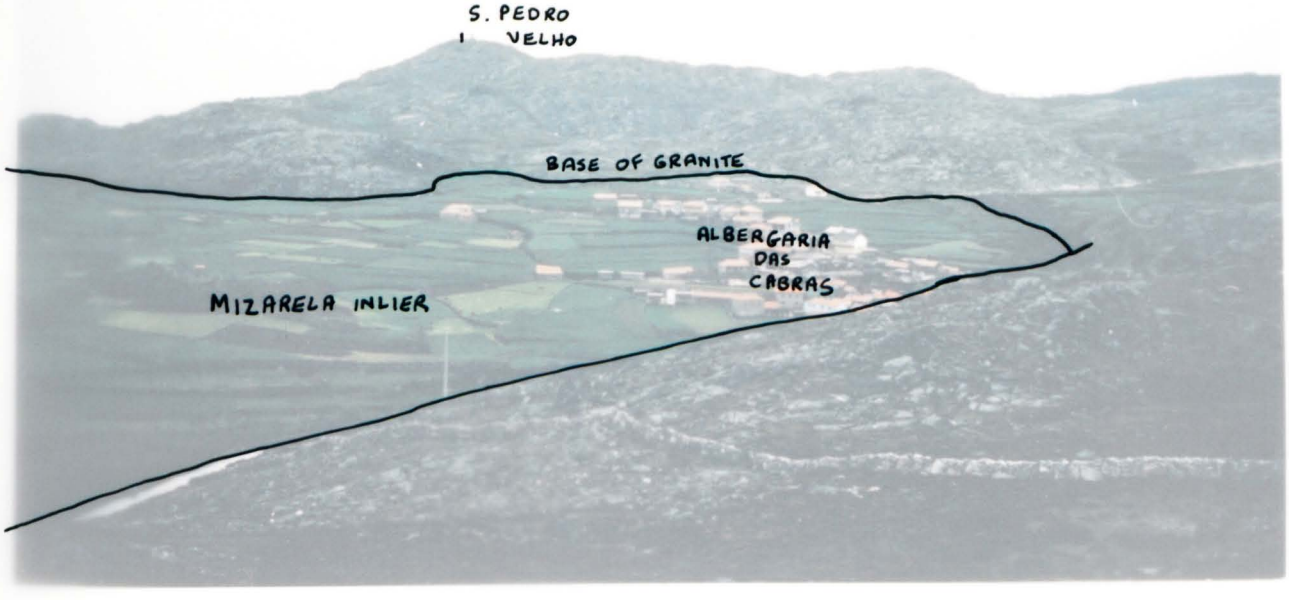

Plates 29 & 30 - The Mizarela inlier viewed from GR 6140 2430. The inlier of schists is well defined by the green fields surrounding Albergaria das Cabras. The suggested lower contact of the granite sheet is outlined

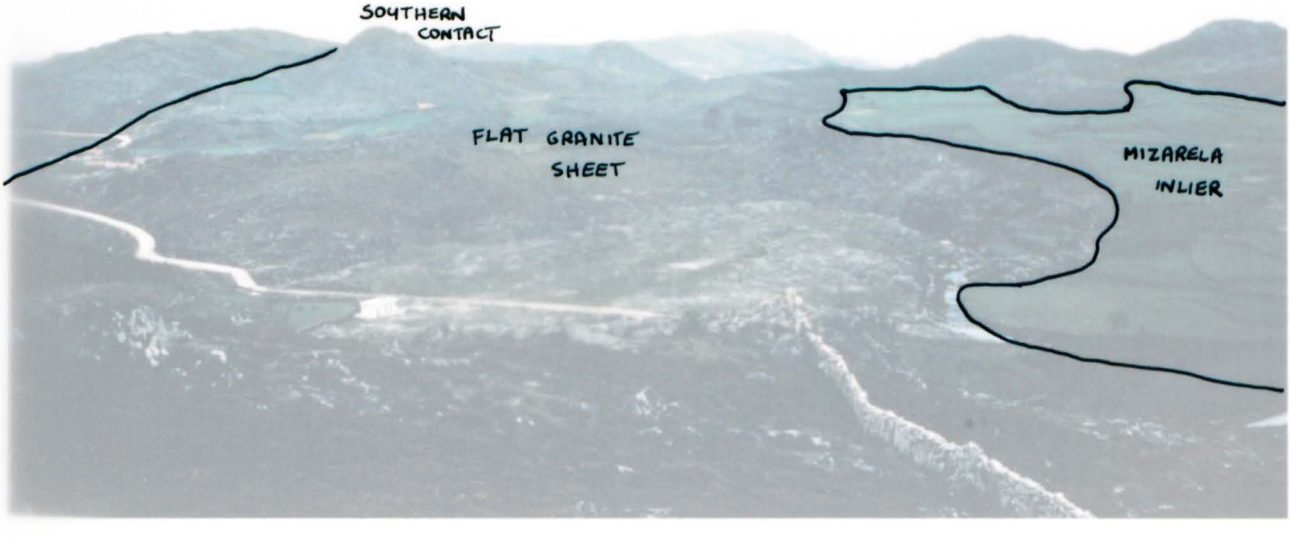

Plates 31 & 32 - Development of mullion structures plunging gently WNW as shown on Figure 4.1

Figure 4.2 - Diagrammatic sketch of the emplacement model envisaged for the Serra da Freita pluton within the shear zone, and its relationships with structures discussed in the text

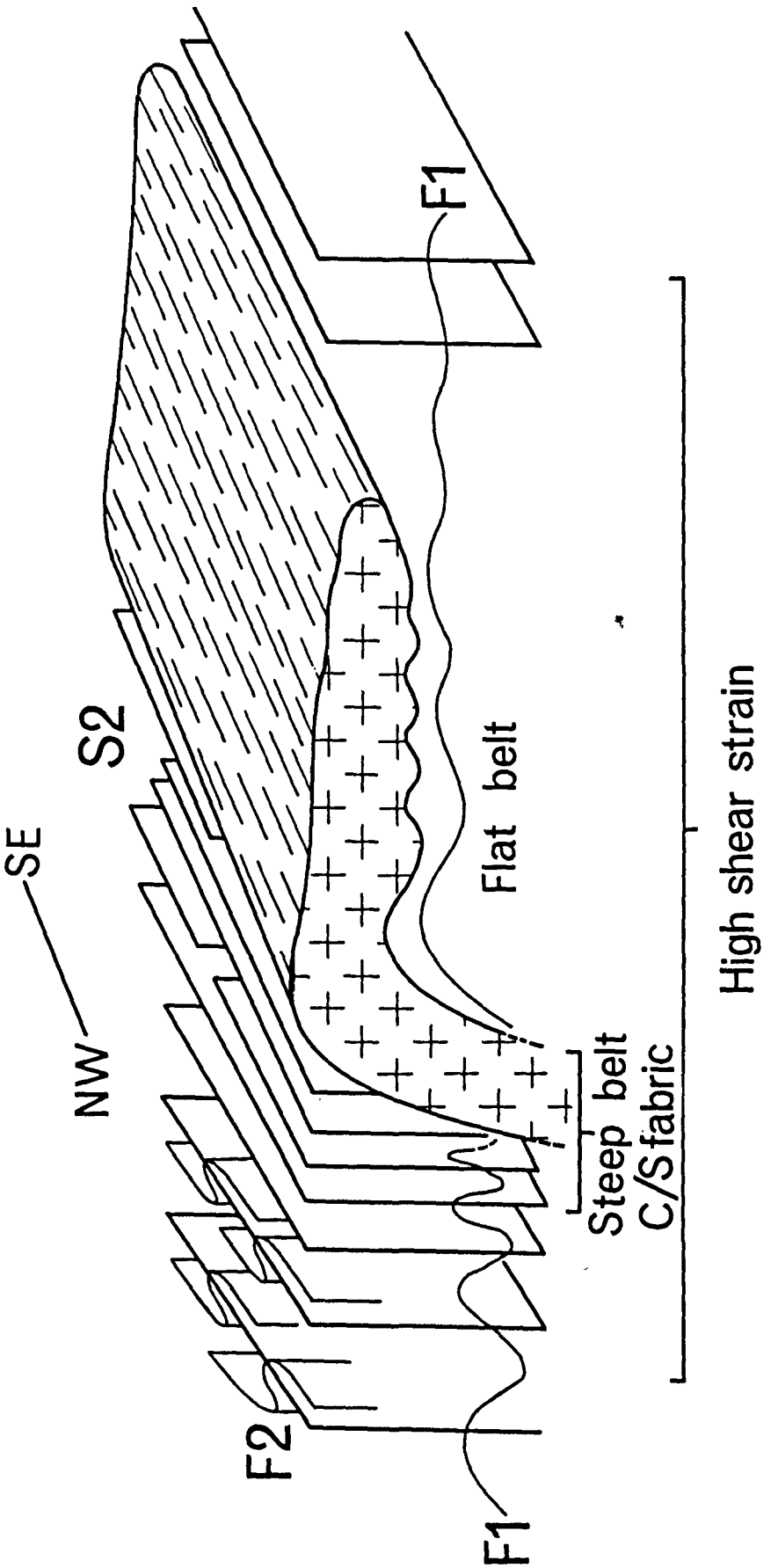

Junqueira inliers is interpreted as an interference pattern between the base of the granite sheet and gently plunging folds. It is difficult to envisage the intrusion as concordant, however the presence of this regional anisotropy is likely to have some effect on the path taken by an intrusion of a viscous melt. The axial zone of the Manhouse inlier, about which the pluton shows apparent symmetry, is a likely major F1 hinge zone.

The variation in shear strain gradient was an important constraint in the final geometrical orientation of the pluton. An initially steeply inclined sheet of magma was emplaced into the zone of highest strain, forming the steep sheet of the northern limb. Further intrusion was inclined across the shear zone and the magma cut south into an area of progressively lower shear strain, giving rise to the flattish sheet of the southern limb. The main magmatic fabric (S2) present in the southern limb was produced by deformation of a viscous crystal mush during emplacement, and can be envisaged as a strain-induced alignment of phyllosilicates, i.e. a flow fabric. As crystallization continued, further transpressive movement intensified the fabric, tightened F1 hinges and accentuated folding in the flat sheet. However the main later shear movements were largely confined to a more restricted zone which involved the steep northern limb of the granite, leading to the development of a C-S fabric of ductile shear bands, reinforcing the steep nature of this root zone. The southern limb shows little evidence of such an intense shear history; although the schists around it still show a penetrative S2, it is more variable in orientation and less steeply inclined (Figure 4.3). Reorientation of S2 has taken place around the Castanheira granite which, although it crops out 600 m from the main pluton, is interpreted as part of the volatile

Figure 4.3 - Variations in strain as recorded by S2 across the Serra da Freita showing the effects of ballooning strain imposed by the Castanheira diapir

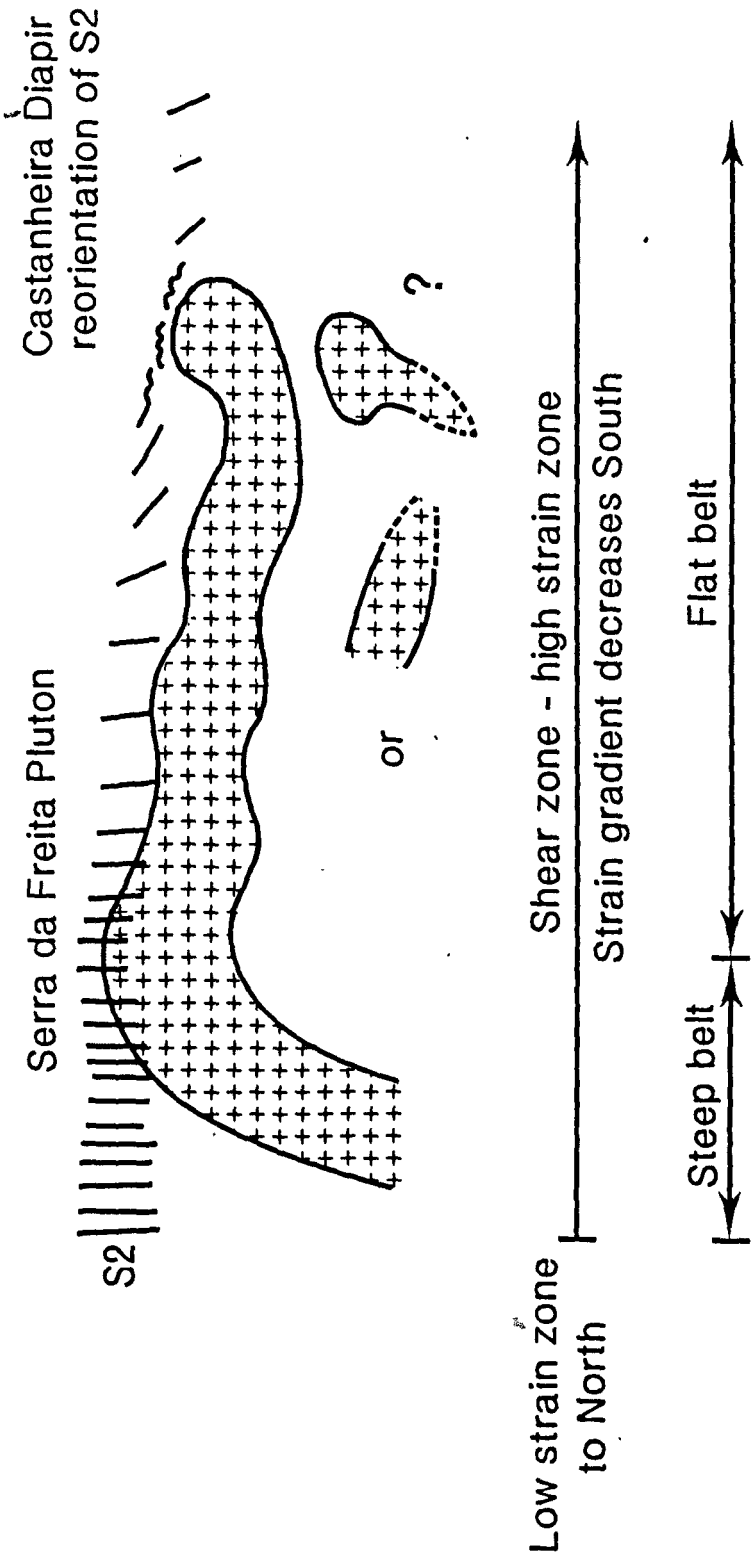

Plates 33 & 34 - Gently SE-plunging folds above the Castanheira diapir

rich roof zone which has risen as a small diapir and ballooned upwards towards the distal end of the flat lying southern limb. Ballooning strains have modified synchronous shear zone strains to produce a composite S2 fabric which is flat, but which still retains the shear zone shear sense, i.e. the stretching lineation which was approximately NW-SE in the main shear zone is now approximately N-S, shown by the X axes of the biotite nodules which characterize the Castanheira granite. This S2 fabric is itself folded at a late stage forming folds which plunge gently NW and SE (Figure 4.3, Plate 33 & 34).

4.4 - Summary

(1) The granite intruded steeply into the shear zone which has a strain gradient decreasing southwards.

(2) Further intrusion was into the area of lower strain. A combination of gravity and early F1 geometry produced a flattish irregular sheet facing south.

(3) Shearing continued throughout, imparting a magmatic flow fabric, preserved in the southern limb where shearing was less intense.

(4) Prolonged deformation continued in the northern area, ultimately forming a C/S fabric in the steep northern limb of the granite and in the schists beyond.

(5) The volatile rich roof of the sheet in the lower strain area to the south locally mobilized and ballooned upwards as the Castanheira diapir.

This sequence enables a close correlation between the regional deformation associated with the development of the Serra da Freita shear zone and the emplacement model for the Serra da Freita granite. Further modifications will be introduced in subsequent sections when variations of granite type within the pluton are discussed.

CHAPTER V -- METAMORPHISM

5.1 - Background

Within the Aveiro-Viseu region several types of metamorphism have been described.

(i) Regional chlorite grade metamorphism produced sericite and chlorite phyllites related to the first Hercynian phase (Schermerhorn, 1956; Oen, 1970).

(ii) The Porto-Viseu metamorphic belt of so-called "plutonometamorphism", (Oen, 1970), gave rise to the chlorite, biotite, andalusite-staurolite, sillimanite zones in the Beira Schists of the Junqueira and S.Pedro do Sul belts (Figure 3.1 & 5.1). Oen suggested that the development of such zones was followed by the emplacement of the Older granites with which they are spatially associated. Such belts, well documented in Iberia, were described as representing a lower pressure facies of the non-almandinous Abukuma type of regional metamorphism in which kyanite and garnet were lacking.

(iii) The Porto - Albegaria-a-Velha belt runs SSE through Oliviera de Azemeis to Albergaria-a-Velha (Figure 3.1 & 5.1) and is characterized by kyanite, staurolite, almandine, sillimanite schists, representing a higher pressure metamorphism of Barrovian type. Where the belts meet near Oliviera de Azemeis, kyanite garnet staurolite schists occasionally contain andalusite and sillimanite, and it was suggested that such rocks were polymetamorphic with a lower pressure overprint on the Barrovian assemblages.

Atherton et al. (1974) reported kyanite and garnet from the Porto-Viseu

Figure 5.1 - Metamorphic belts of north central Portugal

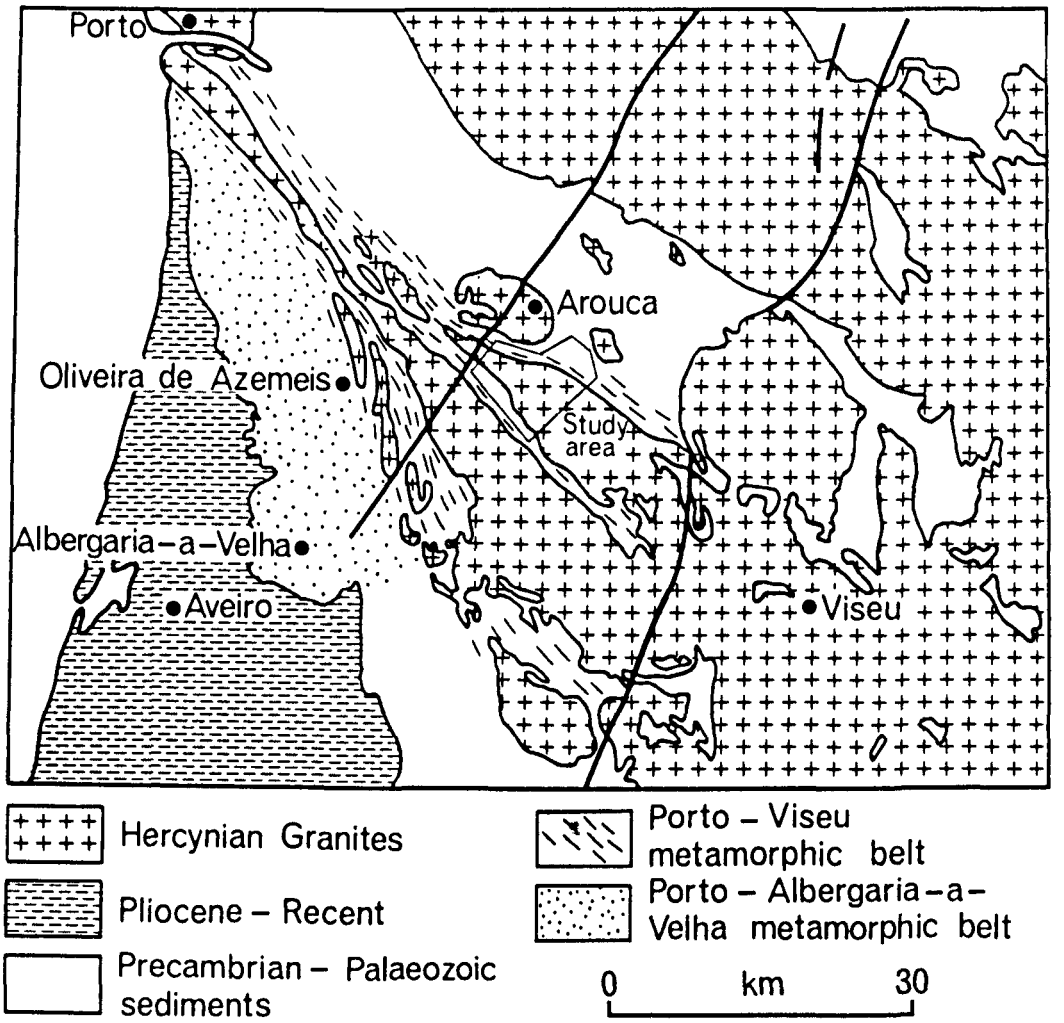

belt, thus throwing into question the low pressure nature of the metamorphism, and also questioned the need for polymetamorphism, maintaining that time relationships could well be similar, e.g. at Cavernais in the supposedly low pressure belt staurolite and kyanite are followed by andalusite and sillimanite in the same metamorphism.

Their second point is not relevant to this study, however the presence of garnet and kyanite is confirmed here in the Serra da Freita region, and the author is in agreement with Atherton et al. (1974) who stated that the low pressure metamorphism as defined by the absence of kyanite is no longer tenable.

(iv) Contact metamorphism associated with the emplacement of the younger granites produces cordierite-bearing hornfelses which overprint all the earlier assemblages. The recognition here of sillimanite in the aureole of the Arouca granite leads to a major modification of the isograds in the region.

5.2 - Metamorphism in the Serra da Freita

The Porto-Viseu metamorphic zones of the S. Pedro do Sul belt must be considered in conjunction with the neighbouring Junqueira and Central belts.

Several previous attempts have been made to understand the complex relations between regional metamorphism, contact metamorphism and different types of plutonism. Oen (1970) used the work of Kluiving (unpubl.), Schermerhorn (1956), and Sluijk (1963) to show plutonometamorphic zones of biotite, andalusite-staurolite, and sillimanite schists (Figure 5.2). Sluijk (1963) also claimed the existence

of an outer chlorite zone in the Regoufe region.

Oen's map (Figure 5.2) shows the following:

(i) a narrow biotite zone,

(ii) the entire Serra da Freita granite falls within the broad andalusite-staurolite zone,

(iii) other granites transect the sillimanite isograd north and west of the Serra da Freita granite,

(iv) cordierite hornfels produced by contact metamorphism occurs around the Arouca granite.

A possible lapse in time between the development of metamorphic zones and plutonic emplacement was the interpretation for the discordant nature between plutonic contacts and sillimanite isograds.

These early studies demonstrated the existence and location of the regional metamorphic zones and the oblique nature of the isograds relative to the granites.

Sheet 13-D of the Portuguese survey shows both regional and contact metamorphic isograds, unfortunately these data are not recorded on Sheet 13-B which was completed earlier (Figure 5.3). On Sheet 13-D, the main re-interpretation is the more widespread occurrence of sillimanite. The country rocks at the NW end of the Serra da Freita granite as well as the inliers within it were all mapped as being of sillimanite grade. The attitude of the sillimanite isograd however appears strangely angular in its relation to both the Arouca and the Serra da Freita granites. It appears that the main problem is due to the sillimanite-bearing rocks within the Arouca granite being mapped as continuous with the sillimanite schists of the regional belt. The nature of the contact metamorphism of

Figure 5.2 - Isograds (Oen, 1970) using data from Kluiving (unpubl.), Schermerhorn (1956), and Sluijk (1963)

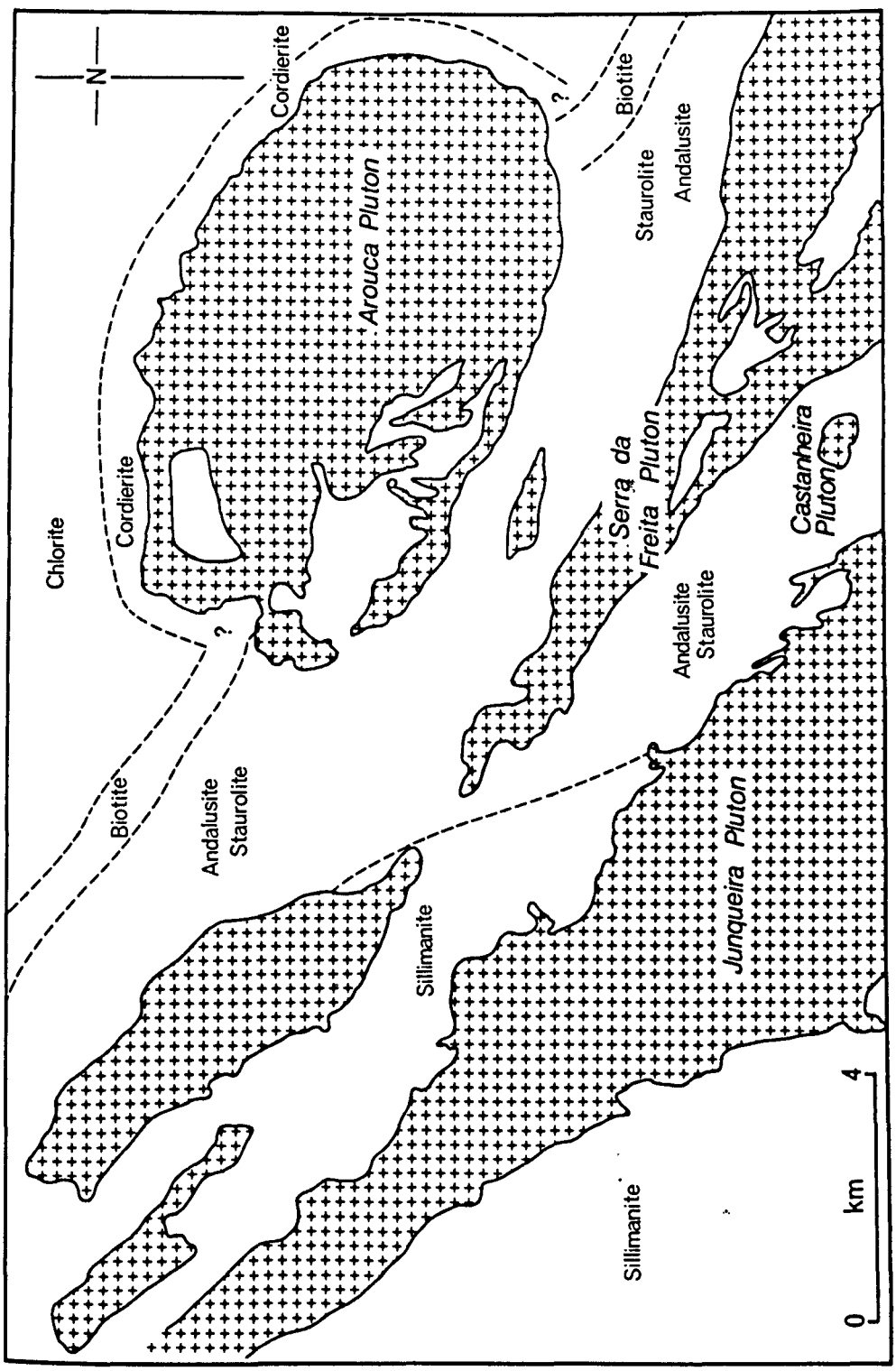

Figure 5.3 - Isograds as shown on Sheets 13-B and 13-D of the Geological Survey of Portugal

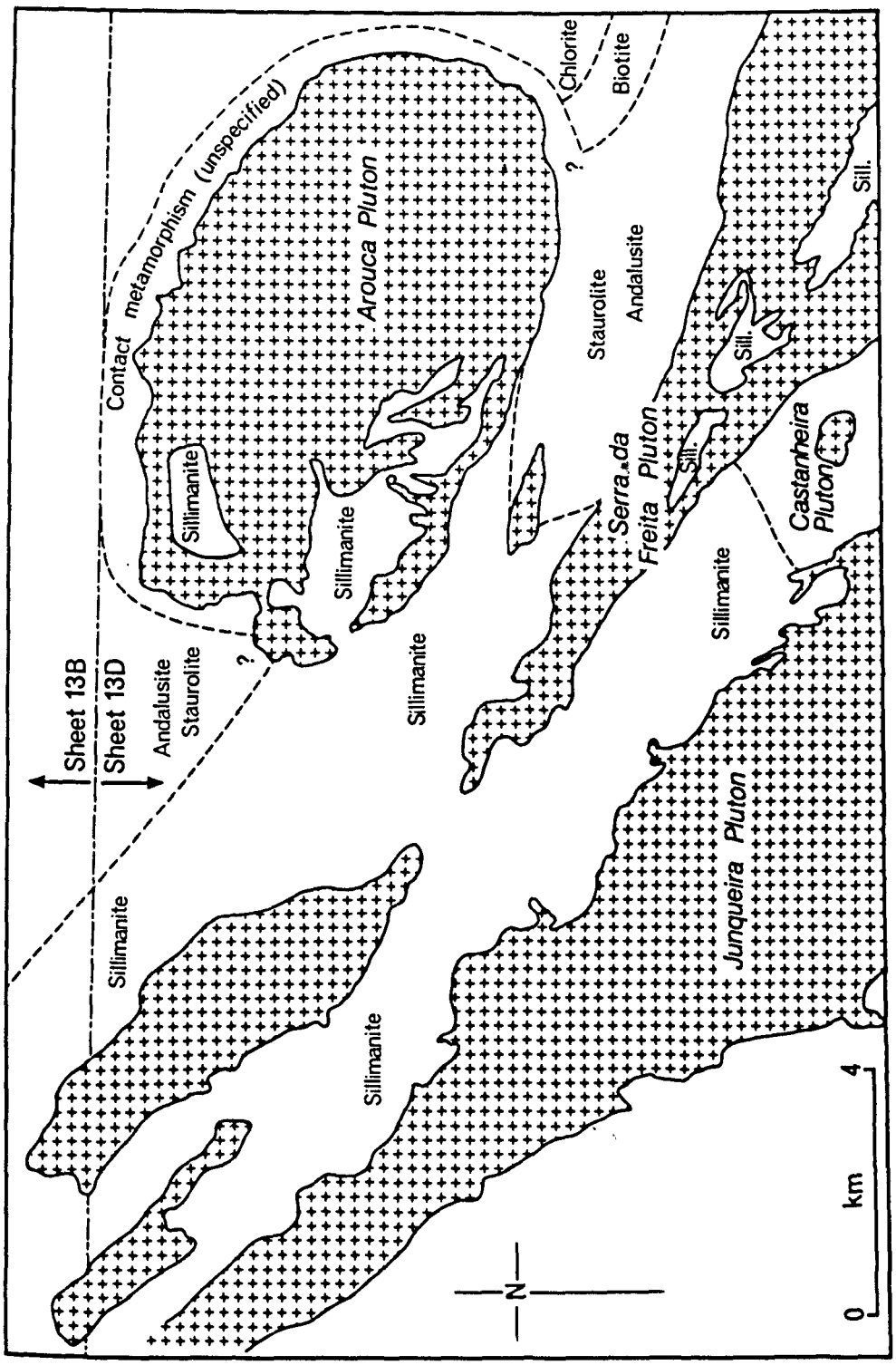

the Arouca granite was not stated, and both its characteristic paragenesis and its relations with the regional metamorphism are unclear.

The present study suggests an alternative interpretation which resolves the above problem and gives new information about the regional sillimanite belt.

5.3 - Field Aspects of Metamorphism

Samples of metasediments were collected on traverses on either side of the Serra da Freita granite and from inliers within it. In addition, several other samples were obtained from localities to the NW and NE outside the main study area (Figure 5.4).

A western and eastern traverse across strike provided 90 whole rock samples for geochemical and petrographic work. The eastern traverse sampled schists on either side of the granite where it reaches its greatest width in the Serlei-Vidoeiro region; it includes the Vale de Cambra road section in the SW and the Rio de Frades ridge to the NE. The latter was chosen as the survey map indicated that this would provide samples of regional low grade metamorphism lying between the contact aureoles of the Arouca and the Regoufe granites. This well exposed ridge also proved most useful during the regional structural analysis. The aims of the western traverse were to investigate the nature of the sillimanite belt and any possible overprint by the aureole of the Arouca granite on the regional belt. Unfortunately steep slopes and lack of exposure limited work SW of the granite at Mizarela, however useful samples were obtained on the Arouca road section running NE from beneath S.Pedro Velho to the northern edge of the plateau.

Figure 5.4 - Suggested isograds based on field and petrographic data presented here. Sample localities outside the main study area are shown, sampling traverses on the Serra da Freita are marked, sample names are shown on the enclosed main map

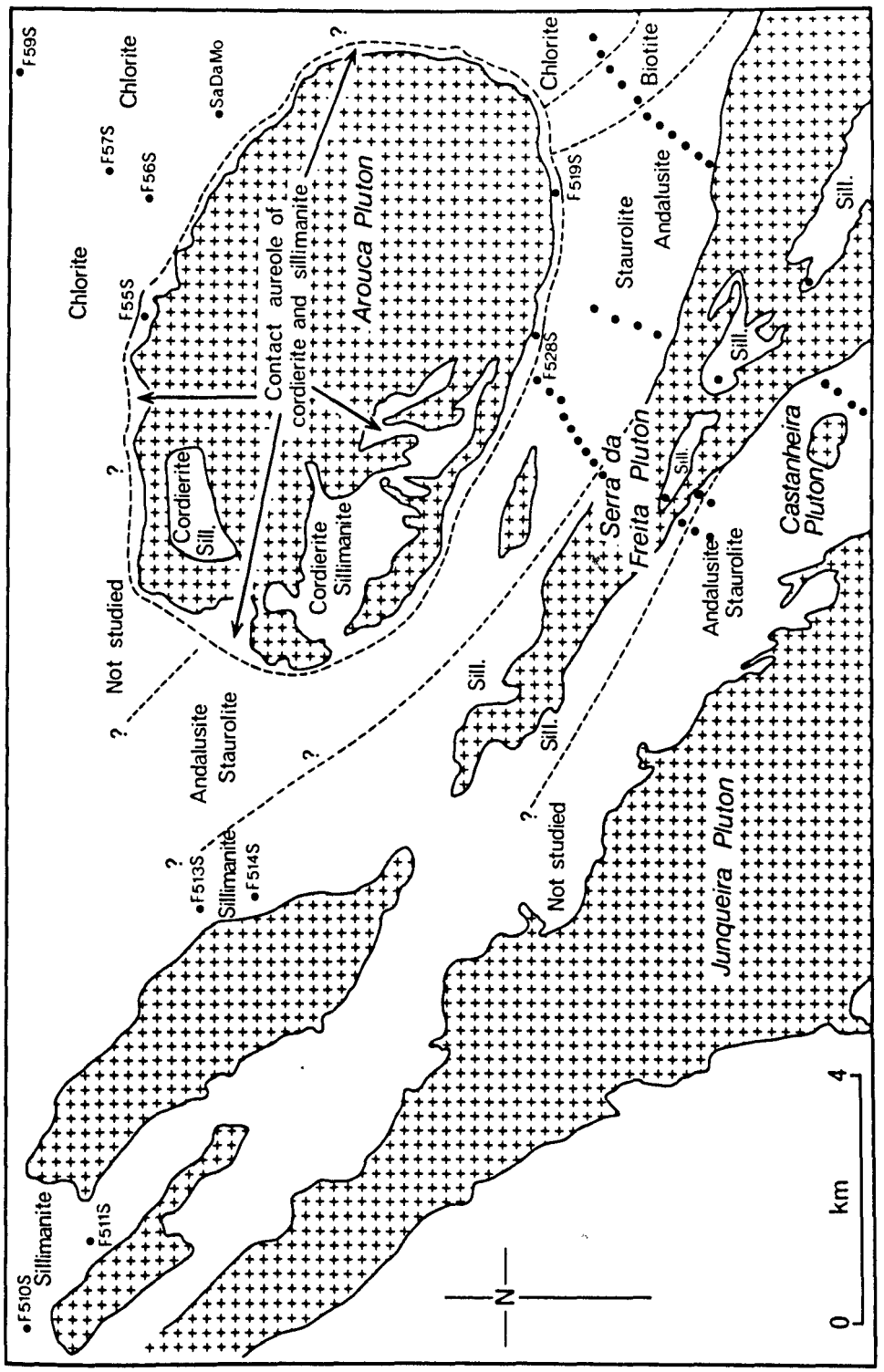

5.3.1 - Chlorite Zone

This is encountered at the north-eastern edge of the Rio de Frades ridge (Plates 35 & 36). At this grade of metamorphism, many of the original sedimentary features are still visible; the lithologies are greywackes with sandstone units up to 0.5 m thick interbedded with shales (Plates 37 & 38). F459S (Plate 39) and F463S show a low grade paragenesis of sericite and chlorite which elsewhere is believed to be related to the first Hercynian phase. Sluijk (1963) recognized a chlorite plutonometamorphic zone in the Regoufe area further east. There is no evidence of this in the Rio de Frades section, the appearance of small biotite porphyroblasts in F465S are the first indicators of a change from the widespread chlorite grade rocks to the north. Samples F56S, F57S, Sa Da Mo (Plate 40), and F59S collected on the Alveringa road NE of Arouca are of similar grade to F459S and F463S.

5.3.2 - Biotite Zone

Small altered biotite porphyroblasts approx. 0.5 mm in size in F465S indicate the crossing of the biotite isograd. Biotite is present in subsequent samples although it is often partially or completely altered to chlorite. On the Rio de Frades section, the biotite zone is approximately 1 km wide before porphyroblasts of andalusite and staurolite mark the onset of medium grade metamorphism.

5.3.3 - Andalusite/Staurolite Zone

This is the widest plutonometamorphic zone seen north and south of the Serra da Freita granite over the entire study area except west of

Plate 35 - The narrowest section of the Rio de Frades ridge, looking NE from GR 6650 2560

Plate 36 - The end of the Rio de Frades ridge (GR 6740 2630) looking SW towards the Serra da Freita

Plates 37 & 38 - Steeply dipping chlorite grade metasediments on the Rio de Frades ridge

Plate 39 - Chlorite, sericite grade schist with zonal S2 crenulation cleavage (F459S, GR 6744 2628, XPL, x 62.5). This paragenesis is believed to be related to the first Hercynian deformation phase, and therefore predates the "plutonometamorphism"

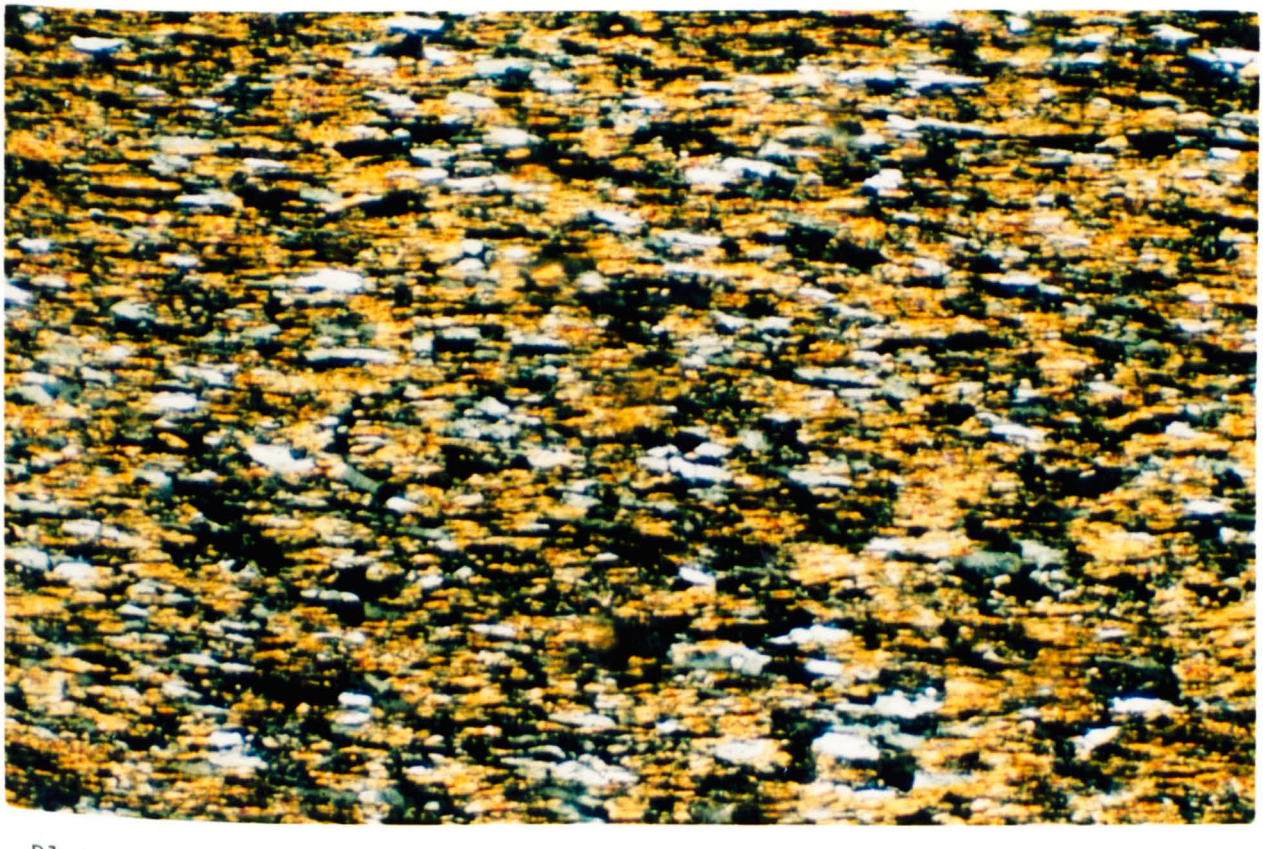

Plate 40 - A similar paragenesis from a sample collected on the summit of Senhora da Mo approx. 5 km N of F459S suggests that there is no chlorite "plutonometamorphic" zone (Sa Da Mo, GR 6465 3150, XPL, x 125)

Albergaria das Cabras where the sillimanite isograd is crossed.

Original sandstones and shales have become psammites and pelitic schists. Due to this varied protolith, the nature of the original sediment is the dominant control on the texture and paragenesis of any particular sample from this zone. Two main lithologies dominate: (i) psammitic layers in which thin micaceous stringers define the main S2 fabric (Plate 41); these often contain small biotite, andalusite and staurolite porphyroblasts; (ii) pelitic units in which phyllosilicates occupy >50% of the rock with quartz being a subordinate constituent. The main S2 fabric is stronger and porphyroblasts are generally syn- to late syn-tectonic. In the field, outcrops in this zone show abundant quartz veining and these often take the form of tension gashes and boudins giving evidence for sinistral shear during D2.

The general paragenesis of schists in this zone is:

quartz + muscovite + biotite + chlorite + andalusite + staurolite + plagioclase.

Tourmaline and ores are almost ubiquitous accessories, the latter strongly aligned along S2 (Plate 42). The groundmass is essentially of quartz, plagioclase and phyllosilicates, the relative proportions reflecting either the quartzitic or pelitic nature of the sediment. Muscovite is the dominant mica present, always exceeding chlorite and biotite. Biotite is usually, but not always, parallel to the main fabric and rotated syn-tectonic porphyroblasts up to 4 mm long which have survived into the andalusite/staurolite zone are also observed (Plate 43 & 44). Both types show partial replacement by post-tectonic chlorite, although fresh biotite is not uncommon. In samples where alteration is

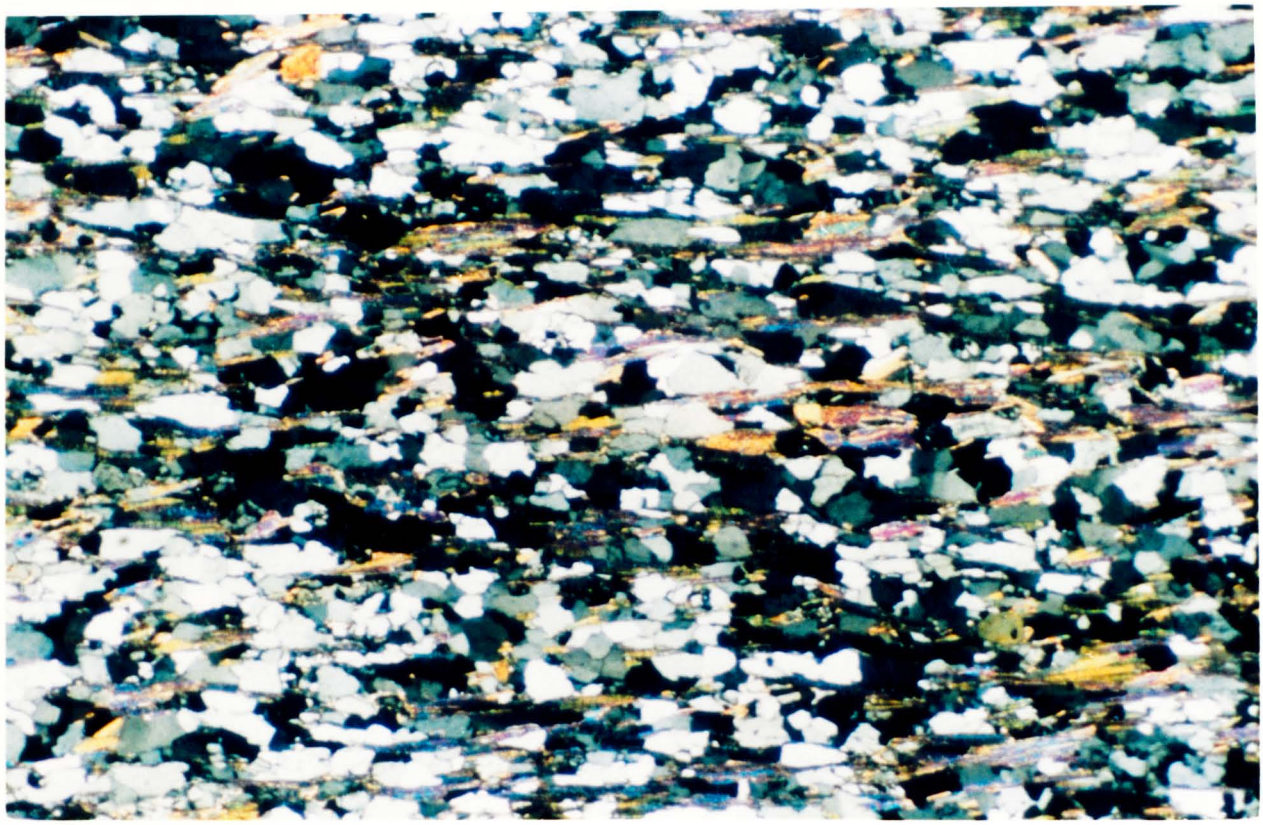

Plate 41 - Psammitic unit of the Beira Schists, S2 is defined by thin micaceous layers (F476BS, GR 6580 2447, XPL, x 31.25)

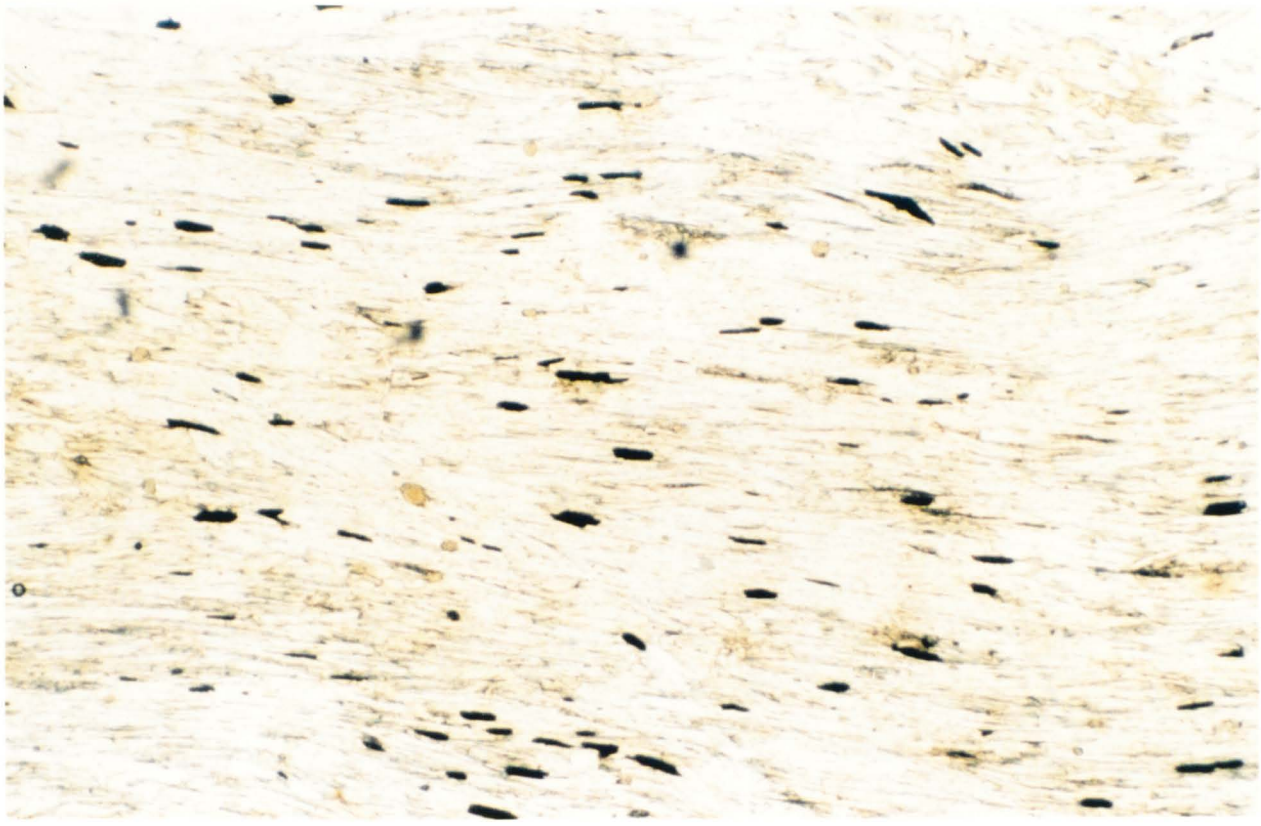

Plate 42 - Strong alignment of opaque ore minerals along S2 (F327S, GR 6188 2190, PPL, x 62.5)

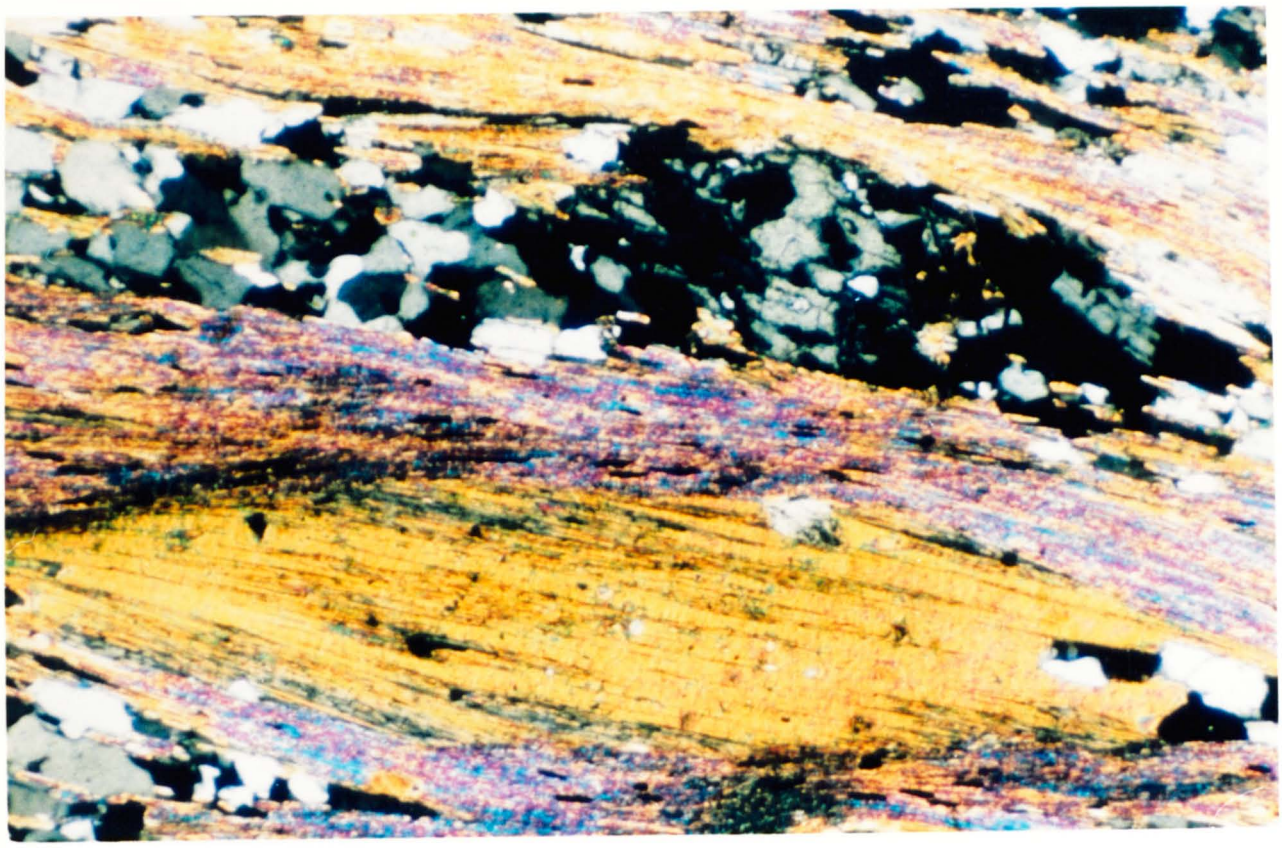

Plates 43 & 44 - Rotated biotite porphyroblasts (mica "fish") giving sinistral sense of shear (Plate 43 - F4113S, GR 6150 2315, XPL, x 62.5; Plate 44 - F46S, GR 5980 2440, XPL, x 31.25)

extensive, the main fabric is almost totally chlorite and muscovite.

Not every sample contains andalusite and staurolite, but one of these minerals is present in every section examined; indeed usually both are present although the relative proportions of each is again a function of the original nature of the sediment. The occurrence of andalusite is very compositionally dependent. Often in a single slide andalusite rich layers (6-7 mm wide) indicate original Al-rich units, showing that locally S2 is parallel to S0 (Plate 45). Layers rich in andalusite porphyroblasts of 3 cm diameter alternate with quartz-rich andalusite-poor lithologies clearly seen in Plate 46. In many samples, andalusite is partially or completely replaced and pseudomorphed by muscovite which grows in a random post-tectonic mass of interlocking crystals. Deformation can be seen on a thin section scale where andalusite has undergone extension and muscovite has grown between the boudins (Plates 47 & 48).

Staurolite grows either as true porphyroblasts (Plates 49 & 50) or enclosed in andalusite (Plate 51); this latter feature suggests that it may have nucleated after the andalusite had formed. Staurolite growth is less compositionally dependent than andalusite; porphyroblasts, which in most cases are 3-5 mm in diameter, are generally evenly distributed throughout the slide (Plate 52). However staurolite-rich bands do occur and in suitable lithologies porphyroblasts can reach lengths of 3-5 cm (Plate 53 & 54). One such unit is so distinctive that it can be used to map an F1 fold trace across the Detrelo de Malhada (Figure 3.3).

Twinning of staurolite is fairly common and the larger crystals are riddled with quartz inclusions (Plate 55 & 56). Replacement is not as pervasive as displayed by andalusite, however late muscovite commonly

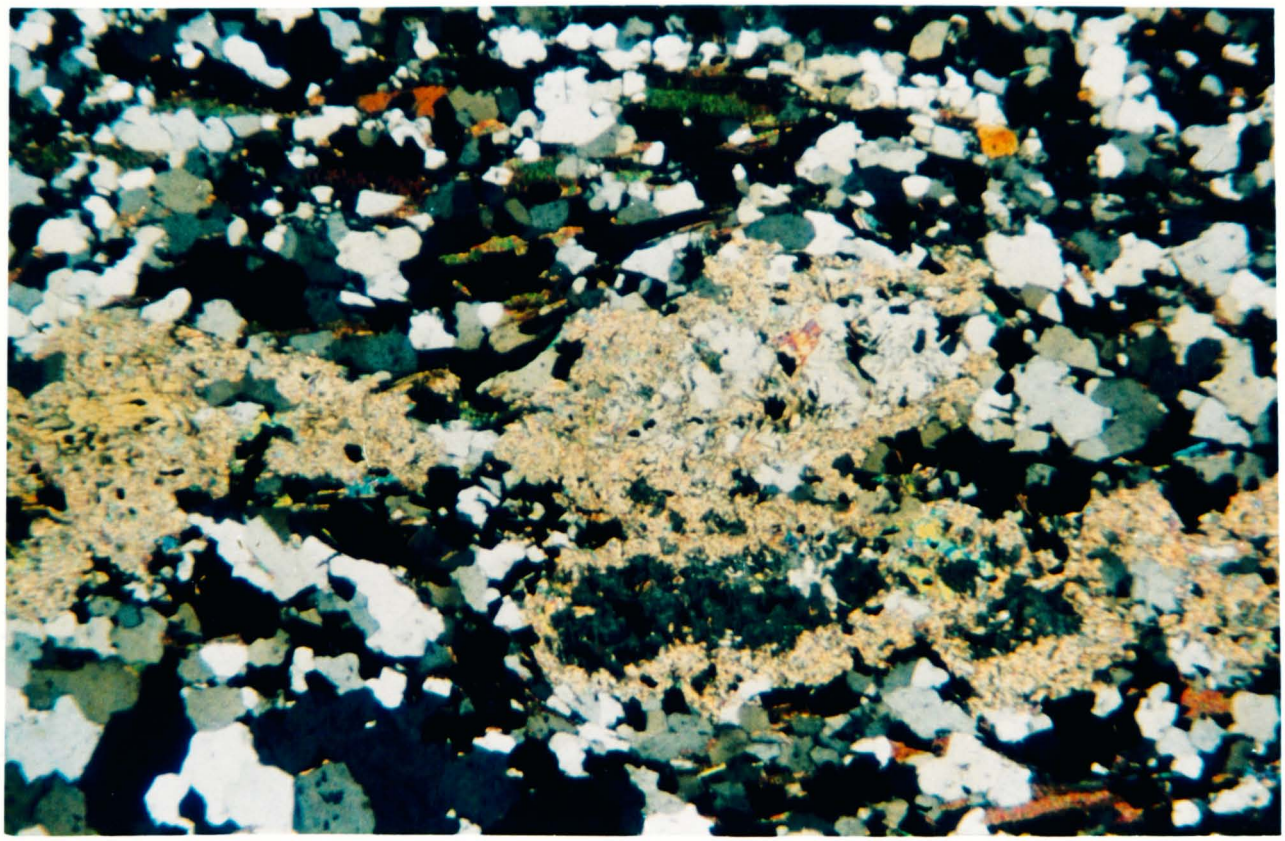

Plate 45 - Andalusite-rich layer showing extensive alteration to fine-grained muscovite (F413S, GR 5949 2476, XPL, x 31.25)

Plate 46 - Layers rich in large andalusite porphyroblasts alternate with psammitic horizons (GR 6445 2610, Coto de Boi ridge)

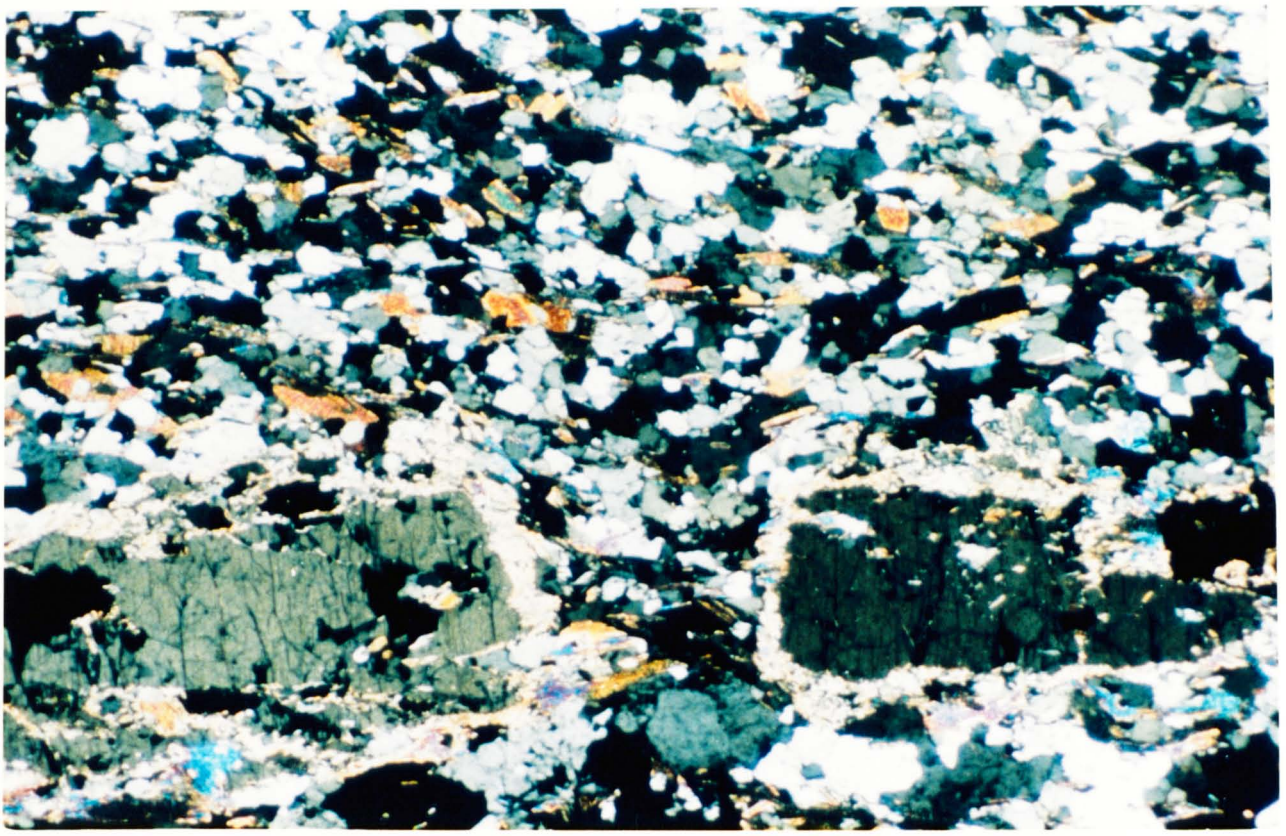

Plate 47 - Boudinage of andalusite crystals (F339S, GR 6210 2545, XPL, x 31.25)

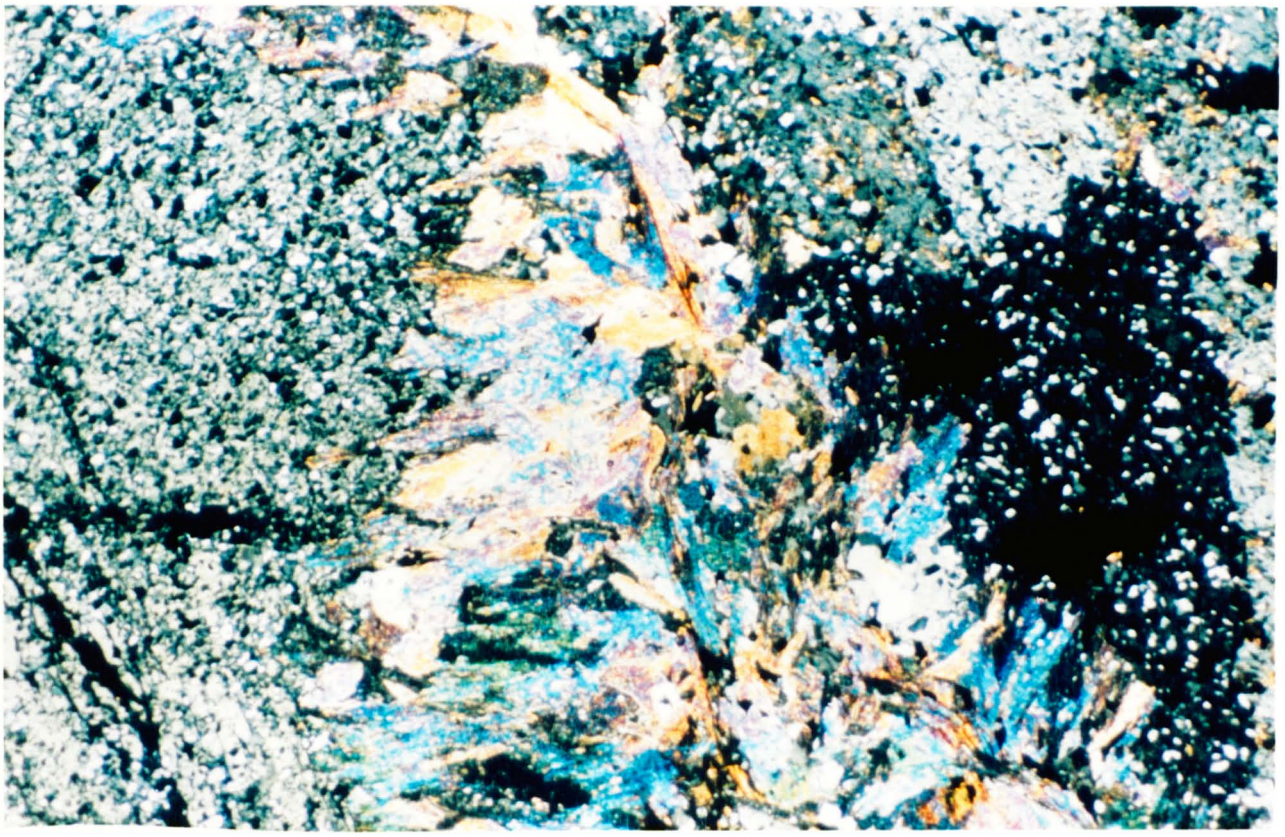

Plate 48 - Late muscovite growing between two boudinaged andalusite porphyroblasts (F344S, GR 5963 2433, XPL, x 125)

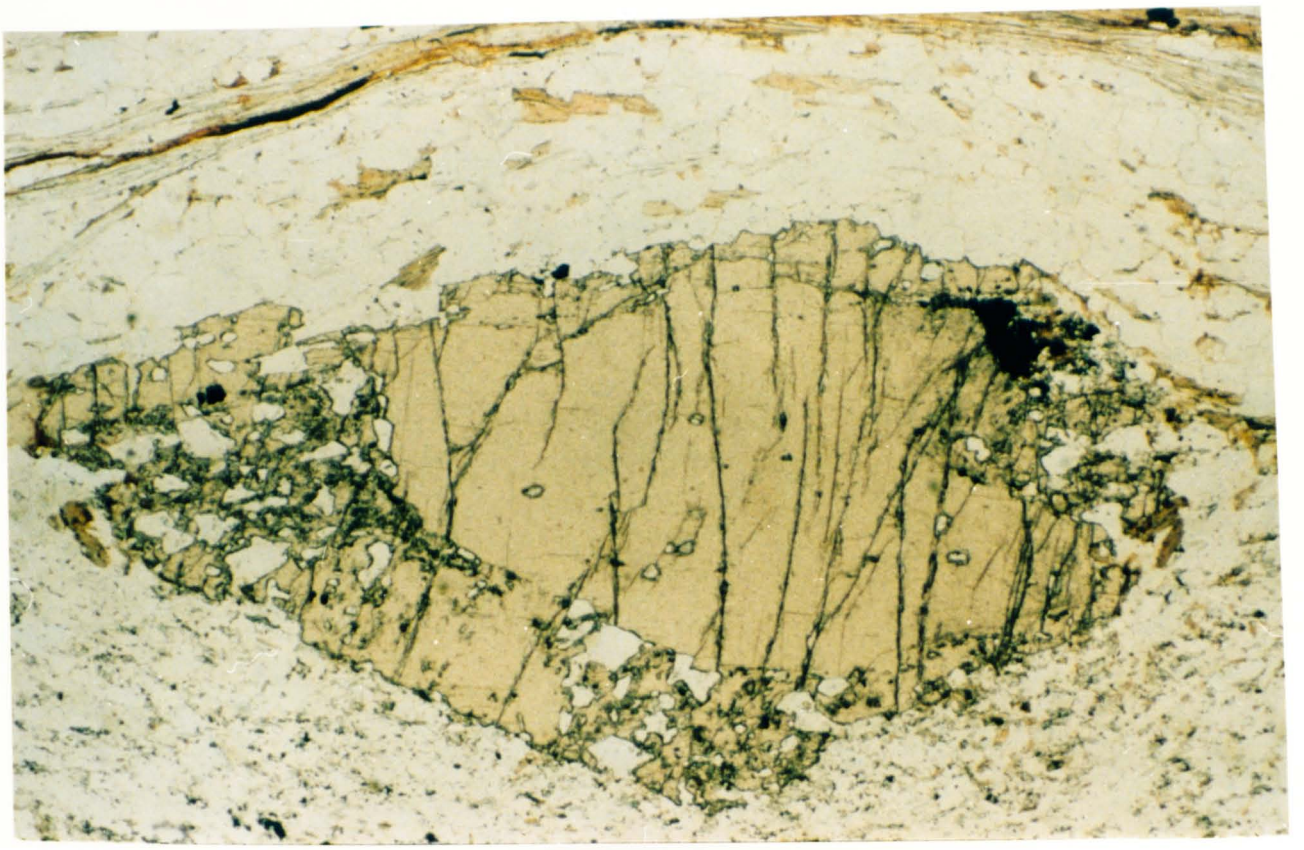

Plates 49 & 50 - Euhedral staurolite porphyroblast (F412S, GR 5951 2471, Plate 49, PPL, Plate 50, XPL, x 31.25)

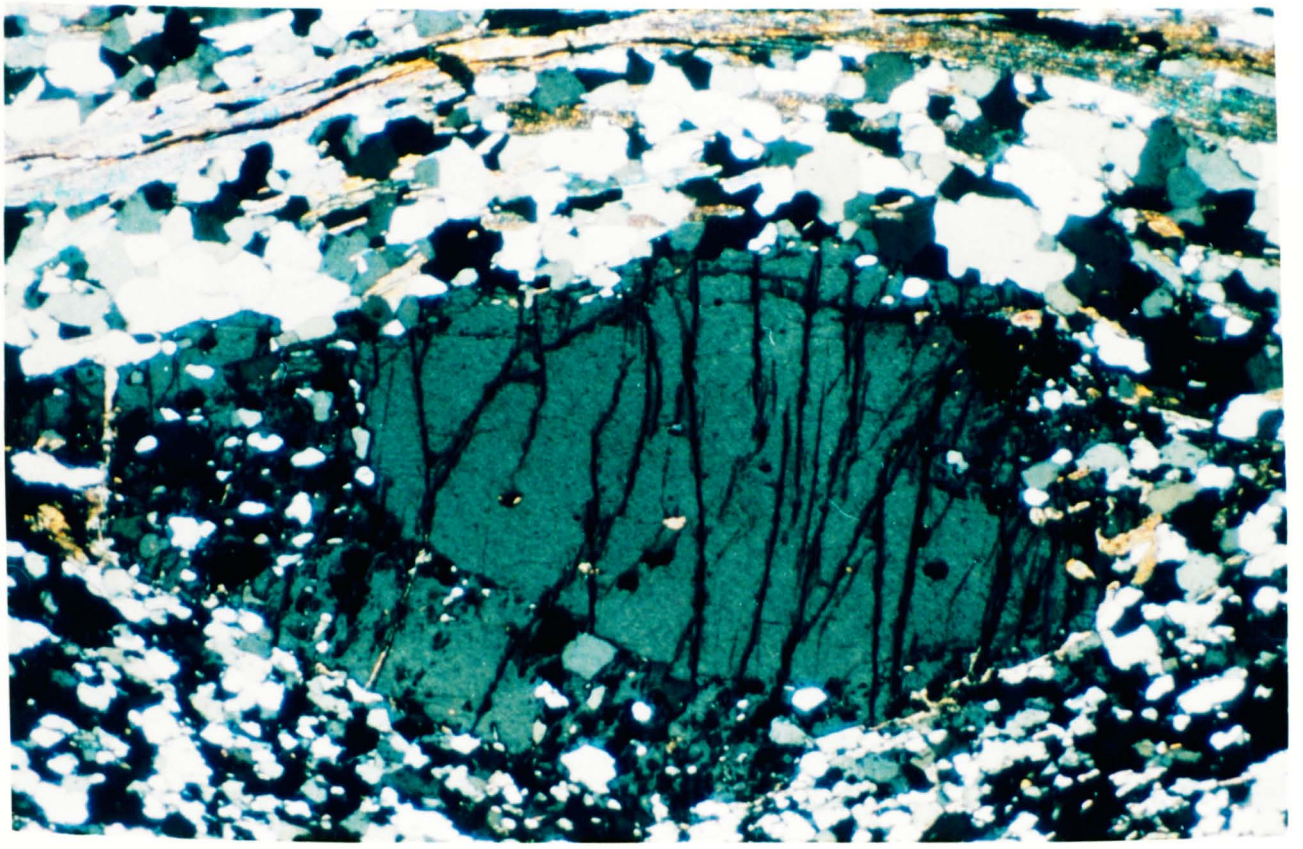

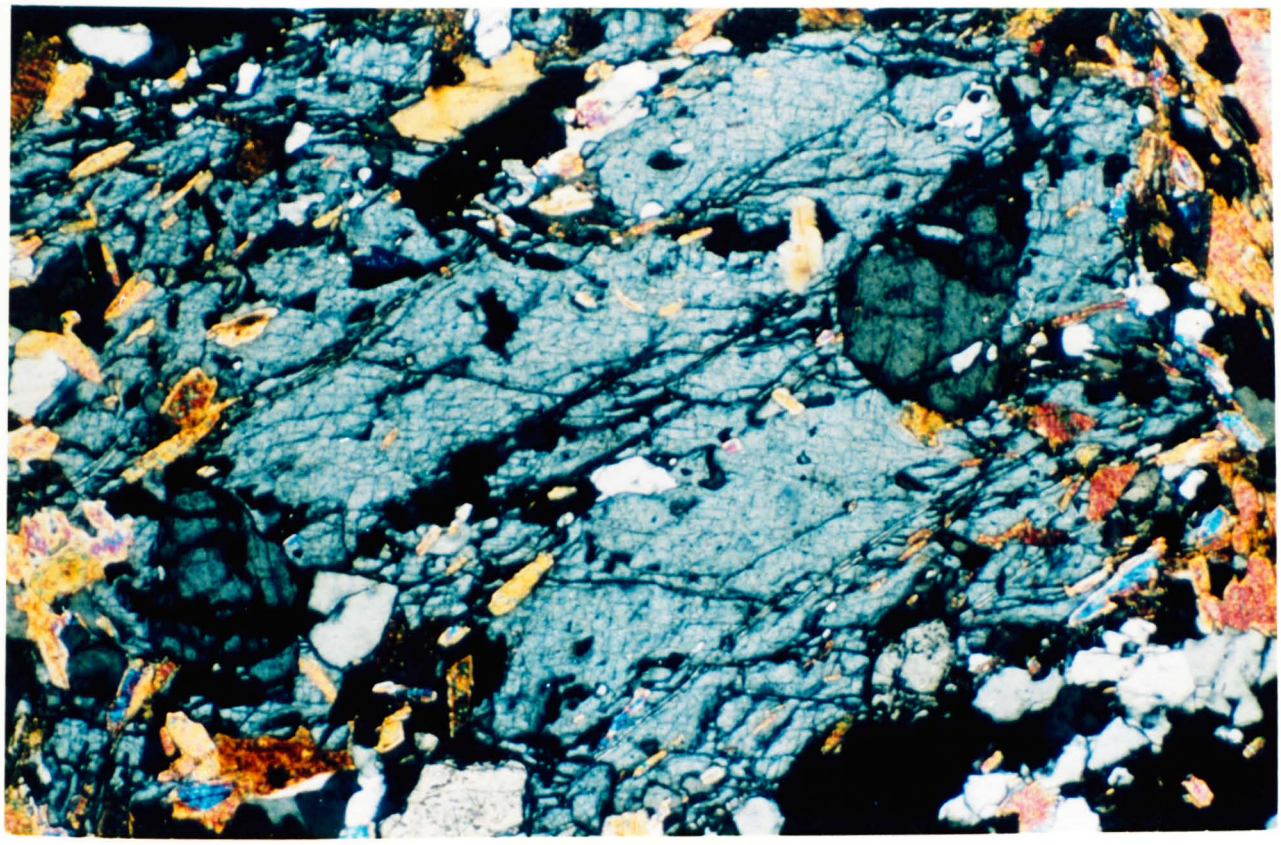

Plate 51 - Staurolite (upper right and lower left) enclosed in andalusite (F337S, GR 6225 2495, XPL, x 62.5)

Plate 52 - Staurolite porphyroblasts show more even distribution than andalusite at thin section scale (F339S, GR 6210 2545, PPL, x 62.5)

Plate 53 - Large staurolite porphyroblasts (GR 6300 2435)

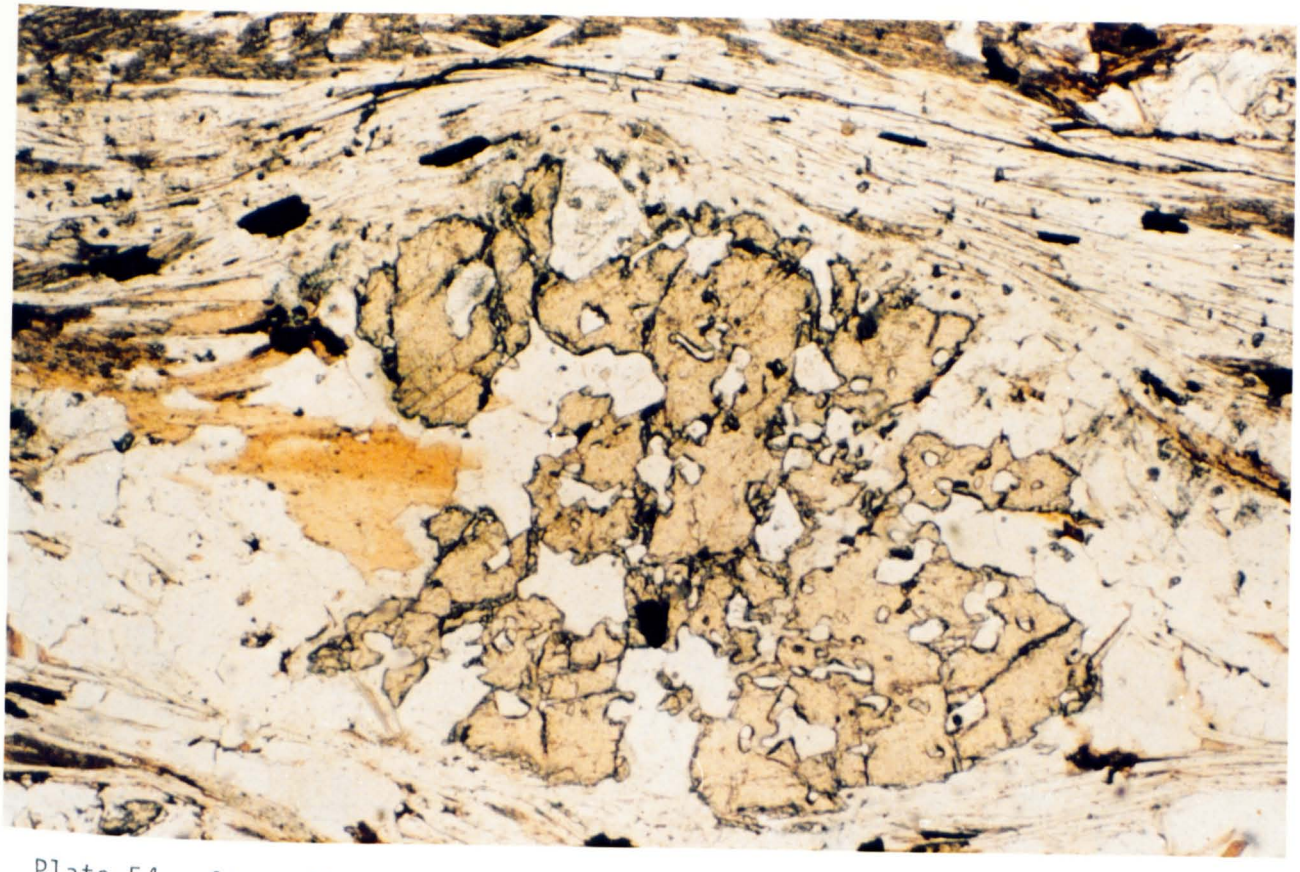

Plate 54 - Staurolite porphyroblast showing large crystal size relative to the groundmass crystals (F425S, GR 6120 2590, PPL, x 62.5)

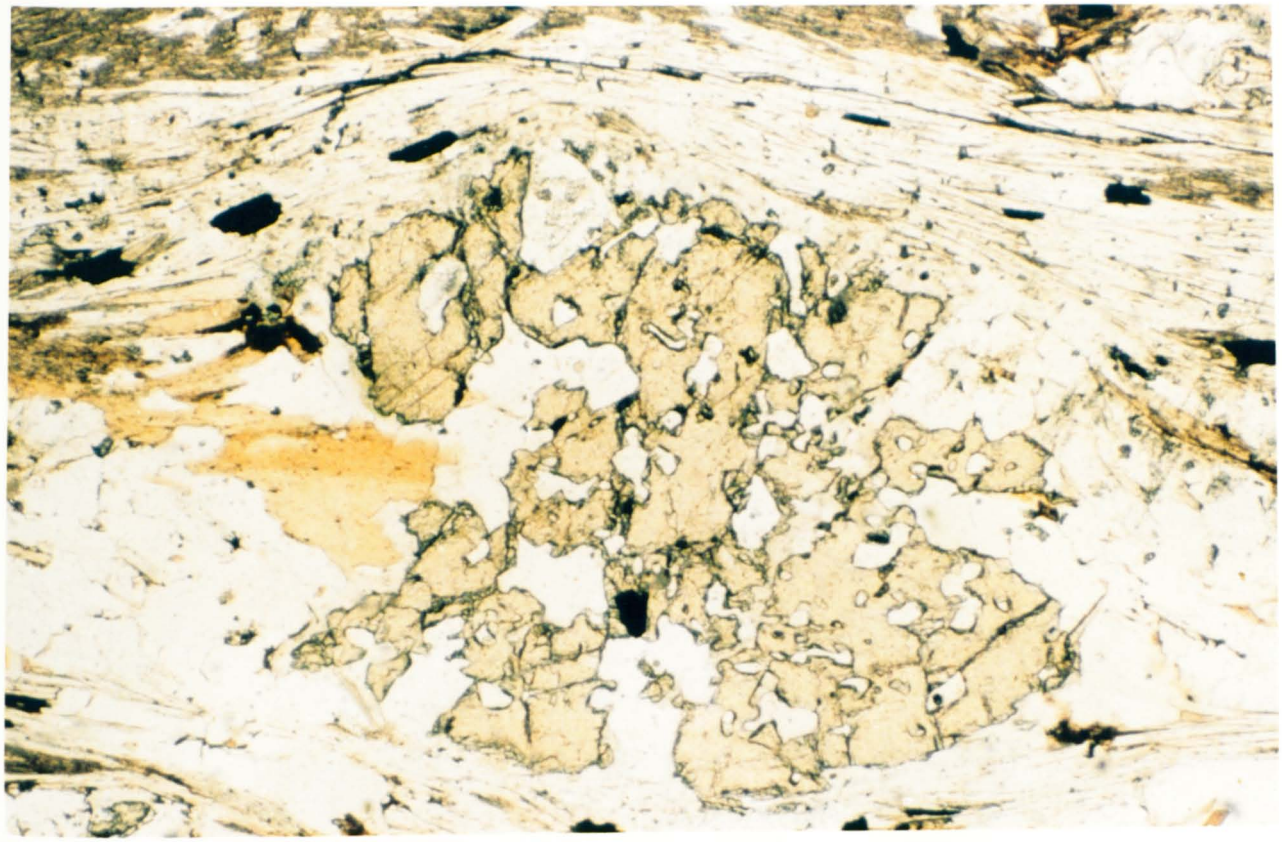

Plates 55 & 56 - Staurolite porphyroblast (Plate 55, PPL; Plate 56, XPL) showing numerous quartz inclusions and (Plate 56) twinning (F425S, GR 6120 2590, x 62.5)

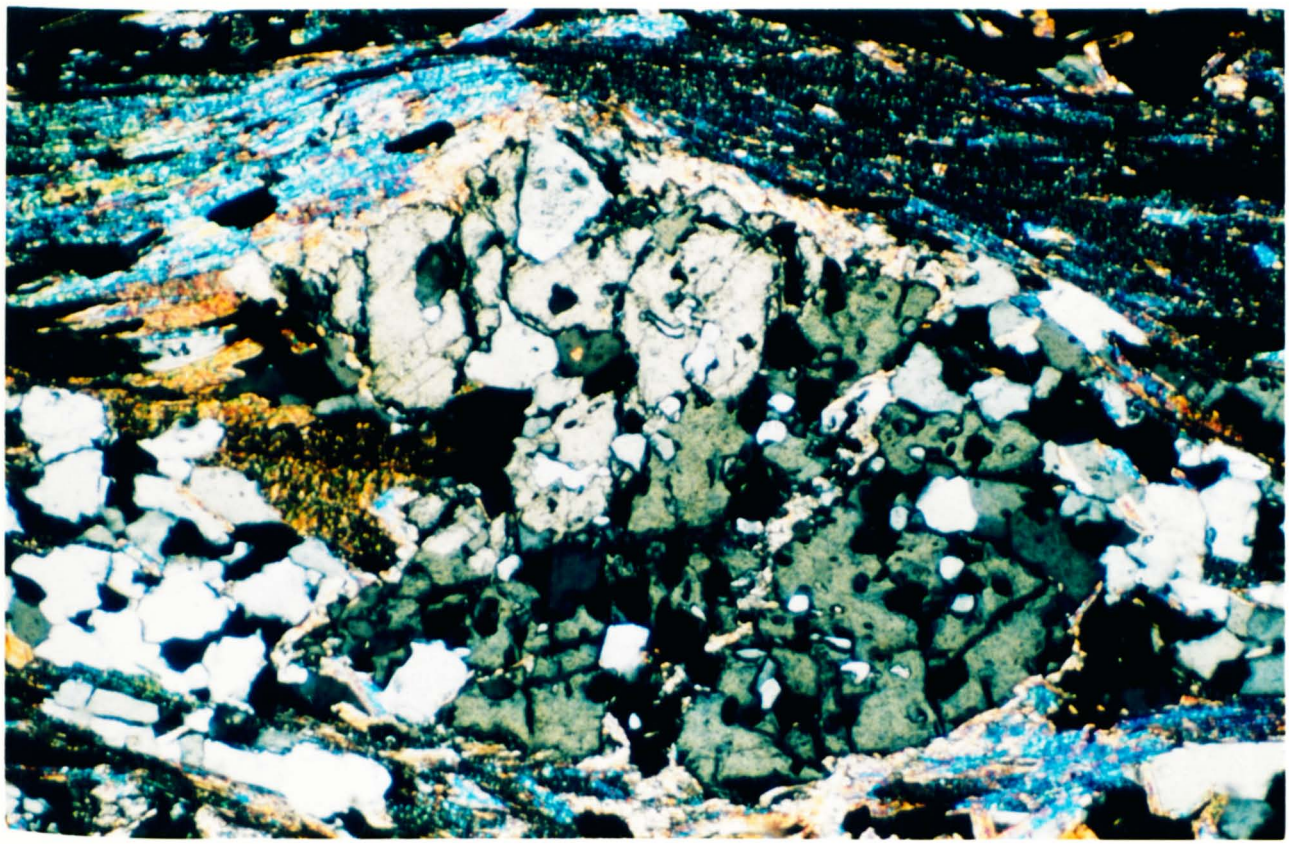

overgrows and surrounds some porphyroblasts (Plate 57 & 58).

5.3.4 - Sillimanite zone

Sheet 13-D indicates widespread outcrop of sillimanite grade schist on either side of the north-western side of the Serra da Freita granite, and in the inliers enclosed by it (Figure 5.3). This is continuous with the sillimanite-bearing rocks both south-west and within the Arouca pluton, which in the Streckeisen (1976) classification is a biotite quartz diorite.

Detailed sampling on the western traverse shows that: (i) the regional sillimanite isograd makes a much more acute angle with the Serra da Freita granite and, especially on the north side, extends further east (Figure 5.4); (ii) the aureole of the Arouca pluton is of cordierite sillimanite type (F519S, (F528S) (Plates 59 & 60); thus all the sillimanite grade rock shown on Sheet 13-D within and adjacent to the intrusion is likely to be a high temperature low pressure hornfels which overprints the regional biotite and andalusite/staurolite zones, rather than a continuation of the regional sillimanite belt. Such a thermal regime is likely around a large high level quartz diorite body. However the polymetamorphic history of the rocks N and W of the Arouca pluton is still unclear, but beyond the limits of this project.

Having recognized this distinction between the two sillimanite zones, further detail can be added to the interpretation of the the regional high grade belt. Samples collected NW along strike (F510S, F511S, F513S, F514S) are all sillimanite schist (Plates 61 & 62, Figure 5.4), confirming the high grade nature of the Porto-Viseu metamorphic belt. The present model is of a high grade thermal axis of sillimanite schist running along strike

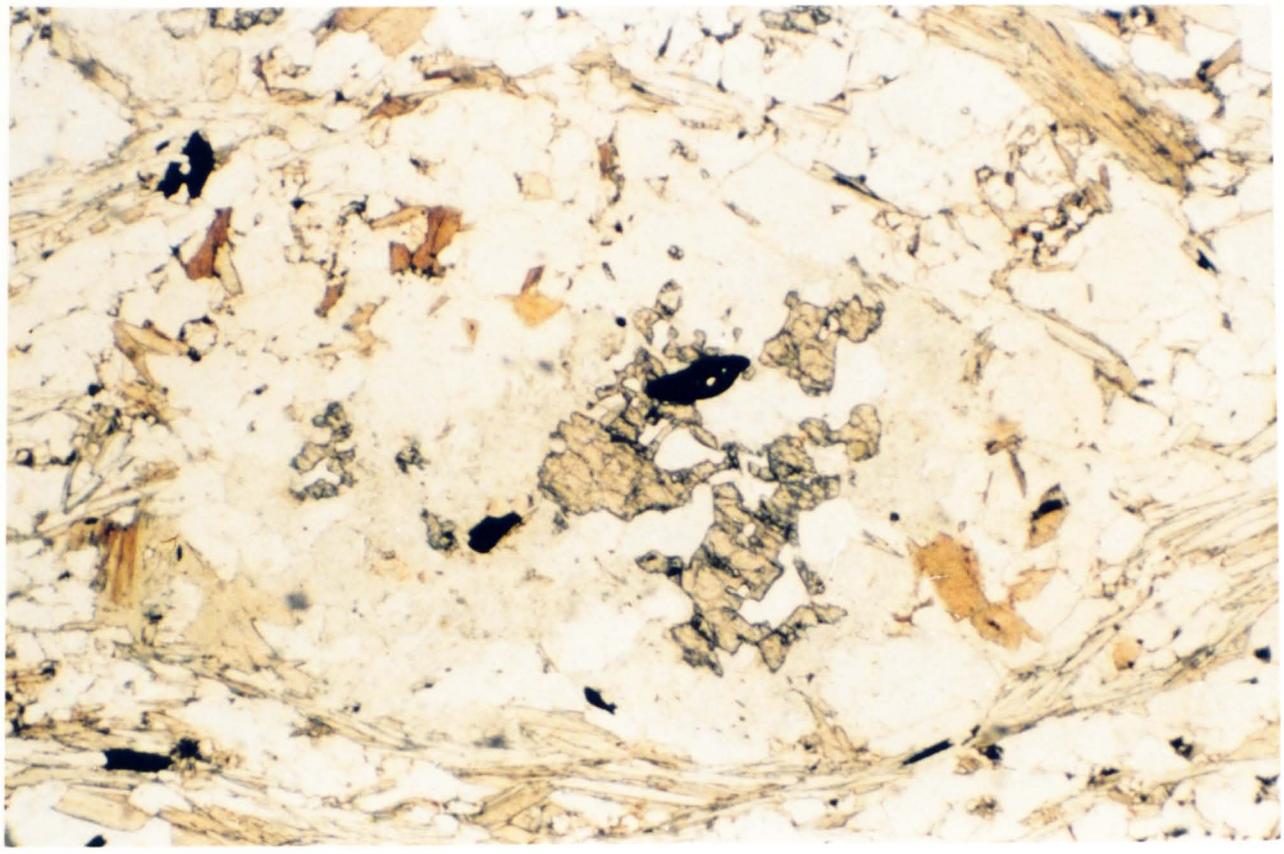

Plates 57 & 58 - Staurolite porphyroblast (Plate 57, PPL; Plate 58, XPL) showing substantial replacement by muscovite (F477AS, GR 6593 2459, x 62.5)

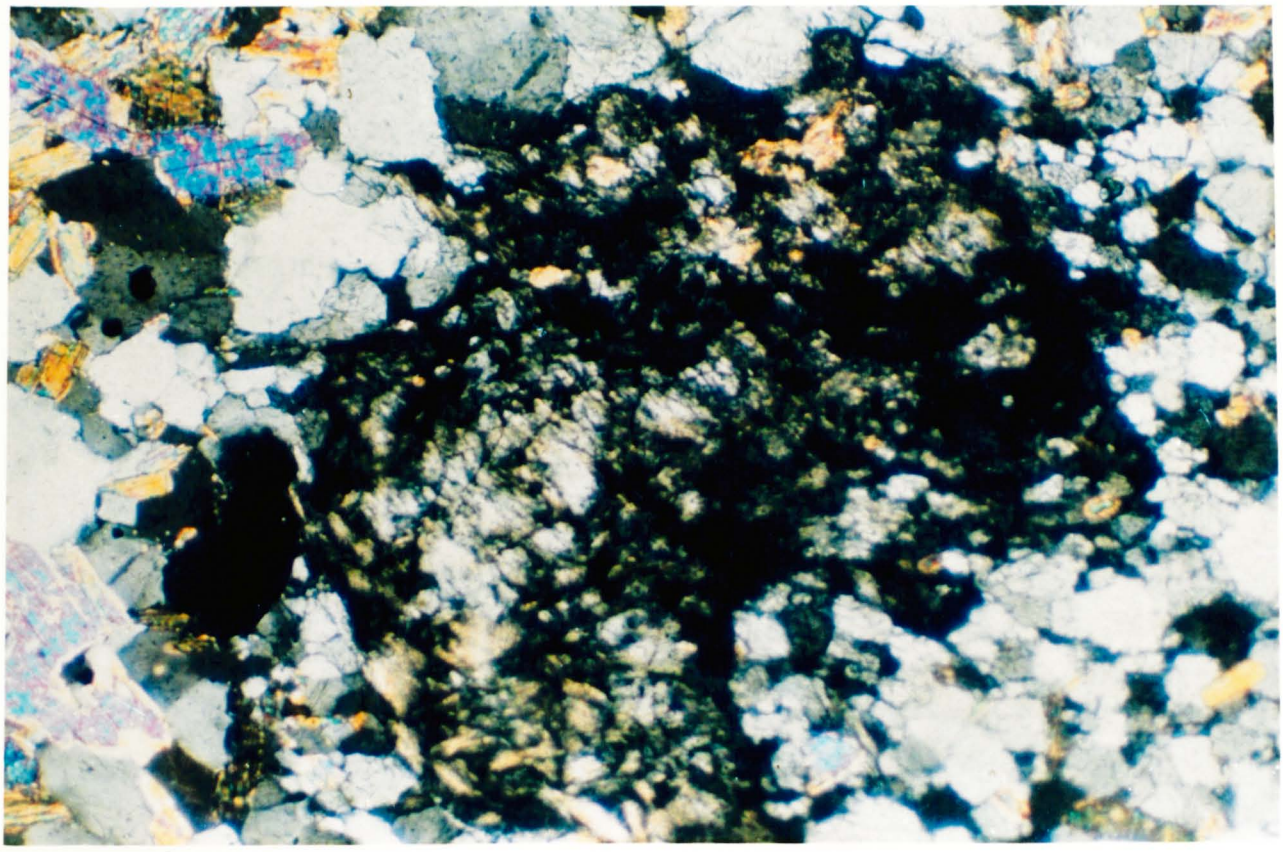

Plate 59 - Cordierite from the aureole of the Arouca pluton (F528S, GR 6285 2710, XPL, x 125)

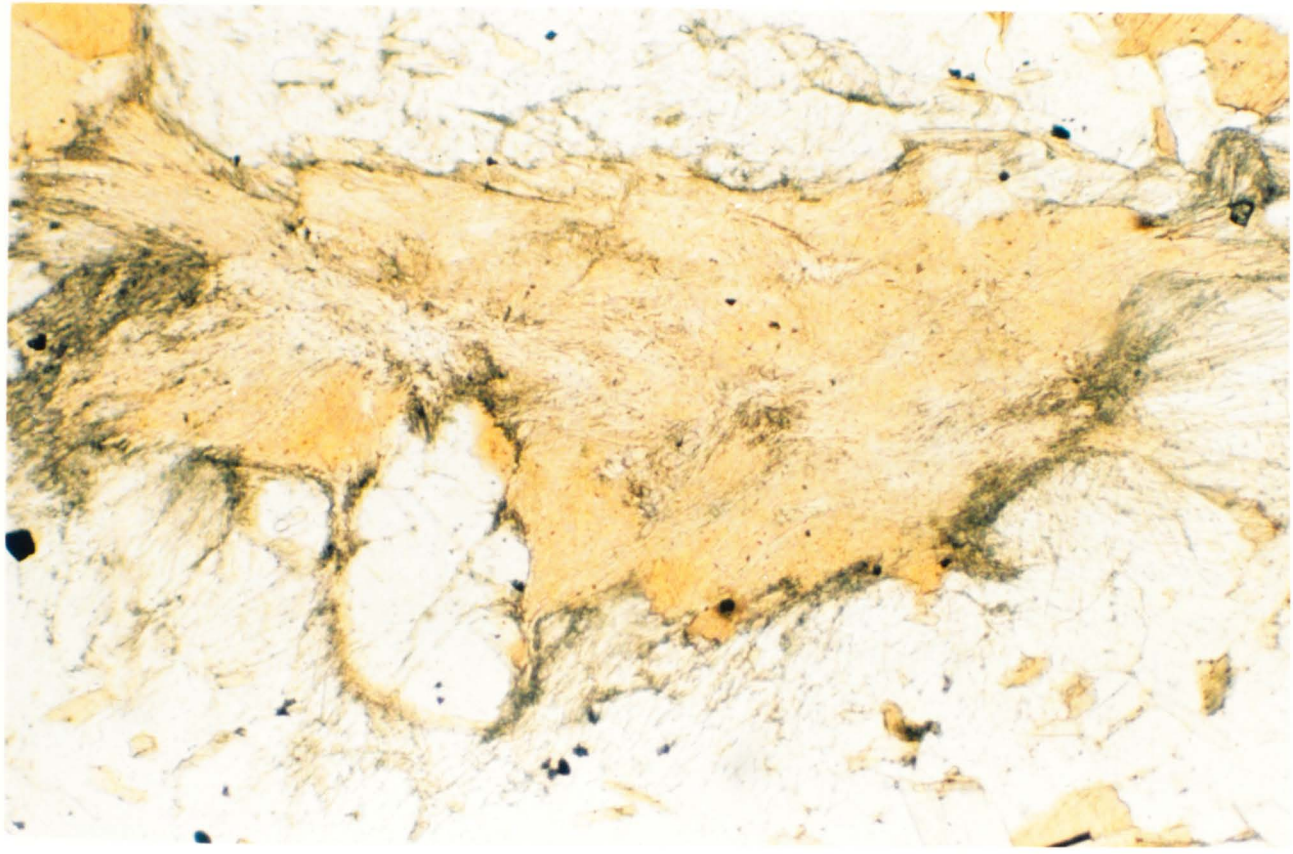

Plate 60 - Fibrolite from the aureole of the Arouca pluton (F528S, GR 6285 2710, PPL, x 125)

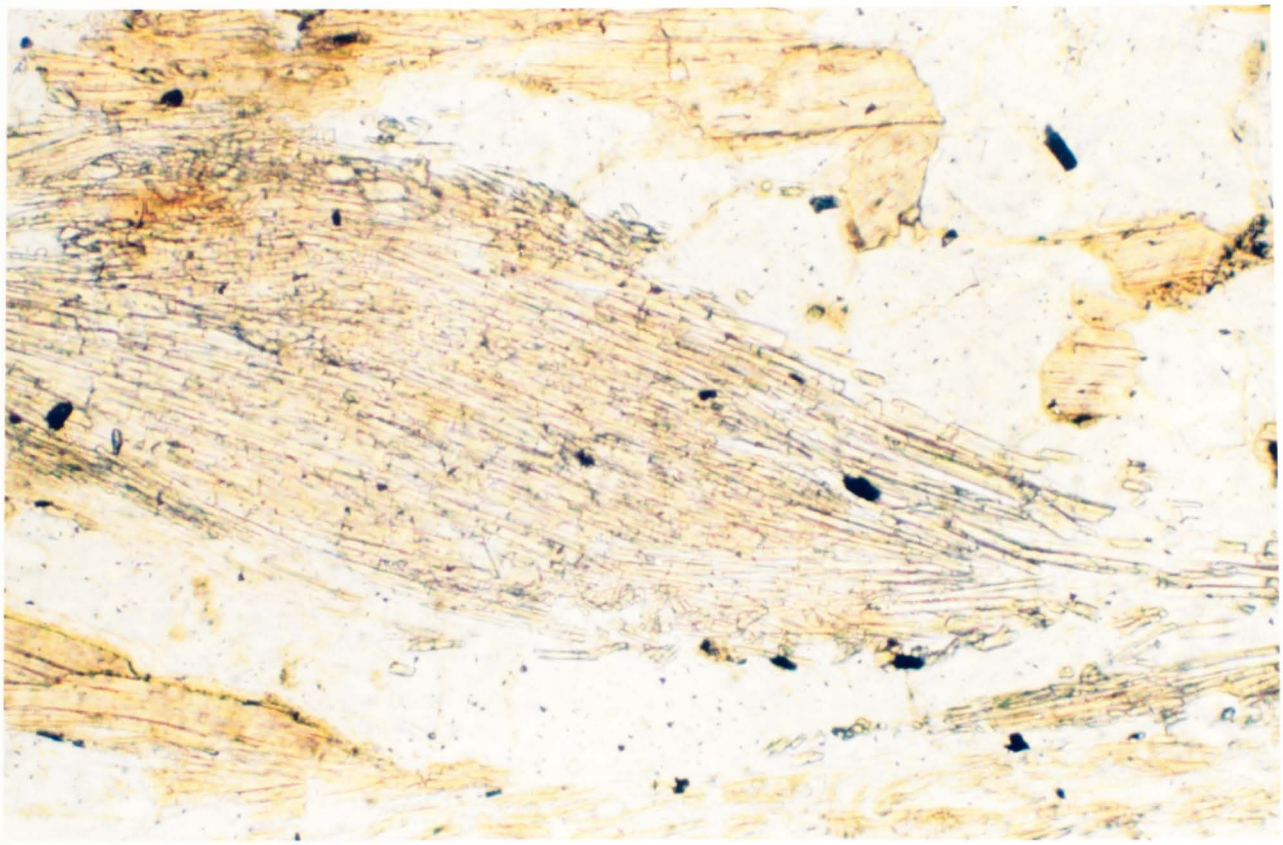

Plates 61 & 62 - Fibrolite, possibly overprinting a biotite "fish", from further along strike to the NW (F510S, location on Figure 5.4, Plate 61, PPL, Plate 62, XPL, x 250)

into which the S.Pedro do Sul belt plutons are intruded. This interpretation explains the oblique contact between the Serra da Freita granite and the sillimanite isograd; the granite is intruded into the sillimanite zone and where the granite widens to the SE, rocks of andalusite/staurolite grade form the envelope, as seen on the eastern traverse. The inliers, shown on Sheet 13-D as roof pendants, but here interpreted as country rock approximately in place beneath a folded granite sheet, represent the continuation of this thermal axis to the SE.

The K-feldspar + Al2SiO5 isograd signifies high grade metamorphism (Winkler) and represents several adjacent reaction isograds. In the western traverse, the nature of the high grade metamorphism can be assessed in samples F420S, F422S and F425S north of S.Pedro Velho, and F41S, F42S and F45S west of Mizarela and is characterized by the appearance of K-feldspar and fibrolite and the progressive loss of muscovite.

The paragenesis in these schists is similar to the preceeding zones; staurolite and andalusite persist although these minerals are obviously being broken down (Plates 63 & 64). In most cases, muscovite and biotite occur in the groundmass although their relationships are complicated by the presence of new biotite forming at high grade and late muscovite replacing andalusite. Muscovite is absent only in the highest grade rocks. Fibrolite is spatially associated with biotite (Plate 65), suggesting that biotite is a nucleation site or that they formed together by reactions such as

staurolite + muscovite + quartz = Al2SiO5 + biotite + H2O

One garnet is observed in F422S (Plate 66), suggesting the following

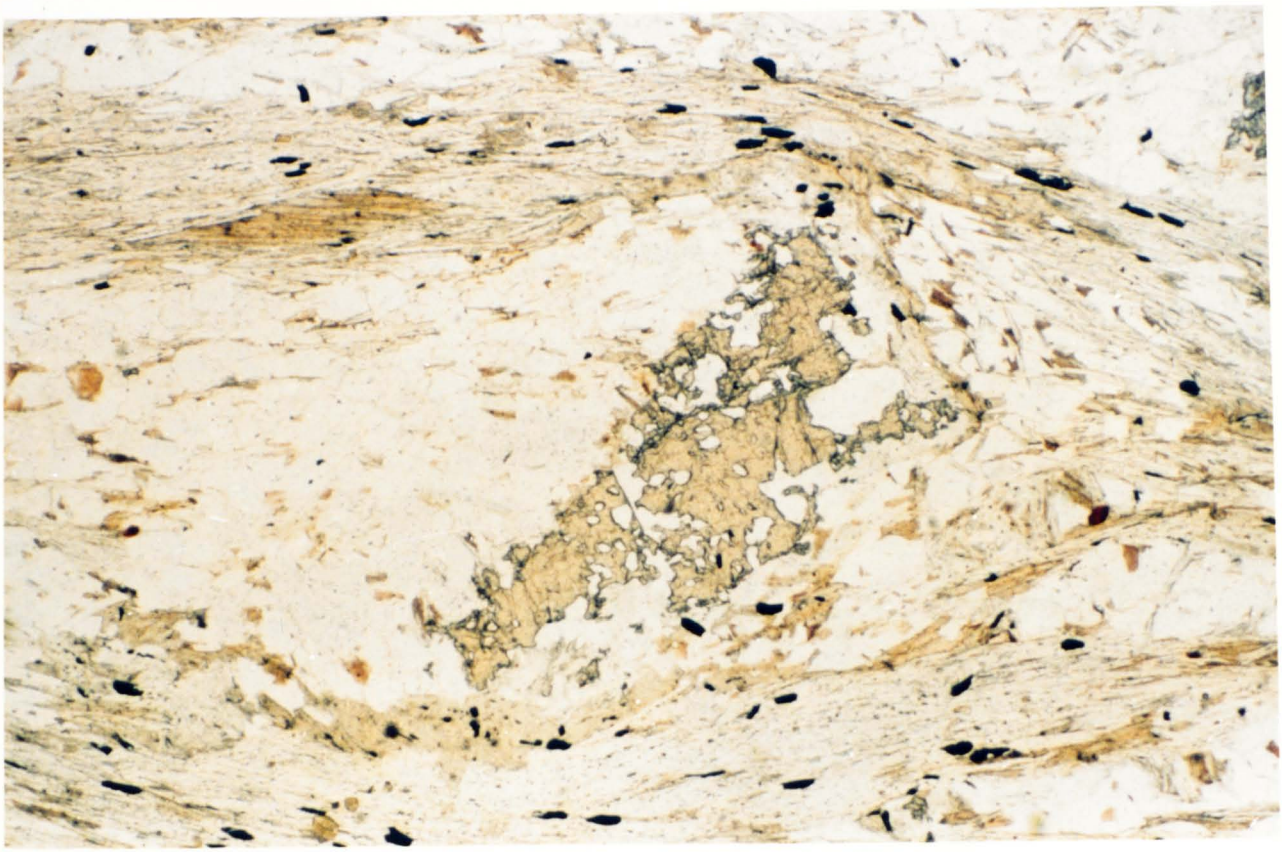

Plates 63 & 64 - Staurolite porphyroblast showing substantial replacement (F425S, GR 6120 2590, Plate 63, PPL, Plate 64, XPL, x 31.25)

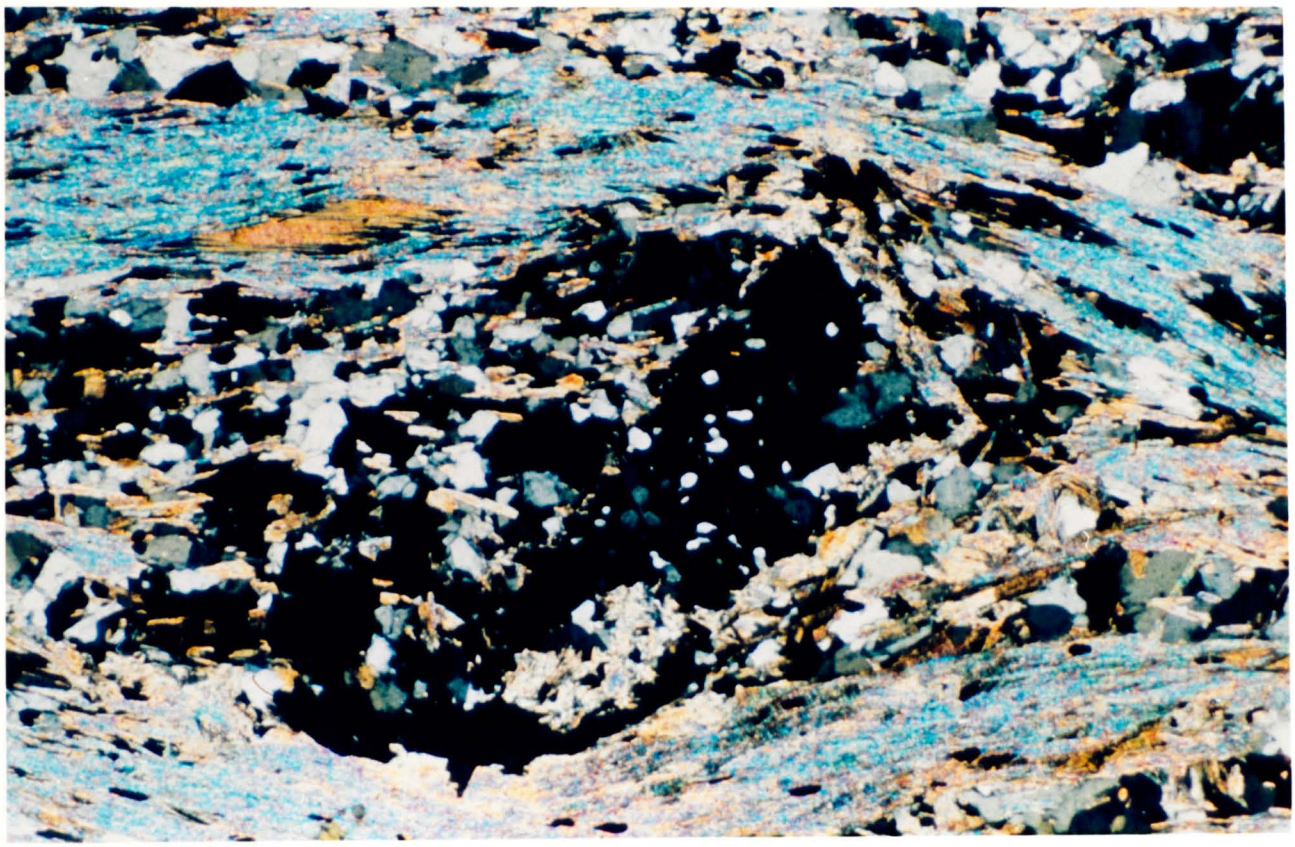

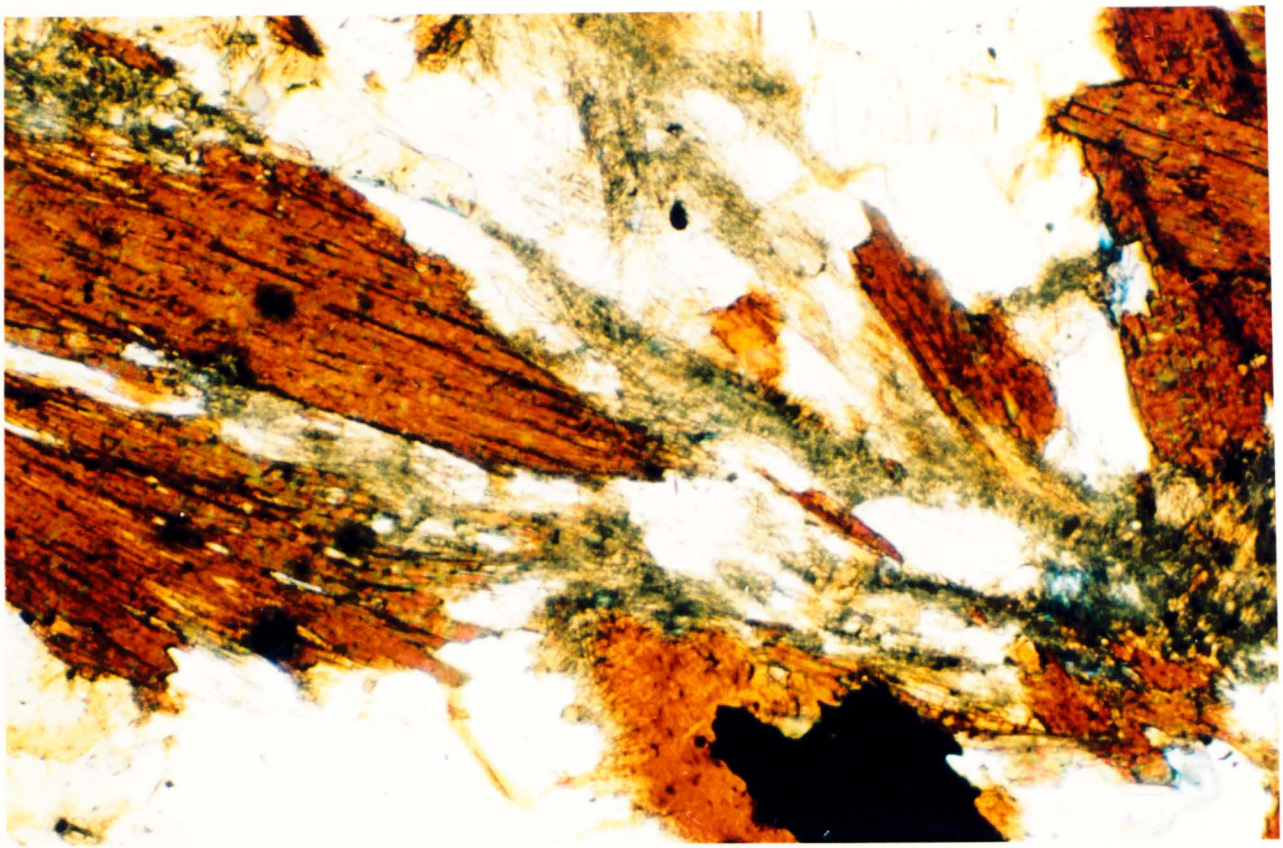

Plate 65 - Fibrolite spatially associated with biotite (F422S, GR 6100 2560, PPL, x 125)

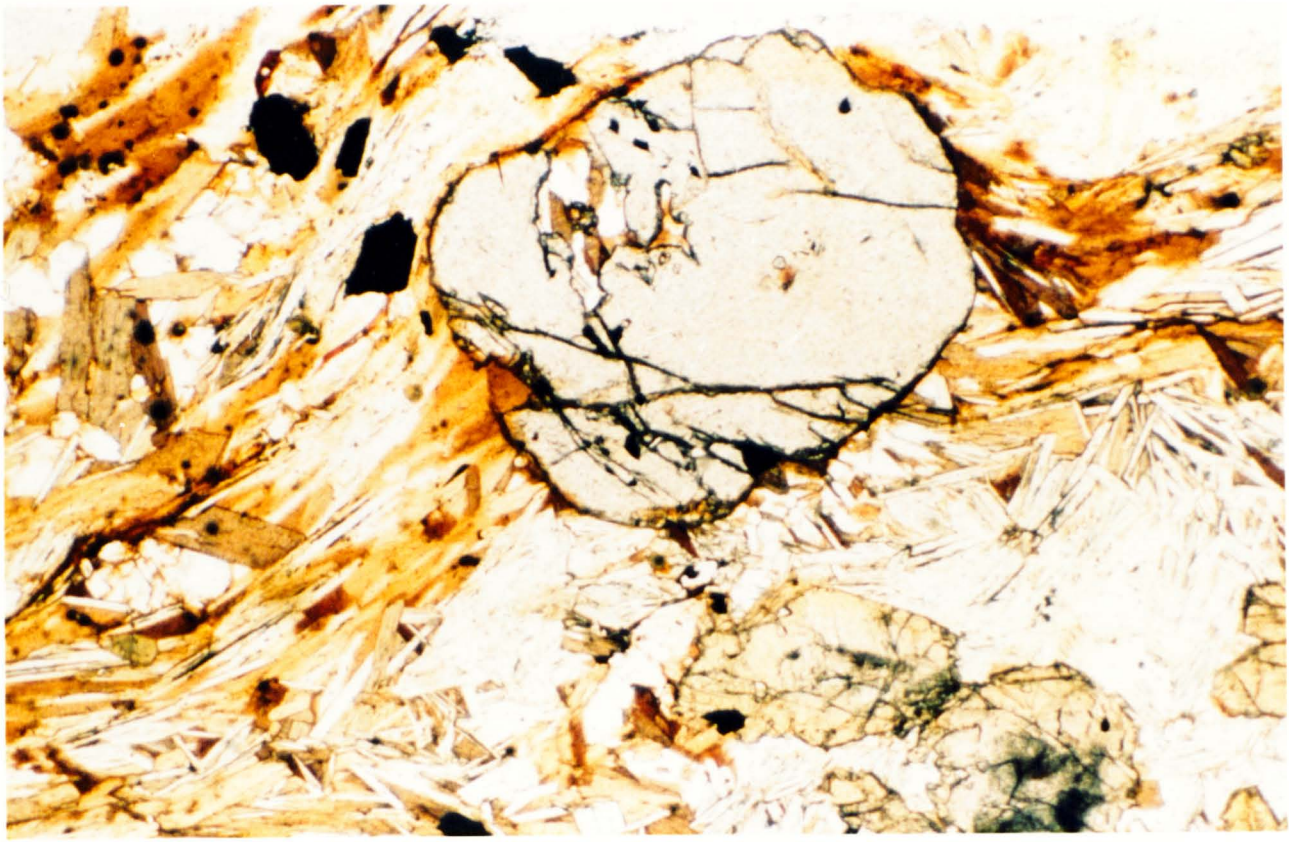

Plate 66 - Garnet, possibly formed by high grade reaction discussed in the text (F422S, GR 6100 2560, PPL, x 31.25)

reaction:

staurolite + muscovite + quartz = Al2SiO5 + almandine + biotite + H2O

Generally fibrolite and K-feldspar form before muscovite disappears; muscovite is abundant in slides F45S, F420S, F422S and F425S, rare in F42S and absent in F41S (Plates 67 & 68), the latter two samples show a marked increase in the amount of fibrolite present (Plates 69 & 70). Fibrolite, associated with fresh biotite, and K feldspar, are characteristic minerals in samples from the Junqueira and Mizarela inliers (Plate 71). Two crystals of kyanite are enclosed in one andalusite porphyroblast in F42S, a texture which suggests a direct local polymorphic transformation (Plate 72).

F519S and F528S were collected within 5 m of the contact between the Arouca pluton and the Beira schists. The paragenesis is quartz, biotite, muscovite, cordierite, sillimanite, plagioclase and it is proposed that rather than representing a continuation of the regional sillimanite belt, this hornfels is evidence of a low pressure high temperature aureole around the quartz diorite body (Plates 59 & 60).

5.4 - Timing of Deformation and Metamorphism

F2 development must have preceeded the main shearing and metamorphic events as F2 folds are steepened and S2 intensified by the main shear movements, and the isograds cut across the F2 fold traces.

The development of the regional biotite, andalusite/staurolite, sillimanite zones in the Beira Schists preceeded the intrusion of the Serra da Freita granite sheet into the axial region of this metamorphic belt oblique to the sillimanite isograd. Porphyroblasts, particularly

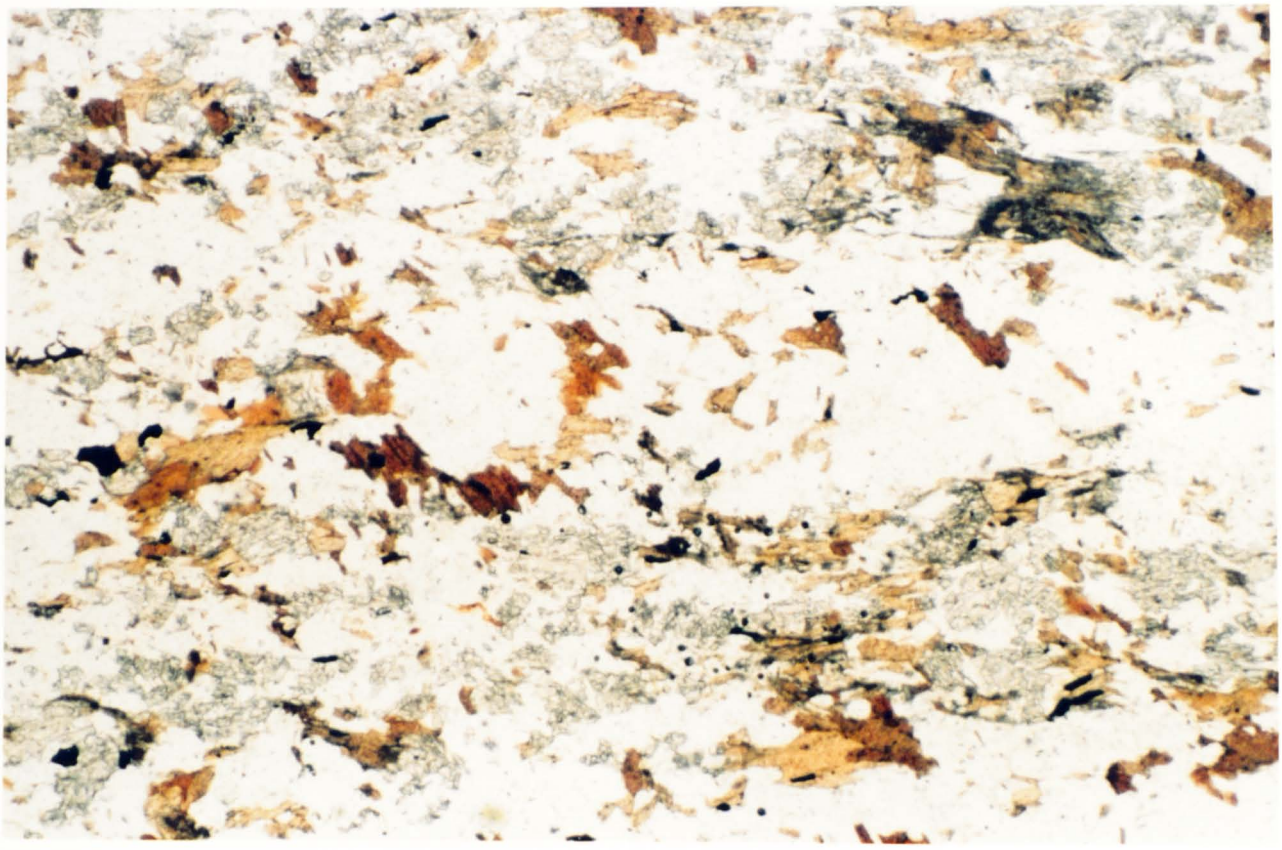

Plates 67 & 68 - High grade assemblage of quartz, K-feldspar, andalusite, fibrolite and biotite. Muscovite is absent (F41S, GR 6031 2421, Plate 67, PPL, Plate 68, XPL, x 31.25)

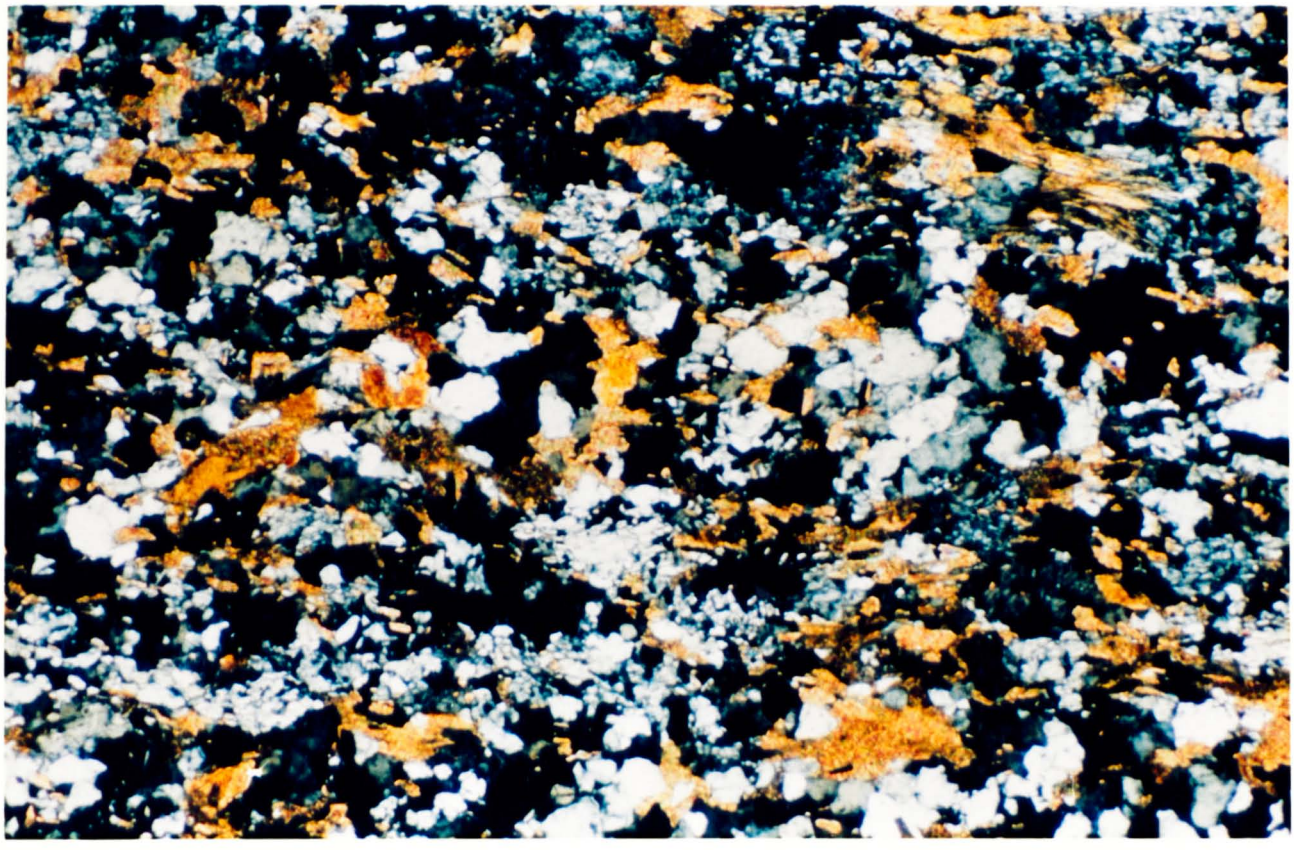

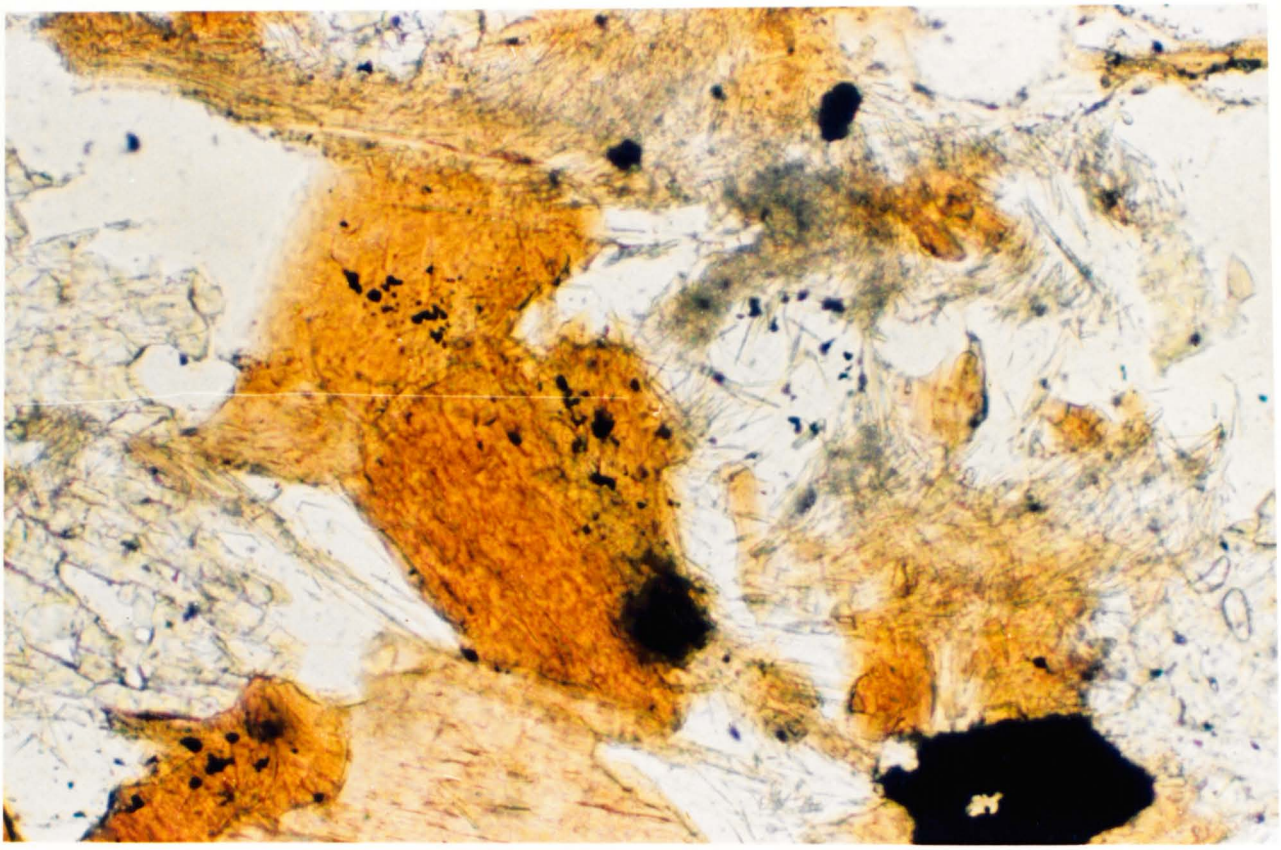

Plates 69 & 70 - Fibrolite overgrowing? biotite (F41S, GR 6031 2421, Plate 69, PPL, Plate 70, XPL, x 250)

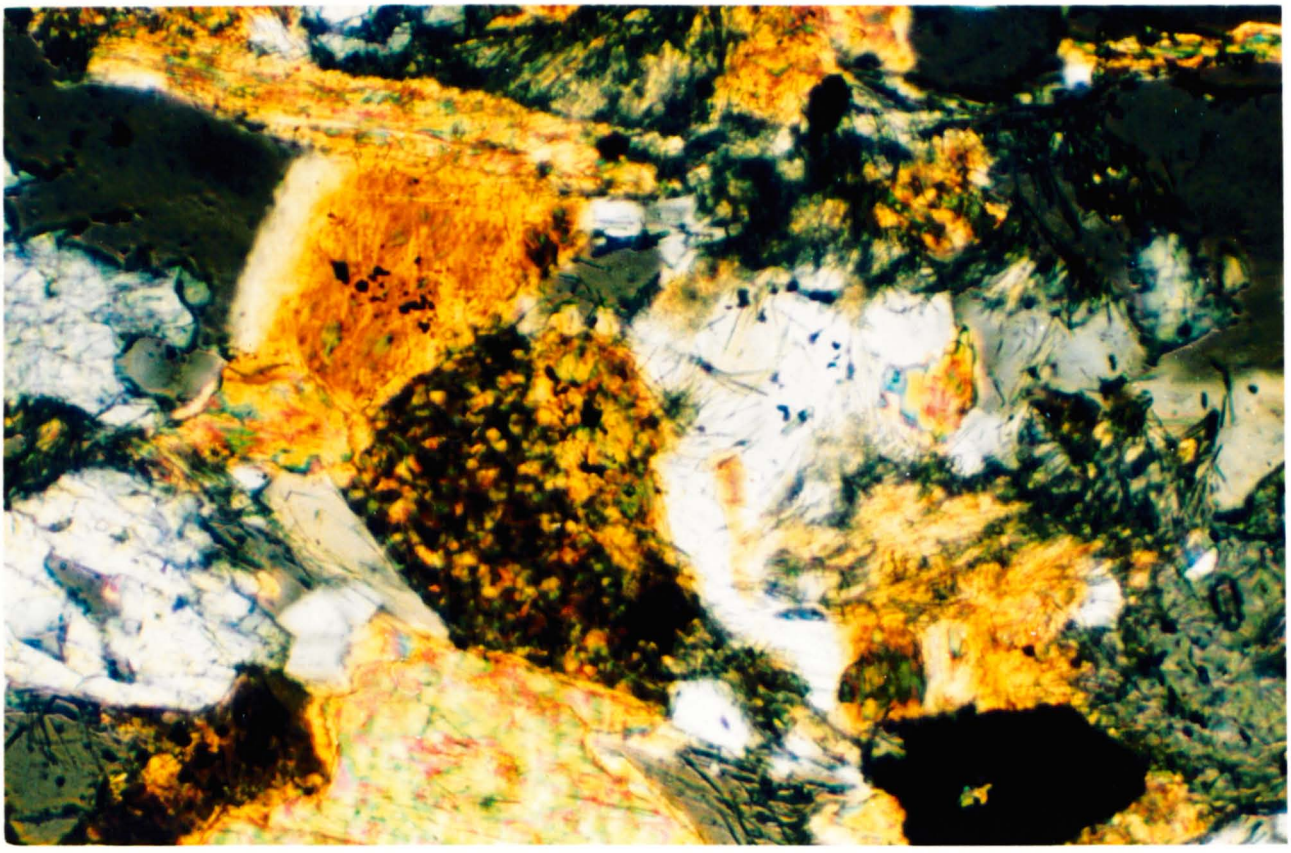

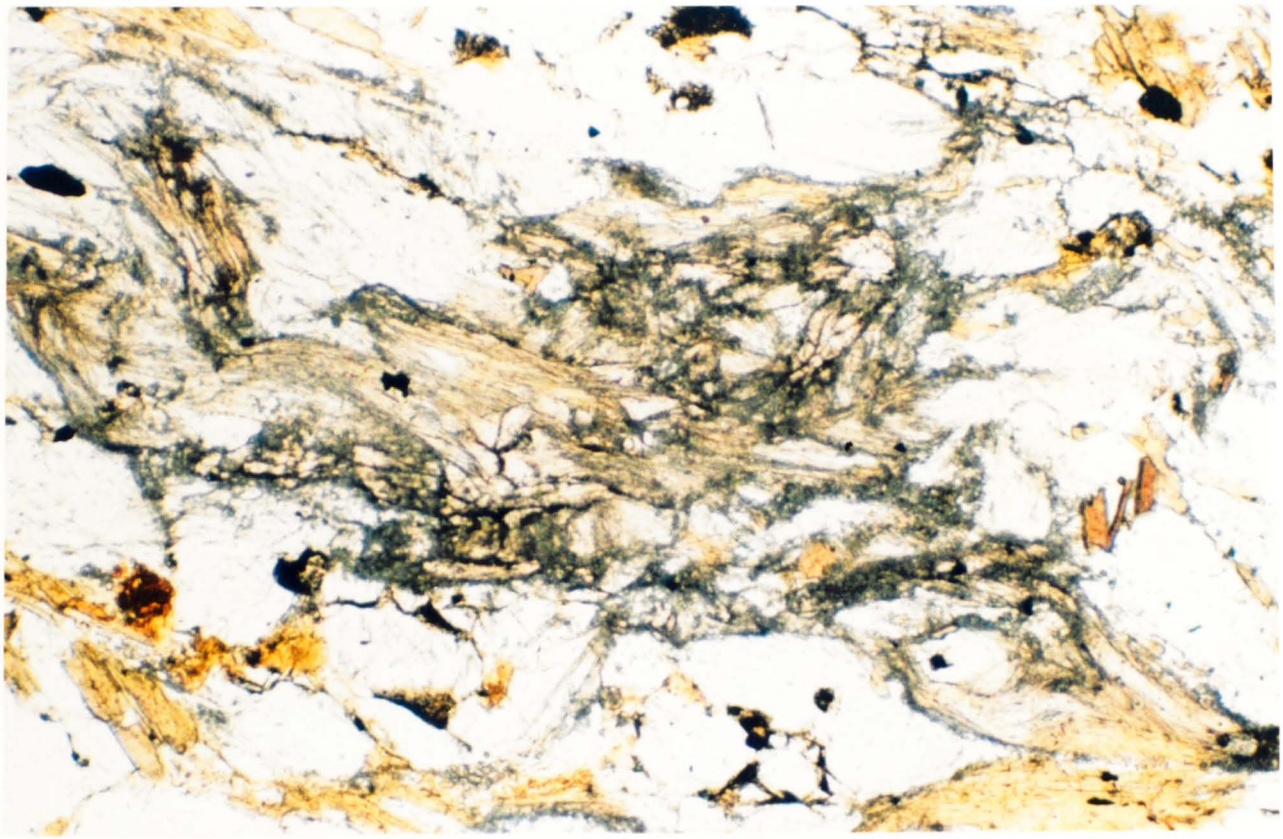

Plate 71 - Fibrolite from the Mizarela inlier (F4121S, GR 5960 2515, PPL, x 125)

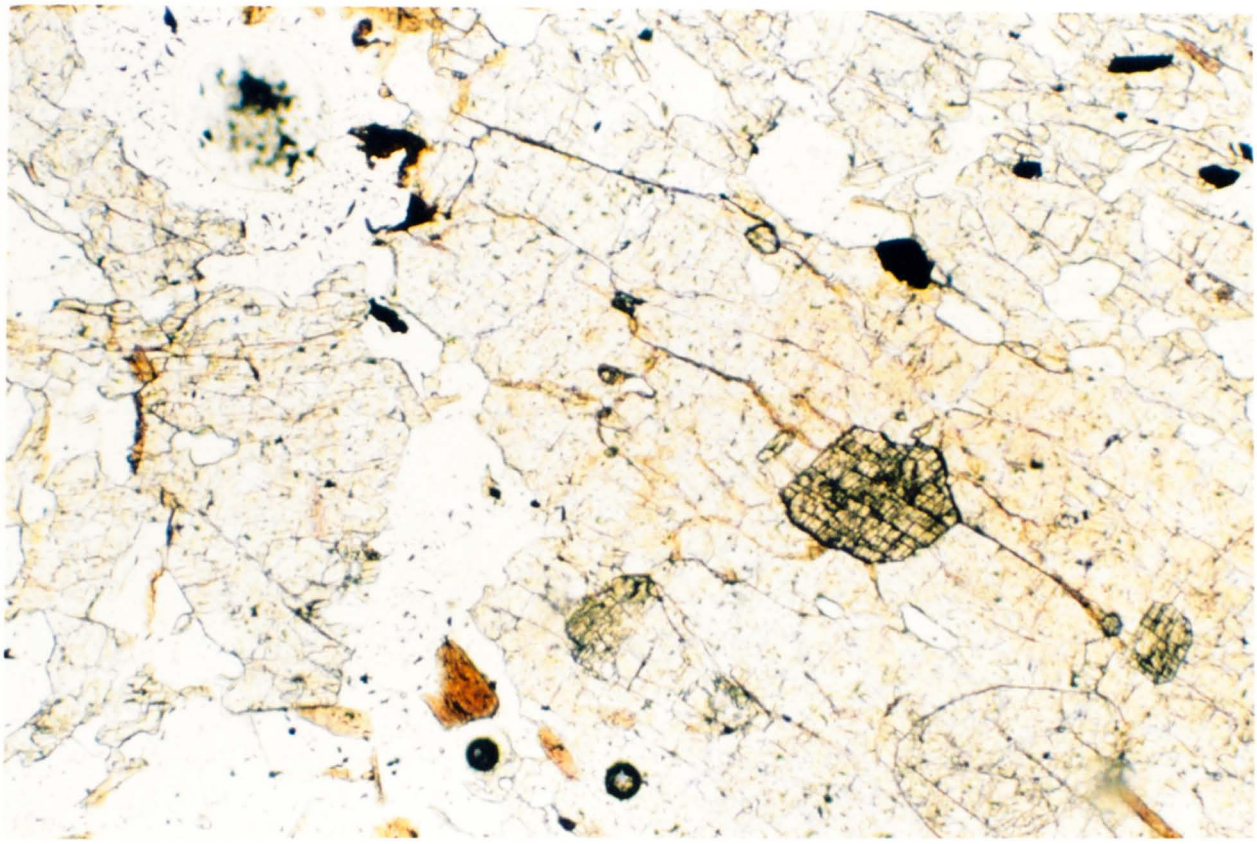

Plate 72 - Kyanite enclosed in andalusite (F42S, GR 6015 2433, PPL, x 125)

biotite and staurolite, show syn-tectonic rotation, and andalusite crystals often form boudins representing syn-tectonic extension; this illustrates that shearing was also active during prograde regional metamorphism.

The Serra da Freita granite has been dated in this study using the Rb/Sr whole rock method at 324±4 Ma, it will be argued later that this represents an intrusion age rather than one which reflects any cooling or subsequent resetting event. In the southern limb of the granite, S2 is a magmatic flow fabric rather than a tectonic fabric (Section 2.5.3); this crucial evidence therefore dates the main shearing as synchronous with intrusion, at about 324 Ma.

CHAPTER VI -- PLUTONISM

6.1 - Introduction

Much information about the granites has been given in preceding sections to support earlier discussions; this is summarized below.

Several granite bodies outcrop on or near the Serra da Freita:

(i) the Serra da Freita pluton;

(ii) the Castanheira cupola, 600 m SW of (i); these both lie in the S.Pedro do Sul belt, and are interpreted as part of one intrusive body;

(iii) the Junqueira pluton, petrographically similar to the Serra da Freita granite situated in the Junqueira belt to the south-west;

(iv) the Arouca and Regoufe plutons in the Central belt to the north-east. These are quartz diorites and the metamorphism around the Arouca intrusion was discussed in Section 5.3.4.

This study has concentrated on the Serra da Freita and Castanheira granites. The outcrop pattern and contact relationships of the Serra da Freita granite are described in Section 2.3.1, whilst the interpretation of the geometry and the emplacement model are put forward in Sections 4.2 and 4.3 respectively. It is now appropriate to consider the variations in granite type recognized during mapping, and their field distributions, showing how these relate to the structural and emplacement models already developed.

On Sheet 13-D of the Portuguese Survey, the Serra da Freita pluton is depicted in the area studied as a medium-grained, foliated 2-mica granite of alkaline type. Much further to the south-east large areas of a porphyritic type and a fine-grained facies are shown. The present study

has revealed that the north-western part of the pluton is much more diverse in terms of granite types than represented by the reconnaissance survey on Sheet 13-D, although the medium-grained 2-mica granite depicted on that map does predominate.

6.2 - Field Geology and Petrography of the Granites - Introduction

Mapping on 1:10000 scale allowed recognition of several granite types or facies within the Serra da Freita intrusion. Three broad divisions are identified.

(A) 2-MICA GRANITES

(1) A medium-grained biotite muscovite granite which comprises the bulk of the intrusion and is called here the main granite.

(2) A coarse-grained facies, possibly reflecting an early pulse, forms the northern margin in the Vidoeiro region. As this part of the intrusion lies exclusively in the zone within which a C-S fabric is developed, the field term sheared granite is used.

(3) Later sheets and wedges of a fine-grained 2-mica granite are termed microgranite.

(B) MUSCOVITE GRANITES

(1) Within 10-15 m of the northern and southern contacts within the schists, biotite decreases and almost disappears resulting in an almost ubiqutous contact leucogranite.

(2) Whereas (1) is derived from the main granite by some modification process, a similar leucogranite is intruded into the main body. Biotite

is confined to drusy pegmatitic segregations within a medium-grained felsic granite.

(3) Fine-grained aplite veins are recorded in several areas.

(C) BIOTITE NODULAR GRANITES

These are of special interest and are found at two localities. The biotite nodules in the Castanheira pluton have been known and regarded for many years as something of a curiosity by Portuguese geologists. However during the mapping of the Serra da Freita granite a new and similar locality was found SE of Gestoso, showing that Castanheira is not unique in the area. Data are presented here which suggest that the Castanheira granite represents part of the roof zone of the main granite.

Any petrographic account of these types is complicated as the fabric varies with deformation intensity across the outcrop. As mentioned in Section 4.3, the following generalizations can be made: (i) in the southern limb, the granite shows only a weak phyllosilicate alignment or no fabric at all; (ii) north of the main pluton axis, the fabric intensifies in the steep belt and the development of a C-S fabric indicates prolonged sinistral shearing. Although this is largely restricted to the northern limb, the situation is obviously more complex, as a good C-S relationship is seen as far south as Gestoso.

6.2.1 - 2-MICA GRANITES

These comprise the bulk of the pluton and represent the typical syn-tectonic Hercynian intrusive of Iberia.

(A-1) - Main Granite - Field Relations

Much of the Serra da Freita pluton consists of a medium-grained biotite muscovite granite, well seen north and south of Albergaria das Cabras. In the Serlei area other facies intrude the main granite, however these are not recorded west of GR 6230; this facies is seen at the contact of the Mizarela and Junqueira inliers and granitic rafts within these inliers are of this type, the largest of these reach lengths of 500 m. This medium grained granite extends NW towards Chave and samples from smaller units collected in the Mansores region some 12 km distant are of similar petrography. This facies is therefore established as the major intrusive unit present, and the field term main granite is used (Plates 73 & 74).

(A-1) - Main Granite - Petrography

F485G (GR 5859 2555) was selected as being representative of the main granite of the southern limb which records low shear strain. The mineralogy is quartz, orthoclase/albite microperthite, biotite, and muscovite; accessories are apatite and zircon. The overall texture is medium-grained inequigranular.

Quartz - the largest crystals present reach sizes of 2 mm; they are anhedral and generally show consertal texture (Plate 75). There is little evidence of strain, although some grain size reduction has taken place in discrete narrow zones resulting in an inequigranular texture.

Feldspars - several types can be distinguished:

Plate 73 - Field photograph of main granite from southern limb (GR 6255 2260)

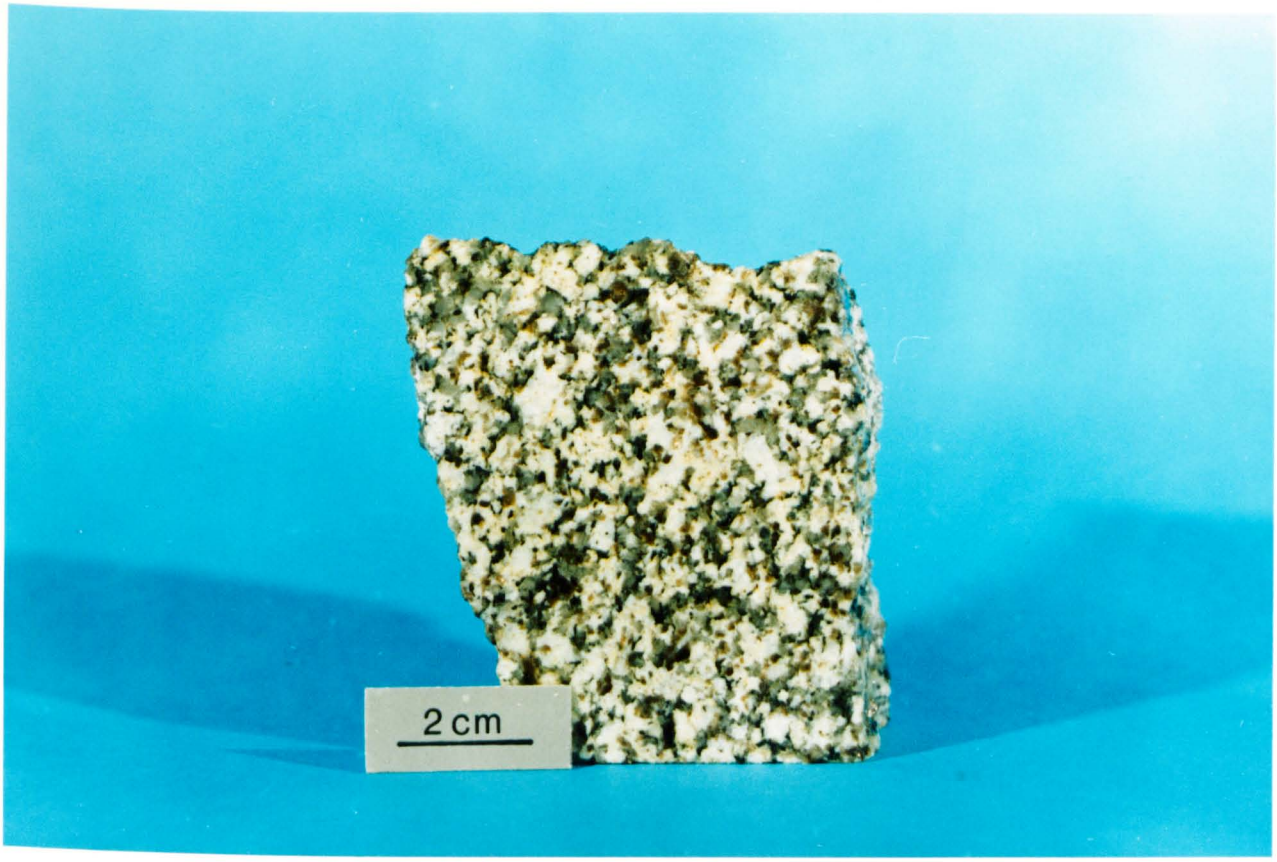

Plate 74 - Hand specimen of F485G (GR 5859 2555), main granite

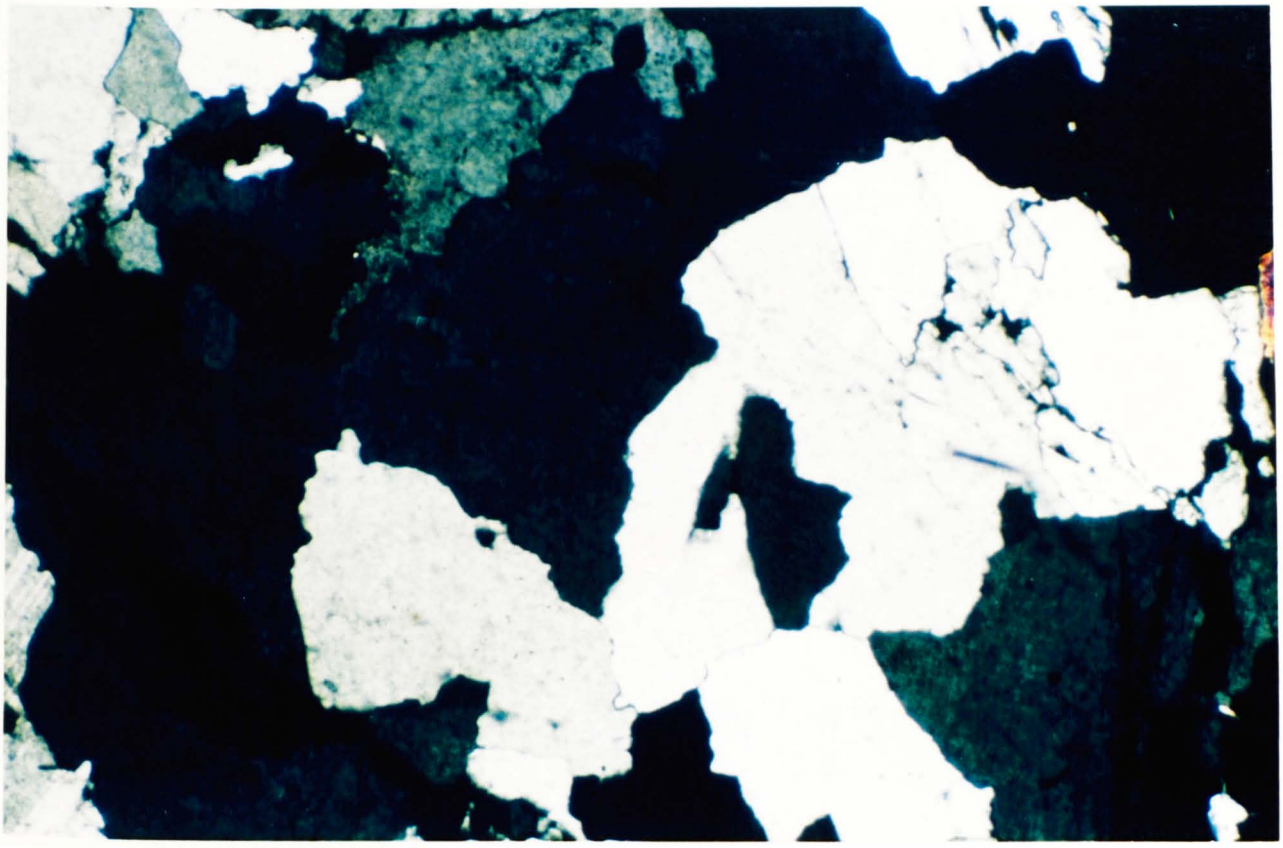

Plate 75 - F485G - Quartz shows consertal texture. Most of the rest of the field of view is orthoclase (XPL, x 62.5)

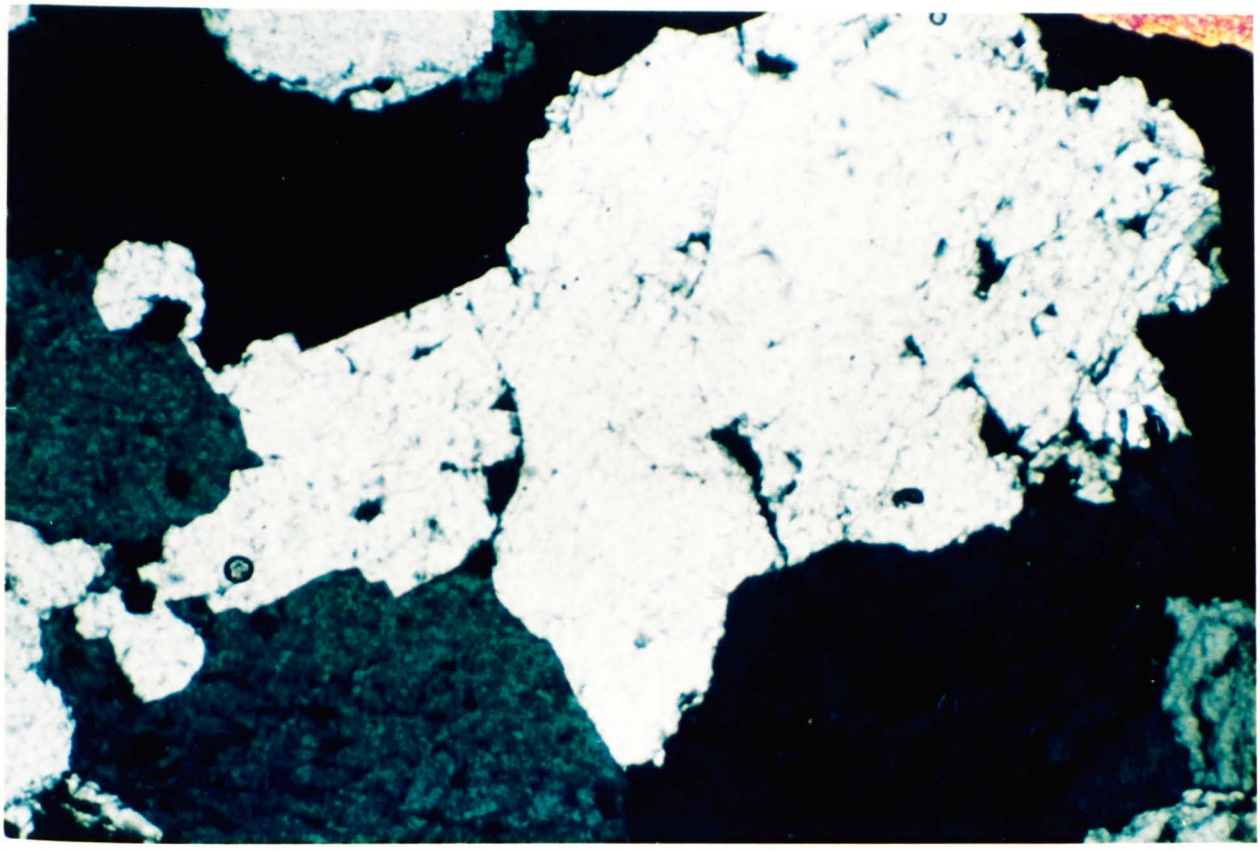

Plate 76 - F485G - Anhedral orthoclase (centre right of field of view) shows no exsolution at this scale (XPL, x 62.5)

(i) orthoclase, in which no exsolution is apparent at microscopic scale (Plate 76);

(ii) albite or Na-rich oligoclase showing minimal exsolution of K-feldspar (Plate 77);

(iii) orthoclase perthite, occasionally microcline perthite (Plates 78 & 79);

(iv) albite antiperthite (Plate 80).

The perthite structure is of penetrative interlocking type, in some cases mesoperthite. Perthite and antiperthite can exist in adjacent crystals. The largest feldspars reach sizes of 4 mm, most are in the range of 1-2 mm and are euhedral to subhedral.

Biotite - biotite is generally euhedral to subhedral and forms flakes of variable size, most are in the range 0.5 - 2 mm although the largest reach 3 mm; most crystals are narrow rather than equidimensional. Some alteration to chlorite has taken place along cleavage in about 15% of the grains, the remainder are fresh but often show pleochroic decay halos. Biotite often grows in association with large muscovites and is taken as being magmatic (Plates 81 & 82).

Muscovite - the occurrence of primary magmatic muscovite is taken as an indicator of strongly peraluminous magma composition and of a depth of crystallization > 11 km (Miller et al., 1981). Reports of primary muscovite in plutons emplaced at depths of 5-10 km mean that either the muscovite is secondary despite its appearance, or that the experimental data are inapplicable to plutonic muscovite; in either case its use for depth estimation would be invalidated. Miller et al. (1981) establish textural criteria for the recognition of primary muscovite. To be primary,

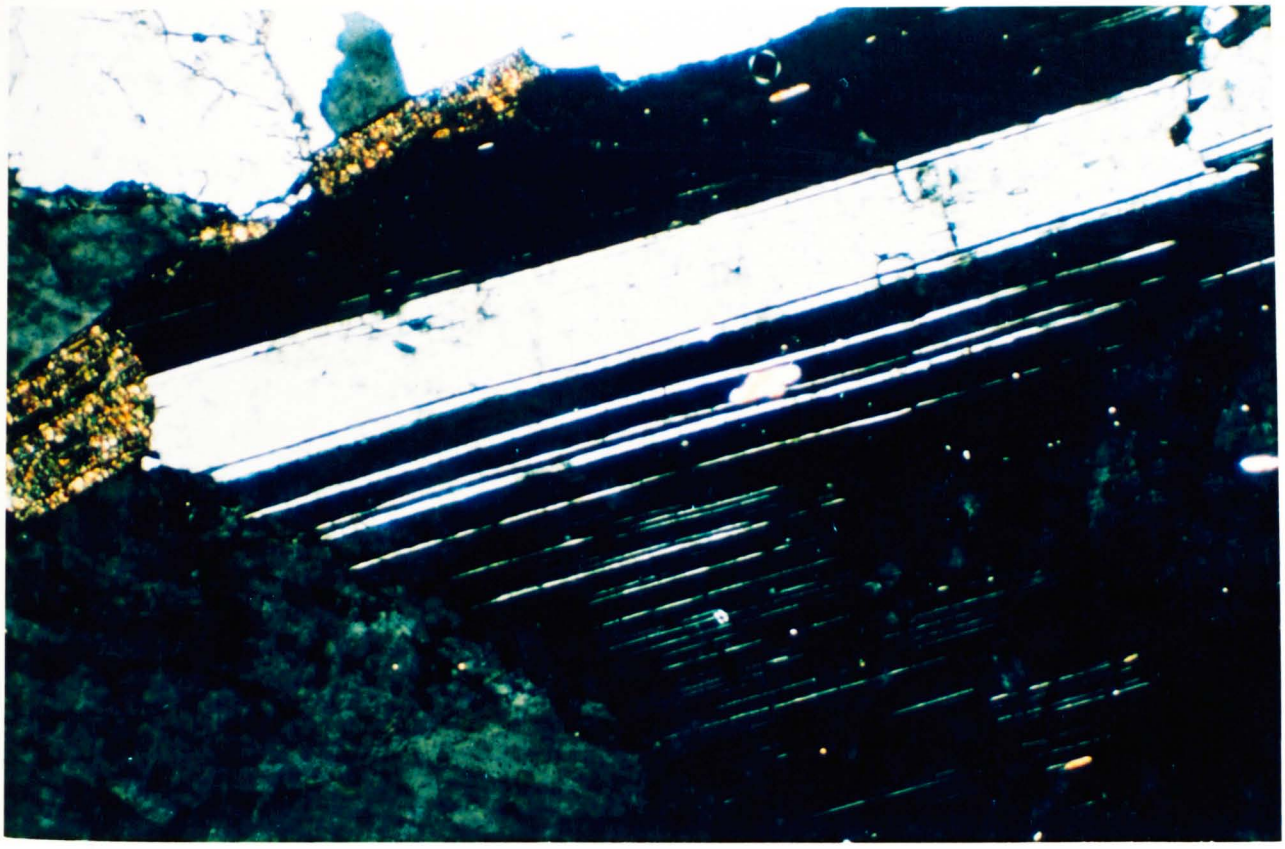

Plate 77 - F485G - Albite showing minimal exsolution of K-feldspar (XPL, x 125)

Plate 78 - F485G - Orthoclase perthite (XPL, x 125)

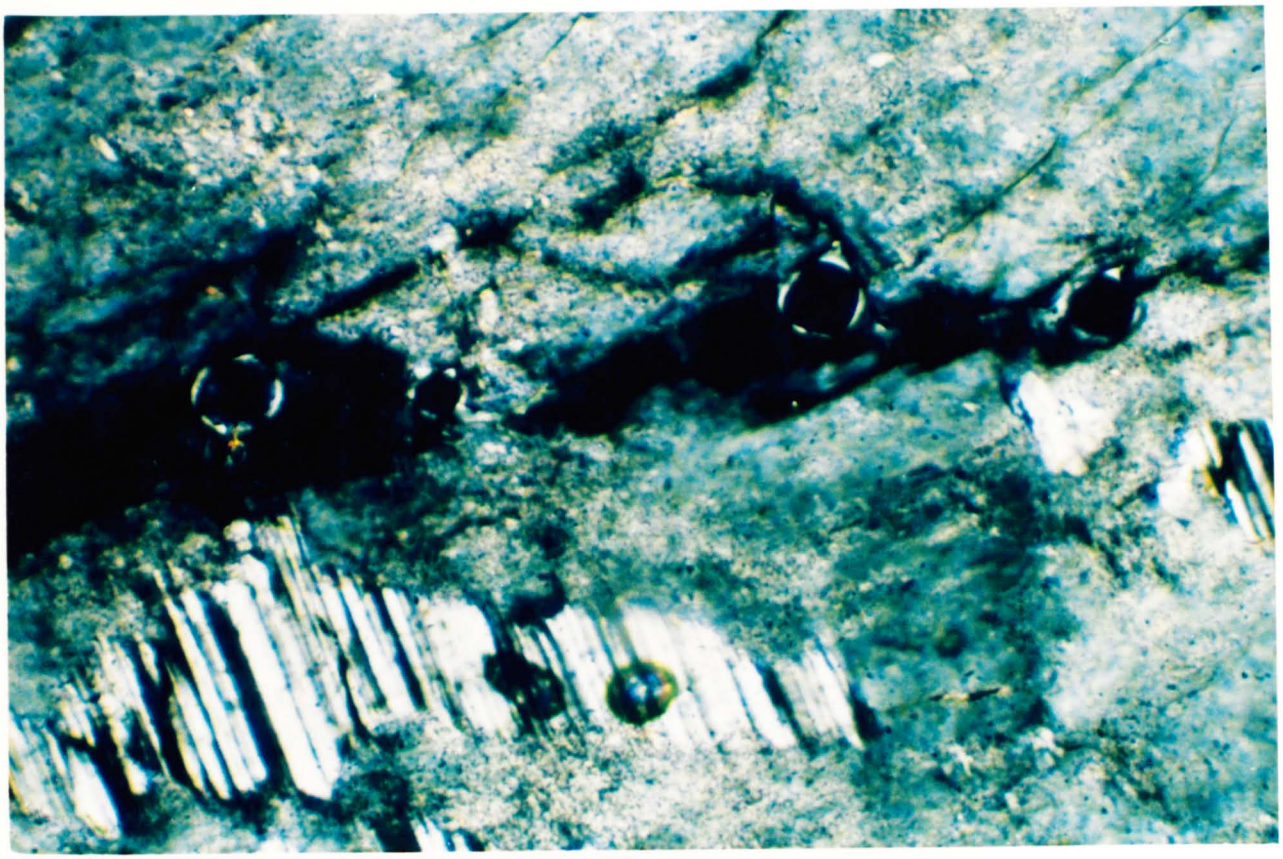

Plate 79 - F485G - Plate 78 at scale x 50. Albite twins are clearly visible

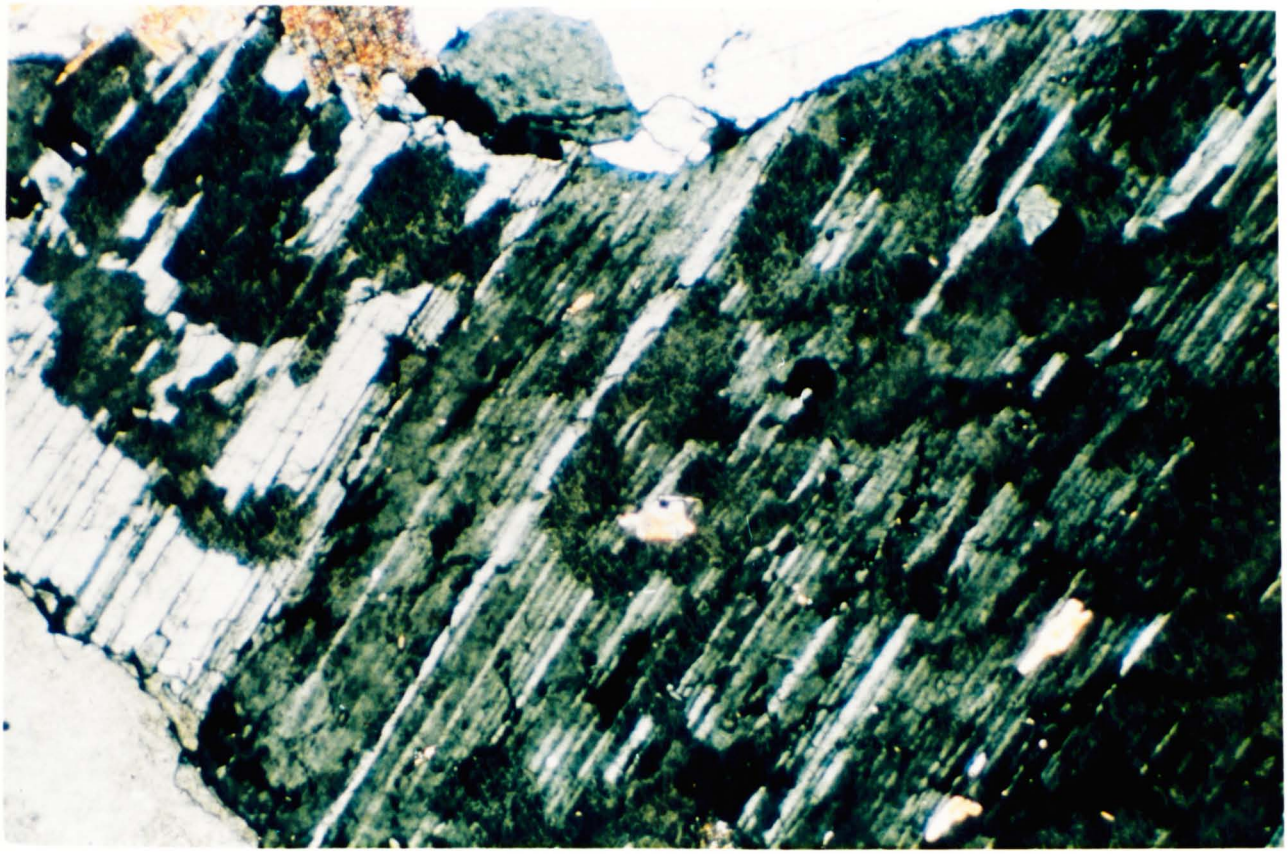

Plate 80 - F485G - Albite antiperthite (XPL, x 62.5)

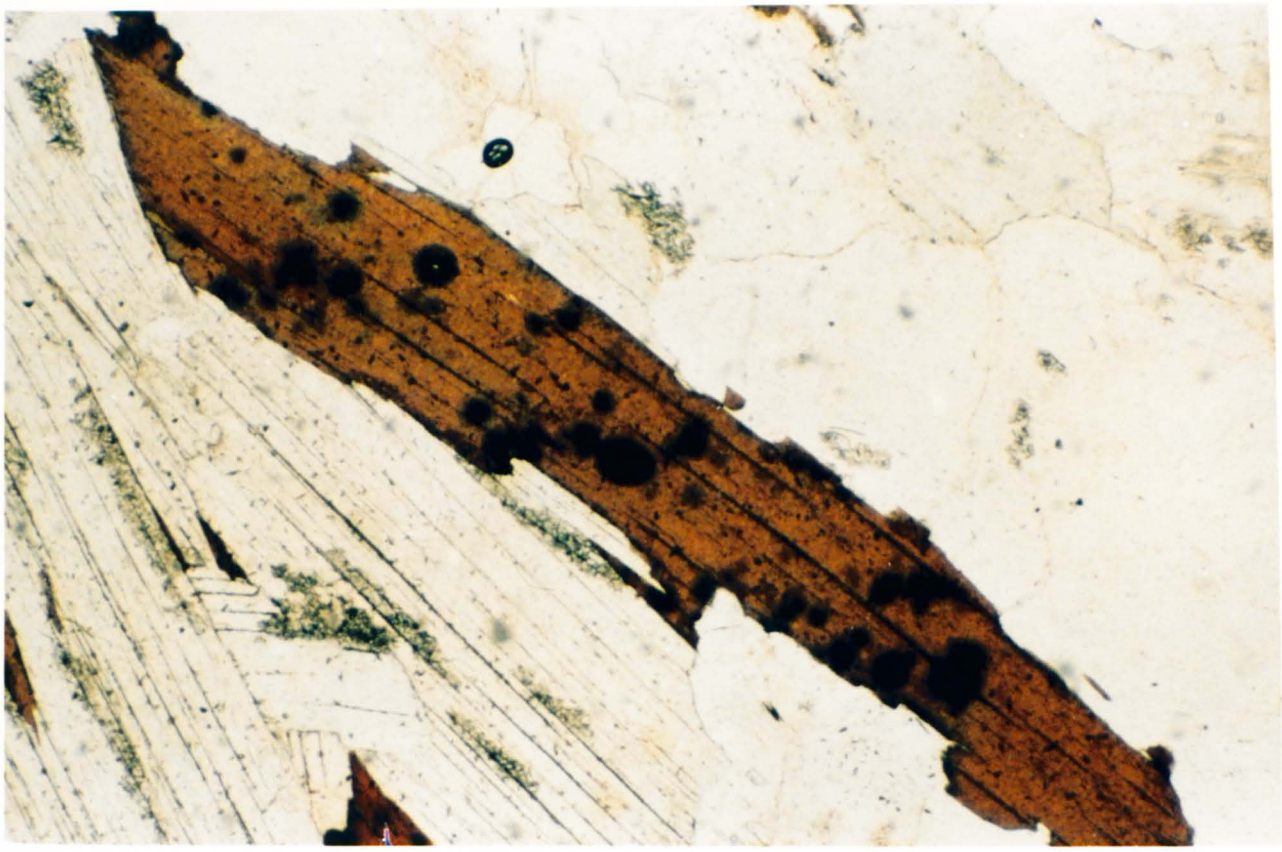

Plates 81 & 82 - F485G - Subhedral biotite with numerous decay haloes aligned NW/SE in the field of view (Plate 81, PPL; Plate 82, XPL) associated with muscovites in lower left of field of view. Quartz and orthoclase comprise the remainder of the photograph (x 62.5)

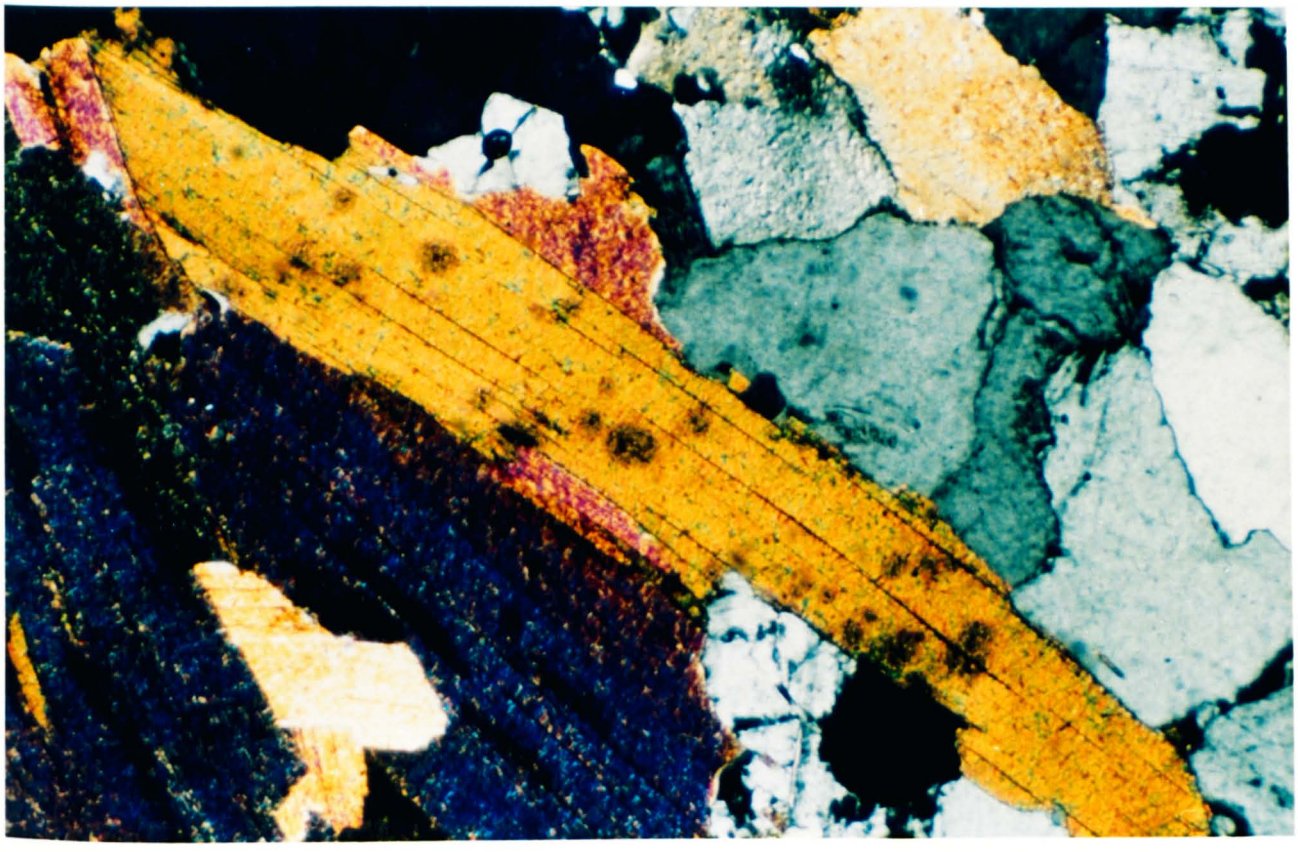

the crystal must (i) have relatively coarse grain size, comparable to obvious primary phases; (ii) be clearly terminated with sub or euhedral form; (iii) not be enclosed by, or raggedly enclose, any mineral of which muscovite is a possible alteration product; (iv) be in a rock with an unaltered igneous texture. It is apparent from these criteria that the several forms of muscovite seen in F485G can be interpreted as representing both primary and secondary growth.

(i) Euhedral often equidimensional grains are interpreted as magmatic. Some of these are as large as 4 mm x 2 mm, but most have lengths of around 2 mm. These frequently show features attributed to post-magmatic deformation including kinking of cleavage (Plates 83), crystal fracturing, and grain boundary recrystallization, notably the development of frayed margins which often suggest later rotation due to shear.

(ii) Smaller narrow crystals, thought to be post-magmatic are commonly seen (a) aligned along grain boundaries defining a weak fabric (Plate 84), (b) as needle-like inclusions within orthoclase or, more commonly, albite (Plate 85). Generally, muscovite crystals are larger than biotite and are modally more abundant.

Accessories - zircon shows characteristic decay halos in biotite (Plates 81 & 82); apatite is quite abundant and usually is enclosed in feldspar or muscovite. Most are large (up to 0.75 mm) and generally have corroded cores and embayed margins (Plate 86). Opaque oxides such as ilmenite or magnetite are noticeable only by their absence.

In the southern limb, a common crude alignment of phyllosilicates is interpreted as representing a magmatic flow fabric initiated as the viscous magma was intruded into the shear system. Moving across the axial

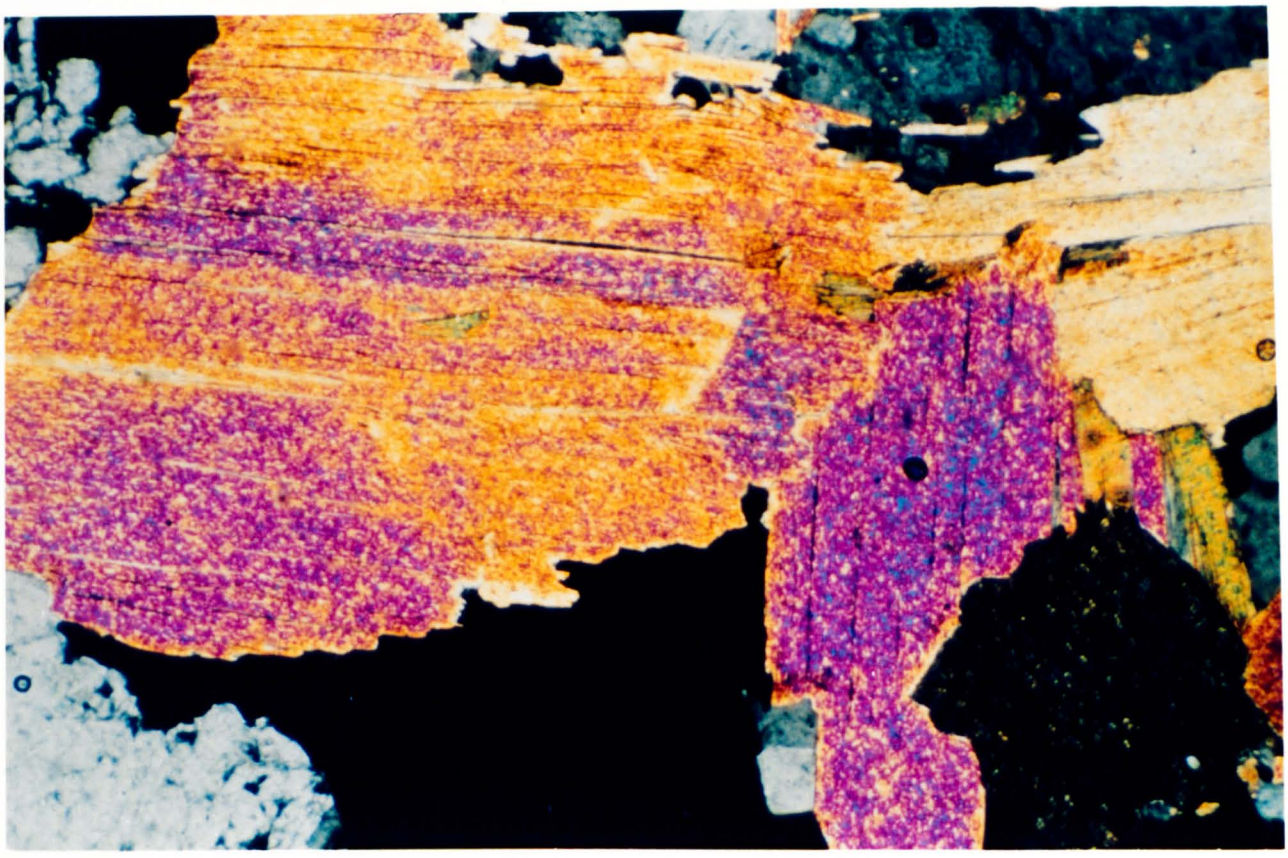

Plate 83 - F485G - Subhedral equidimensional muscovite, thought to be magmatic. The large crystal centre left of the field of view shows some kinking of cleavage, attributed to post-magmatic deformation (XPL, x 62.5)

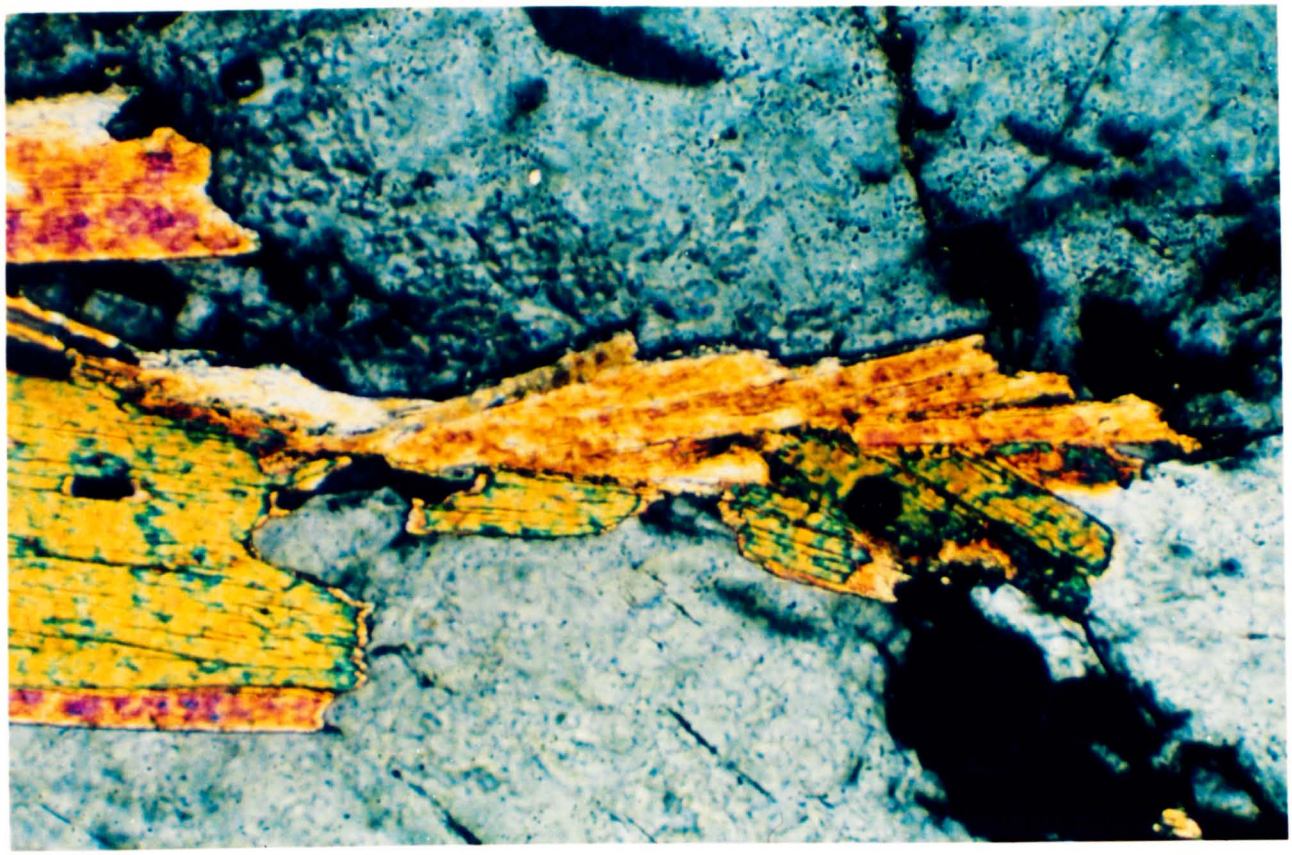

Plate 84 - F485G - Narrow bladed muscovites aligned between two orthoclase crysta are thought to be post-magmatic (XPL, x 250)

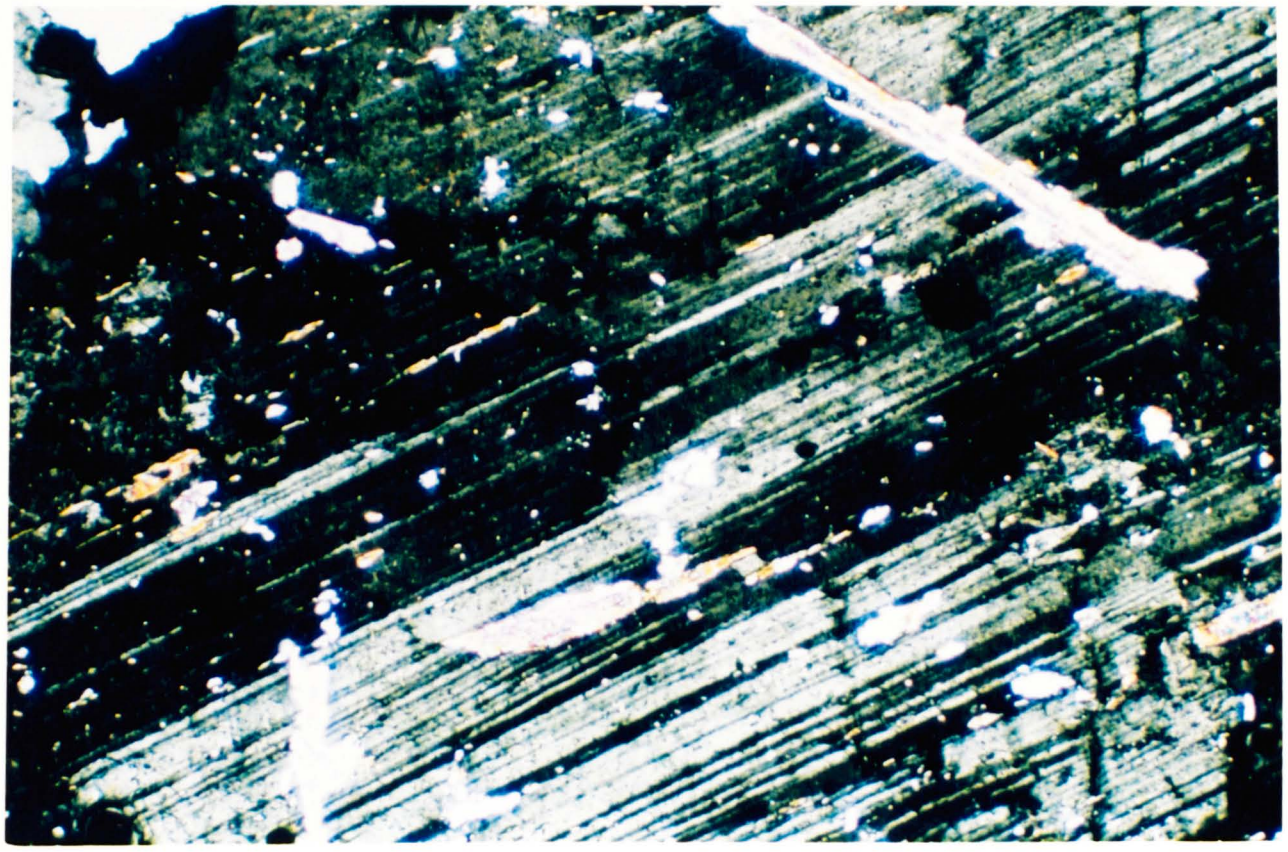

Plate 85 - F485G - Needle-like inclusions of muscovite in albite may be replacive (XPL, x 250)

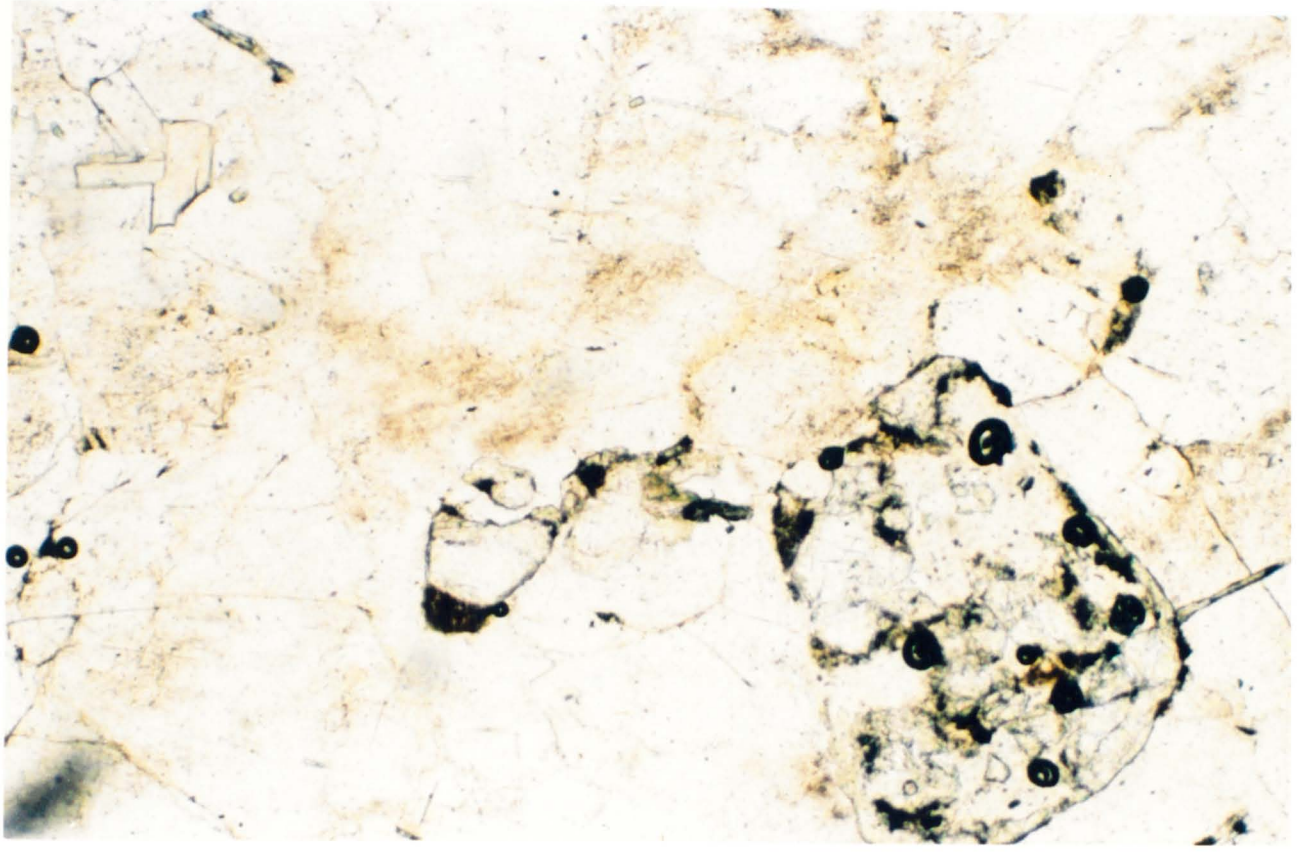

Plate 86 - F485G - Large anhedral apatite with corroded core in lower right of field of view (PPL, x 125)

zone into the steep belt of the pluton, the main fabric represented is increasingly one produced by deformation of the consolidated mass, though still at high temperature as ductile structures predominate.

F4133G (GR 6170 2450) from the northern limb shows a protomylonite fabric (Plate 87). Primary muscovite shows "fish" structures rotating back in the sense of shear (sinistral) with substantial recrystallization along the margins (Plate 88). The C surfaces of this type II C-S mylonite are defined by trails extending across the section linking the mica fish (Plates 89 & 90). These often correspond with narrow zones in which quartz shows intense grain size reduction and annealing, i.e. zones of intense shear strain.

(A-2) - Sheared Granite - Field Relations

The NE part of the intrusion in the area studied is of a much coarser facies in which feldspars reach a size of 1 cm, distinct enough from the main granite to be mapped as a separate unit. The contact relations between the two facies are obscured by a major swarm of aplite sheets which are concentrated along this zone, running SE from the 1053 m summit of Vidoeiro to the Ribeiro de Abundancia. This line is marked topographically, but there is no field evidence of a faulted contact.

This part of the intrusion lies in the locus of the prolonged sinistral shear movements which produced the C-S fabric in the northern limb. The coarser grain size of this facies means that the sheared fabric is much more distinct than in the corresponding main granite, therefore "sheared granite" was introduced as a field term (Plates 91 & 92).

(A-2) - Sheared Granite - Petrography

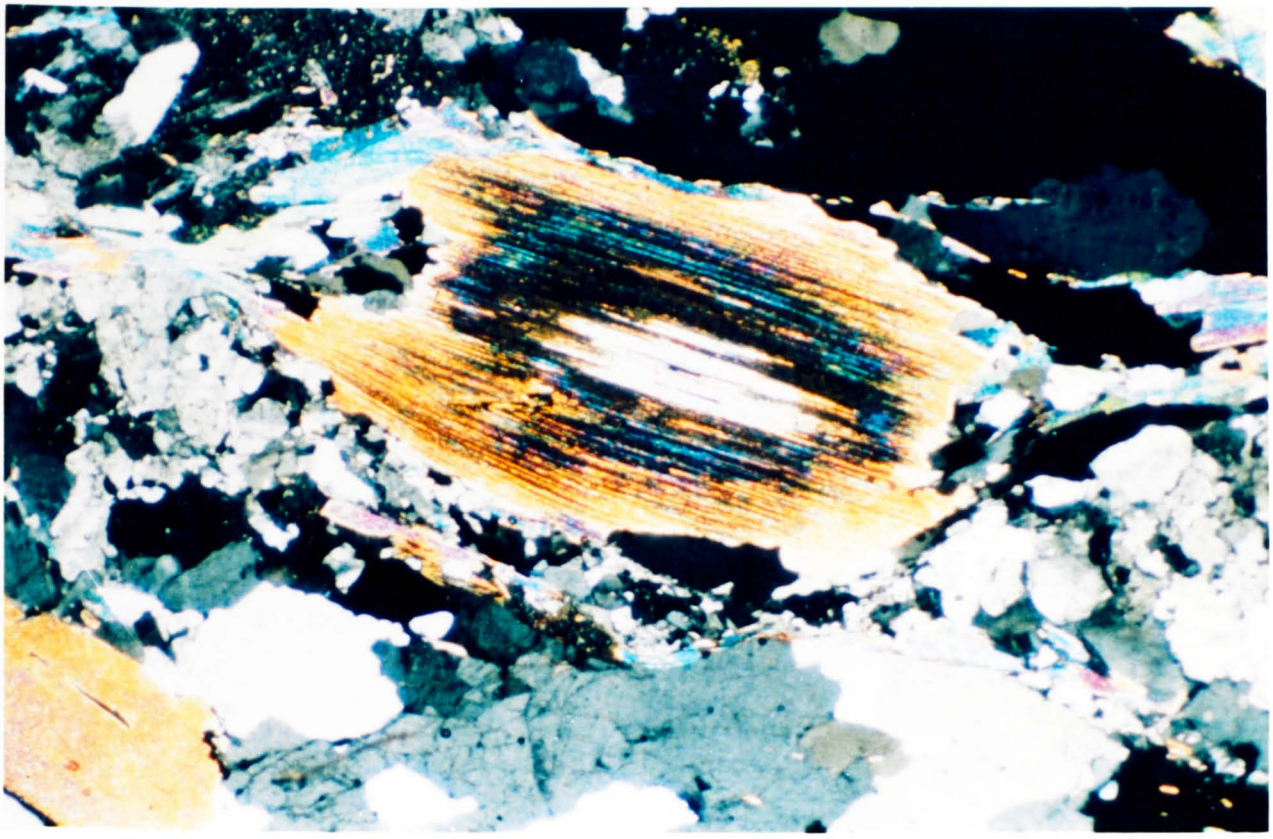

Plate 87 - F4133G, (GR 6170 2450), main granite from the northern limb. Large muscovite "fish" is rotated giving sinistral sense of shear. Recrystallization along the margins is apparent, one zone of high strai (C plane) in which quartz and feldspar recrystallize runs across the field of view (XPL, x 31.25) Centre of muscovite may be sillimanite

Plate 88 - F4133G - Hand specimen, compare with Plate 74

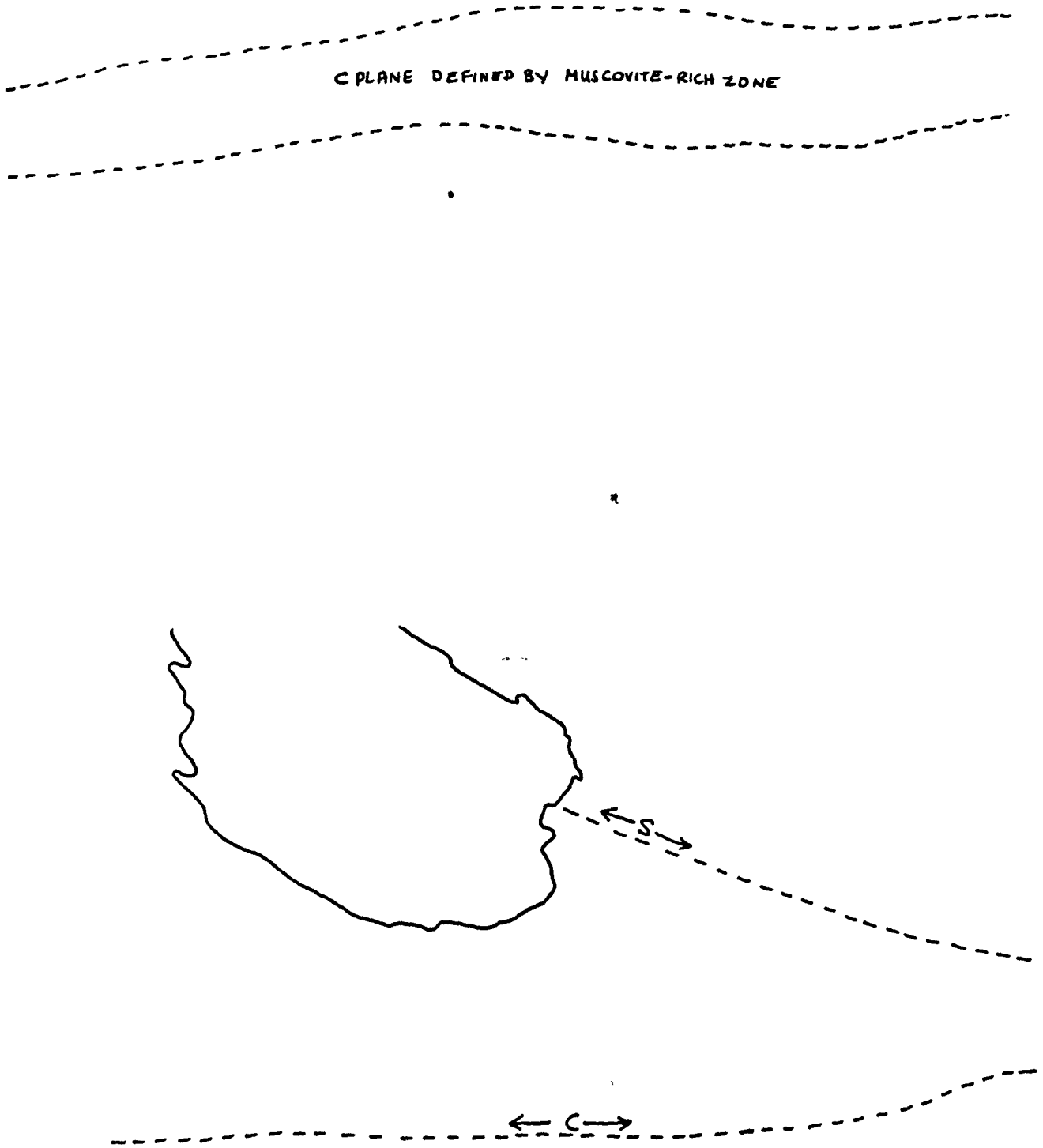
C PLANE DEFINED BY MUSCOVITE-RICH ZONE
S
C

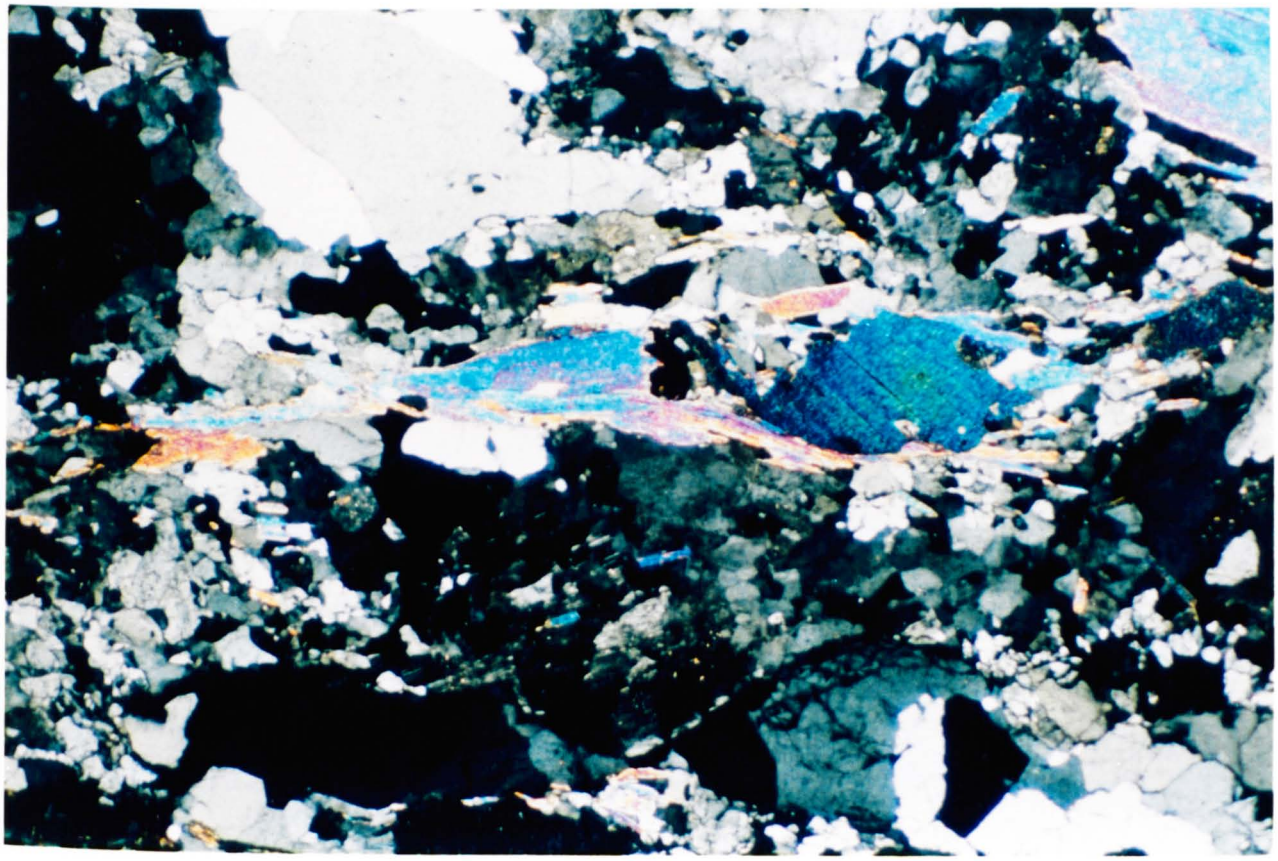

Plates 89 & 90 - F4133G - C planes defined by thin micaceous zones approximately W/E in the field of view, associated with intense recrystallization of quartz and feldspar. In Plate 90, large rotated muscovite defines original S plane (XPL, x 31.25)

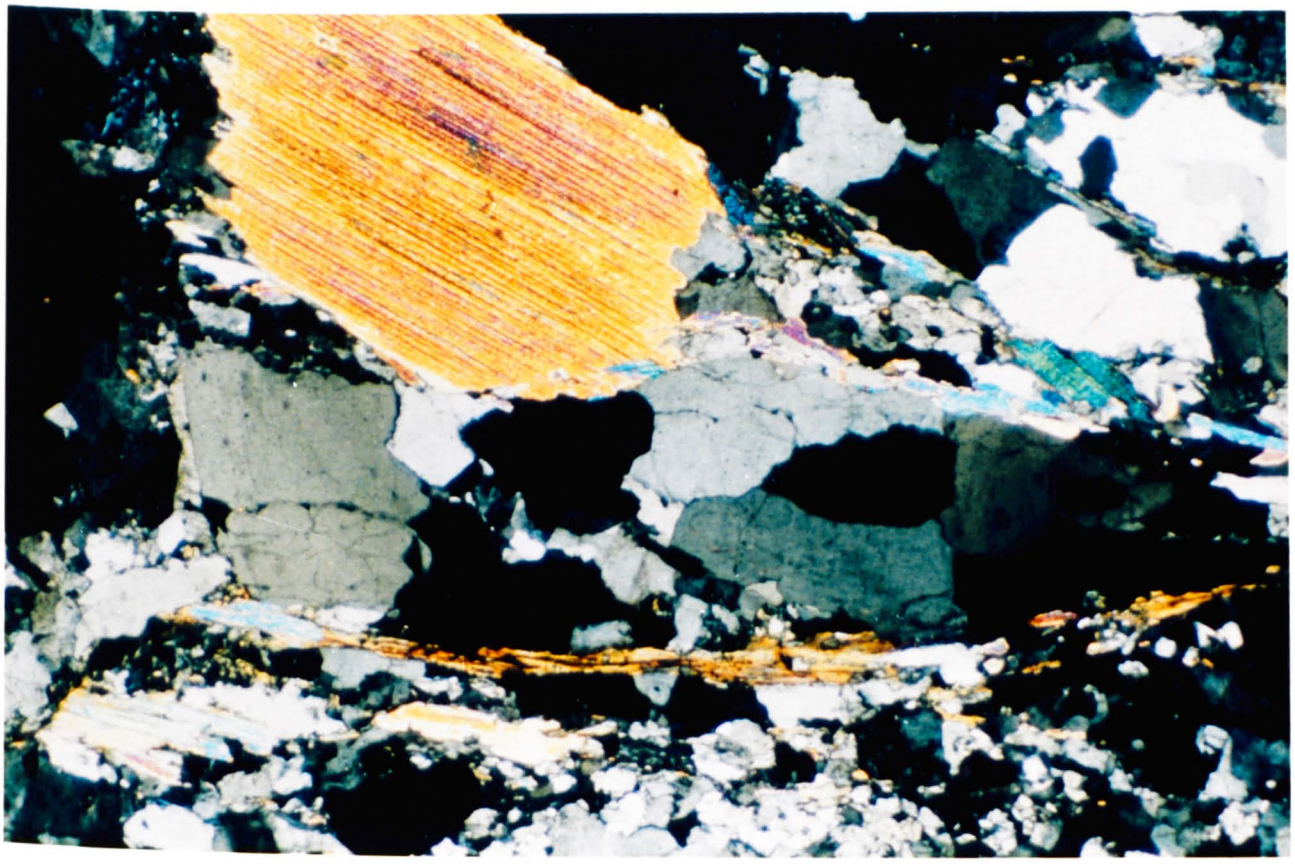

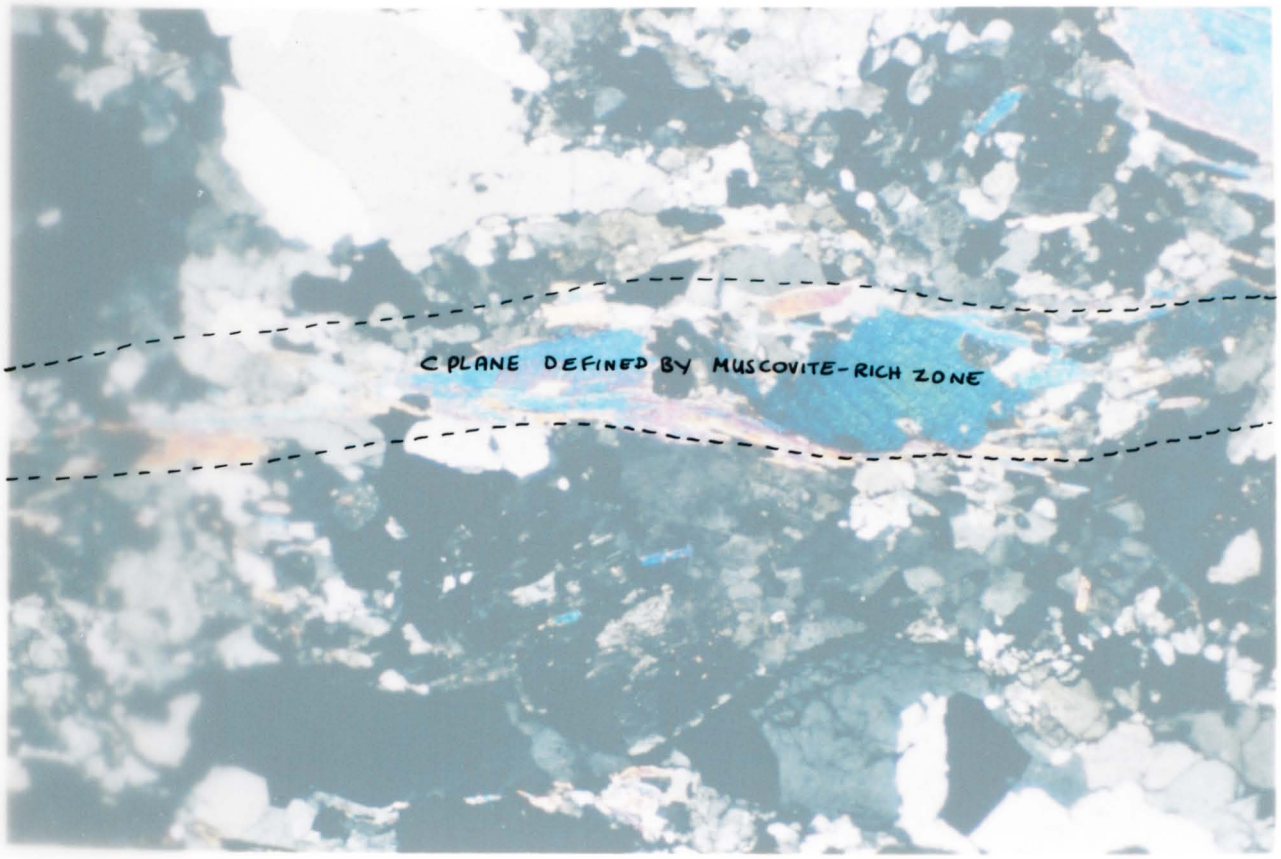

Plates 89 & 90 - F4133G - C planes defined by thin micaceous zones approximately W/E in the field of view, associated with intense recrystallization of quartz and feldspar. In Plate 90, large rotated muscovite defines original S plane (XPL, x 31.25)

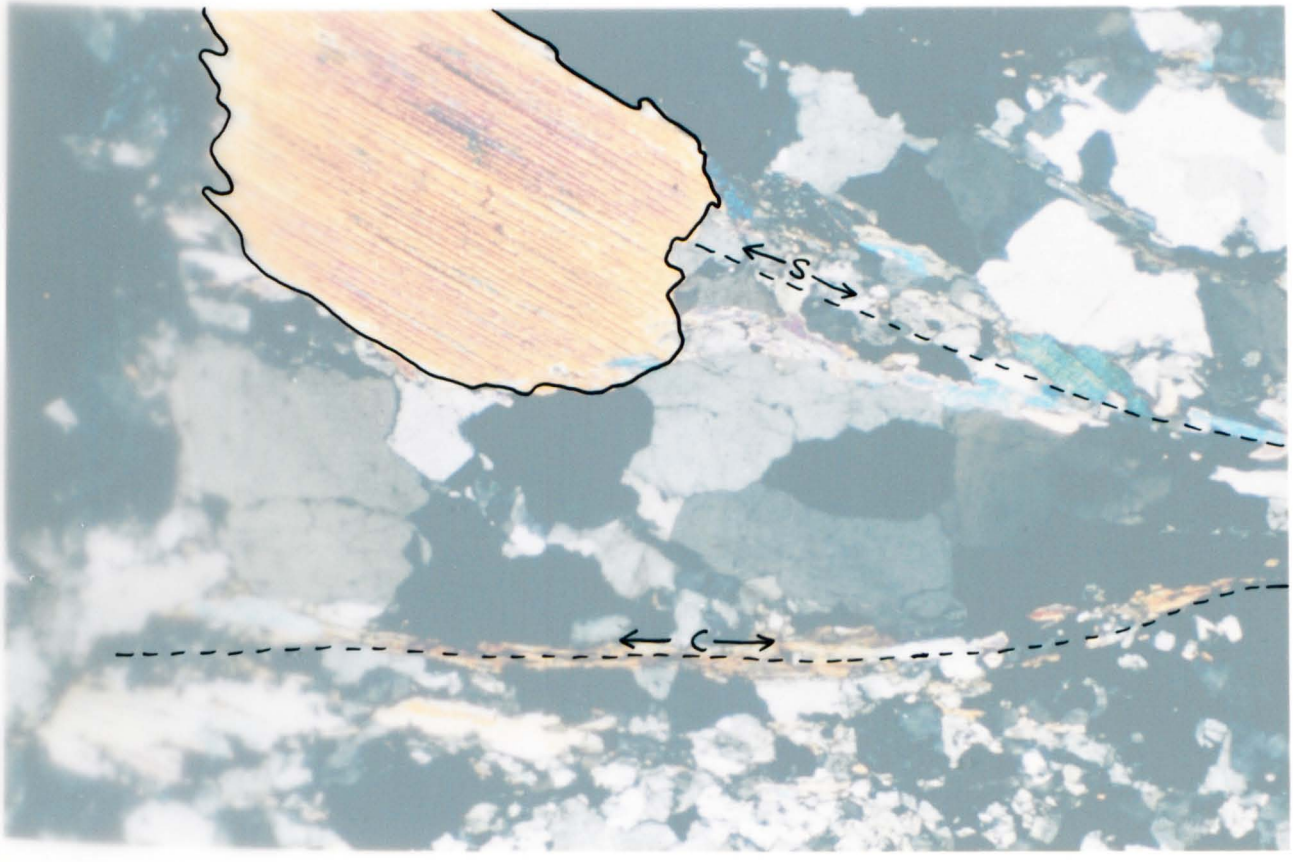

Plate 91 - Field photograph of sheared granite (GR 6470 2420). Pen is parallel to original S plane

Plate 92 - Hand specimen of F441G (GR 6527 2383), sheared granite

Sections examined of this facies show very similar petrography to the medium-grained granite. The mineralogy consists of quartz, albitic plagioclase, orthoclase, biotite, and muscovite; apatite and zircon are present as accessories. The feldspars commonly contain randomly orientated needles, thought to be sillimanite (Plate 93). Microcline perthite is more abundant (Plate 94) than in the medium grained granite but is still subordinate to orthoclase perthite.

In the field S2 and S2a are readily mapped especially where feldspars up to 1 cm diameter are wrapped. However this C-S fabric is too coarse to be well represented in thin section; it is present but is not as marked as at outcrop (Plates 95 & 96). In F441G (GR 6527 2383) it is less easy to distinguish between primary and secondary mica. Certainly a tectonic fabric now completely overprints any relics of magmatic flow. Along C surfaces, a recrystallized residue of quartz, feldspar and mica diplays a finer grain size than average for the rock. Between C surfaces the grain size is generally close to that of the original granite, but quartz in these zones shows undulatory extinction. Overall the texture, both in outcrop and thin section is more that of a gneiss than a granite.

The exact nature of this coarse unit is not well understood. However if the junction between the sheared and main granite is extrapolated on to the smaller scale of Sheet 13-D, it is apparent that the width of the intrusion would be more uniform if the coarse grained facies were absent. This strongly suggests that the 2 facies are separate pulses; the coarser grained type may represent a batch of magma intruded within the Serra da Freita shear zone system before the main granite. This leads to the idea that the intrusion of the Serra da Freita pluton was not one simple event,

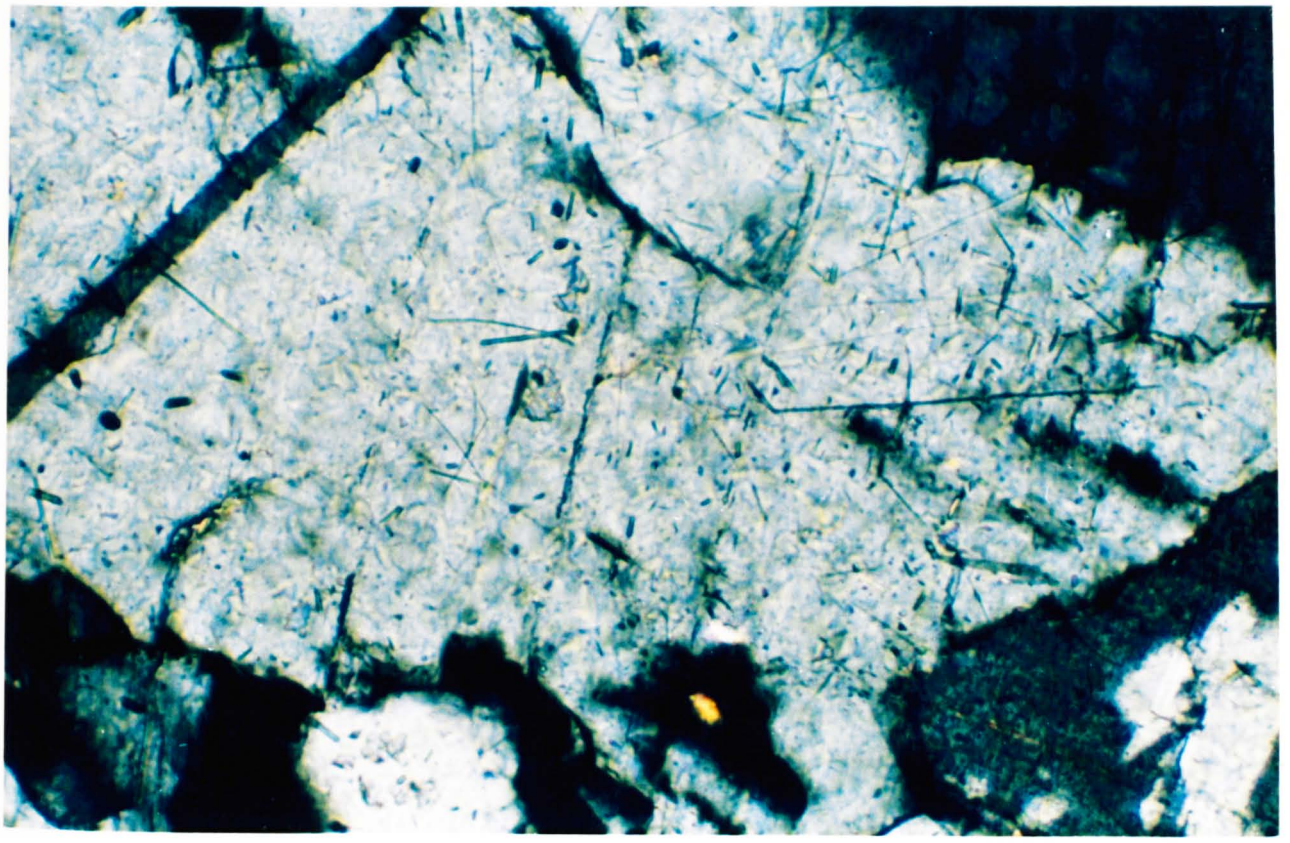

Plate 93 - F441G - Sillimanite? needles in orthoclase (XPL, x 250)

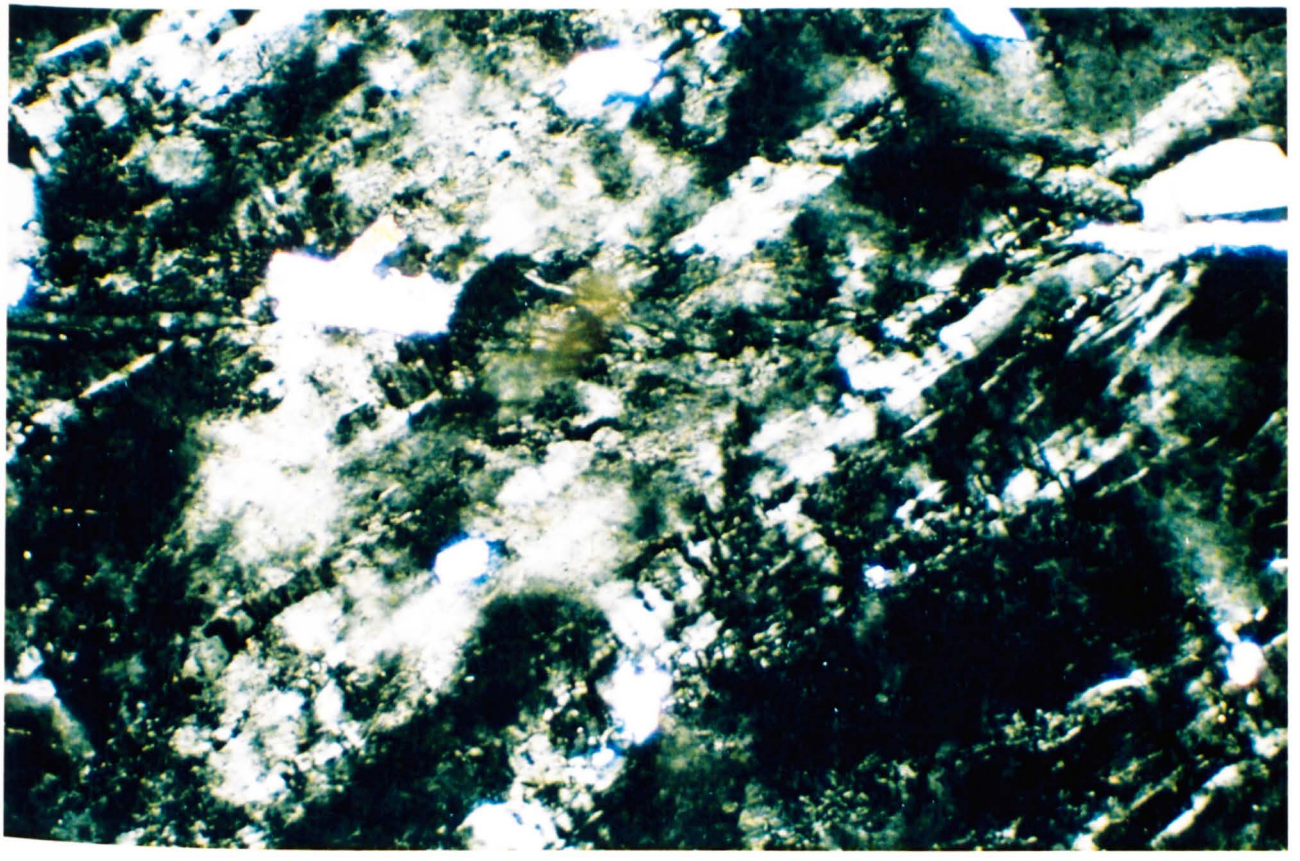

Plate 94 - F441G - Microcline perthite (XPL, x 125)


S


C

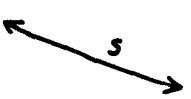
S

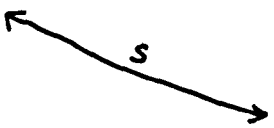
S

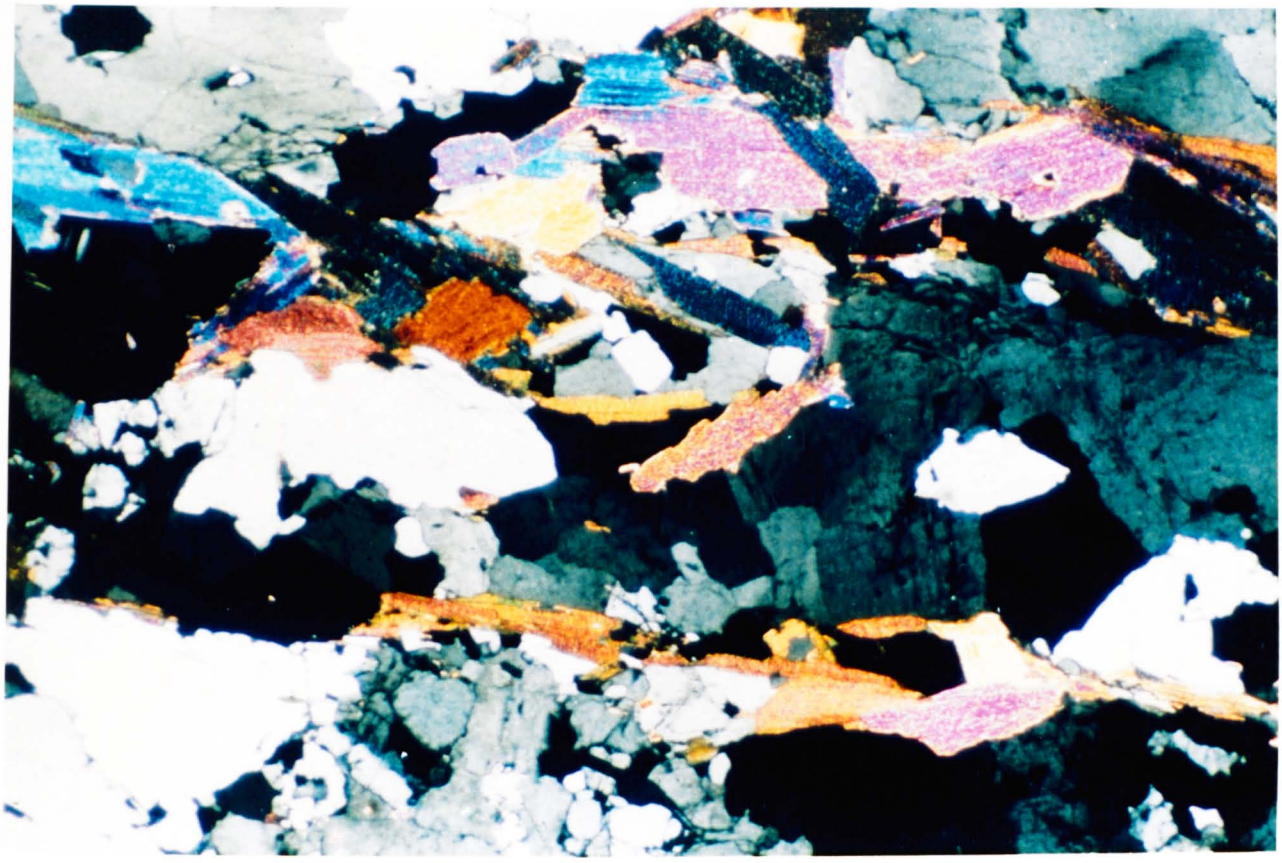

Plates 95 & 96 - F441G - C-S fabric in the sheared granite. These two photograp
show C planes across the field of view, however in Plate 96, a
possible S plane is highlighted. The sense of shear is sinistr
(XPL, x 31.25)

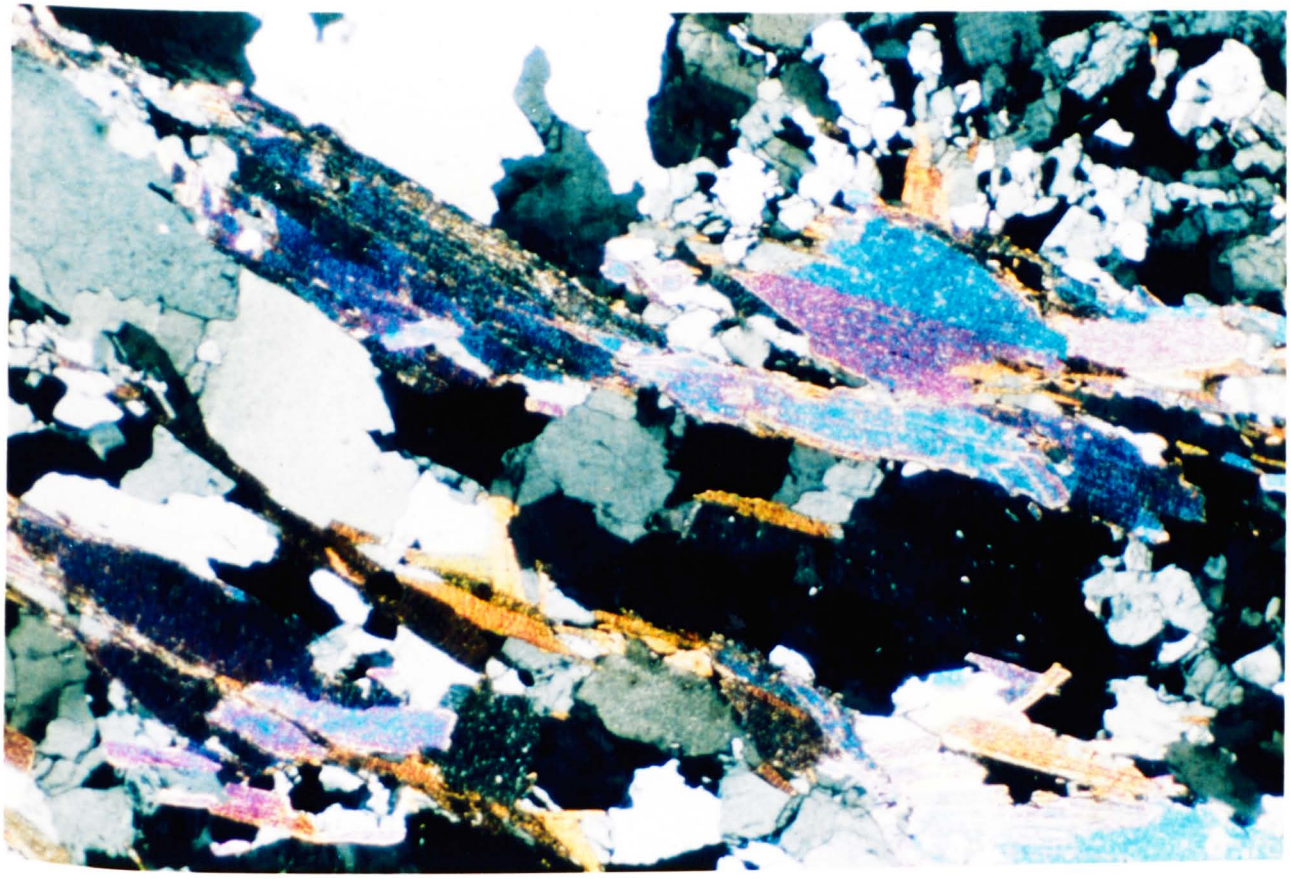

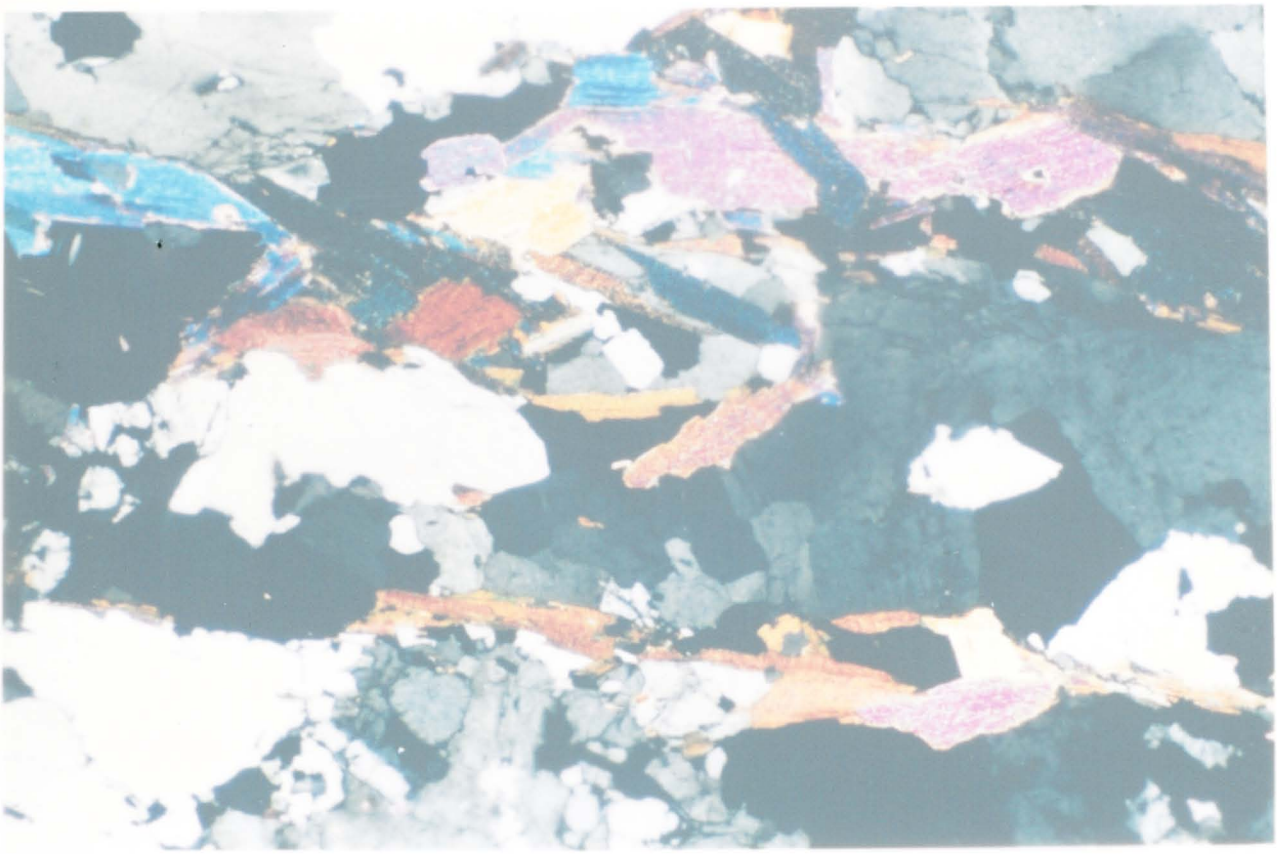

Plates 95 & 96 - F441G - C-S fabric in the sheared granite. These two photograp
show C planes across the field of view, however in Plate 96, a
possible S plane is highlighted. The sense of shear is sinistr
(XPL, x 31.25)

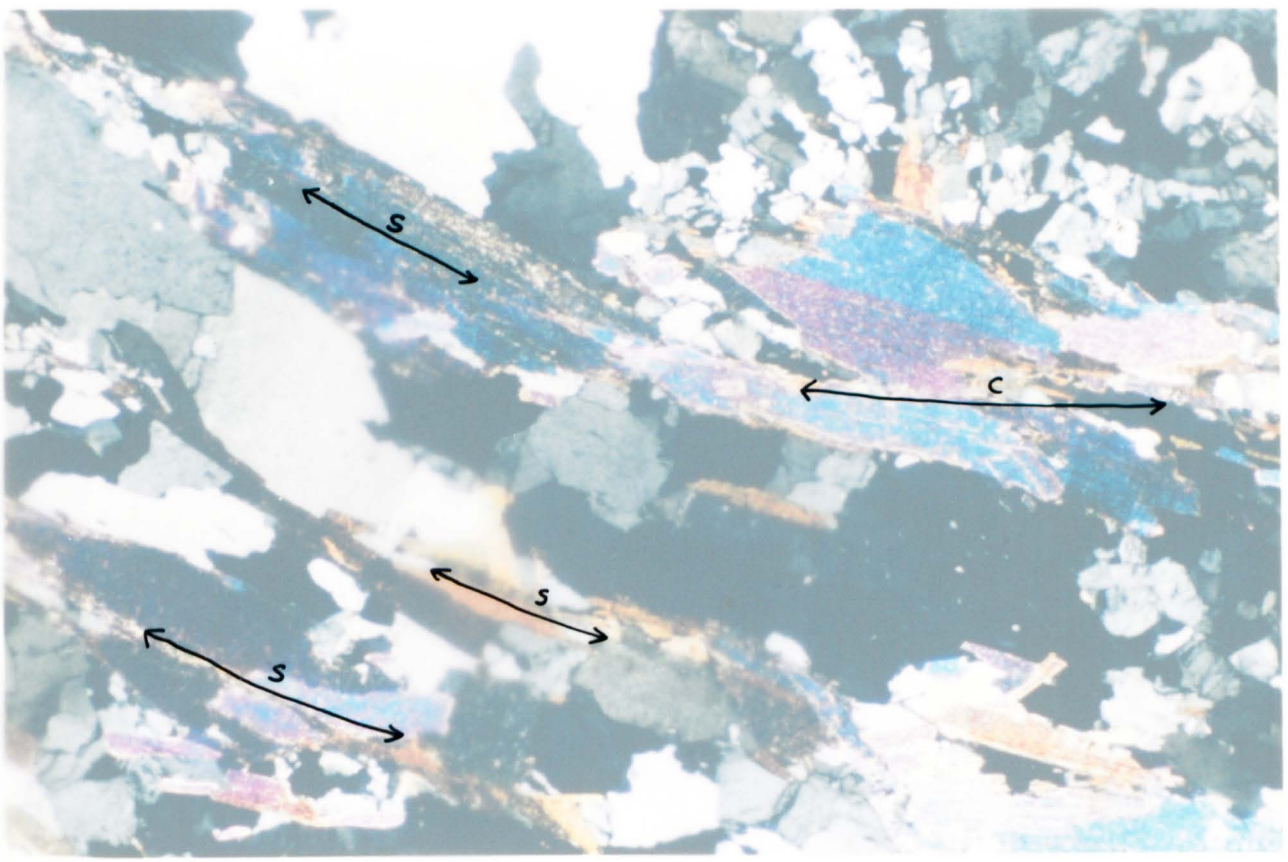

but a series of discrete pulses injected within the shear system.

(A-3) - Microgranite - Field Relations

Numerous sheets of microgranite intrude the medium-grained granite around and SE of Serlei. The average grain size of this facies is 2 mm and it is mineralogically similar to the main granite. Most of these bodies are 300-400 m long and some 40-60 m wide; the largest can be mapped from near the summit of Serlei as far as Gestoso and is approximately 700 m by 150 m in extent. Immediately west of the Gestoso track, a zone of small scale sheeting occurs over a distance of 1 km. In this zone, some 30-35 sheets of microgranite alternate with the main granite, each sheet being less than 2 m across (Plates 97 & 98).

(A-3) - Microgranite - Petrography

Most of the samples of these sheets are strongly deformed, however F4138G (GR 6370 2280) is not and shows a magmatic inequigranular texture (Plates 99 & 100). The mineralogy is: quartz, plagioclase, orthoclase, biotite, and muscovite with accessory apatite and zircon. The inequigranular texture is not caused (in F4138G) by deformation and grain size reduction as seen previously. The largest crystals are of anhedral orthoclase and quartz which reach sizes of 2 mm, but most are between 1 and 2 mm. Perthite is very rare, only present as ca.5% of feldspars of this grain size. The anhedral nature of these minerals could be produced by resorption of early formed phases. A finer grained groundmass in which the average crystal size is between 0.25 and 0.5mm is composed of quartz, albite/sodic oligoclase and orthoclase. Perthite is absent from these feldspars which are generally subhedral (Plate 101).

Micas- subhedral equidimensional muscovite crystals of between 1 and 2 mm are quite common and can be regarded as equidimensional with the larger

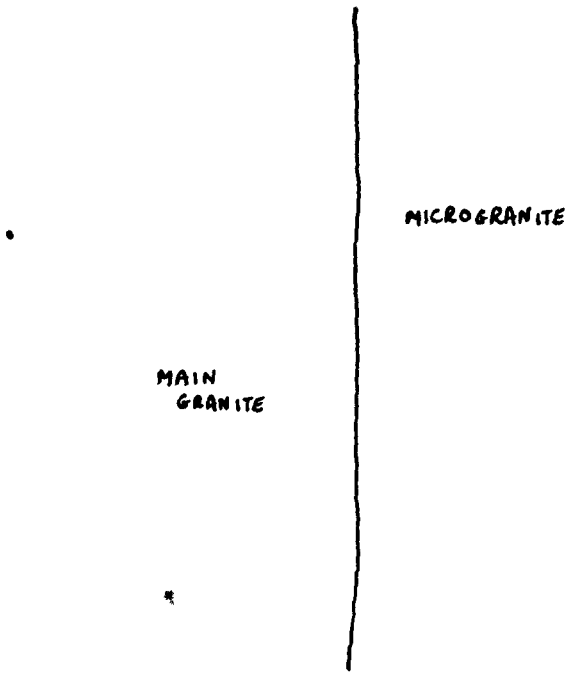
MICROGRANITE
MAIN
GRANITE

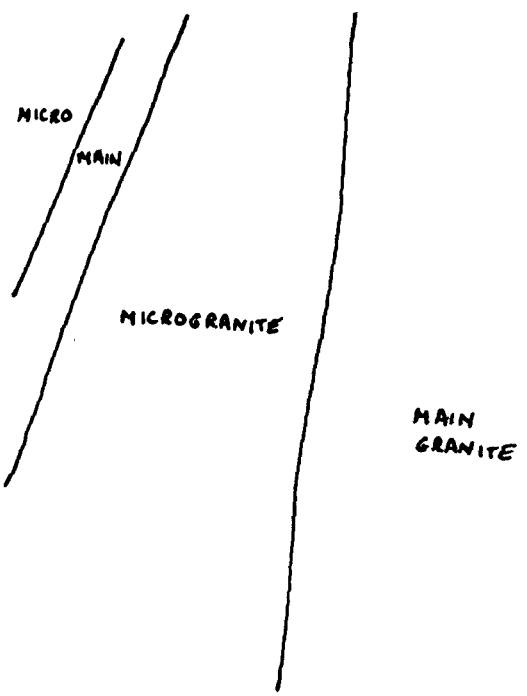
MICRO
MAIN
MICROGRANITE
MAIN
GRANITE

Plates 97 & 98 - Small scale sheeting of microgranite within the main granite facies, west of the Gestoso track

Plates 97 & 98 - Small scale sheeting of microgranite within the main granite facies, west of the Gestoso track

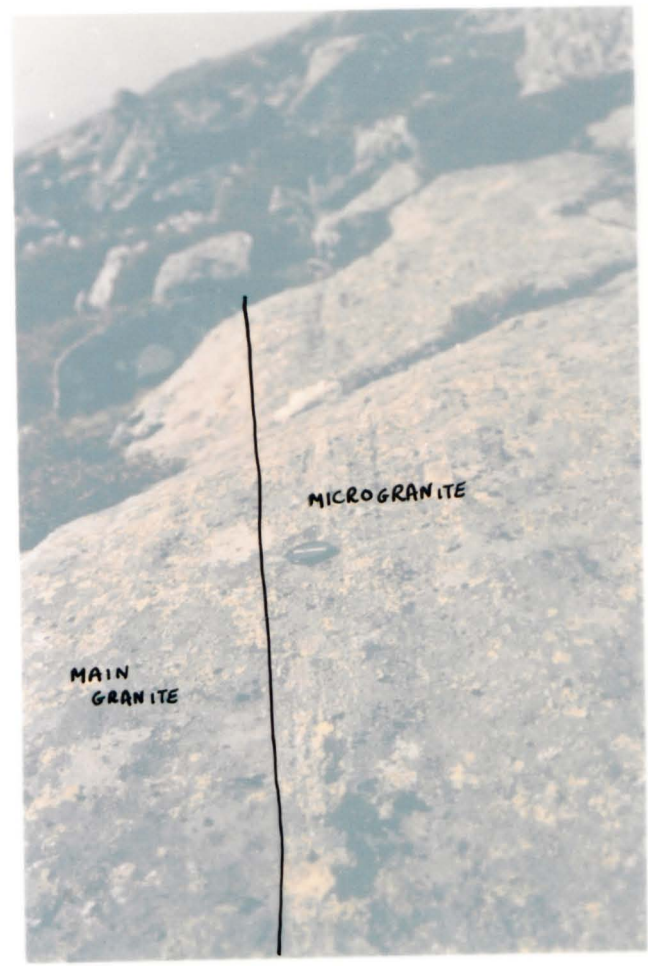

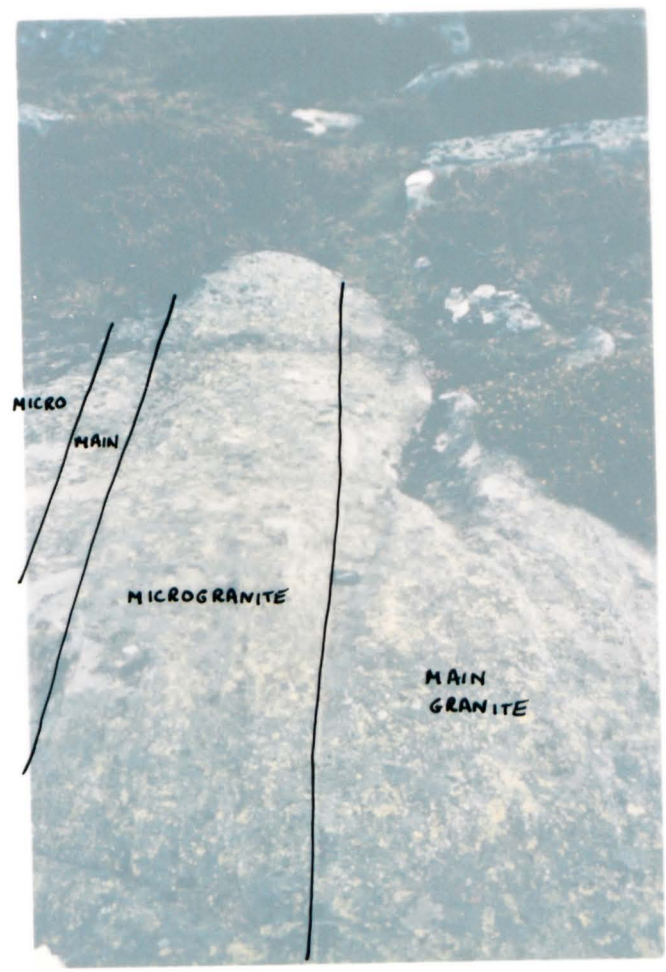

Plate 99 - Hand specimen of F4138G (GR 6370 2280), microgranite

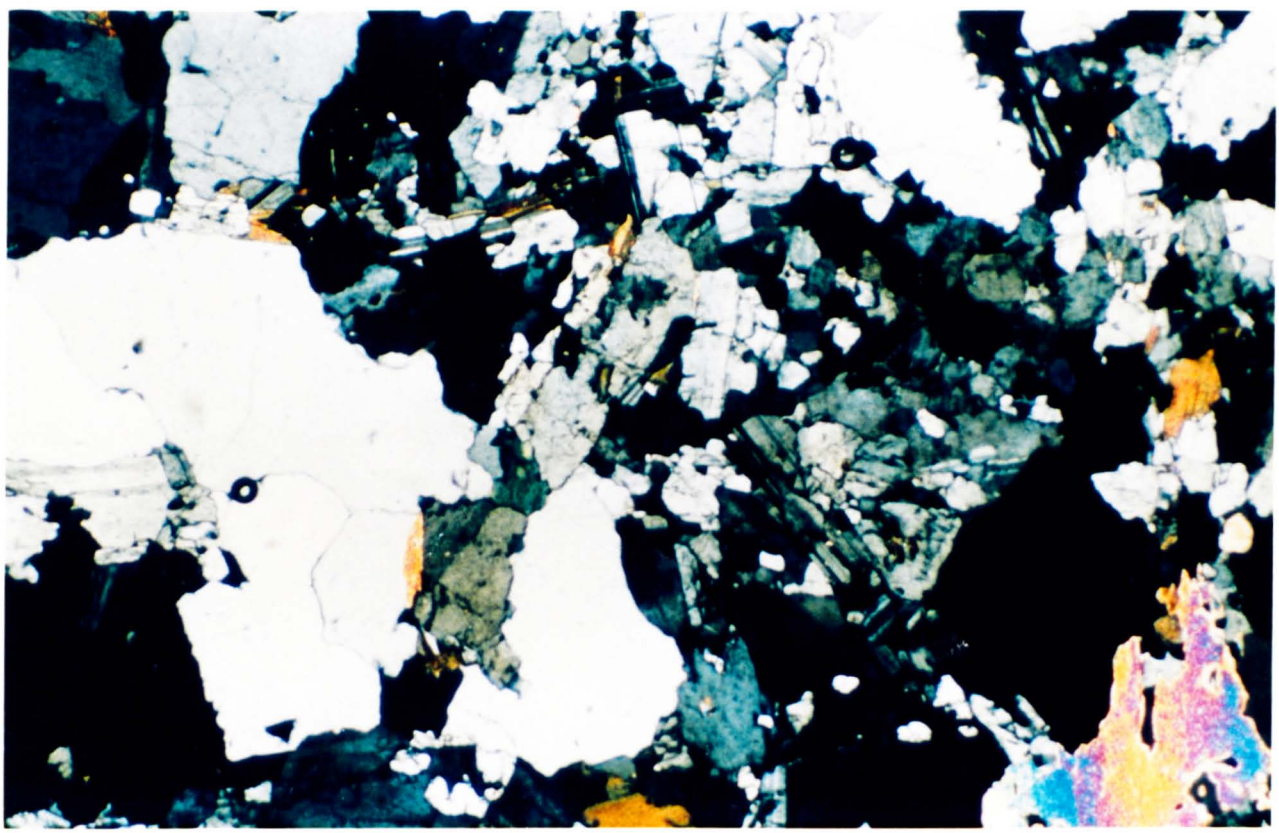

Plate 100 - F4138G - Magmatic inequigranular texture. Much of the upper centre of the field of view consists of quartz and feldspar of comparatively finer grain size than the rest of the rock. Discussion in text (XPL, x 31.25)

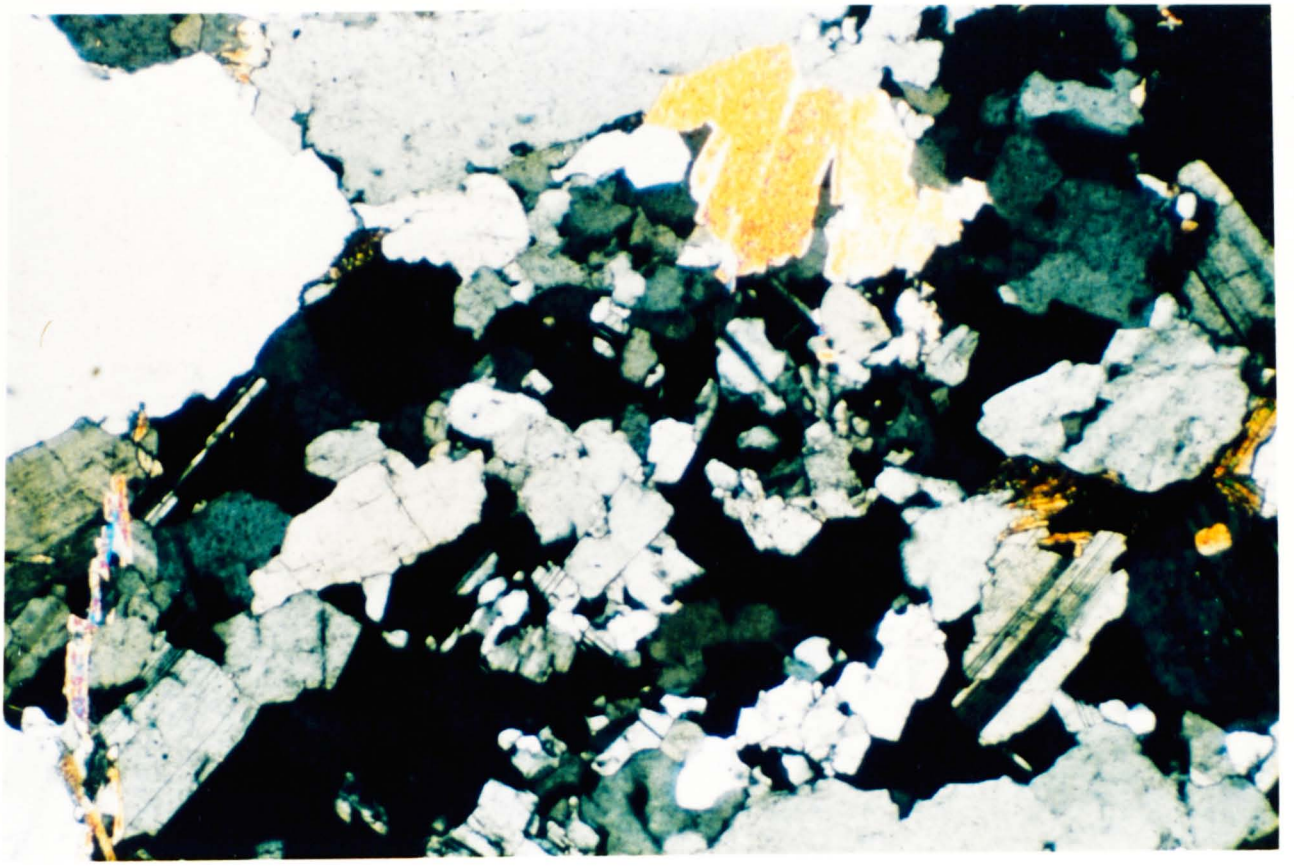

Plate 101 - F4138G - Fine grained groundmass of quartz, plagioclase and orthoclase (XPL, x 62.5)

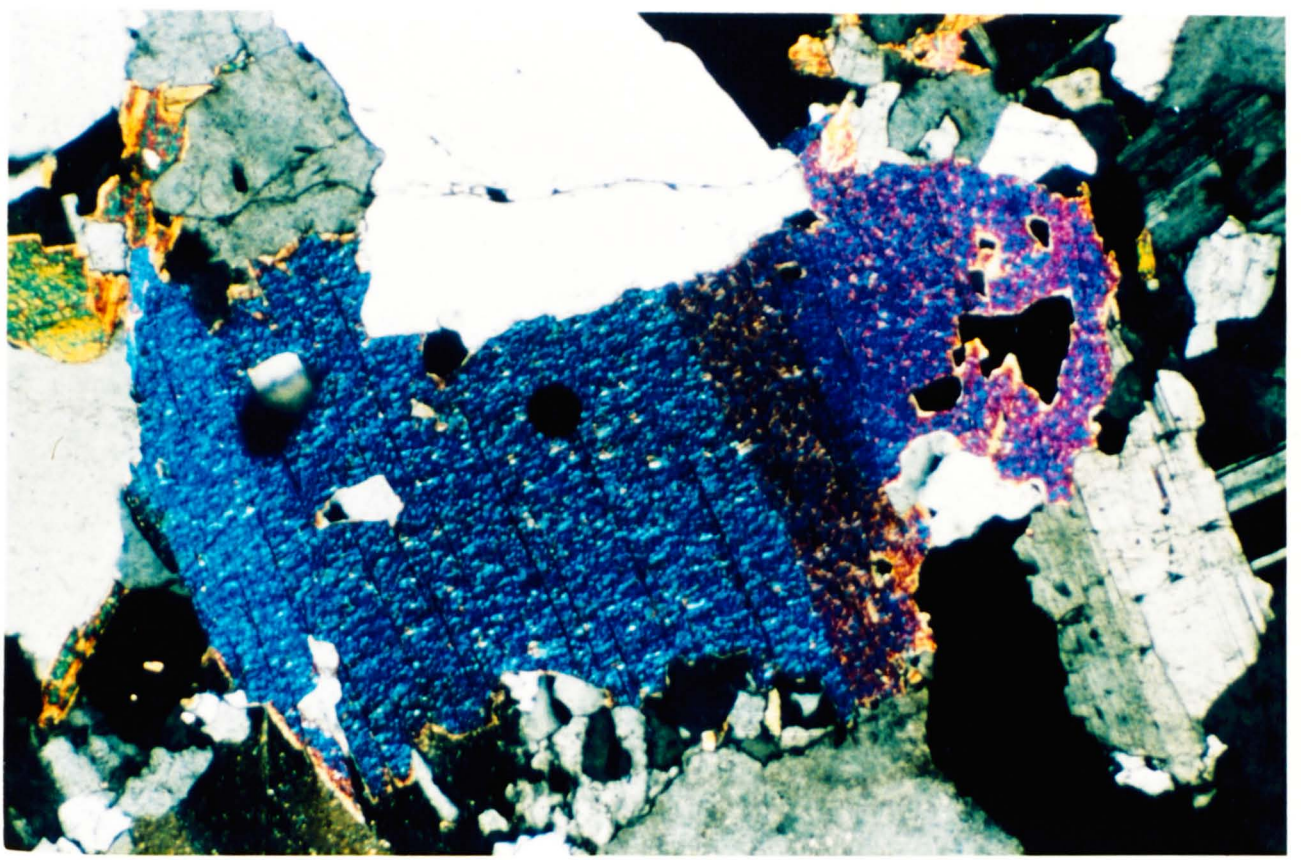

Plate 102 - F4138G - Magmatic? muscovite showing embayments (XPL, x 62.5)

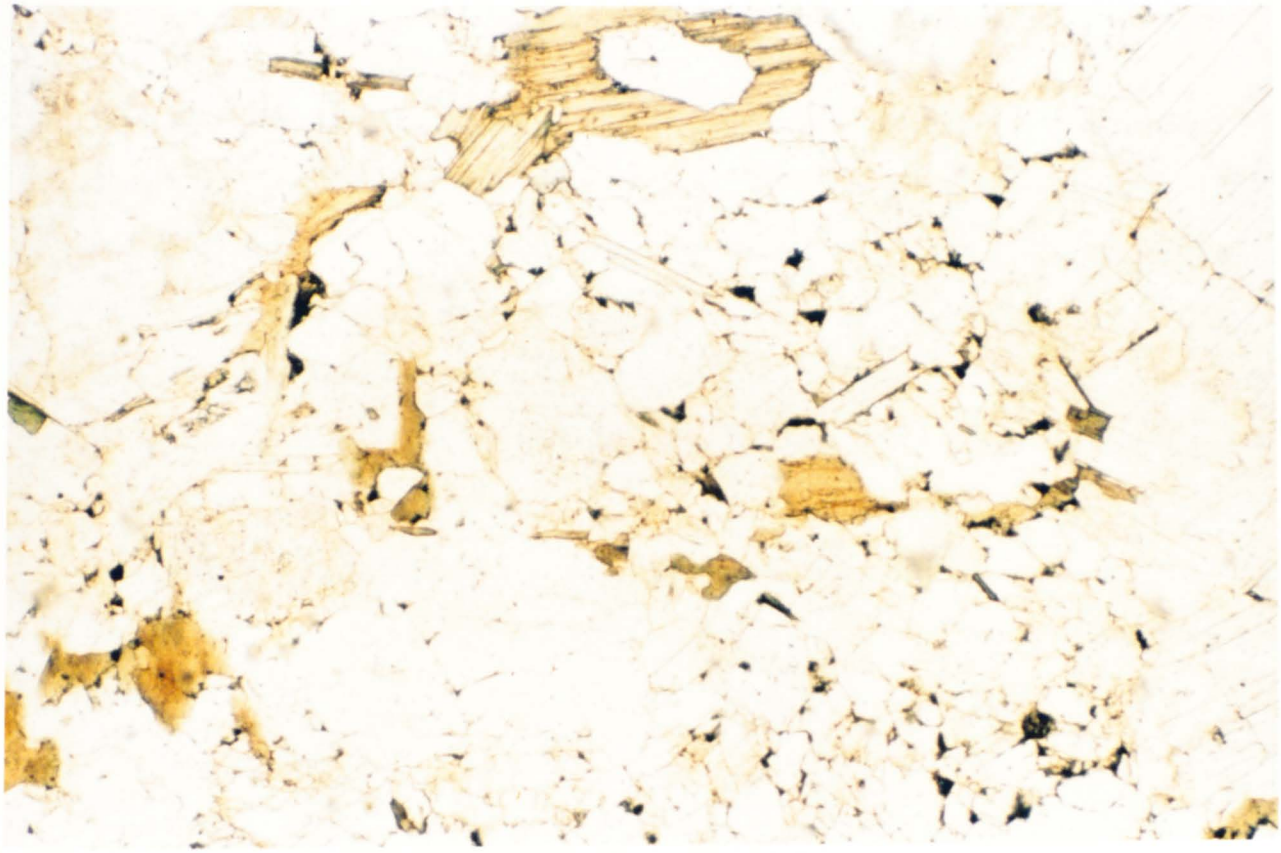

Plates 103 & 104 - F4138G - Biotite randomly orientated in the fine-grained groundmass (Plate 103, PPL, Plate 104, XPL, x 62.5)

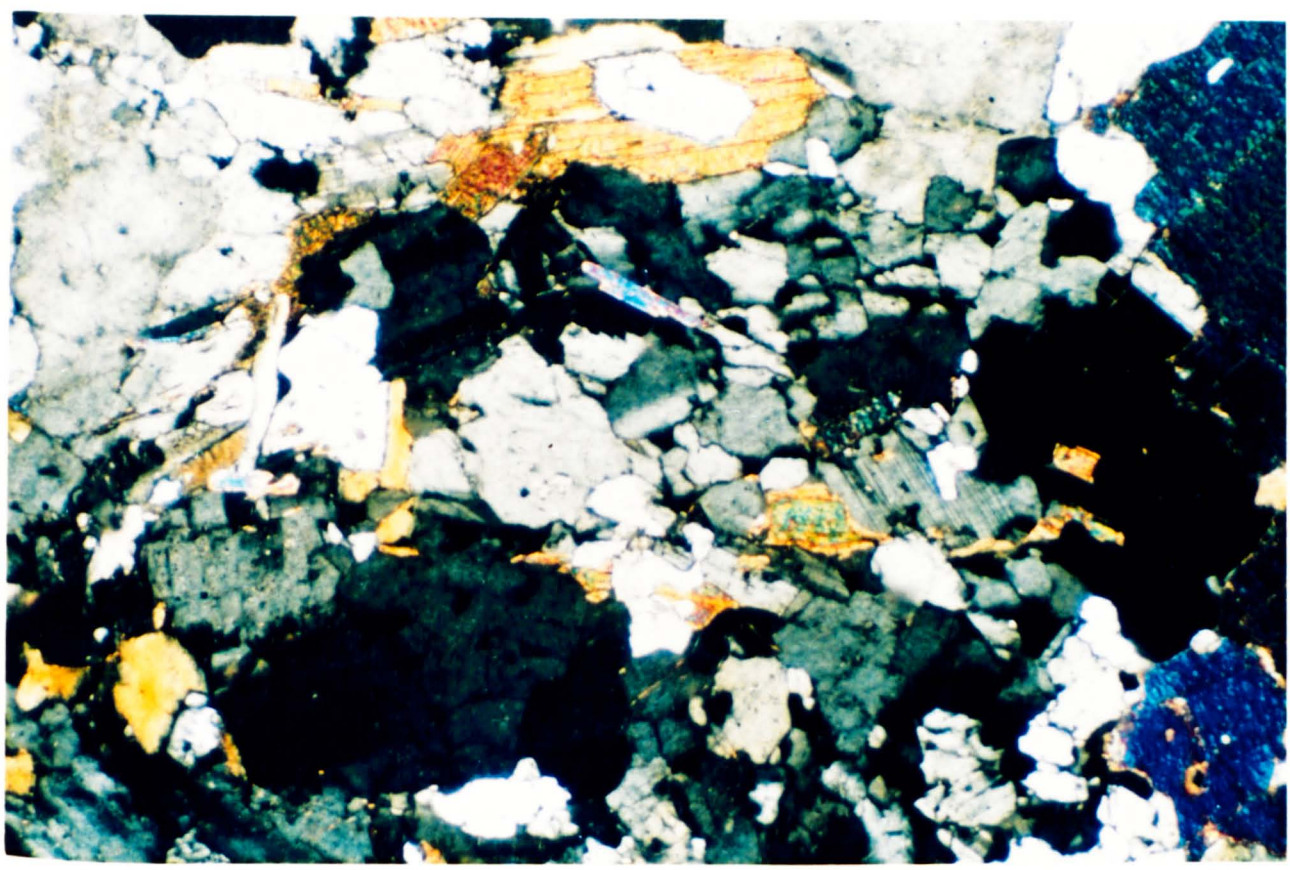

feldspars and quartz, these may be magmatic and generally show embayments possibly produced by resorbtion (Plate 102). However muscovite is almost completely absent from the finer groundmass of quartz and feldspar. Biotite is much more abundant than muscovite and subhedral to anhedral approximately equidimensional laths up to 0.75mm are randomly orientated in the groundmass (Plates 103 & 104). The overall texture is interpreted as representing a two-stage evolution; early formed crystals being resorbed by the melt followed by relatively more rapid crystallization of the groundmass minerals. Such a sequence can be explained by intrusion and rapid cooling of a later wedge within the main granite body.

Modal Analyses of the Serra da Freita Main Granite Facies

As has been shown, petrographic descriptions are complicated by inequigranular magmatic fabrics and by deformation-induced fabrics which increase in intensity northwards across the outcrop. Eight thin sections of the main granite from the relatively undeformed southern limb were point counted (1000 points per slide) to obtain a representative modal analysis for the main facies of the pluton (Table 6.1). The proportions of felsic minerals were re-calculated and plotted on a QAP triangle. All the analyses fall within the "granite ss" field, i.e. the monzogranite and syenogranite sub-fields.

Table 6.1 - Modal Analyses of the Serra da Freita Main Granite

Sample	F334G	F43G	F49G	F448G	F485G	F4118G	F4120G	F4148G
Quartz	17.6	20.6	23.2	22.9	23.7	26.6	27.6	29.7
Alkali Feldspar	39.4	41.2	31.8	34.5	25.4	34.3	29.0	28.4
Plagioclase Feldspar	19.0	13.5	28.6	21.2	25.5	14.7	20.2	19.2
Biotite	10.4	8.7	9.6	11.1	10.1	13.3	11.8	7.9
Muscovite	11.7	14.9	5.8	9.6	13.8	9.3	10.1	13.5
Accessories (Apatite, zircon)	1.7	1.1	0.9	0.6	1.4	0.7	1.3	1.2

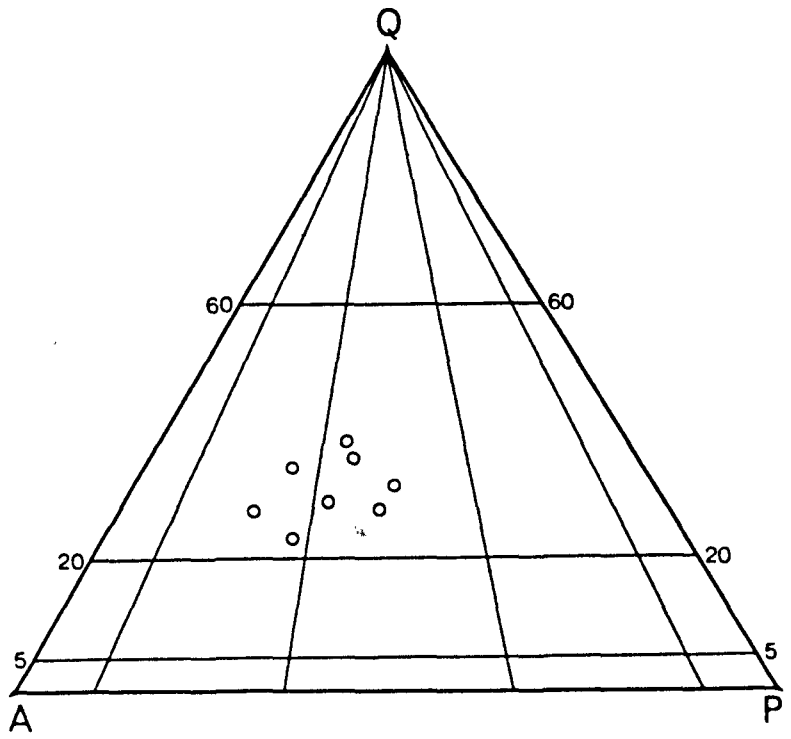

6.2.2 - MUSCOVITE-BEARING BIOTITE-POOR GRANITES

(B-1) - Contact Leucogranite - Field Relations

A narrow zone is mapped along the northern and southern contacts of the main granite in which biotite is almost absent. Samples collected at the contact have similar grain size to the rest of the main granite (Plate 105), and it is thought that the gradual reduction in modal biotite clearly seen in the field over a 10-15 m traverse to the contact implies some metasomatic effect produced by reaction with the envelope over a very short distance, rather than a sheet of almost biotite-free magma intruding along the entire length of the northern and southern contacts. There is no textural evidence that biotite has been lost from this contact leucogranite, therefore any explanation must assume that conditions along the northern and southern contacts were never suitable for its crystallization on any appreciable scale; this will be considered in detail in subsequent sections.

Samples from the northern contact, in common with the main granite from the northern limb, show strong fabrics produced by deformation. The southern contact however affords an opportunity to compare what represents a magmatic fabric with that of the weakly foliated main granite of the southern limb, (F4110G, GR 6200 2280).

(B-1) - Contact Leucogranite - Petrography

The mineralogy is quartz, orthoclase, albite/sodic oligoclase, muscovite; apatite is the only apparent accessory phase. The overall texture is phanerocrystalline hypidiomorphic granular. Plagioclase is generally euhedral-subhedral and forms crystals between 1-2 mm. Subhedral-anhedral

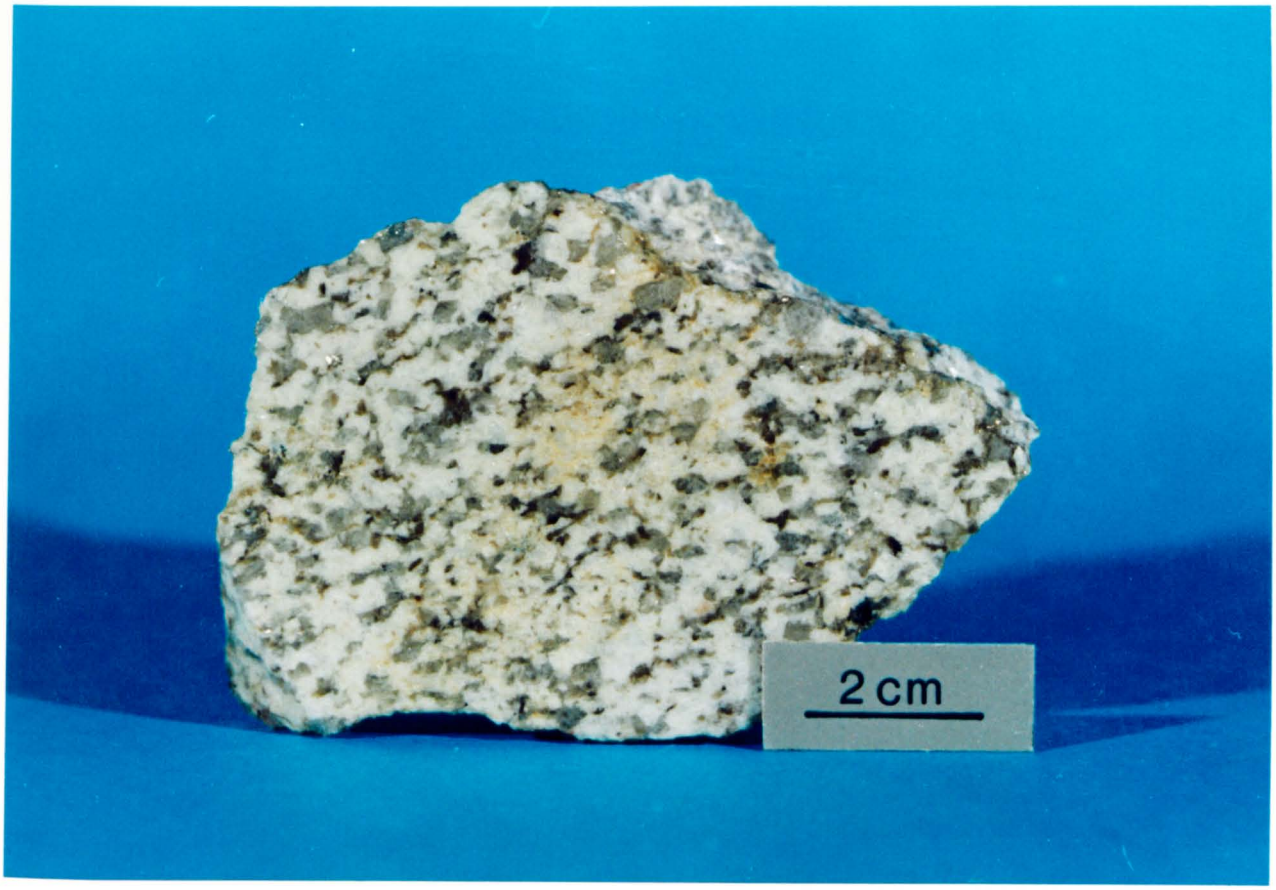

Plate 105 - Hand specimen of F4110G (GR 6200 2280), contact leucogranite

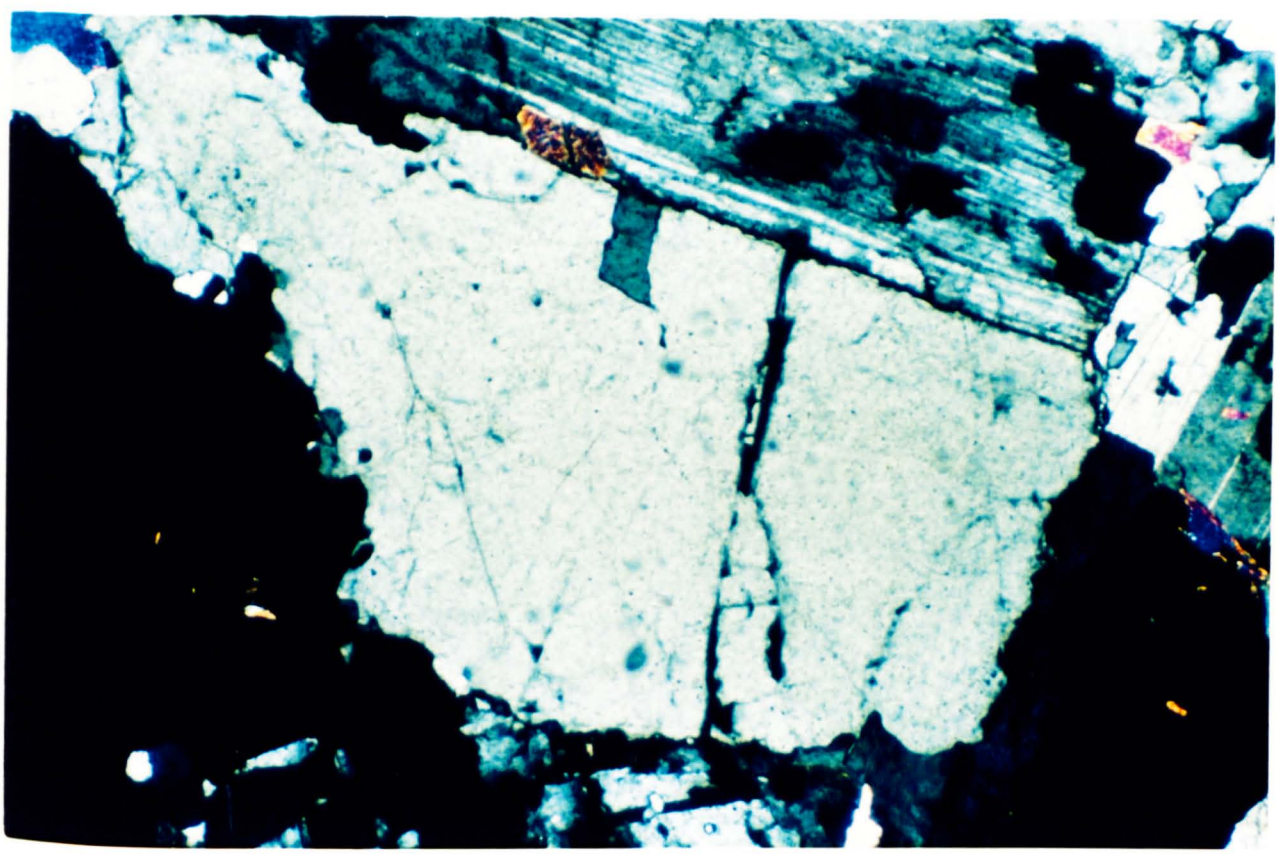

Plate 106 - F4110G - Subhedral orthoclase in centre field of view (XPL, x 62.5)

orthoclase averages 2-3 mm (Plate 106), but some crystals attain 4 or 5 mm. Meso antiperthite is common (Plate 107) and more abundant than meso perthite. Anhedral quartz of 0.5-2 mm shows consertal texture and generally strained extinction (Plate 108), although there is no evidence of grain size reduction. Muscovite is again present in two forms: larger subhedral crystals most of which are approximately equidimensional and average 1-1.5 mm in size (Plate 109), the largest being ca. 2.5 mm, are interpreted as being of magmatic origin; needle-like or bladed crystals 0.25-0.5 mm enclosed in plagioclase, lying along grain boundaries, or free in the groundmass are probably post-magmatic (Plate 110). The overall mineralogical and textural features of this rock strongly suggest that it is a biotite free equivalent of the main medium-grained 2-mica granite. There is certainly no evidence that biotite was ever present.

Two problems with this facies are apparent:

(i) its absence along the internal contacts; as noted earlier, the main 2 mica granite occurs adjacent to the inliers beneath the sheet;

(ii) this facies is not present along the outer contact of the coarse-grained granite in the Vidoeiro region.

(B-2) - Felsic Granite - Field Relations

The granite types described above have been 2-mica granites of varying grain size and a metasomatic alteration product derived from one. However, in the Gestoso region, a large mass of felsic granite intrudes the main facies in a fairly restricted area in the southern limb. The largest of these bodies is some 1200 m by 200 m and several smaller sheets crop out within a few hundred metres of this. The only occurrence beyond this is a

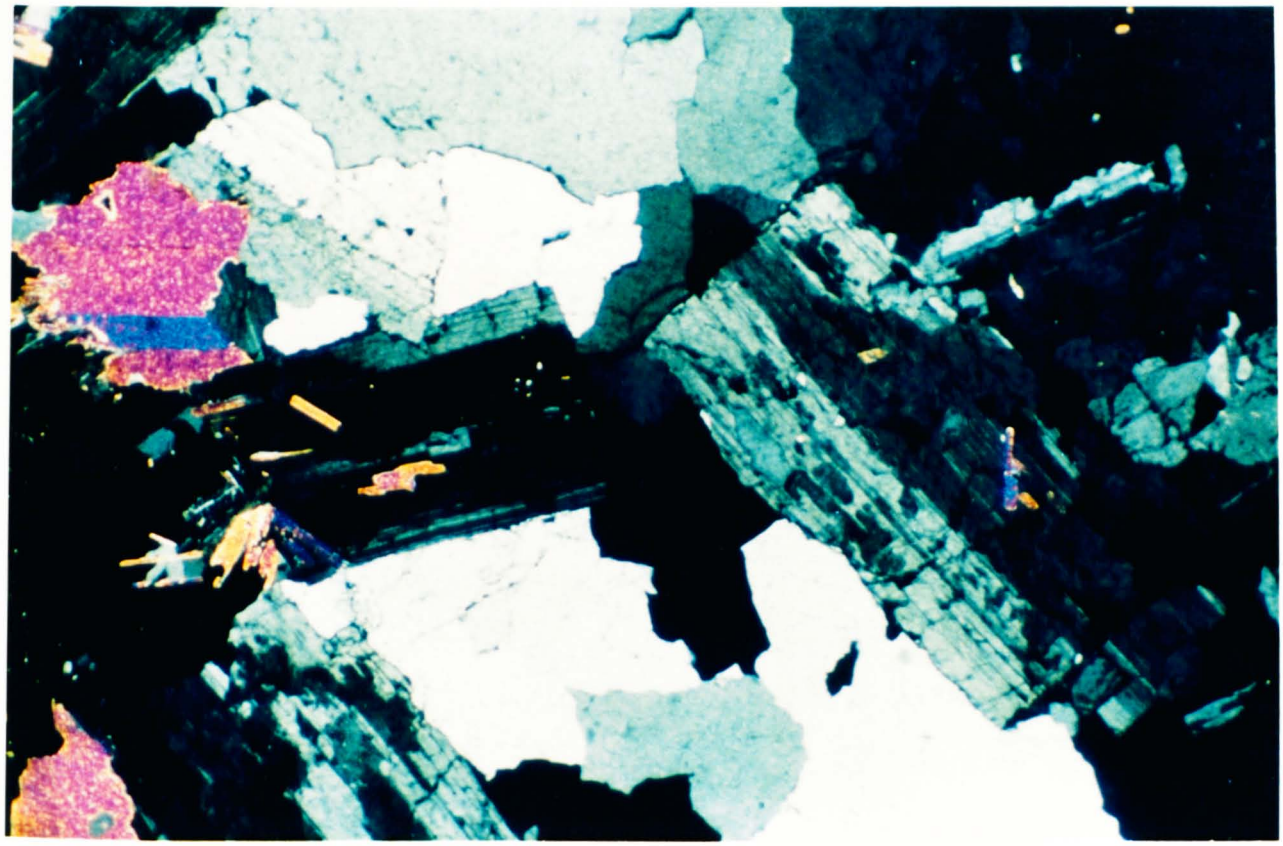

Plate 107 - F4110G - Antiperthite developed in three euhedral albite crystals (XPL, x 31.25)

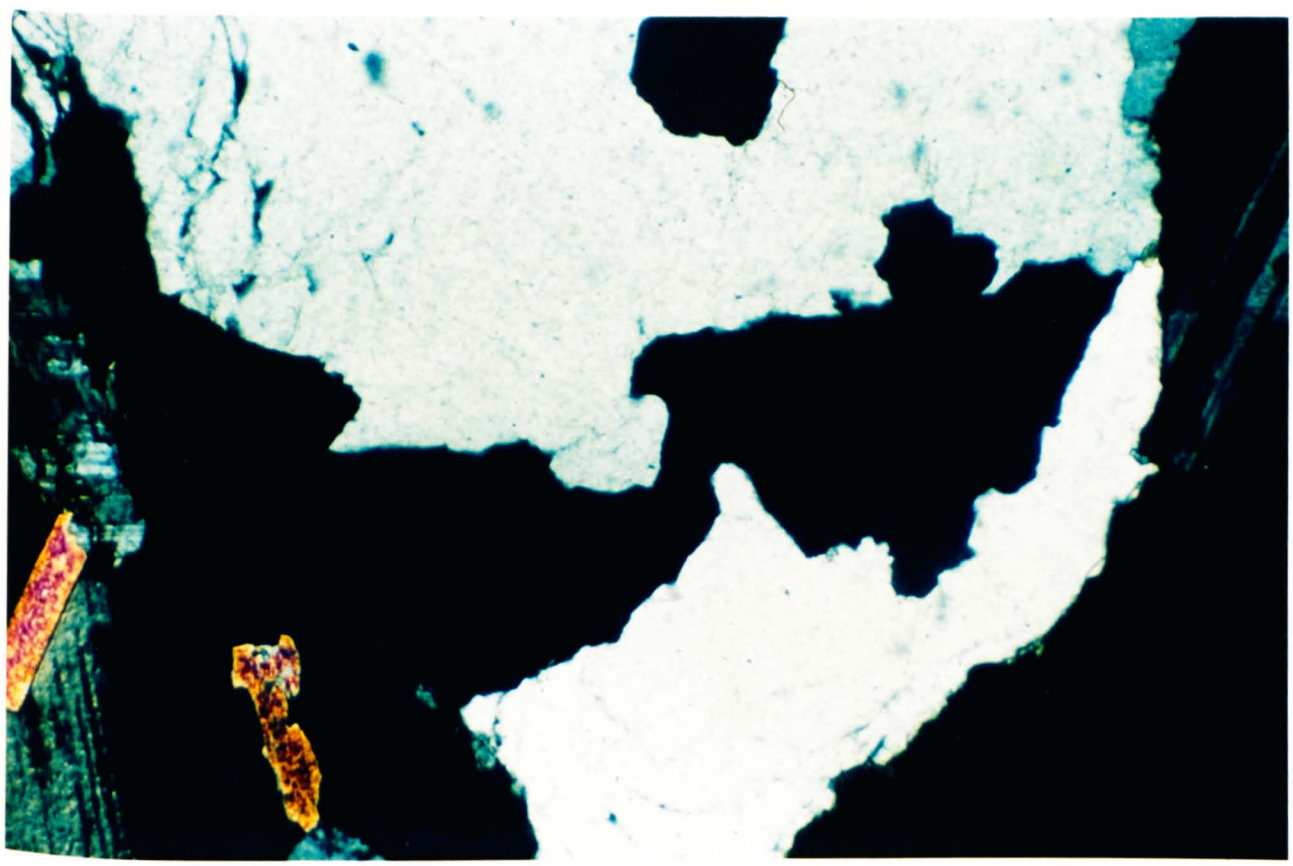

Plate 108 - F4110G - Consertal texture in quartz (XPL, x 31.25)

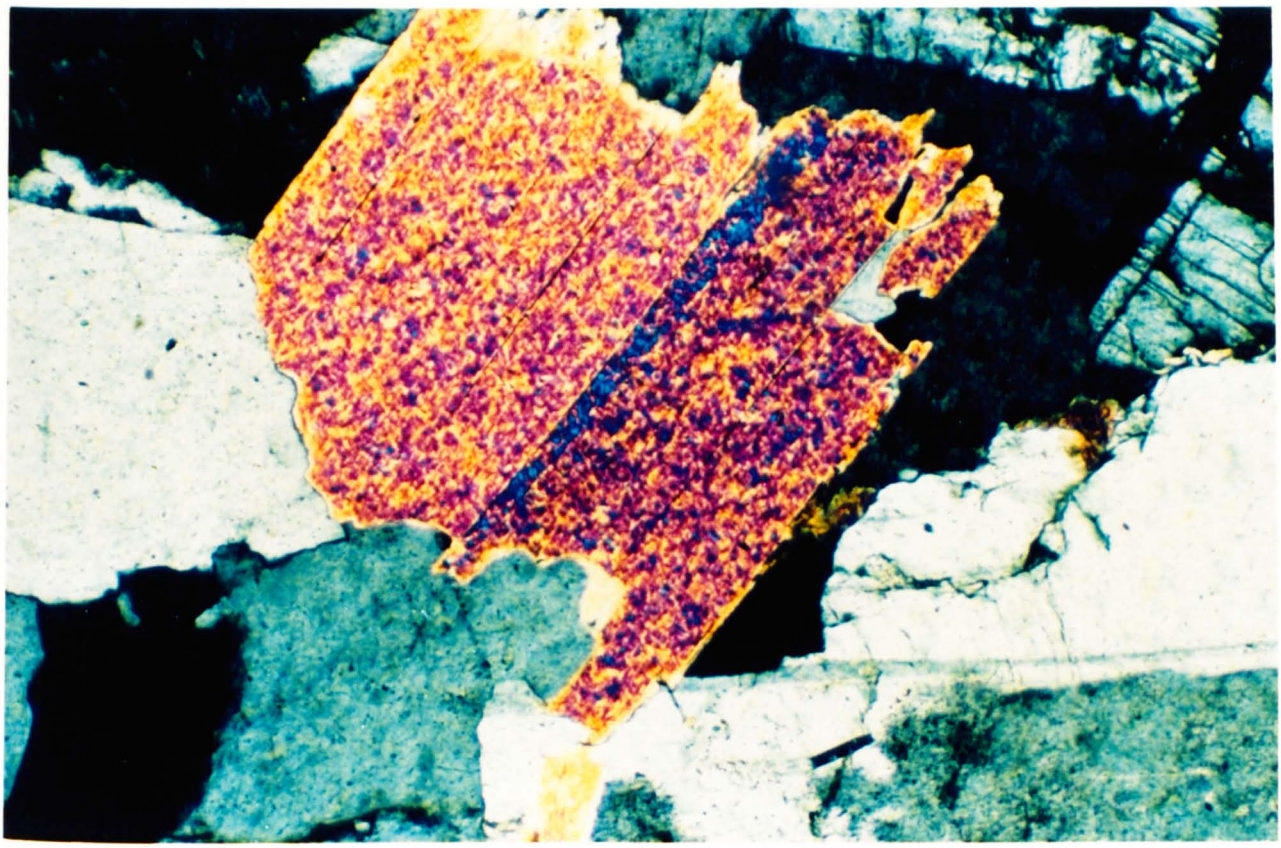

Plate 109 - F4110G - Equidimensional magmatic? muscovite (XPL, x 125)

Plate 110 - F4110G - Needle-like crystals of post-magmatic muscovite (XPL, x 250)

thin sheet near the outcrop of the Gestoso nodular granite discussed later.

Biotite is absent from the general groundmass of the rock and is present only in small drusy cavities which are generally 1-2 cm across but larger biotites in pegmatitic segregations reach sizes of 2-3 cm (Plate 111 & 112). The contact with the main granite is well exposed in freshly cut blocks and although sharp, is often irregular or lobate suggesting that the felsic granite was intruded before complete consolidation of the host (Plate 113 & 114).

(B-2) - Felsic Granite - Petrography

All samples examined of this facies proved to be petrographically similar and showed a magmatic inequigranular texture. F4150G (GR 6320 2270) was chosen as being representative. As this felsic granite is intruded into the southern limb, the fabric is generally weak with no evidence of recrystallization. The mineralogy is quartz, muscovite, albite, and orthoclase, biotite is very sparse and usually shows preferential alteration to chlorite along cleavage. Apatite is present as an accessory phase. Larger anhedral quartz crystals of 1-1.5 mm show a consertal texture, though those in the groundmass are much smaller. Feldspars again show two size ranges. (i) Large subhedral crystals reach 5 mm although most average 2-3 mm. Meso antiperthite is more abundant than albite, the latter often shows kinking of albite twins (Plate 115). Orthoclase and orthoclase perthite is subordinate in abundance. (ii) A finer grained groundmass consists of mostly subhedral interlocking quartz, plagioclase and orthoclase in which perthite is absent (Plate 116). Few good equidimensional muscovite crystals are seen, those present are up to 2 mm

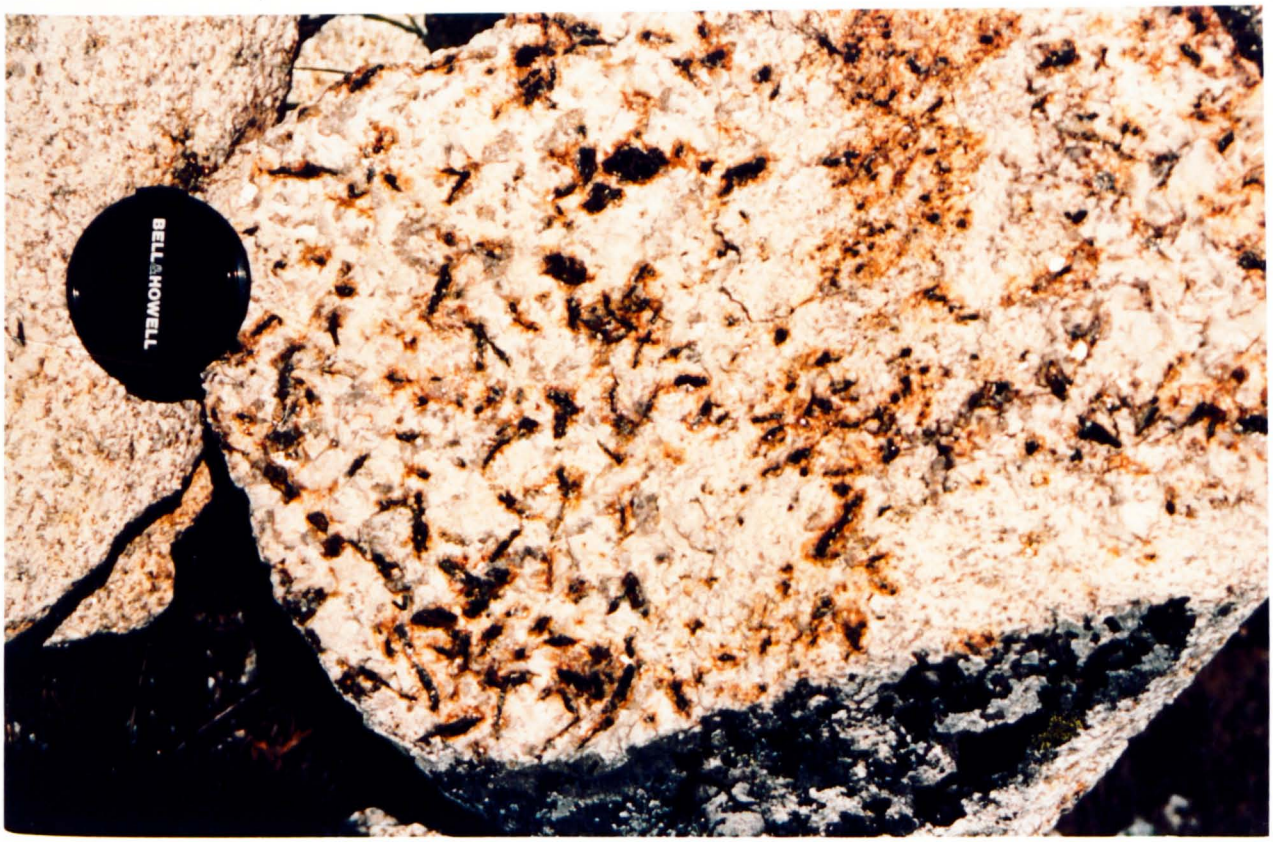

Plate 111 - Field photograph of felsic granite (GR 6330 2260) showing pegmatitic development of biotite

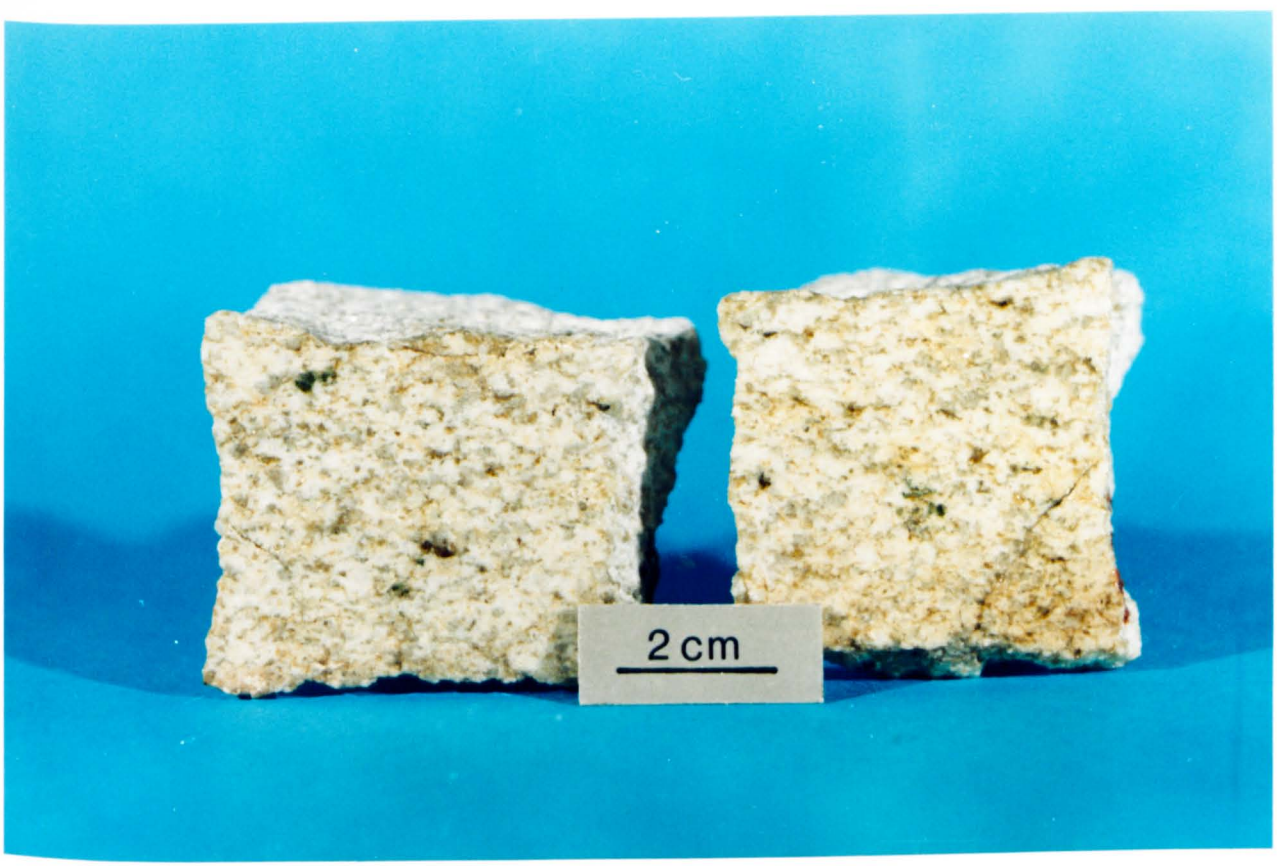

Plate 112 - Hand specimen of F4150G (GR 6320 2270), felsic granite. The groundmass is almost biotite-free

Plates 113 & 114 - Field photographs of the contact between the felsic granite and the main 2-mica granite. Contact is sharp but lobate, Plate 113 (upper left) shows typical occurrence of biotite in drusy patches (GR 6335 2270)

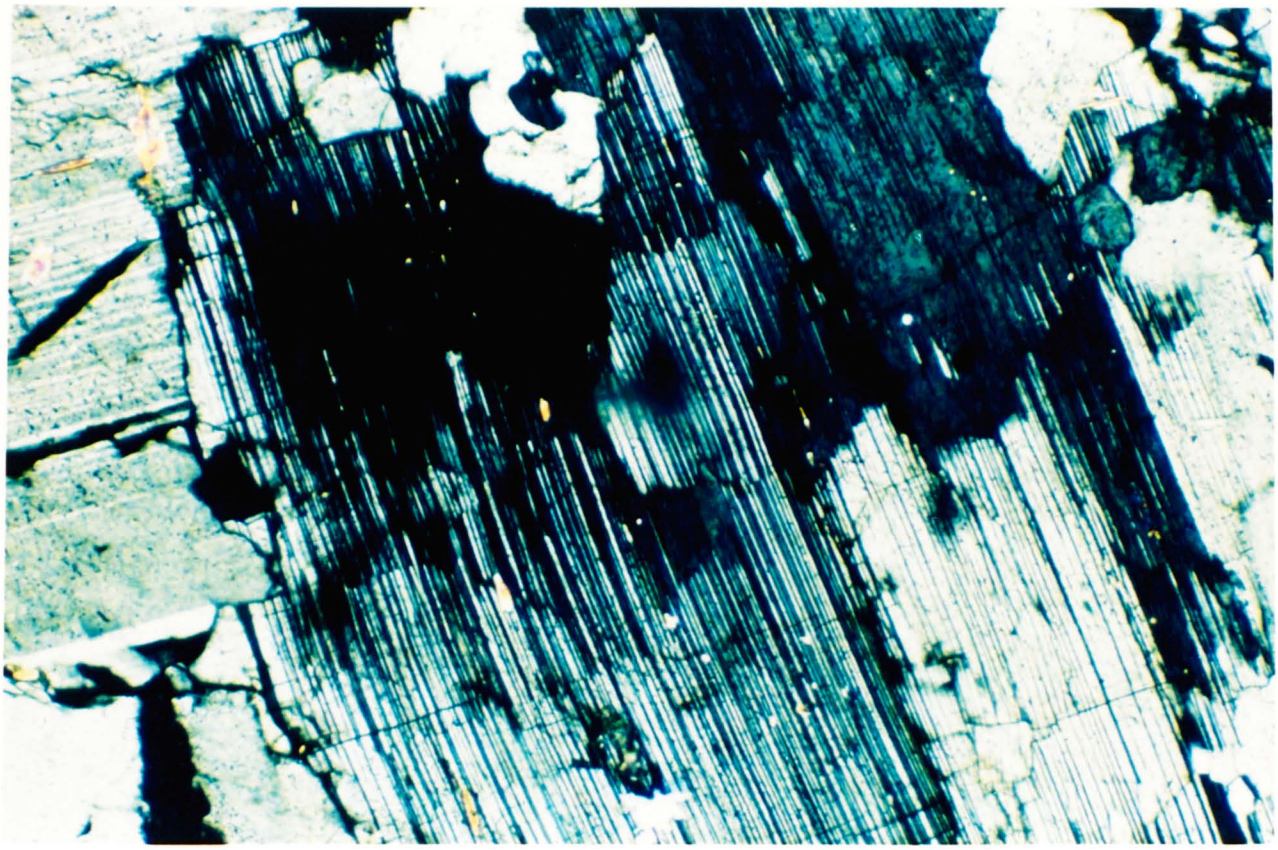

Plate 115 - F4150G - Kinking of albite twins (XPL, x 250)

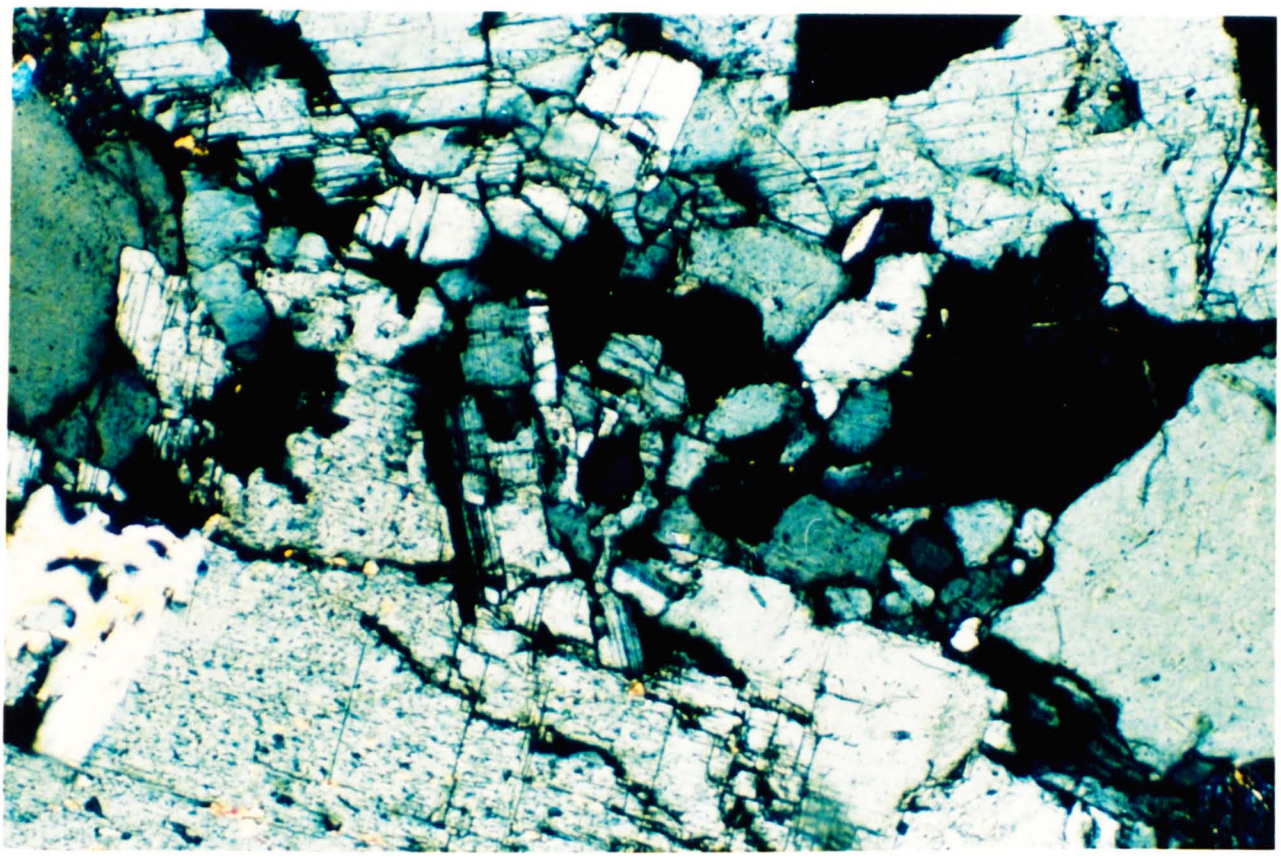

Plate 116 - F4150G - Fine-grained groundmass of quartz, plagioclase and orthoclase (XPL, x 250)

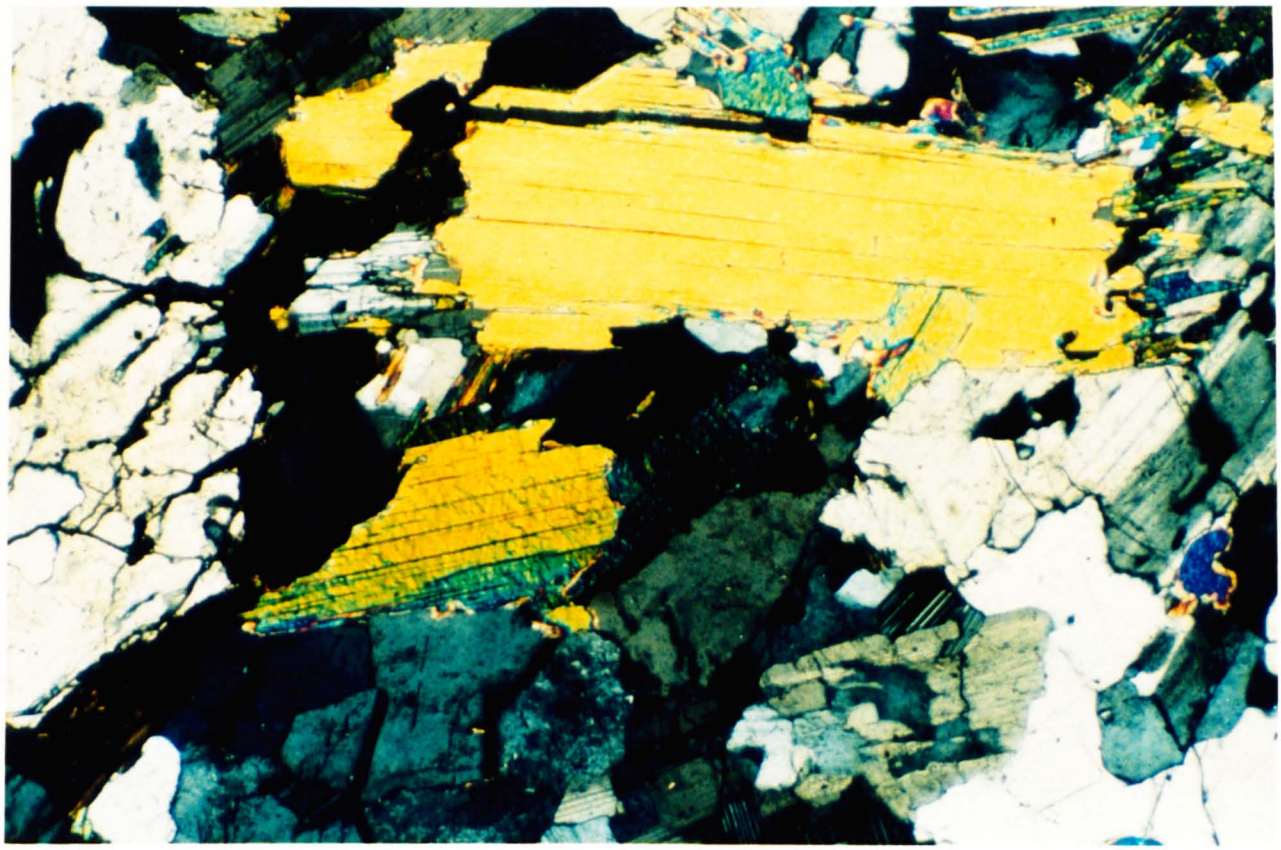

Plate 117 - F4150G - Magmatic muscovite, note some post-magmatic recrystallizatio
at extreme right of large crystal (XPL, x 62.5)

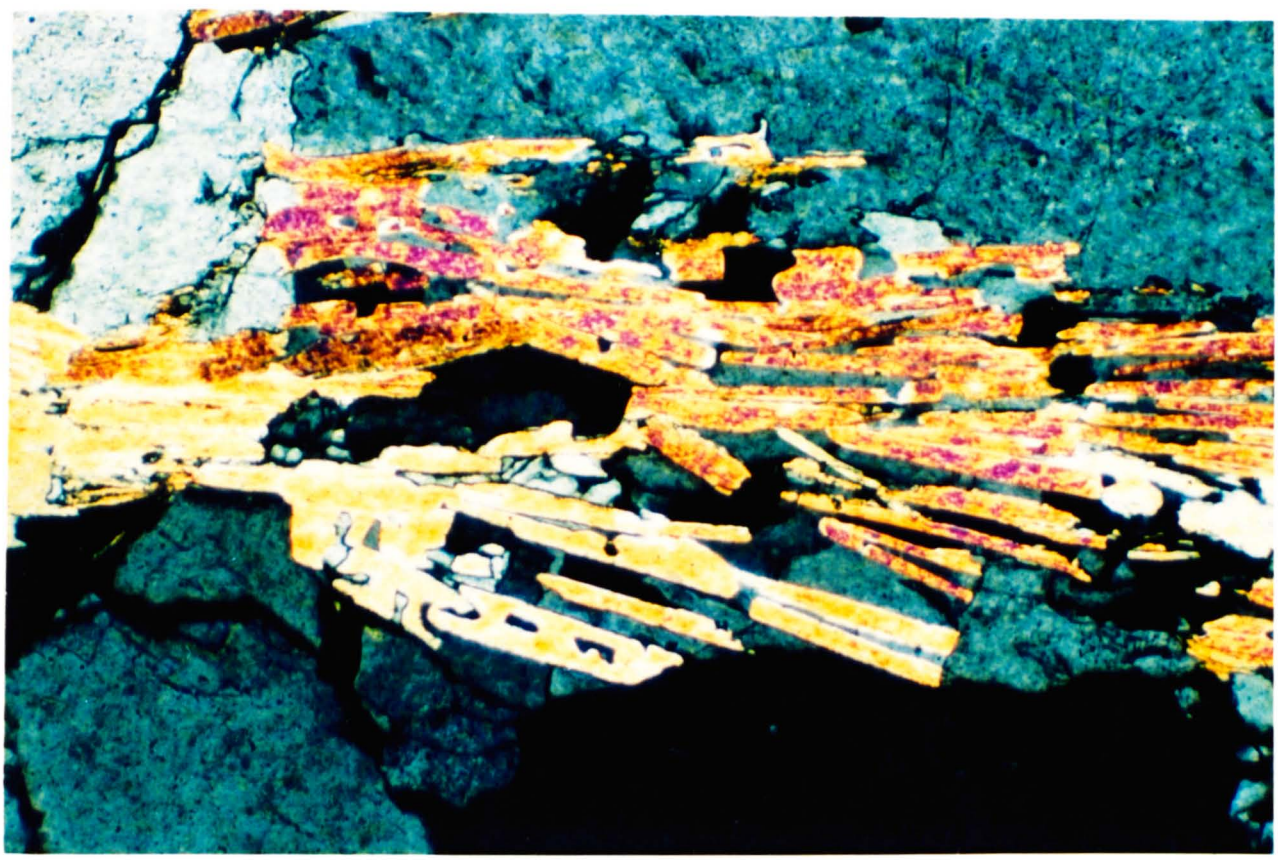

Plate 118 - F4150G - "Sieve" textures in muscovite (XPL, x 125)

in length and display evidence of recrystallization along their margins (Plate 117). Most are narrow, lie along grain boundaries, and show sieve textures with surrounding felsic phases; they may be either partially resorbed magmatic crystals or alternatively entirely post-magmatic (Plate 118).

These sheets of felsic granite, in common with those of microgranite show evidence of a two-stage magmatic history: early formed crystals are surrounded by finer grained equivalents; presumably the magma existed as a crystal mush and nucleation of new sites in the remaining melt ensued following intrusion of the body into the main granite.

(B-3) - Aplopegmatites - Field Relations

The contact region between the main and coarse grained 2-mica granite is complicated by the intrusion of numerous aplopegmatite sheets.

Mapping along the northern contact of the pluton for 1 km around Vidoeiro reveals 3 sub-parallel sheets or dykes 2-3 m wide (Figure 6.1). These intrusions show strong C-S fabrics in common with their hosts.

The southernmost sheet was intruded between the main and sheared granites, and as this is followed SE, numerous thin parallel sheets mark the contact zone. The second sheet cuts the sheared granite, but gradually thins and cannot be traced beyond 200 m into the pluton. The northernmost sheet is intruded along the margin of the pluton, effectively forming the northern contact itself for some 500 m, before being cut out by a late fault striking 040/220 across the granite (Plates 119-122).

(B-3) - Aplopegmatites - Petrography

Large parts of these sheets are coarsely pegmatitic in character with

Figure 6.1 - Map of the Vidoeiro area

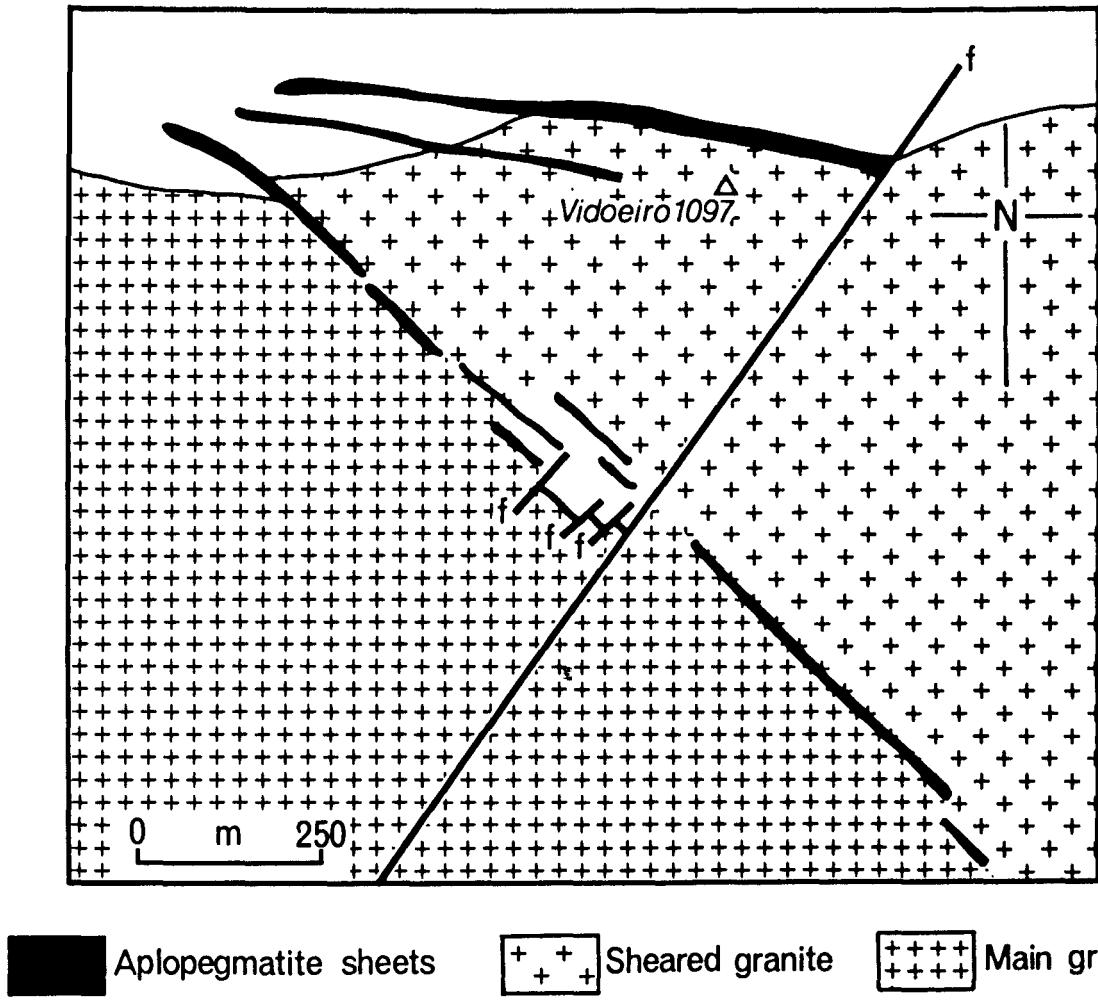

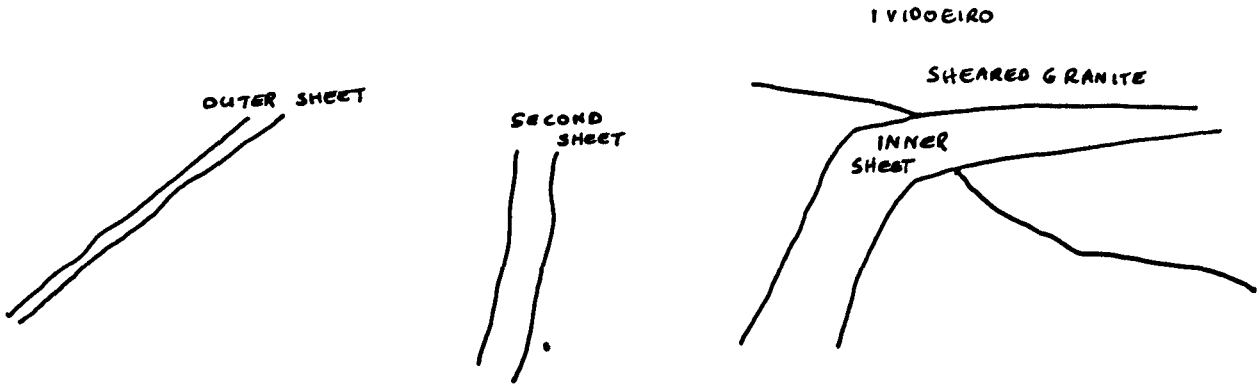
IVIDOEIRO
OUTER SHEET
SECOND SHEET
SHEARED GRANITE
INNER SHEET

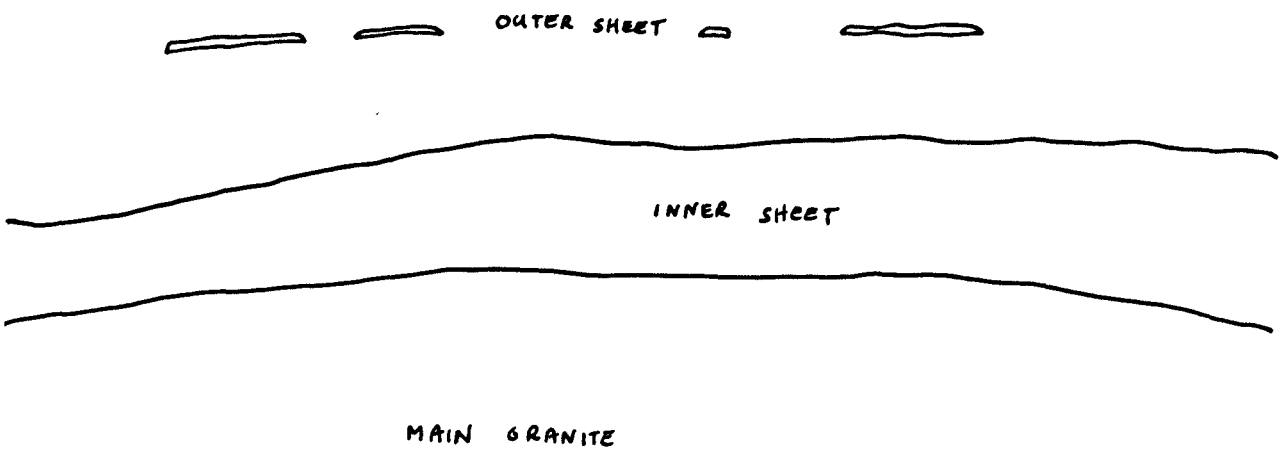
OUTER SHEET
INNER SHEET
MAIN GRANITE

(Plates 119-122 - refer to Figure 6.1) Plate 119 - Looking east at the three aplopegmatite sheets, details on overlay. Vidoeiro on horizon

Plate 120 - The southernmost (inner) sheet entering the main pluton, the northern most (outer) intrusion can be seen on the near ridge

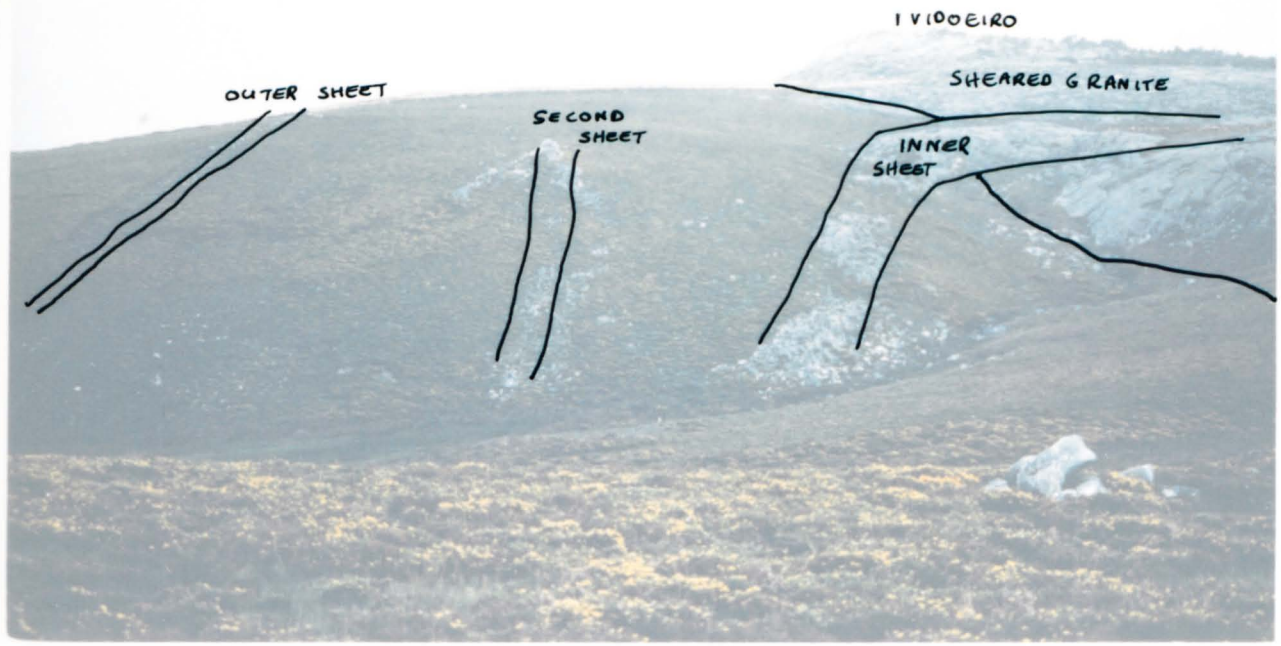

(Plates 119-122 - refer to Figure 6.1) Plate 119 - Looking east at the three aplopegmatite sheets, details on overlay. Vidoeiro on horizon

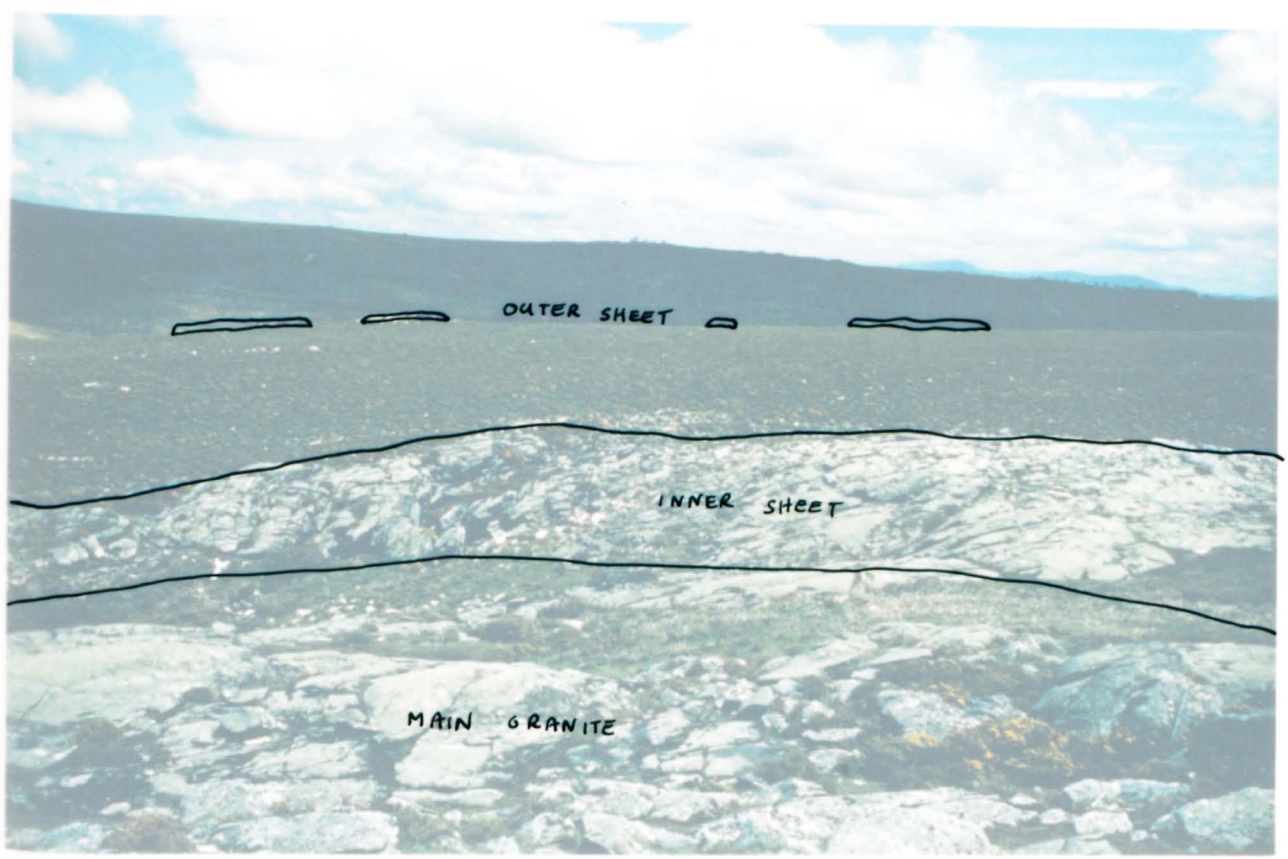

Plate 120 - The southernmost (inner) sheet entering the main pluton, the northern most (outer) intrusion can be seen on the near ridge

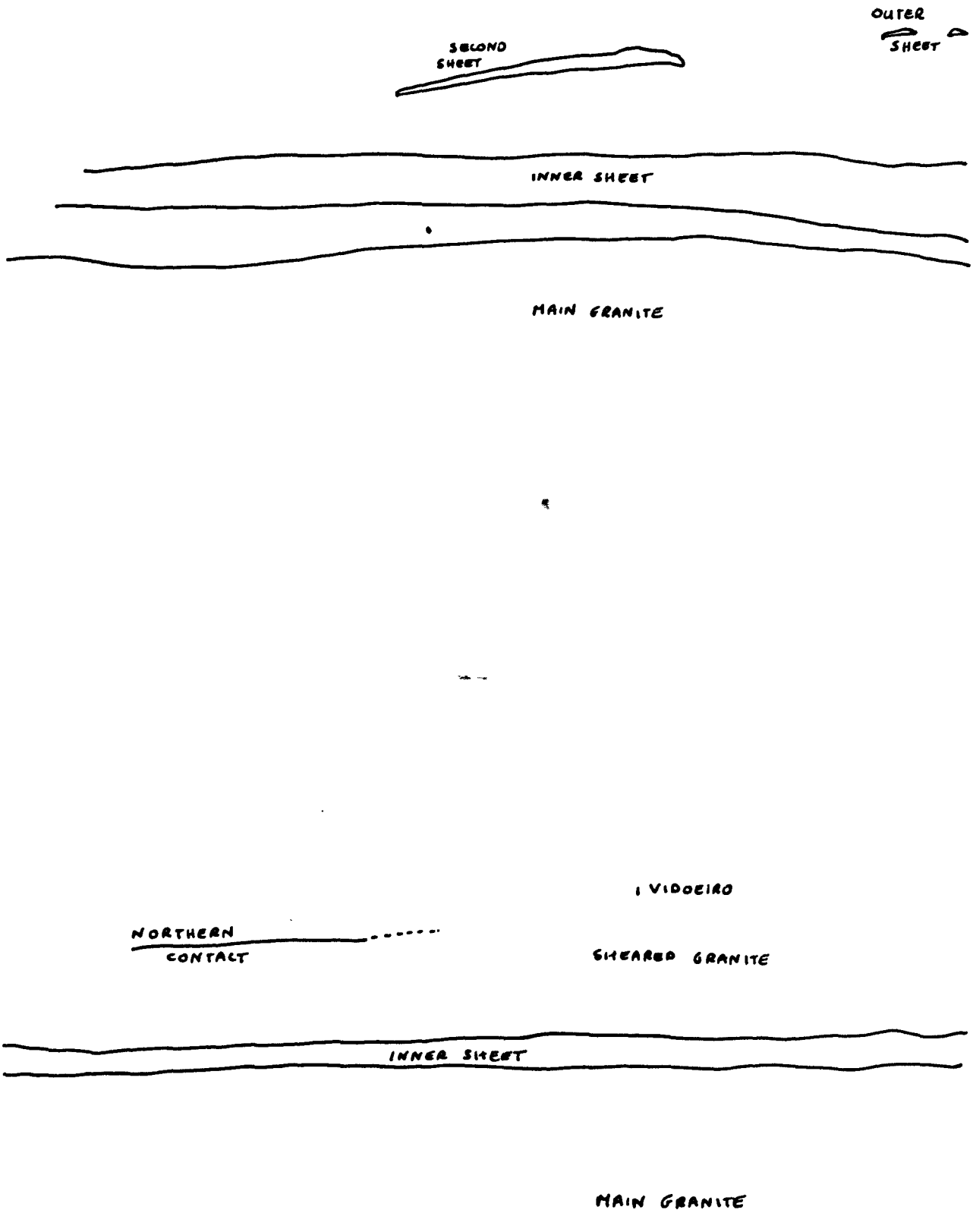
OUTER
SHEET
SECOND
SHEET
INNER SHEET
MAIN GRANITE
VIDOEIRO
NORTHERN
CONTACT
SHEARED GRANITE
INNER SHEET
MAIN GRANITE

Plate 121 - The second and inner sheet viewed from 10 m west of camera position in Plate 120

Plate 122 - View east from the main granite towards Vidoeiro on the horizon. The background is sheared granite and the aplite sheet which runs along the contact can be clearly seen in the lower centre of the photograph

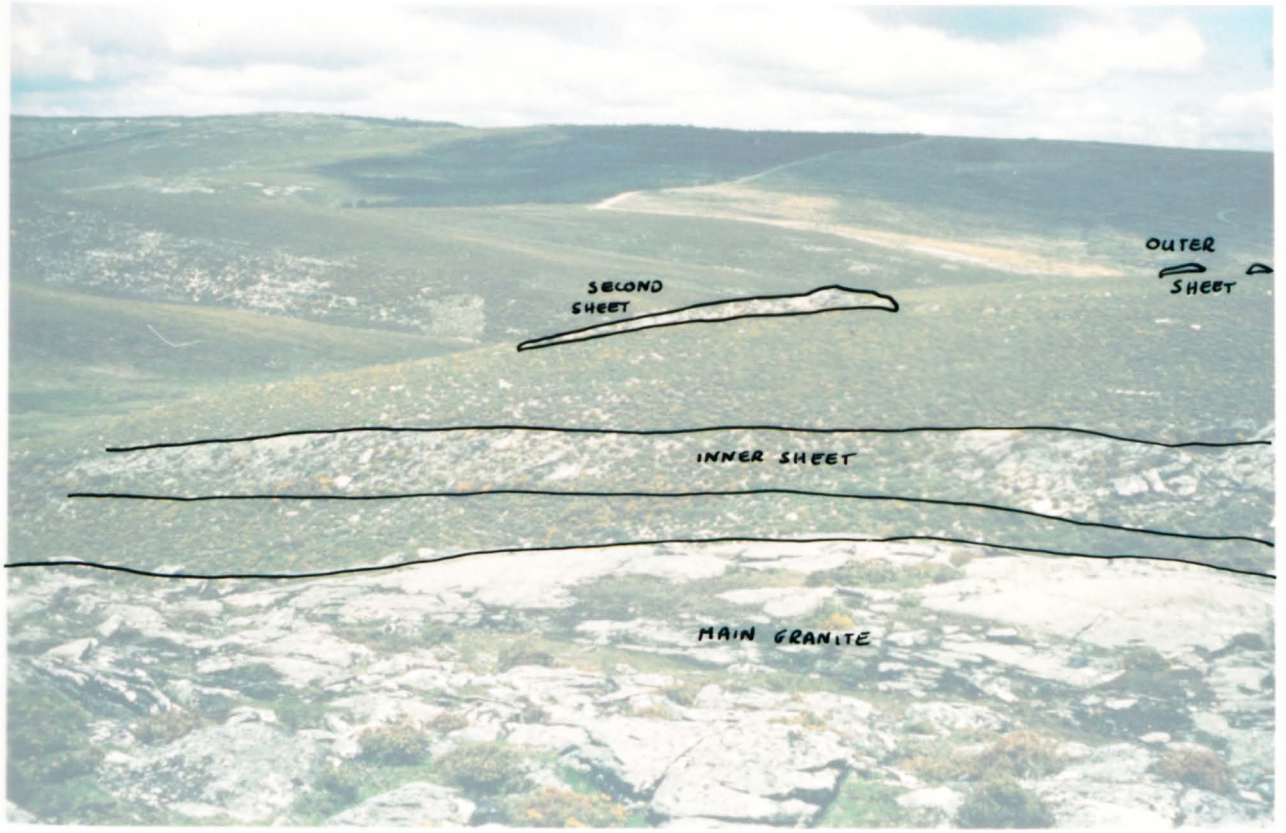

Plate 121 - The second and inner sheet viewed from 10 m west of camera position in Plate 120

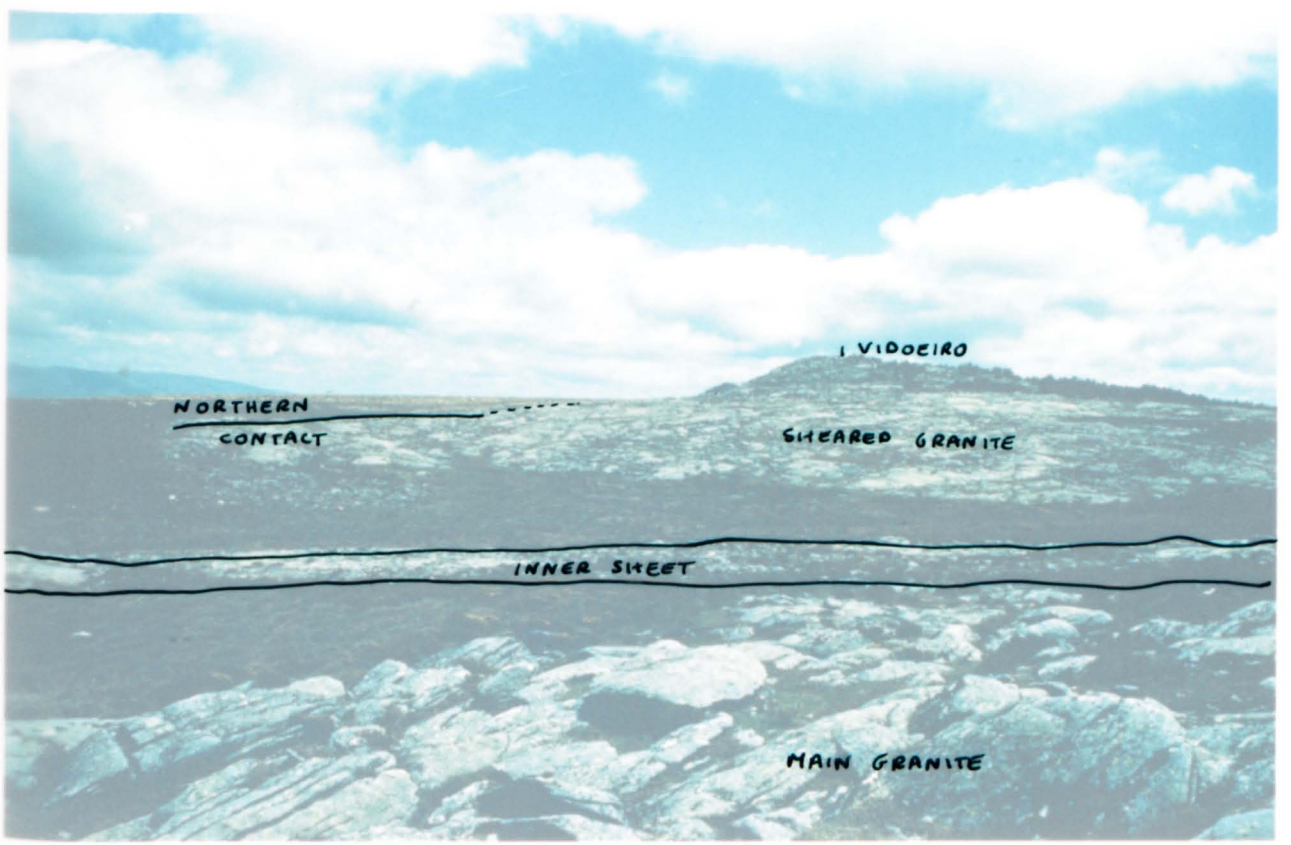

Plate 122 - View east from the main granite towards Vidoeiro on the horizon. The background is sheared granite and the aplite sheet which runs along the contact can be clearly seen in the lower centre of the photograph

feldspars and muscovites up to 3 cm across. Although displaying a simple paragenesis of quartz, albite, orthoclase, muscovite and accessory apatite, the texture of these sheets is very variable due to (i) great variations in initial grain size, and (ii) the development of shear bands. In general larger feldspars are perthitic, whilst smaller crystals show no evidence of exsolution. As seen elsewhere, an inequigranular texture is produced by recrystallization and grain size reduction along C planes.

6.2.3 - BIOTITE NODULAR GRANITES

These occur at two localities:

(i) the Castanheira pluton which is 600 m distant from the main granite of the Serra da Freita and is an oval body 1000 m x 600 m in outcrop;

(ii) within the main pluton in a restricted area 1km SE of Gestoso 20m away from the contact with the Manhouse inlier. The outcrop concerned is approximately 250 m x 40 m in extent.

It is the presence and abundance of discoidal biotite aggregates that makes these localities so remarkable. The nodular granite of Castanheira had been described as early as 1954 by Portuguese workers (Plate 123), however the outcrop at Gestoso is reported here for the first time (Plate 124).

(C-1) - Castanheira - Field Relations

The Castanheira pluton is not as well exposed as the Serra da Freita granite as part of it underlies the fields around the village after which the intrusion is named. However a good river and road section are available and these provide some useful vertical relief.

At GR 6050 2265, 6115 2220, and 6140 2240, the contact between the intrusion and the flat-lying schists is well exposed. The attitude of the contact is variable, but is never greater than 40°, suggesting that it represents the roof of the intrusion. The contact is sharp, but within 3 m the schists are riddled with sub-horizontal quartz veins, some up to 0.5 m across. Tourmaline is abundant in the schists above the intrusion and in places the term tourmalinite is appropriate (Plates 125 & 126).

The field evidence points to a model in which the Castanheira intrusion

Plate 123 - The enigma of the Castanheira biotite nodules, first described in 1954

Plate 124 - The main outcrop of nodular granite at Gestoso, described here for the first time

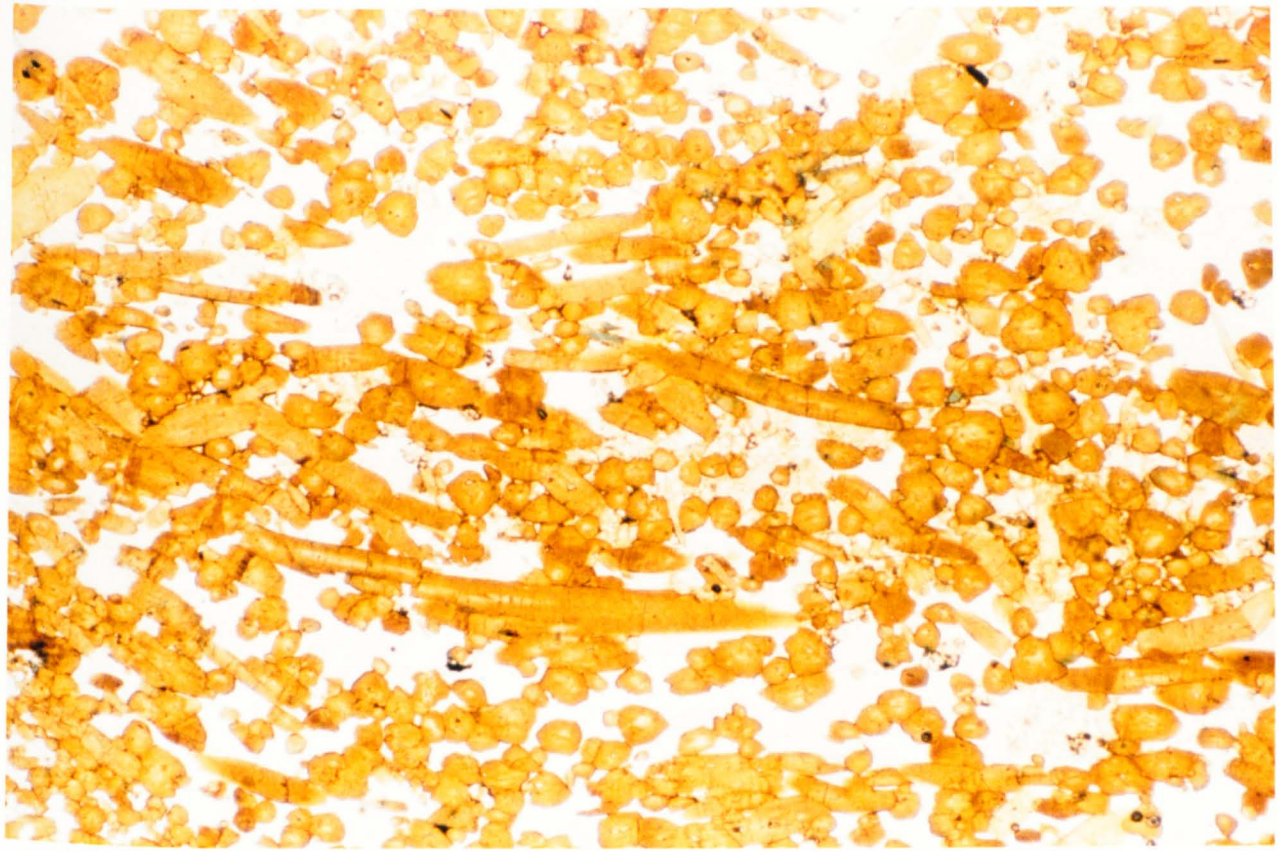

Plates 125 & 126 - Tourmaline-rich schists in the Castanheira roof (Plate 125, PPL, Plate 126, XPL, x 31.25

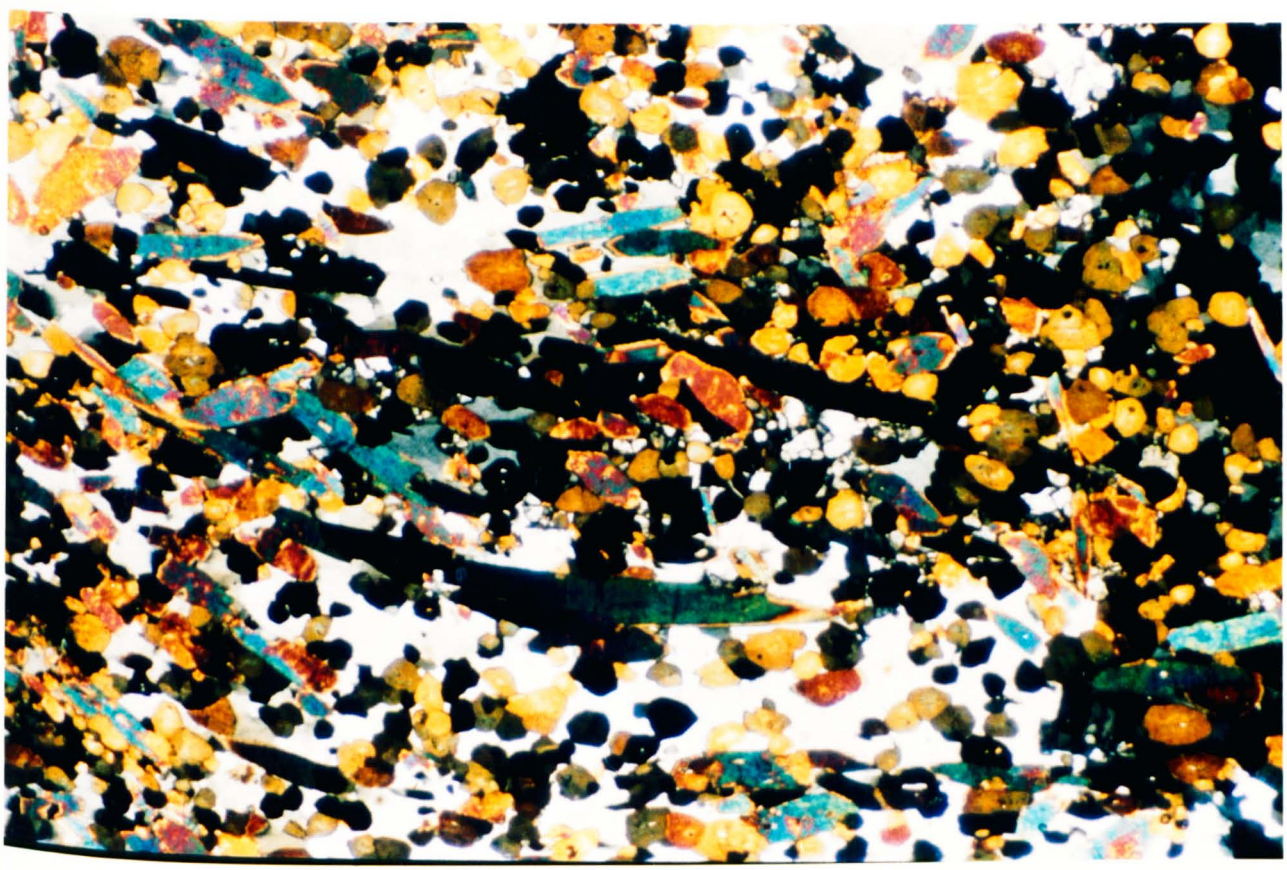

is part of the volatile-rich roof zone of the distal end of the flattish southern limb of the Serra da Freita granite. Structurally it represents a small diapir which has ballooned upwards; ballooning would be aided by (i) a fluid rich magma, and (ii) a low intensity of shear strain.

Both these conditions are locally achieved at Castanheira. The abundance of tourmaline and quartz veining in the country rocks above the granite provides ample evidence for large scale circulation of fluids, particularly those rich in boron and halogens.

S2 south of the main granite is much more variable in its orientation and immediately above the Castanheira granite has been reorientated and modified by ballooning strains locally producing a flattish composite S2/S0? (Figure 4.3). This fabric is itself deformed by gently NW and SE plunging folds, presumably related to the ballooning process (Plate 33). The NW plunging stretching lineation indicative of sinistral transpression recorded in the main shear zone is now recorded by the N-S alignment of the X direction of the elliptical biotite nodules within the Castanheira granite.

The nodular granite itself is the medium-grained biotite muscovite granite which forms the bulk of the main intrusion. A leucocratic contact facies exists within 20 m of the roof which is exposed in several places. The absence of both nodules and groundmass biotite from this zone seems to lend weight to the earlier argument that the leucocratic facies of the main granite was originally a biotite-poor magma.

The nodules are very variable in size, the smallest being less than 1cm in diameter, none was found with a diameter greater than 12 cm (Plates 127 & 128). The actual size at any one locality appears totally random, there

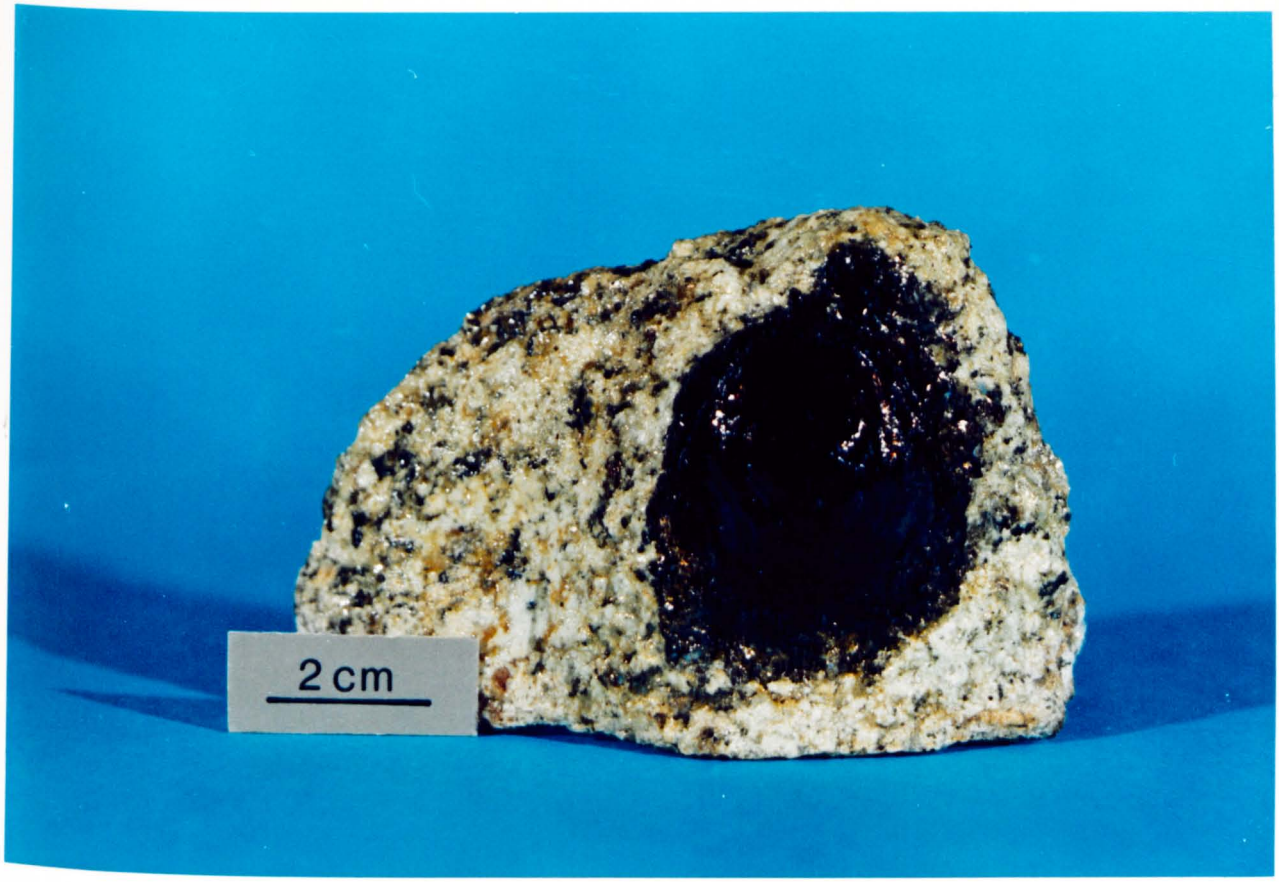

Plate 127 - Plan view of nodule within its host granite

Plate 128 - Size variation in nodules

is no trend of size vertically or laterally within the pluton. Without exception, each nodule contains a nucleus or core of granite (Plates 129 & 130), this is often only 7-8 mm in diameter in a 6-7 cm nodule but occasionally they can be much larger an occupy > 50% of the total volume. These cores are undeformed showing no apparent fabric. On foliation surfaces, nodules tend to be circular in outline (Plates 131 & 132), i.e. X≈Y; in vertical exposures in the river section, most are elliptical with horizontal XY planes (Plates 133 & 134), thus their three dimensional form approximates to an oblate spheroid. Most are asymmetric with respect to their XY plane, being oversheared to the north-west, i.e. sinistral.

Nodules and sections through them are well displayed throughout the granite, they also tend to weather out of the host rock (intact) resulting in many hundreds being scattered over the outcrop.

(C-1) - Castanheira - Petrography and Texture

The inter-nodular granite has an assemblage of quartz, plagioclase, orthoclase, biotite and muscovite. The feldspars are often zoned with highly altered cores of fine grained white mica (Plates 135 & 136). Muscovite defines a weak fabric which, as it is associated with some recrystallization of quartz, is assumed to be post-magmatic in origin. Thin biotite flakes lie along grain boundaries but alteration to chlorite along cleavage is widespread and fresh grains are rare.

The nodule cores are mineralogically similar to the host granite which surrounds them (Plates 137 & 138). Quartz, orthoclase and plagioclase display a granular texture with both biotite and muscovite present. Moving outwards from the core, biotite tends to form parallel sheaves which assume a tangential orientation relative to the core (Plates 139 & 140).

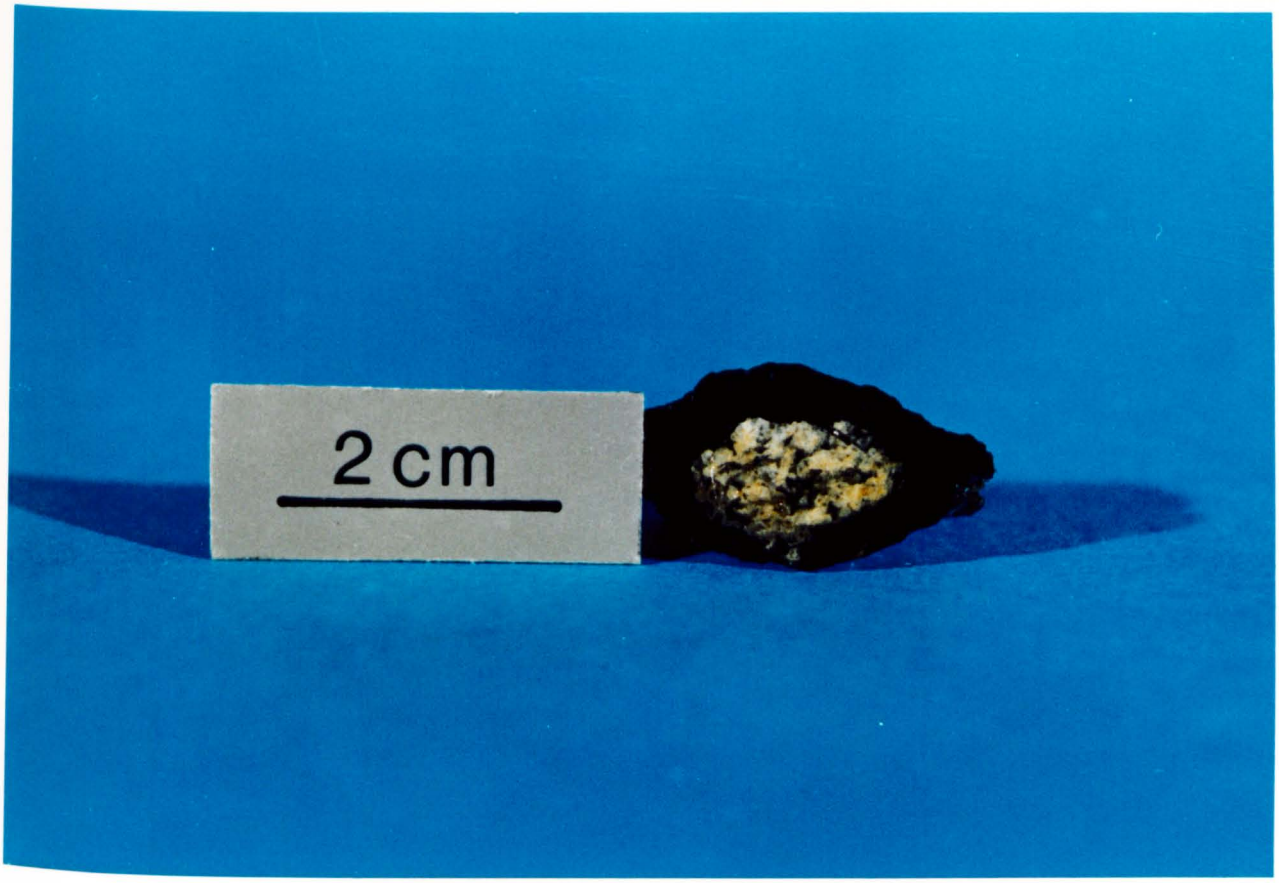

Plate 129 - Nodule cut open to show undeformed granite core

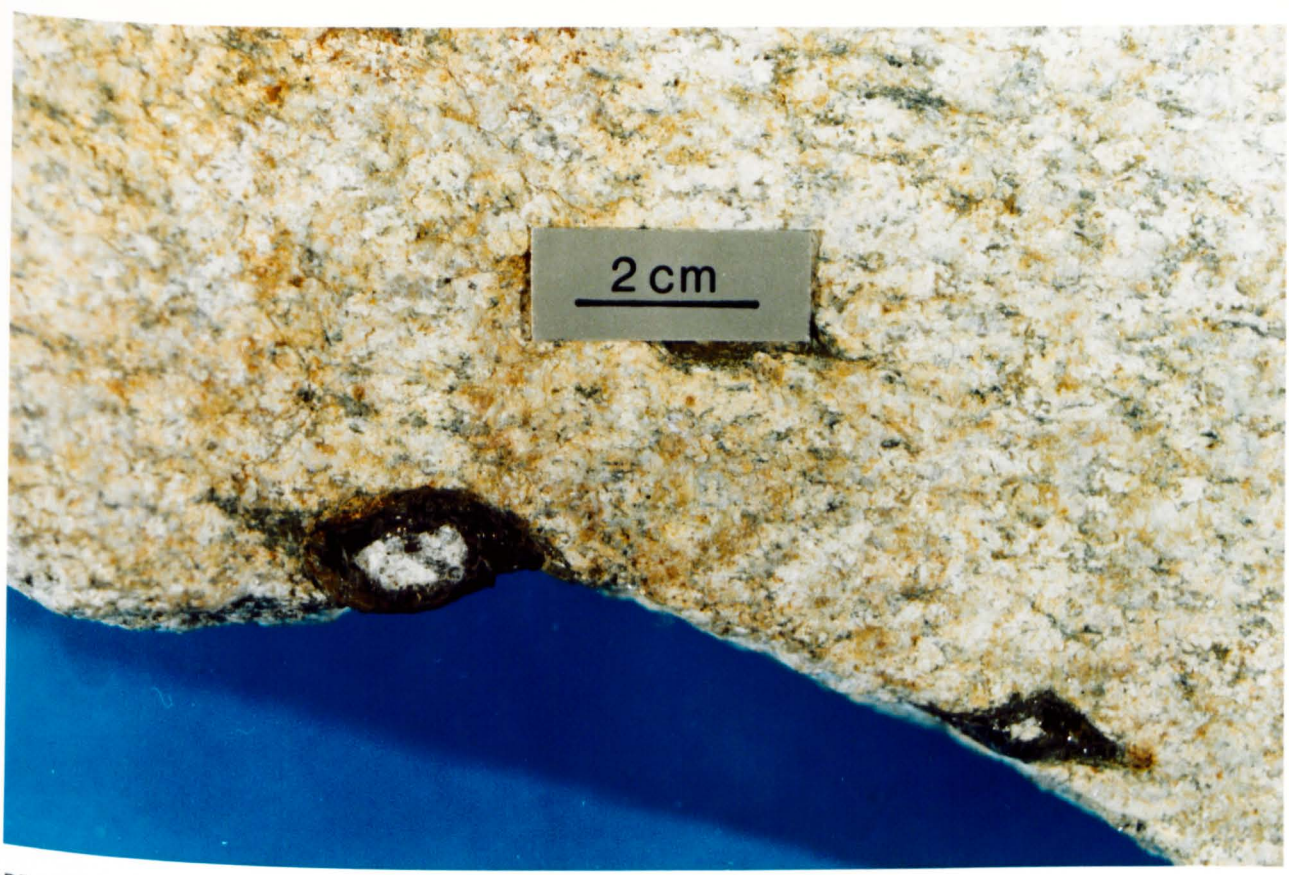

Plate 130 - Cores revealed by weathering in loose block

Plates 131 & 132 - Circular outline of nodules on foliation surfaces

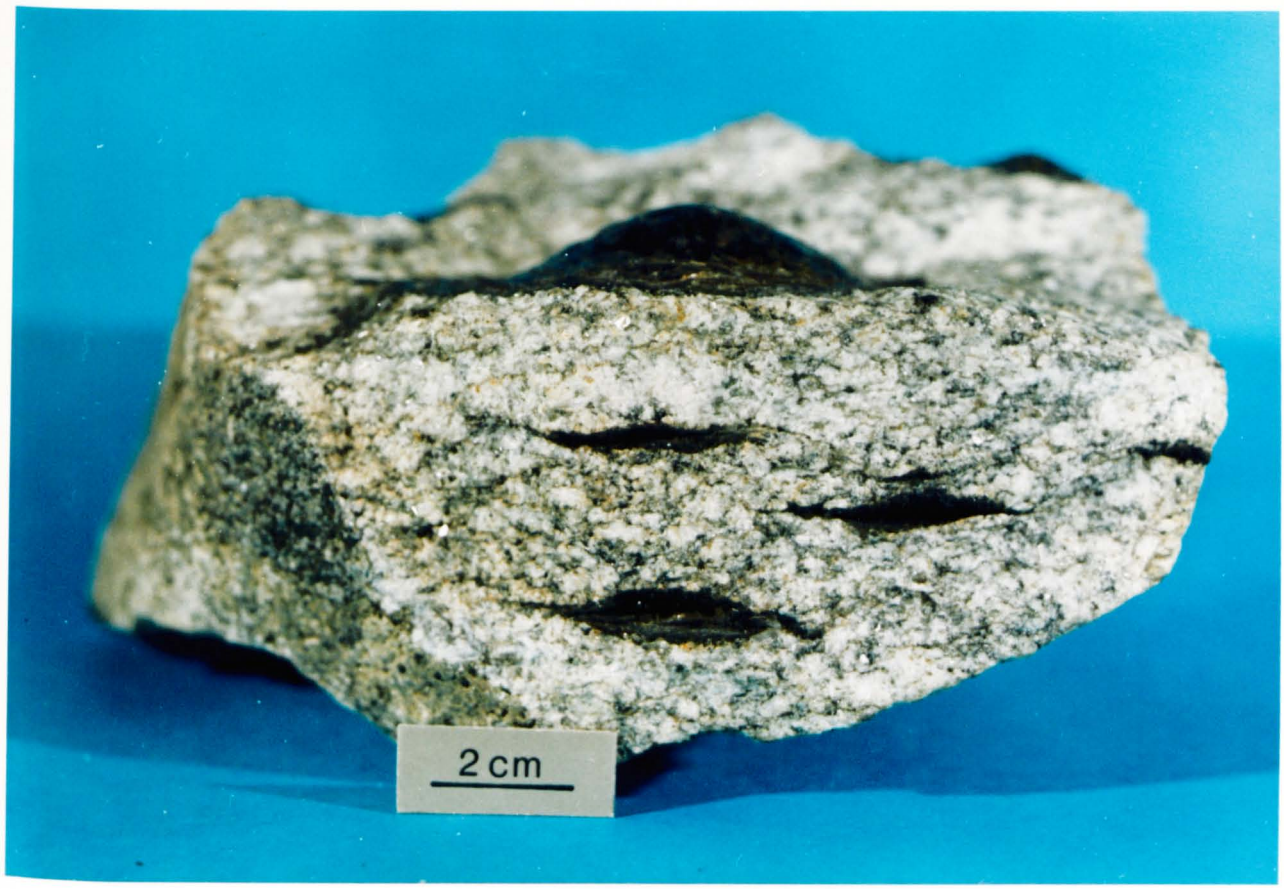

Plate 133 - End on view of block showing eliptical nature of nodules with horizontal XY planes

Plate 134 - Small vertical cliff in river section shows horizontal eliptical XY planes

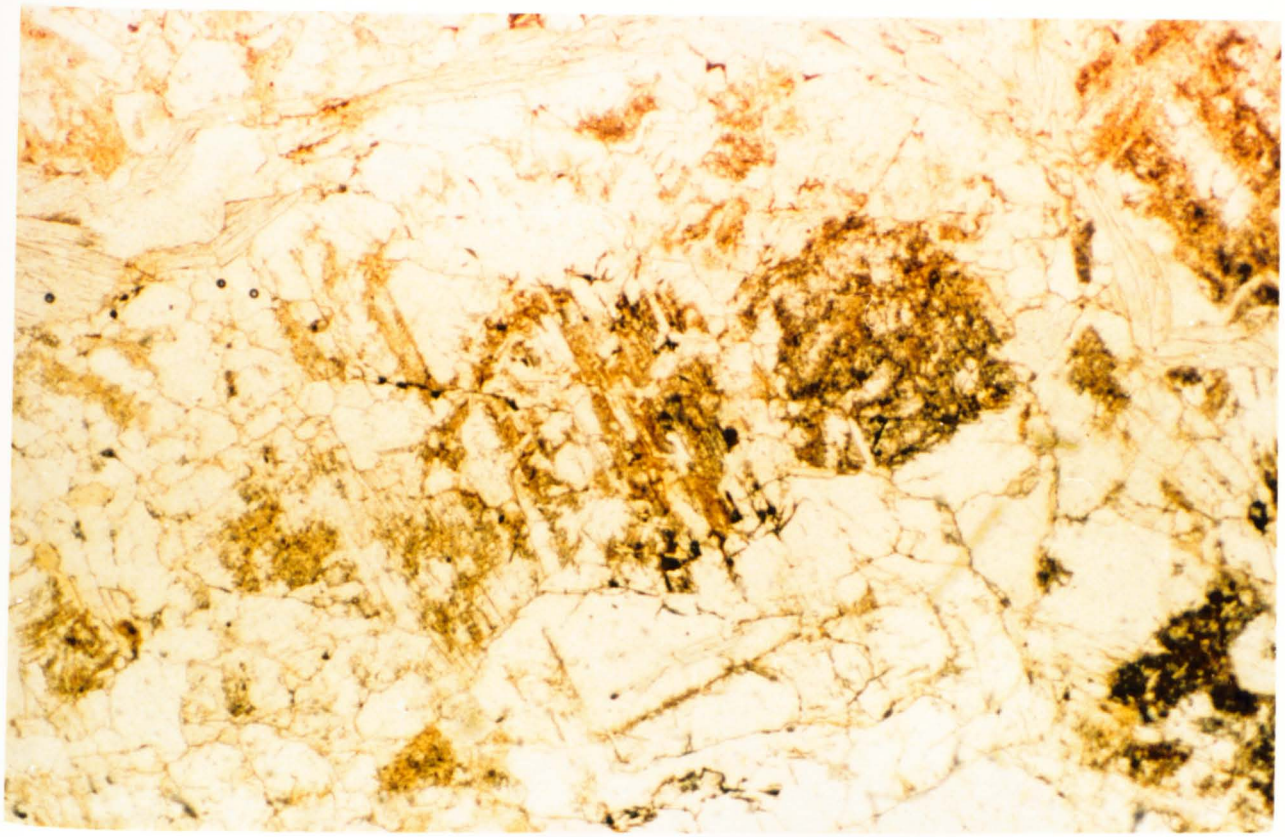

Plates 135 & 136 - F313G - (GR 6100 2240), internodular granite. Zoned plagioclase with altered cores of fine-grained white mica (Plate 135, PPL, Plate 136, XPL, x 31.25)

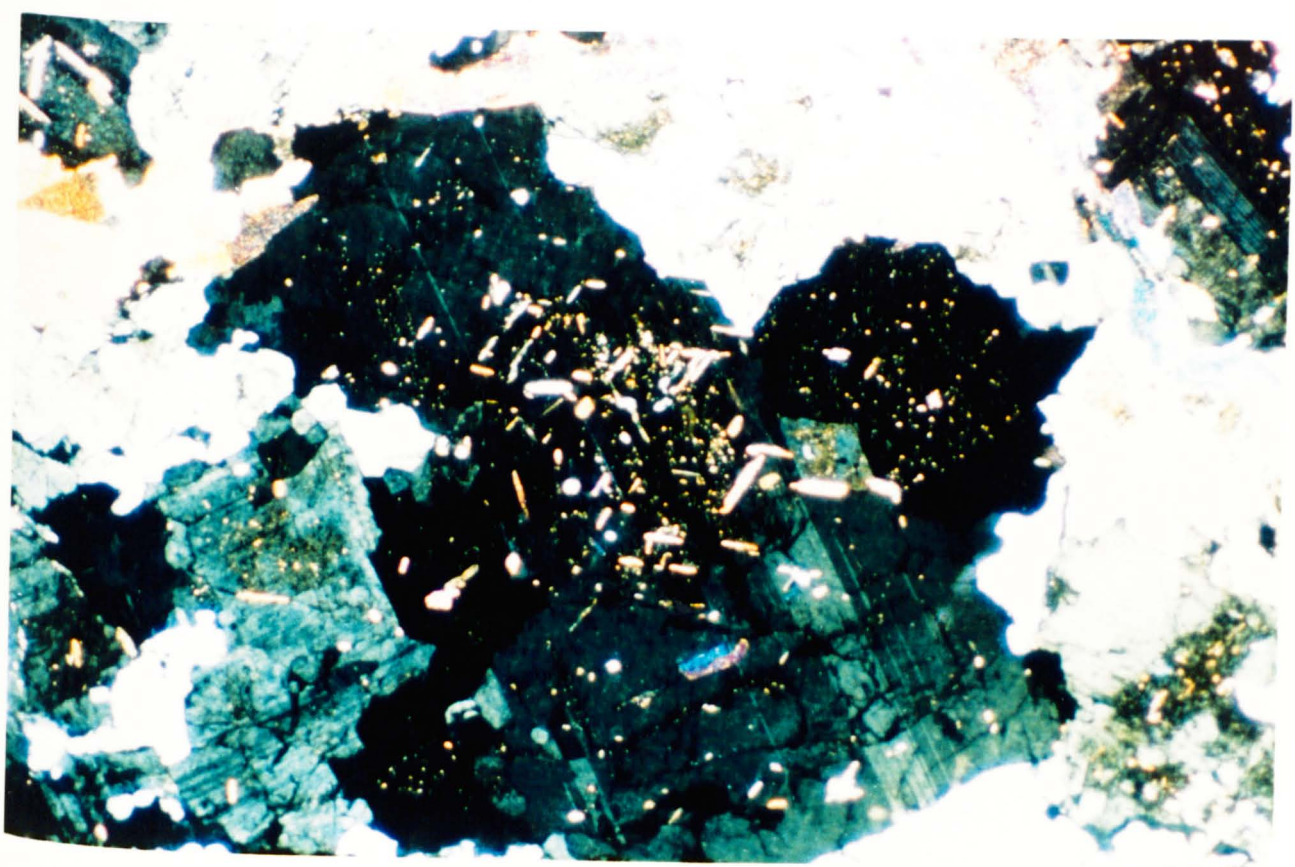

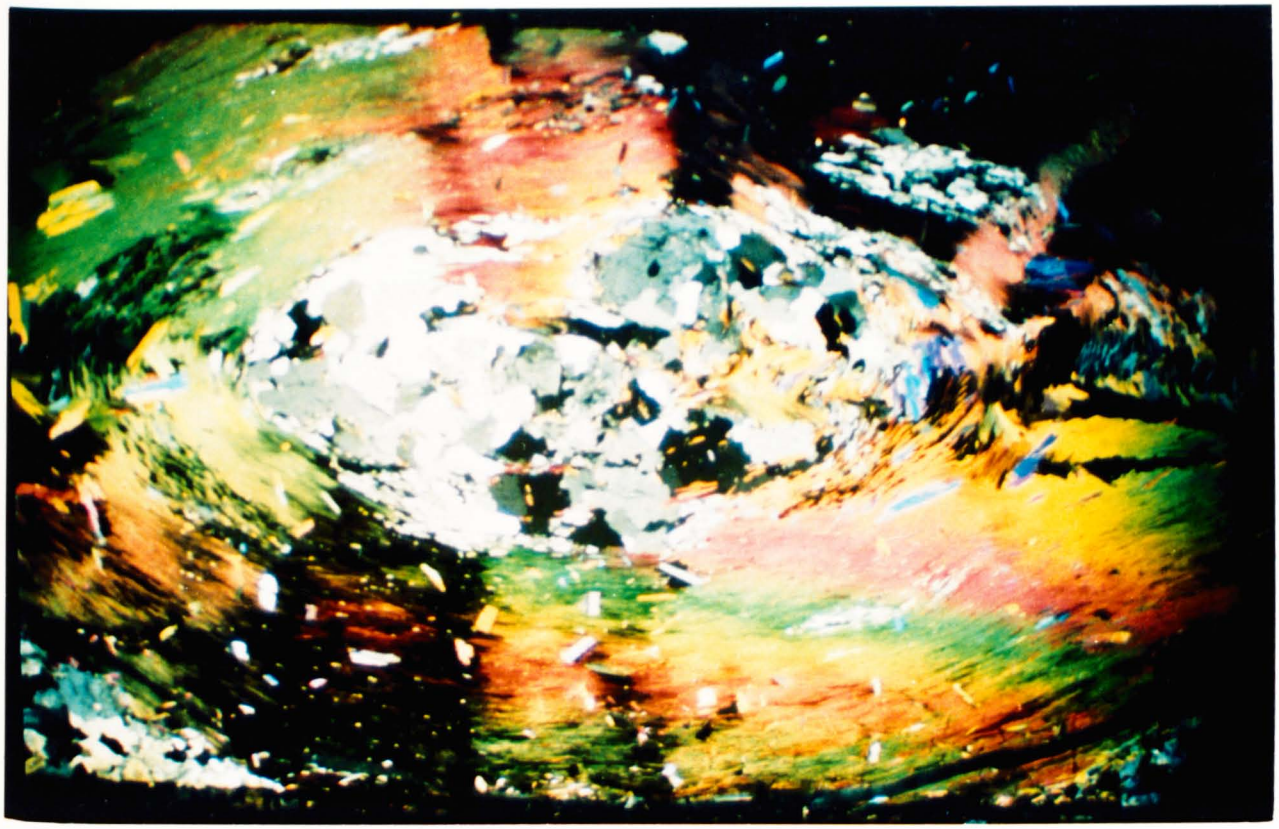

Plates 137 & 138 - Nodule cores of undeformed granite give way to parallel sheaves arranged tangentially (Plate 137, XPL, x 5.625, Plate 138, XPL, x 13.75)

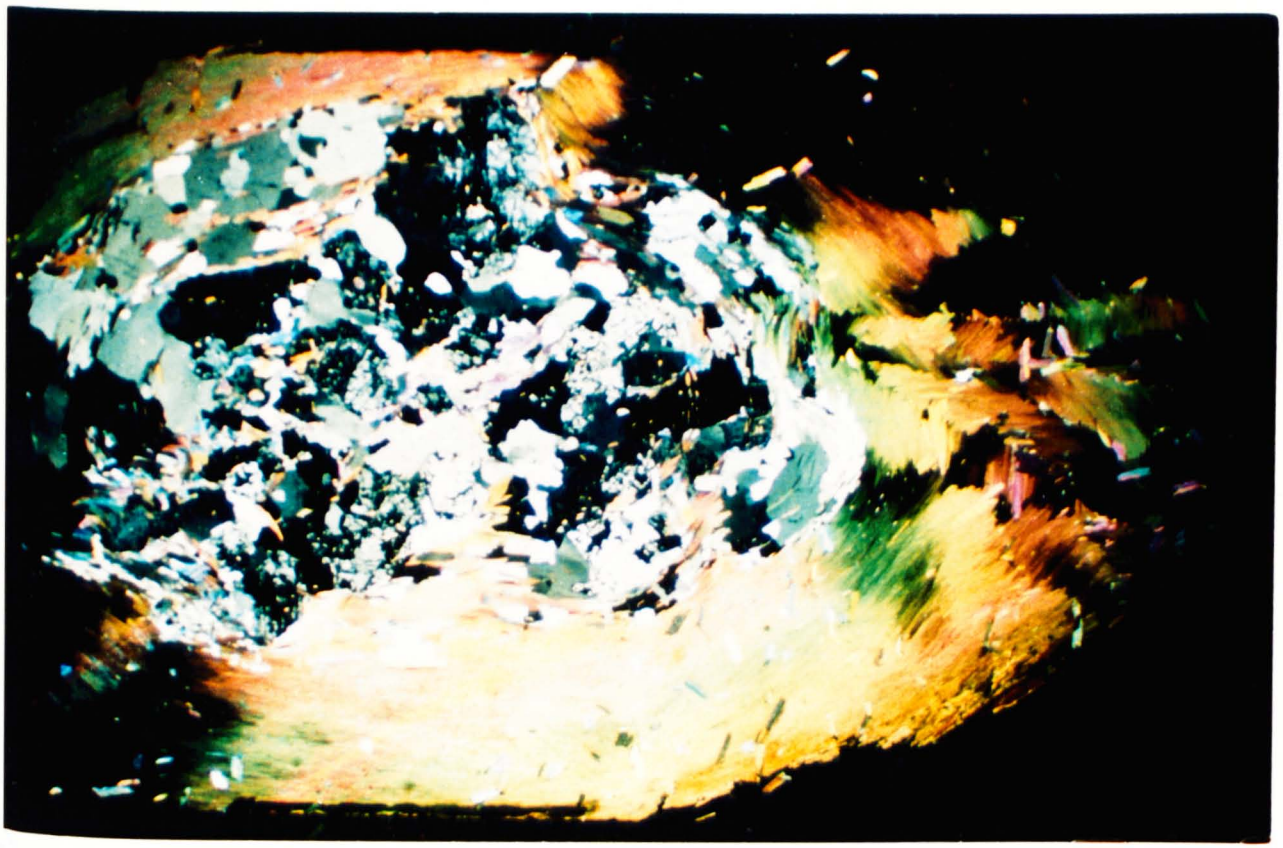

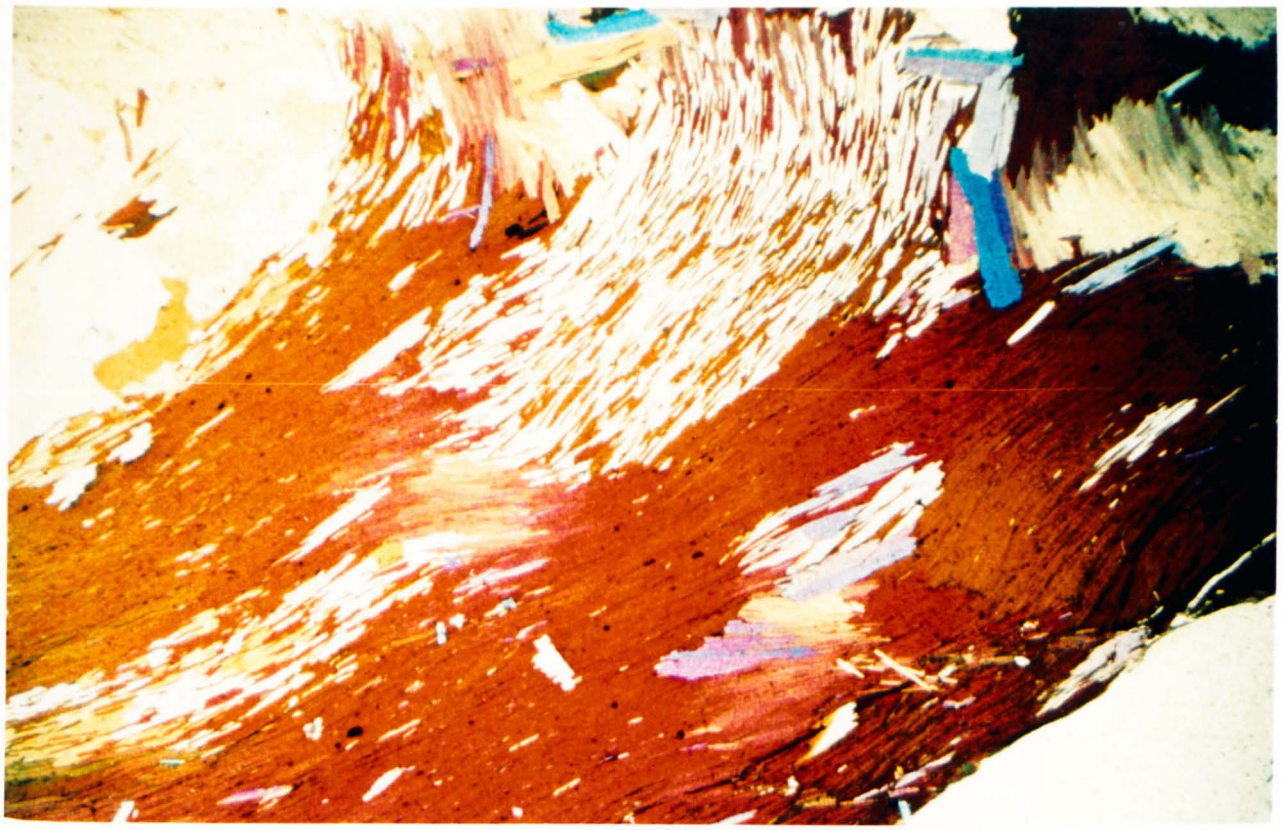

Plates 139 (PPL) & Plate 140 (XPL) - Cross-section from core to margin of nodule A transition is apparent in biotite structure moving from tangential sheaves in the lower part to tight crenulations in the equatorial region (top of field of view) (x 37.5)

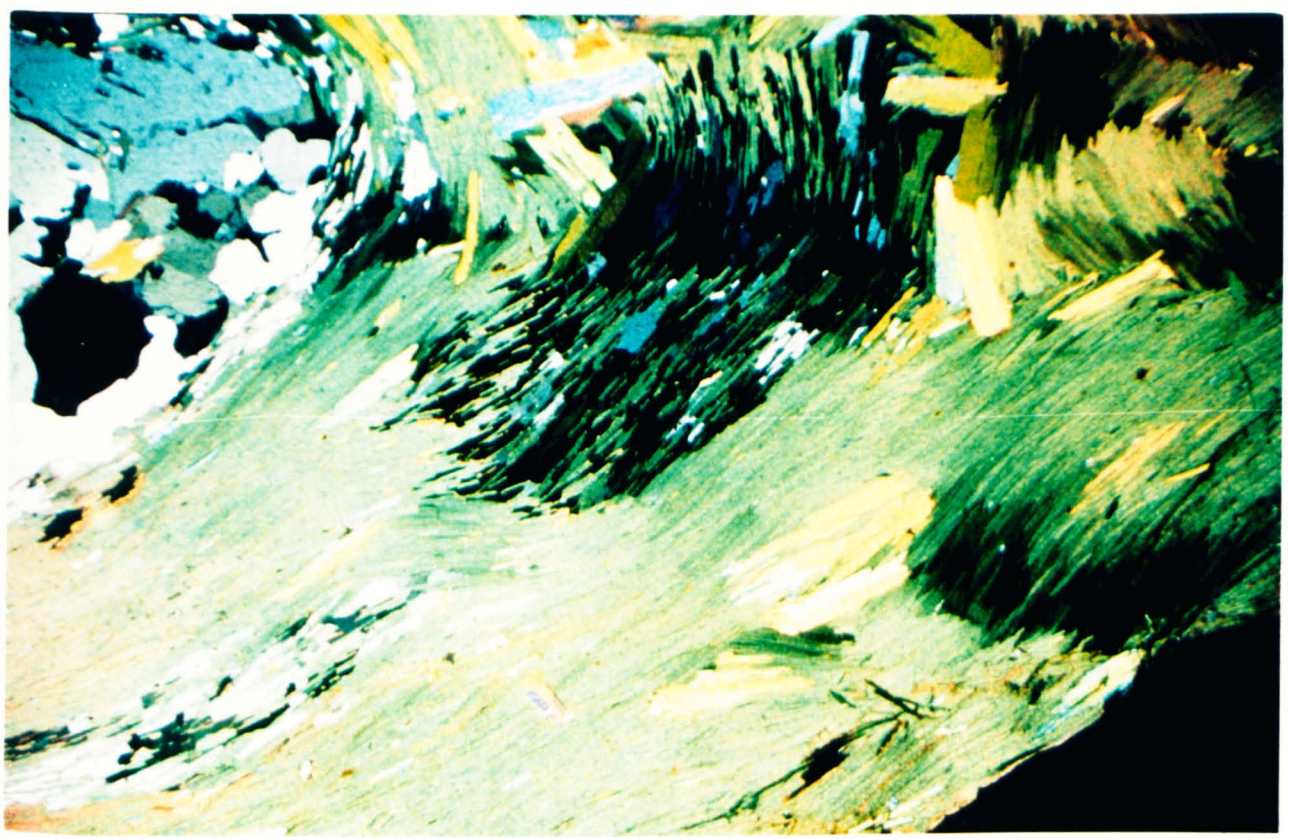

The outer layers consist of interlocking layers which are almost mono-mineralic, though small euhedral muscovites lie across the biotite layers obliquely (Plate 141). These crystals have a random orientation and are often twinned. The equator of the nodules i.e. along the XY planes are crenulated in outcrop suggesting tight folding around the nucleus (Plate 142). The structures produced by this folding are complicated by a continuation of growth tangential to the core producing mutual interference of closely packed layers resulting in an interlocking array of biotite stacks which are in optical continuity (Plates 143-146). Muscovite is often concentrated in zones where sheaves interlock.

The only known published account of such structures are those in the "Bullseye Granite" of Craftsbury, Vermont (Van Diver, 1970) where a Devonian granodiorite contains biotite orbicules. The granite cores often protrude through weathered biotite layers giving rise to the term "bullseye". The description of these structures is so similar to the Castanheira nodules that a similar model to explain their formation seems feasible. At Castanheira, textural evidence, principally tangential wrapping around a core, combined with geochemical data presented later, point to a magmatic source being more likely than any xenolithic/restitic explanation.

Van Diver (1970) demonstrated the mimicking of clay flocculation by biotite flakes in heavy liquids; loosely stacked biotite clots formed after agitation of 200-250μm crushed flakes in a methylene iodide/acetone mixture. Two possible processes were suggested to explain magmatic formation of these aggregates. The first involves flocculation of biotite flakes to form nuclei, followed by loosely packed cohesion of

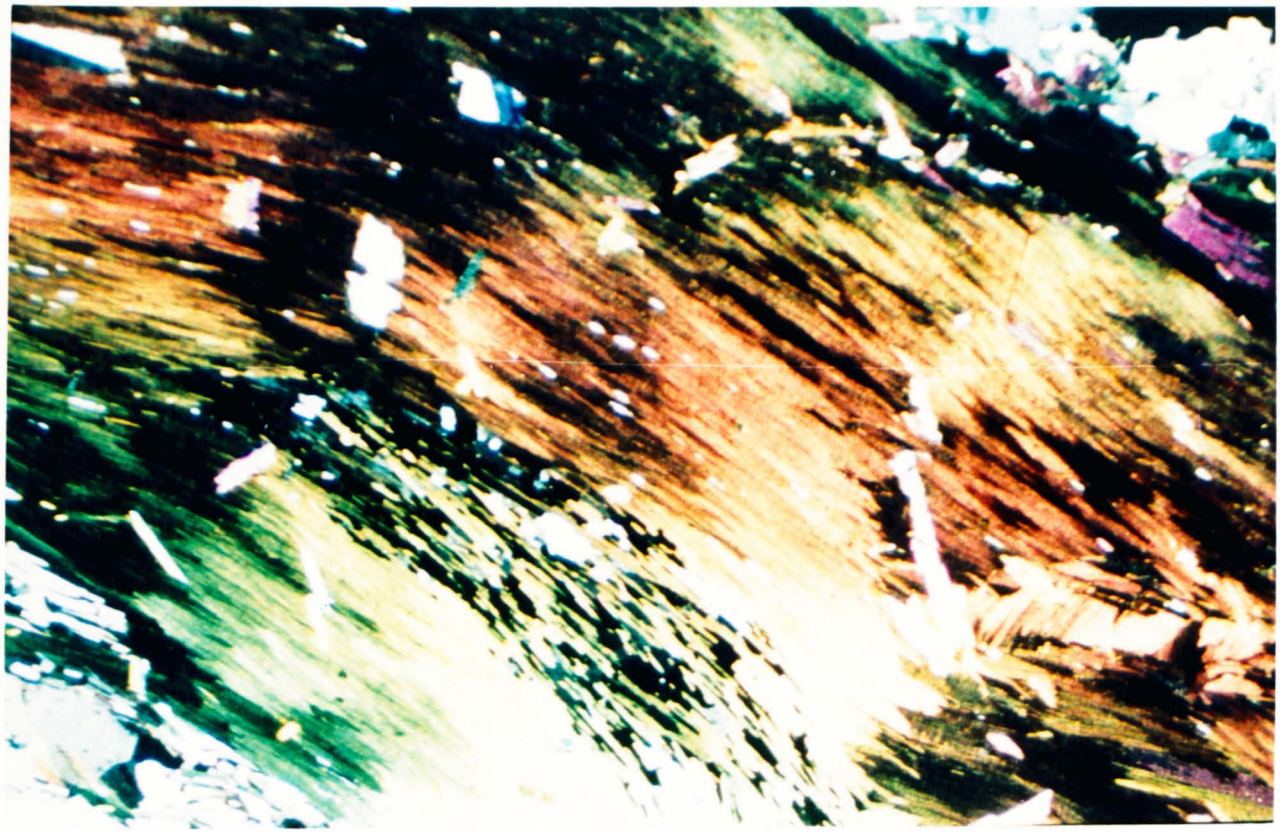

Plate 141 - Euhedral muscovites growing obliquely across the biotite layers (XPL, x 43.75)

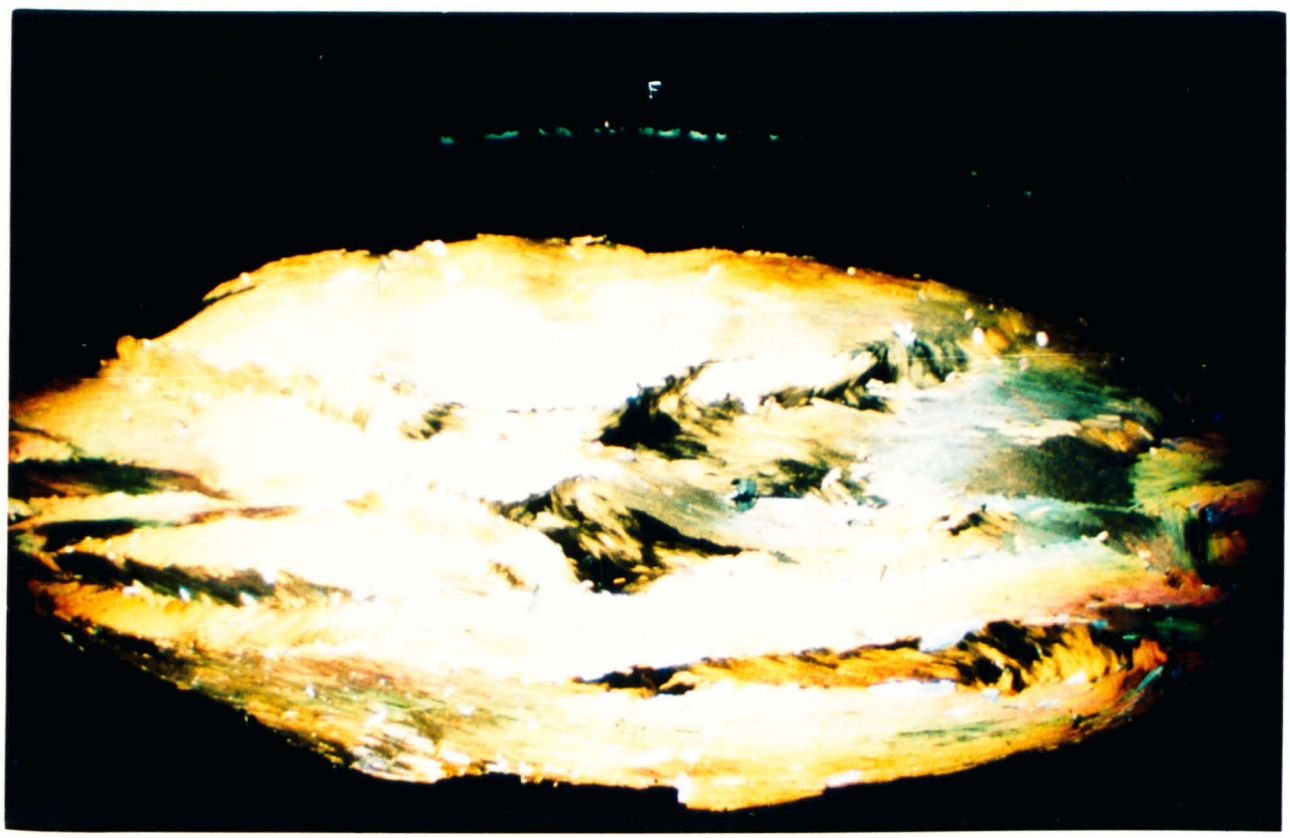

Plate 142 - Cross-section through a crenulated outer margin normal to the XY plane (XPL, x 12.5)

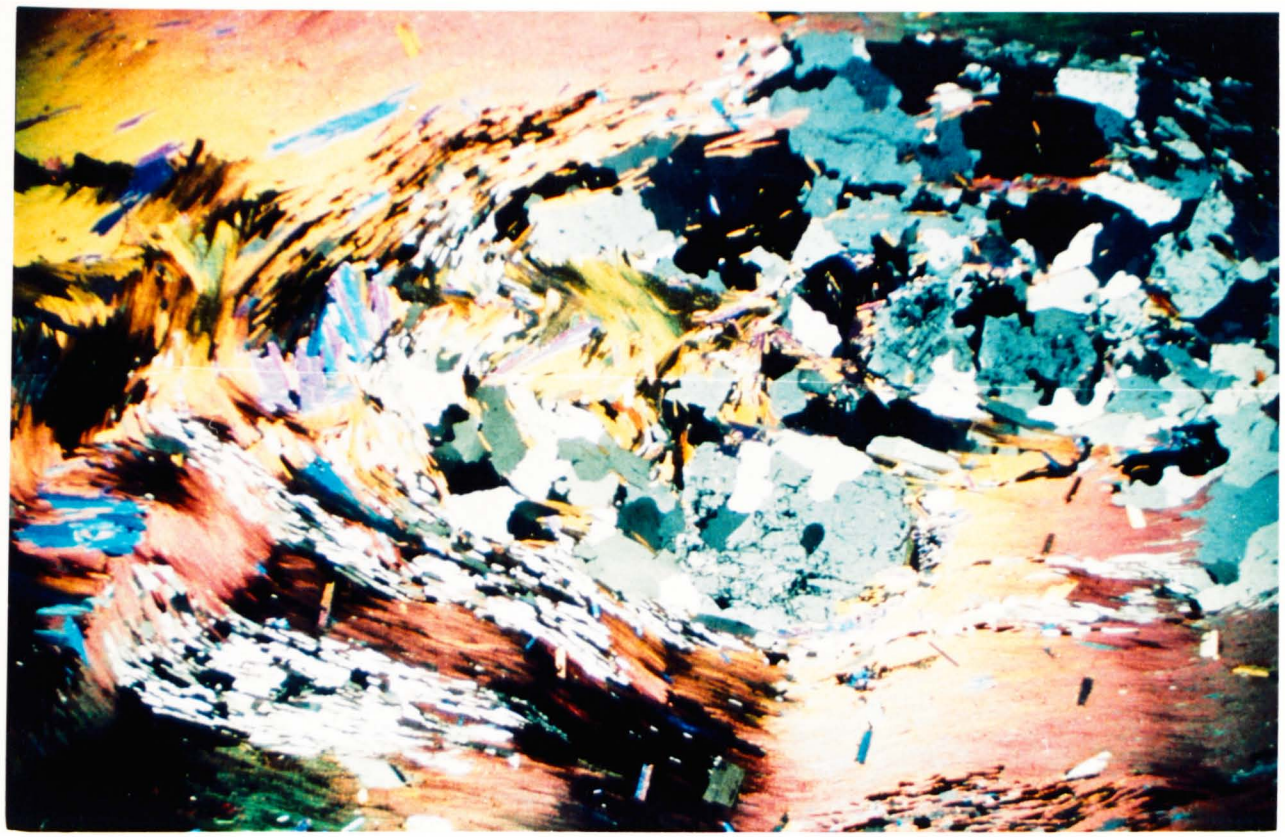

Plates 143-146 - Changing magnifications slightly to the left of a core showing interlocking arrays of biotite stacks which are in optical continuity (XPL, Plate 143, x 25, Plate 144, x 31.25, Plate 14 x 43.75, Plate 146, x 50)

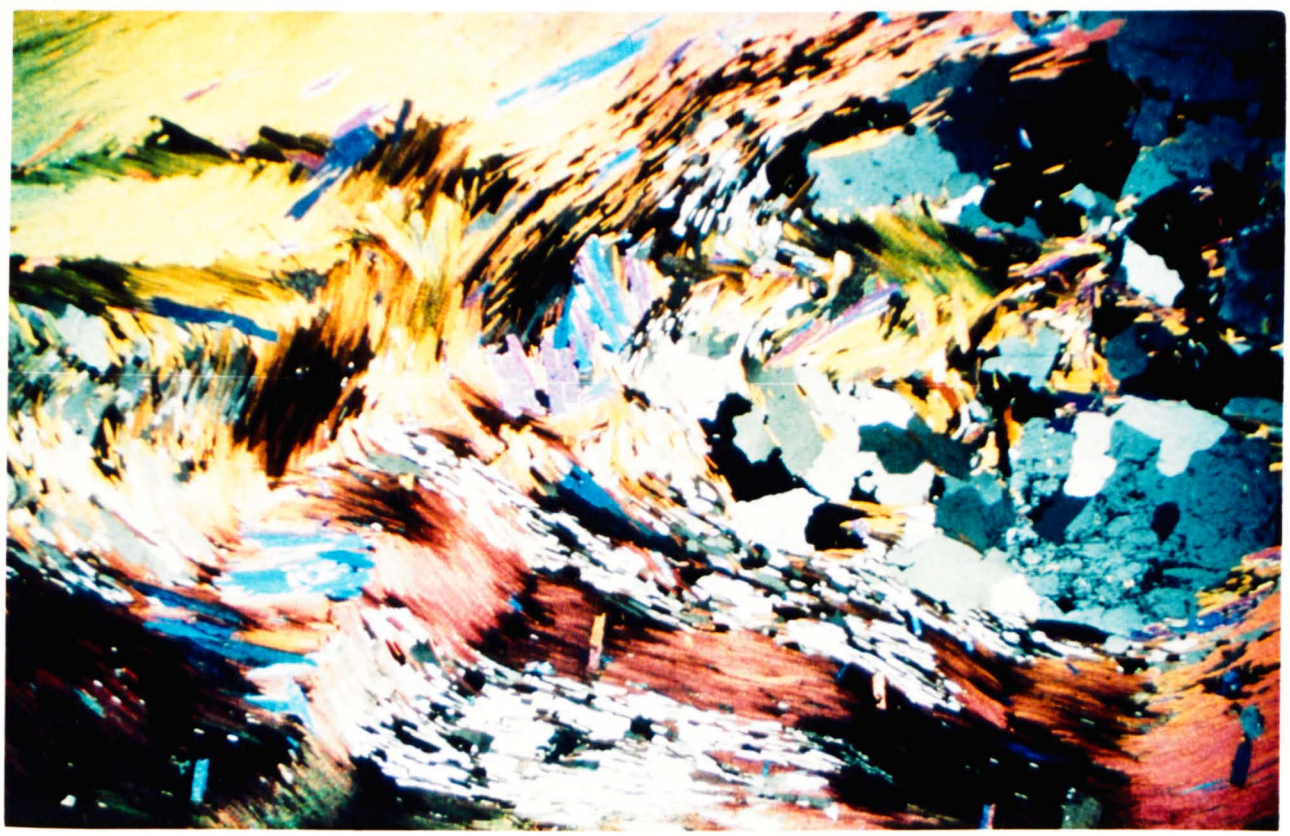

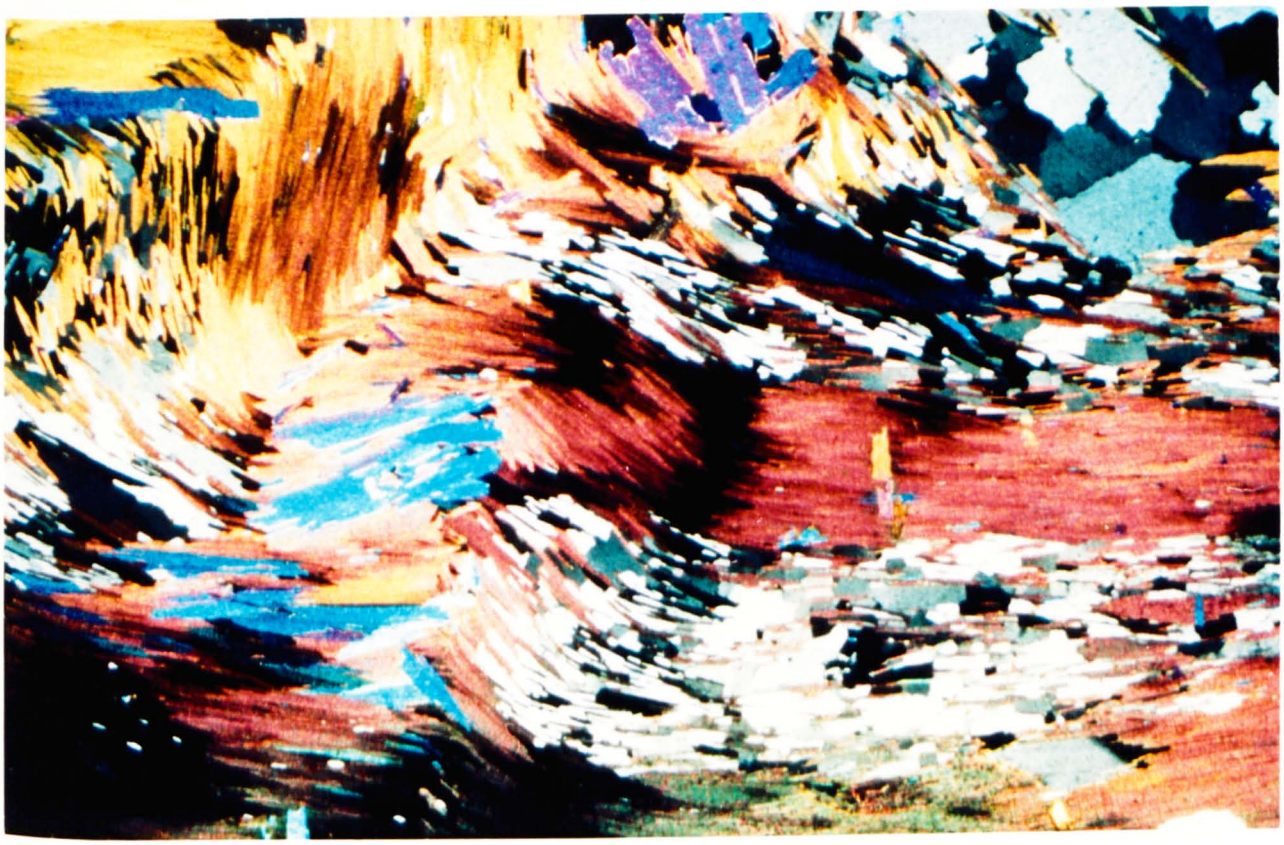

subsequent layers progressively richer in biotite and poorer in liquid. The resulting ball would have a liquid rich core with biotite concentrated in the shell. The second process, regarded by Van Diver as more likely, "involves accumulation of biotite flakes around gas bubble nuclei. Given the necessary attractive forces between the bubbles and biotite crystals, as well as between crystals, it would be possible for these to grow to very large size as the buoyant bubbles work upwards through the magma. Acquisition of additional small bubbles by these proto-orbicules would enhance their buoyancy."

If this model is correct, concentration of gas bubbles in the fluidized roof of a volatile-rich melt seems a reasonable explanation for both the presence and abundance of biotite nodules in this situation.

Measurements of the XYZ parameters of nodules (discussed later) clearly illustrate an increase in flattening near the roof. Van Diver's idea that flattening occurred by gas bubble collapse against intrusive margins raises the possibility that these structures are only found in the upper parts of intrusive bodies.

Extensive hydrous alteration of plagioclase in the American case is taken as indicating a high PH2O. This would encourage early biotite crystallization (Wones and Eugster, 1965), lower the viscosity of the magma, and possibly aid nodule nucleation. At Castanheira, plagioclase shows similar alteration suggesting the magma was fluid rich, and as discussed above, the abundance of tourmaline in the schists above the roof lends support to a model of a fluid volatile-rich magma in which free movement of biotite crystals and gas bubbles would be promoted.

(C-1) - Castanheira - Strain Analysis of Nodules

Such an abundance of ellipsoidal bodies allowed easy measurement of the principal axes of what approximates to a oblate spheroid. The aim was to dicover if any spatial variations in bulk strain were recorded by nodule shape. It proved difficult to obtain many measurements of all three X, Y, and Z parameters, however in outcrop X/Y and X/Z (or Y/Z) were easily recorded from foliation surfaces or vertical sections, especially in the river section. Measurements from nodules scattered on the surface lacked spatial control as they were not in situ. Selection of localities was dictated both by exposure and ease of achieving both vertical and horizontal sections within a few metres. Under these constraints, measurements were recorded at eight localities (Figure 6.2).

The raw data are shown in Table 6.1.

Results and Conclusions

Within the pluton, X/Y ratios show no significant (i) spread, and (ii) spatial variation, the only possible source of error in these measurements arising from erosion of nodules on exposed foliation surfaces which would tend to produce a more circular outline. However, this is not likely to have occurred on an appreciable scale.

Y/Z ratios show a much greater spread and a definite increase approaching the roof (Plates 147 & 148). The highest values were recorded at localities 1, 2, and 6, nearest the contact which, as mentioned above, represents the intrusion's roof. The main conclusion of this study is that nodules become more oblate, i.e. the "b" parameter on a Flinn plot increases towards the margins of the diapir, probably reflecting an increase in ballooning strains (Figure 6.3). This process would be augmented by migration, accumulation and flattening of gas bubbles near

Figure 6.2 - Map of the Castanheira intrusion showing the locations used in the strain analysis of biotite nodules

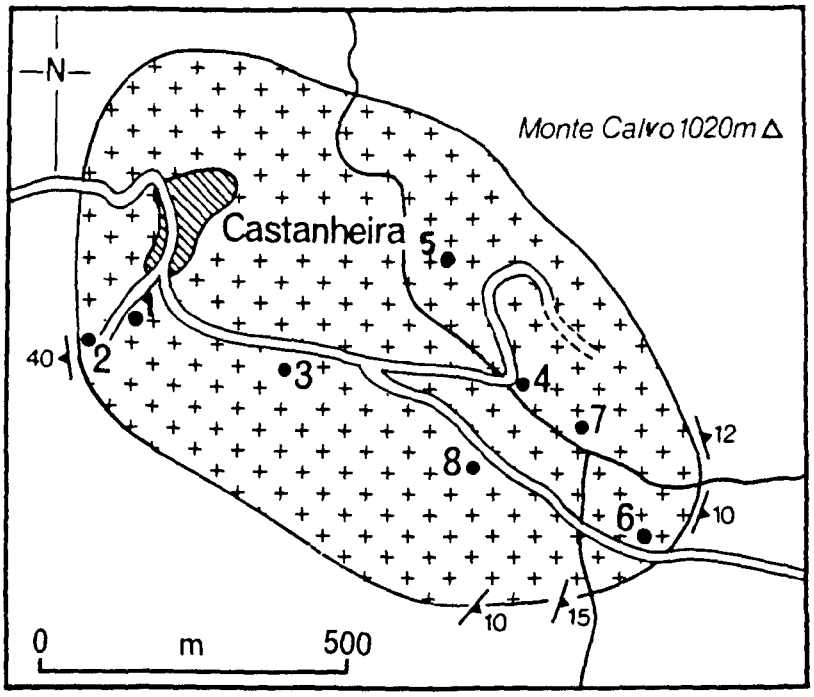

TABLE 6.2

CASTANHEIRA STRAIN DATA

Sample Locality	Means	
	X/Y	Y/Z
1	1.315 (30)	3.04 (24)
2	1.27 (30)	3.03 (39)
3	1.295 (31)	2.117 (31)
4	1.244 (38)	2.79 (33)
5	1.226 (50)	2.559 (47)
6	1.254 (50)	2.932 (47)
7	1.367 (24)	2.657 (36)
8	1.194 (36)	2.615 (48)

(Number of measurements in brackets)

Plate 147 - Profile planes of nodules, 40 m from the roof in the Castanheira river section

Plate 148 - Profile planes of nodules 10 m from the roof in river section, an increase in flattening can be seen from base to top of the photograph

Figure 6.3 - Flinn plot of Castanheira nodules demonstrating an increase in flattening strain towards the roof of the intrusion

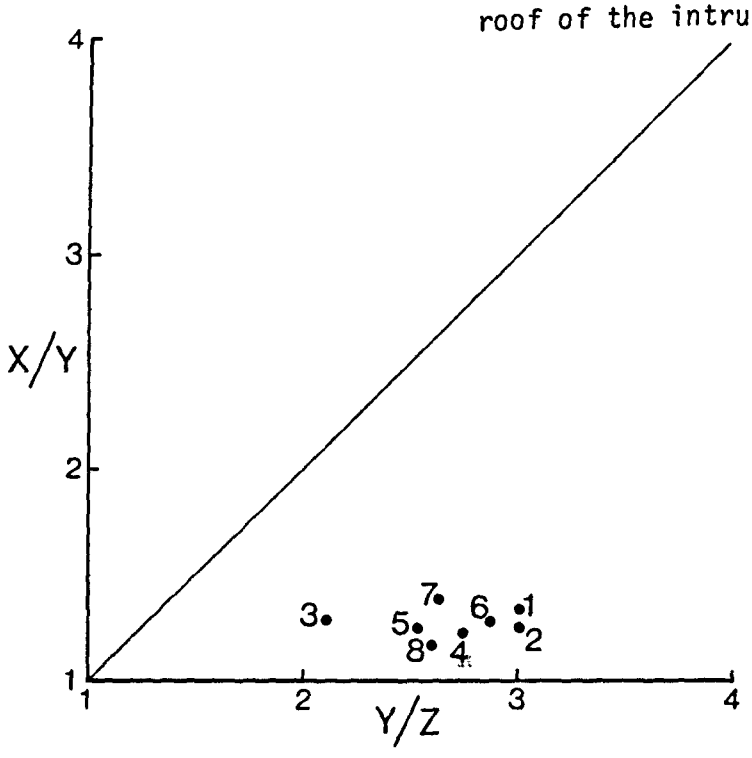

intrusive margins, as suggested by Van Diver.

(C-2) - Gestoso

The outcrop of nodular granite at Gestoso was recognized during this study for the first time and was mapped in detail (Figure 6.4). Its shape suggests that it was intruded as a wedge-like body, therefore its relationships with the host of main granite are similar to those of the felsic granite and microgranite which concentrate in this axial zone of the Manhouse inlier. On the NE it is flanked by a sheet of felsic granite, the only intrusion of this type in the northern limb; to the south it is bounded by the main granite only 50 m from the contact with the schists (Plate 149).

Although broadly similar to the situation at Castanheira, the nodules here are much more strongly deformed (Plate 150 & 151). At Castanheira, the nodules exhibited flattening strains with their X-axes aligned along the principal extension direction, however at Gestoso a strong C-S fabric is developed in the host granite around the biotite masses; often the trailing edges are aligned along "C" planes, i.e. the entire nodule is behaving like a "mega mica fish" (Plate 152). The "nodules" are now recrystallized irregular clumps of biotite interlocked in a seemingly random orientation and showing a wide range of grain size (Plate 153). Only rarely is anything recognizable as a granitic core preserved, but where it is seen, remnants of biotite wrapping are clearly seen (Plate 154). Most of the field evidence points to major similarities between the nodules at both Castanheira and Gestoso - (i) nodules are of similar size, (ii) granite cores are present in both, (iii) the host at both localities

Figure 6.4 - Map of the Gestoso nodular granite outcrop

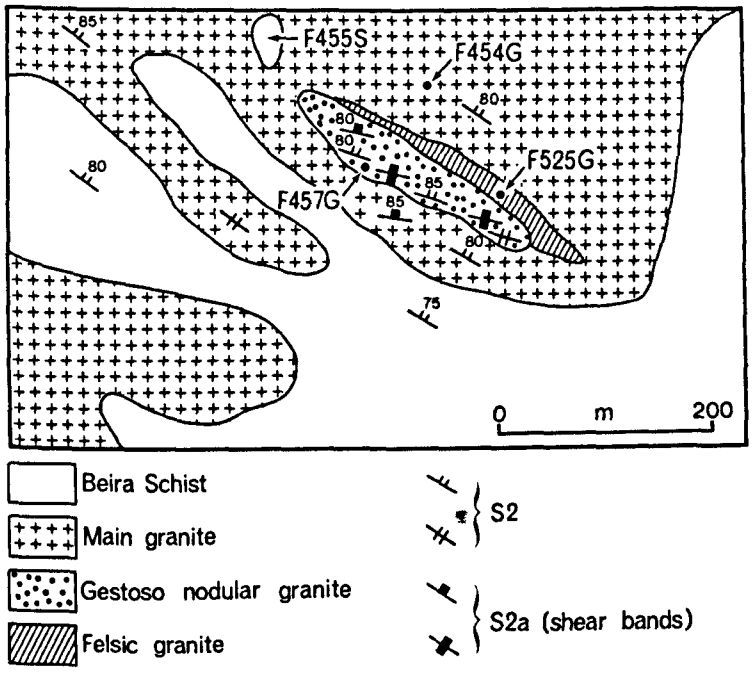

Plate 149 - Looking NE across the main outcrop of the Gestoso nodular granite, felsic granite in the background

Plate 150 - Deformed nodules, Gestoso nodular granite

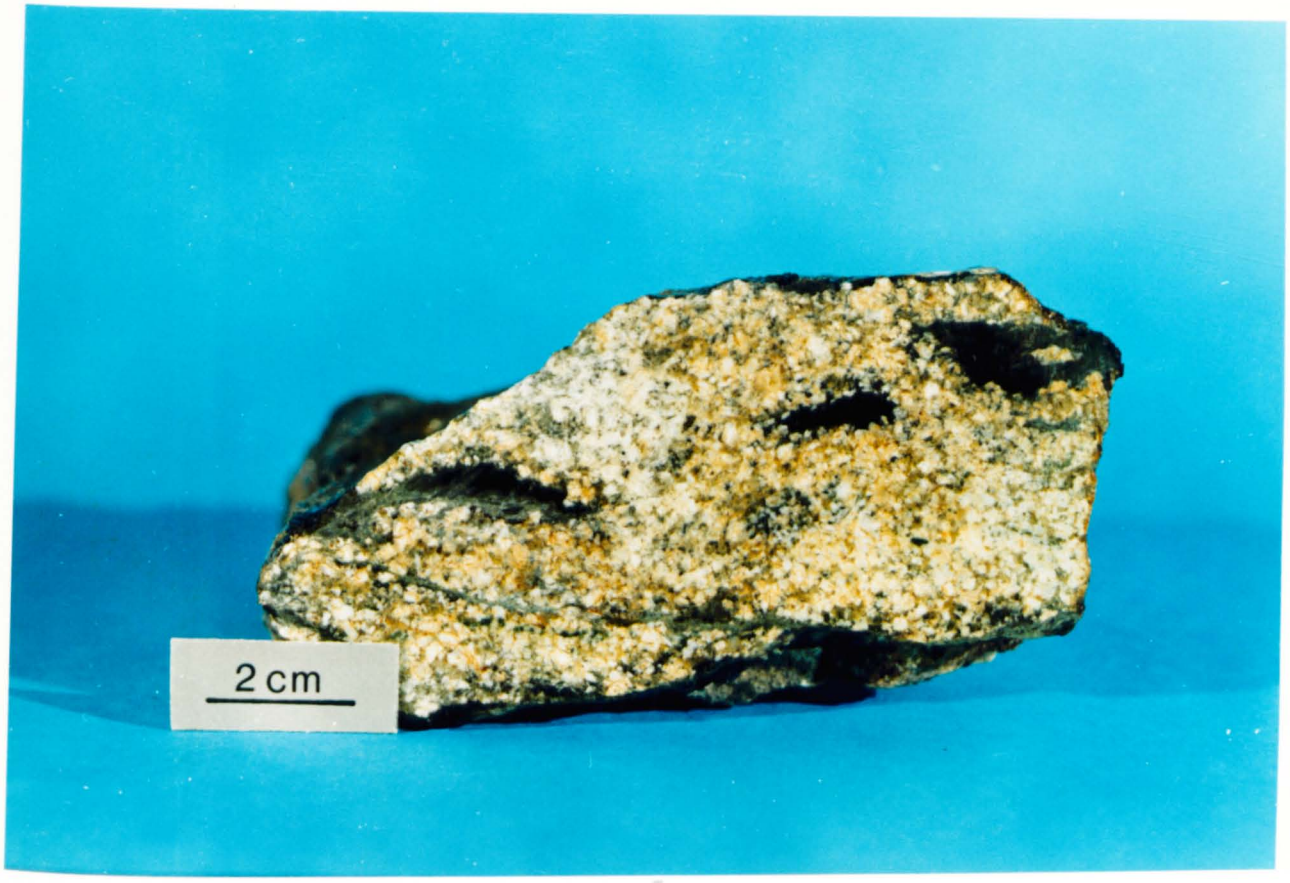

Plate 151 - Deformed nodules from same locality, note remnant granite core at top right of block

Plate 152 - C-S fabric developed in the nodular granite. Sense of shear is sinistral

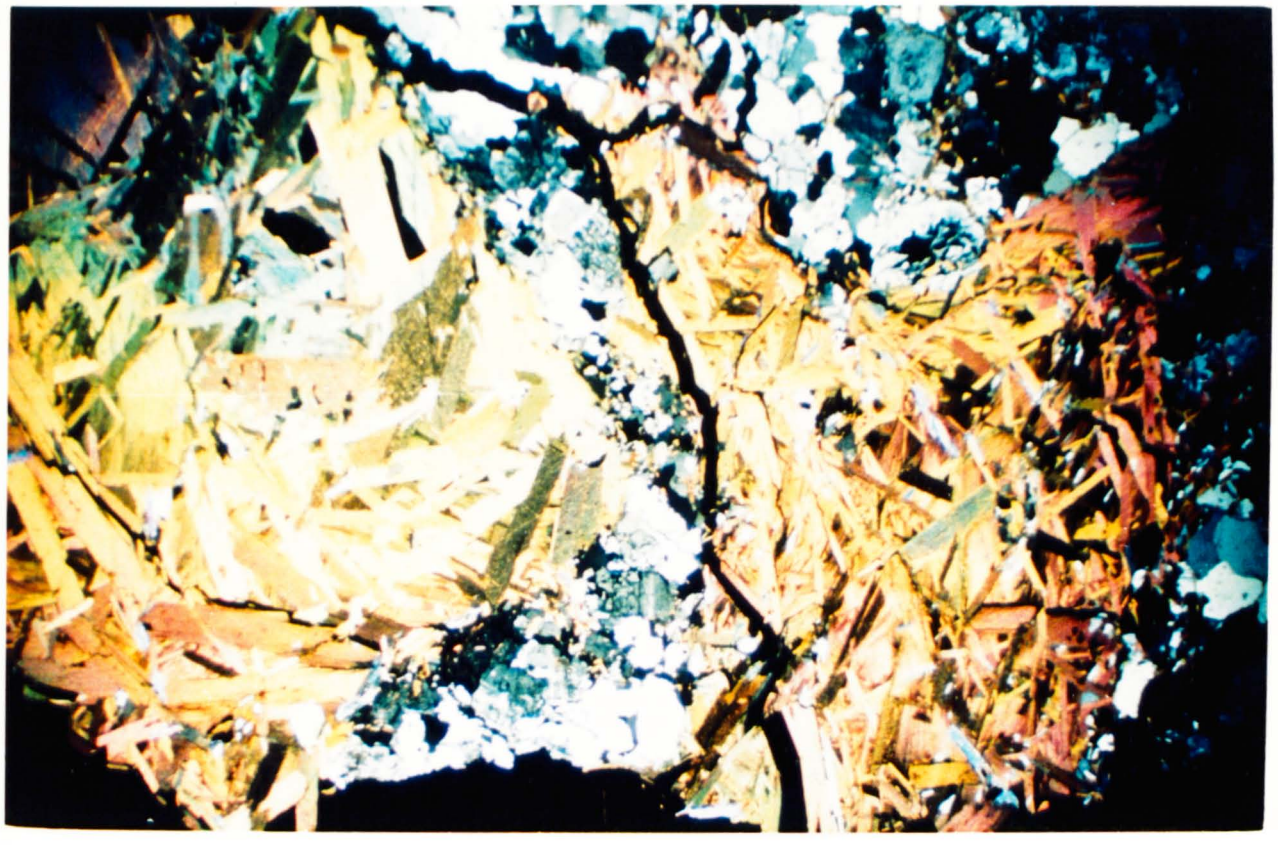

Plate 153 - Thin section cut through parts of 2 nodules, showing random interlocking biotite crystals, compare with Castanheira plates (XPL, x 18.75)

Plate 154 - Rare nodules showing possible remnant granite cores

Plate 155 - Nodules in southern part of outcrop showing relatively low shear strain

Plate 156 - Highly strained nodules 12 m north of those in Plate 155

is the main biotite muscovite granite and (iv) the XY planes of the nodules are in both cases parallel to the main foliation. The main difference is that at Gestoso, the nodular granite was intruded into a zone of higher shear strain. A marked increase in XZ ratios with distance northwards across the outcrop demonstrates that shear strains were both intense and inhomogeneous (Plate 155 & 156).

The existence of two localities of this unusual rock type within such a small area, strongly infers a similar petrogenetic mode of origin. The case for a volatile rich magma in a roof zone setting has been proposed for Castanheira. The precursor of what now forms the Gestoso outcrop may have represented something analogous before disruption and emplacement within the northern limb. These ideas are expanded below.

6.3 - Summary

It is possible at this stage to expand the proposed emplacement model (Section 4.3) to incorporate ideas developed from the study of these other facies. The shape and geometry of these bodies are all wedge or sheet-like, with their long axes generally parallel with both the main fabric and overall shape of the intrusion.

Lobate contacts between the main granite and the later facies show that conditions were still plastic when these sheets were emplaced. Their inequigranular textures indicate a two-stage magmatic history; crystallization began before intrusion to a higher level took place.

It is proposed that the granite is generated from partial melting of the high grade Beira Schists; this hypothesis is tested and discussed in Part III. As the entire pluton was intruded within a long-lived shear zone system, a model is envisaged in which discrete batches of melt were periodically generated and emplaced fairly rapidly as sheets or wedges over a protracted time period. Intrusion of successive melts to a high structural level relative to their source region can help to explain: (i) the absense of true migmatites, (ii) the generally sharp contacts with the schists and (iii) the absence of pelitic xenoliths, presumably complete melting and assimilation and/or separation of restite would have occurred by the time the melt reached a high level.

Within the steep belt, the coarse-grained granite found in the north-east may represent the earliest pulse of 2-mica granite, possibly fixing a locus for later intrusions. As noted in Section 6.2.1, numerous sheets of microgranite are concentrated near the edge of the Manhouse inlier and these can be envisaged as being injected successively into the southern

edge of the steep belt. So within the three facies of 2-mica granites represented in the Serra da Freita pluton, a possible sequence of southward migration of magma emplacement through time can be seen, with the most voluminous type being the medium-grained granite which was intruded southwards to form the southern limb. This model can also explain why the felsic granite, which is more evolved and hence presumably later, intrudes the southern limb. Although the southern limb is flat lying, intrusions into it are of similar orientation to those in the northern limb, implying that intrusion of the felsic granite sheets took place after the main pluton shape had been achieved. Finally, the nodular granite of Gestoso may represent the volatile-rich roof zone of a small batch of 2-mica granite magma which was at one stage separate from the main body and was sheeted in along with the microgranite. In conclusion therefore, field and petrographic evidence has enabled an overall emplacement model for the Serra da Freita pluton to be developed within which relationships between different granite types can be explained.

SUMMARY OF CONCLUSIONS FROM FIELDWORK (PART II)

The following are the main conclusions from the mapping study.

Structural Analysis

(1) Recognition and naming of the Serra da Freita sinistral transpressive shear zone.

(2) Detailed structural analysis of pre-, syn-, and post-shear zone structures.

(3) Recognition that the geometry of the granite is much more complex than that shown by the simple cross-section on Sheet 13-D; the granite is an inclined sheet with a flat lying distal end.

(4) Presentation of an emplacement model for the pluton within a sinistral transpressive shear zone.

Metamorphism - Revision of the Existing Isograd Map of the Area

(5) Demonstration that the Serra da Freita granite lies in the thermal axis of a regional metamorphic belt, and that this belt continues to the north-west.

(6) Recognition of the distinction between the regional sillimanite belt and the cordierite/sillimanite thermal aureole of the Arouca quartz diorite.

Plutonism - Detailed Mapping of the Serra da Freita Pluton

(7) Mapping of the pluton's geometry leading to (3) above.

(8) Recognition of several different facies of granite showing that the pluton is not one single homogeneous body, integration of their intrusion style with (4) above.

(9) Interpretation of the small intrusion of Castanheira as a biotite

nodular volatile rich fluidized roof zone of the main granite.

(10) Strain analysis of these nodules reflecting an increase in ballooning strains approaching the roof.

(11) Discovery and mapping of the nodular granite outcrop at Gestoso and its correlation with Castanheira.

The association between deformation, metamorphism and plutonism shown by detailed field and petrographic work has now been demonstrated, the remainder of this study is aimed at using major element, trace element and isotopic geochemical data from both granite and schist to understand these relationships in terms of petrogenetic processes.

PART III -- GEOCHEMISTRY

CHAPTER VII--MAJOR AND TRACE ELEMENT GEOCHEMISTRY

7.1 - Introduction

The preceding chapters have been concerned with the interpretations gained from mapping the Serra da Freita, the main conclusions of which have just been stated. The other main aim of the field study was the collection of samples of both granites and metasediments for geochemical analysis. The analytical procedures used are summarized in Table 7.1. Details of all laboratory procedures, sample localities and full major and trace element analyses are given in Appendices 1-3.

From the 218 samples collected, 189 were fresh enough for geochemical work. Samples were selected to include all facies of the granite recognized during mapping and a range of metasediments of all regional metamorphic grades and lithologies (Table 7.2).

7.2 - Aims

The main aims of this section are to consider the bulk geochemical characteristics and variations within the granite types and between the granites and schists, and to discuss these in terms of petrogenetic relationships.

7.3 - Geochemical Characteristics of the Serra da Freita Granites

Seven granite types (or facies) were established in the field, and are now characterized in terms of geochemical variations.

Notation on diagrams

Table 7.1 - Procedures and techniques employed in geochemical analysis

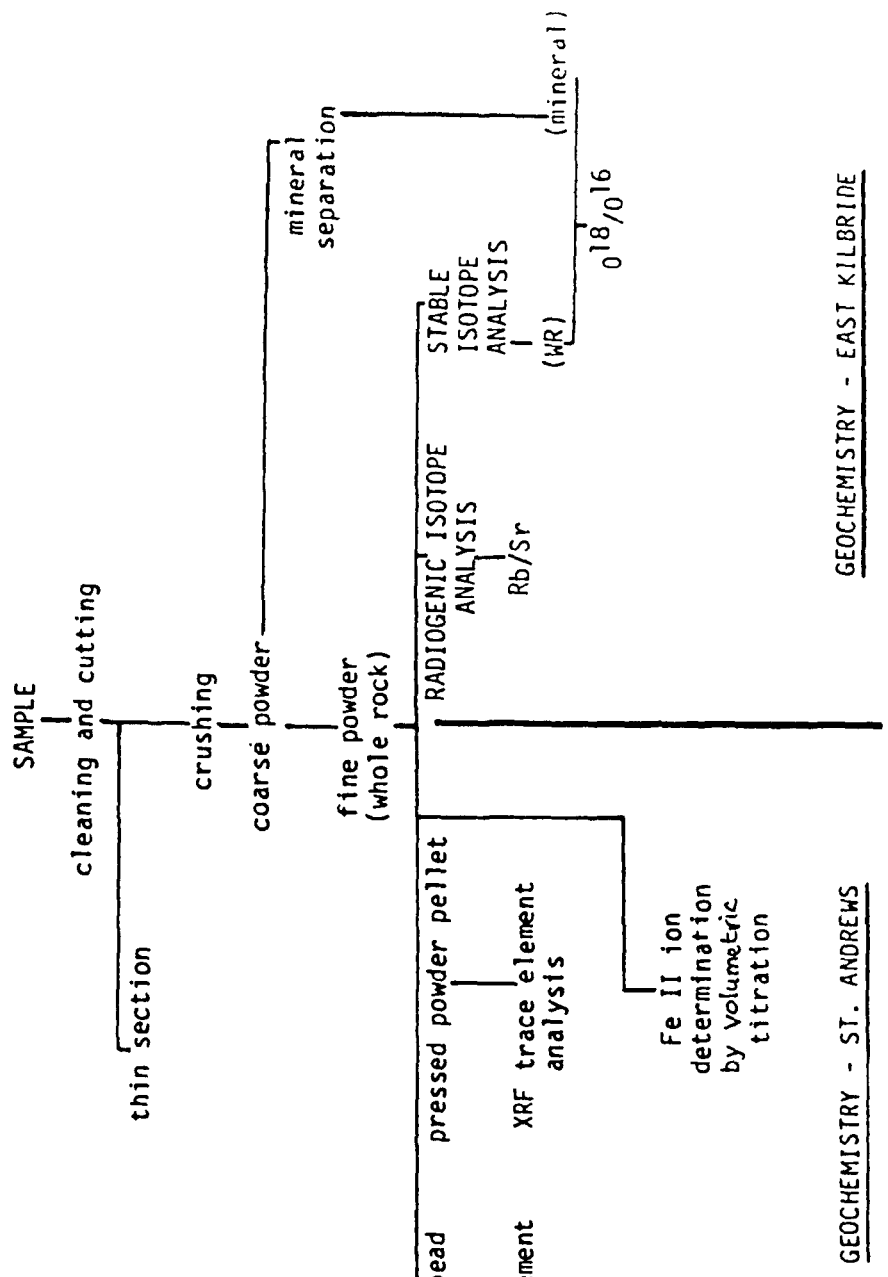

Table 7.2 - Sample types and numbers analysed

Main Granite	57
Microgranite	7
Sheared Granite	6
Contact Leucogranite	13
Felsic Granite	8
Aplite	7
Castanheira/Gestoso	3
(Total)	(101)
Metasediments	88

The 2-mica granites are depicted using variations on a cross (+, main granite; x, microgranite; and ✕, sheared granite). The muscovite granites are shown by open symbols (▽, contact leucogranite; ◇, felsic granite; and △, aplite.) Castanheira and Gestoso samples are grouped together (⊡). F313G (Castanheira) and F457G (Gestoso) are 2-mica inter-nodular granites; F522G is from the biotite-free Castanheira roof zone, field relations are similar to the contact leucogranite of the main body and its geochemical affinities will be considered. F512G was collected from the north-westward continuation of the Serra da Freita pluton near Fermedo (Figure 2.2). It is of the main 2-mica granite and lies within that field for all plots.

MAJOR ELEMENTS (WEIGHT% OXIDES)

SiO2

SiO2 values fall in a very restricted range between 69.5% - 76.0%; the 2-mica granites have values of 70% - 74% and the muscovite granites are slightly more acid ranging from 72% - 76%.

Al2O3

Again a narrow field is defined with most samples ranging between 14% and 17%. There is no systematic variation between facies (Figure 7.1a).

FeO, Fe2O3, MgO, TiO2

FeO values (0 - 1.8%) are higher than those of Fe2O3 which are, with one exception, <0.6% implying that the granites are generally in a fairly reduced condition. No trend is apparent within the Fe2O3 values but the muscovite granites show a depletion in FeO relative to the 2-mica granites (Figure 7.1b-c). As Fe(III) values are approximately constant, this represents an overall depletion in Fe(tot) (Figure 7.1d) and a lower

Figure 7.1 - a, b, c

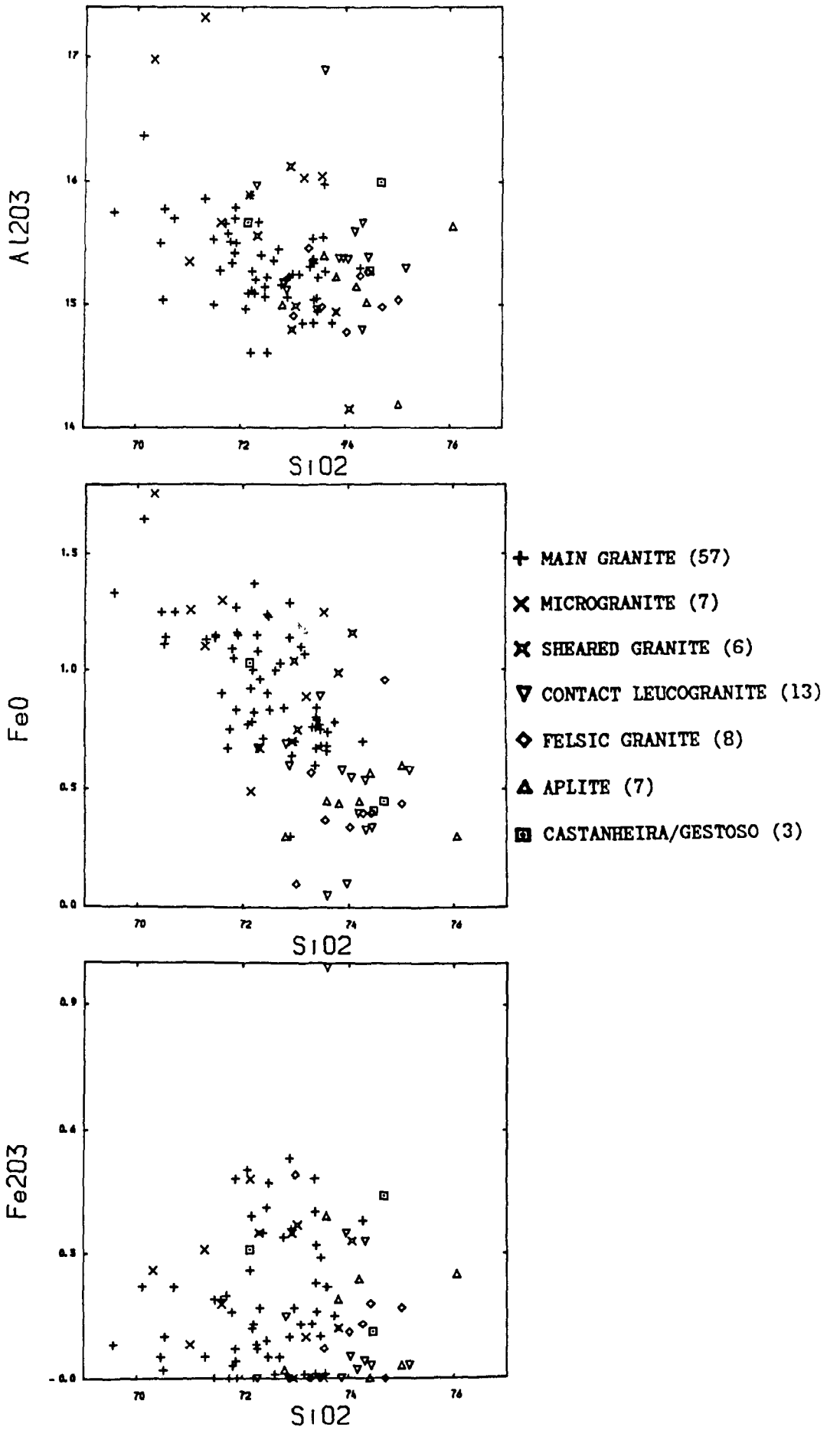

Figure 7.1 - d, e, f

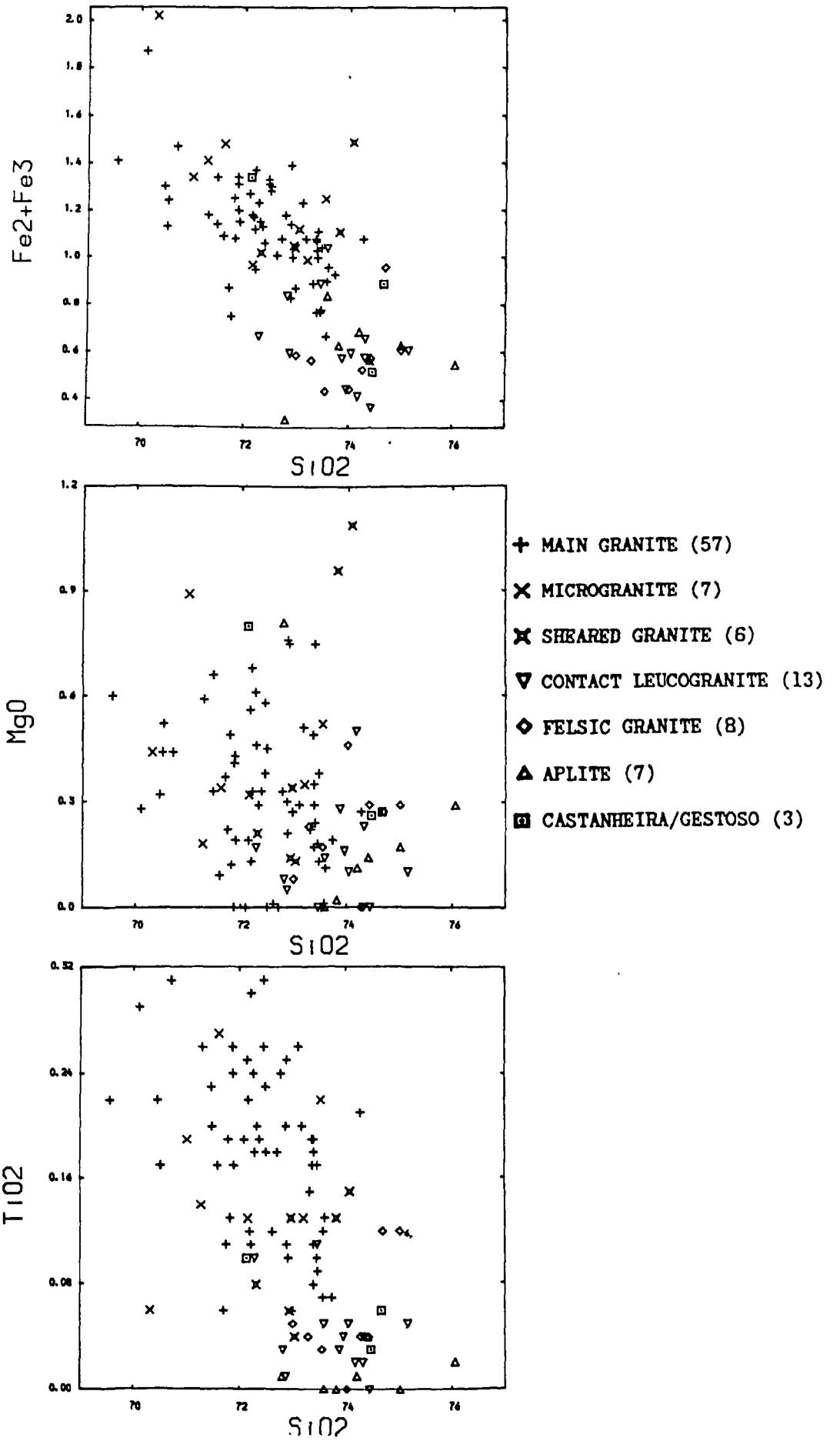

Fe(II)/Fe(III) ratio in the muscovite granites.

MgO shows minimal depletion in the muscovite granites (Figure 7.1e), but the TiO2 trend is similar to that of FeO (Figure 7.1f).

CaO, Na2O, K2O

Values for CaO of 1.64% (F313G) and 1.5% (F457G) are more than 3 times higher than in the other granites which, as a group, show a very slight CaO depletion in the muscovite granites (Figure 7.1g).

The muscovite granites are markedly enriched in Na2O (Figure 7.1h) and depleted in K2O (Figure 7.1i) compared with the 2-mica granites. The internodular granites are the most sodic (Na2O around 6%) and show a severe depletion in K2O, well away from the main trend (Figure 7.1j). Overall, total alkalis are fairly constant, between 7% and 9% (Figure 7.1k).

P2O5

There is no overall pattern in P2O5, although the Castanheira/Gestoso samples show some depletion (Figure 7.1l).

Summary

Major element behaviour can be summarized as follows:

(i) SiO2, Al2O3, and Fe2O3 show no systematic variations between facies.

(ii) FeO values exceed those of Fe2O3.

(iii) The 2-mica granites (i.e. the main granite, microgranite and the sheared granite) form a coherent group.

(iv) The muscovite granites can be characterized as depleted in FeO, TiO2, and K2O, slightly depleted in MgO and CaO, and enriched in Na2O relative to the 2-mica granites.

(v) The inter-nodular granites are enriched in CaO and Na2O, and depleted

Figure 7.1 - g, h, i

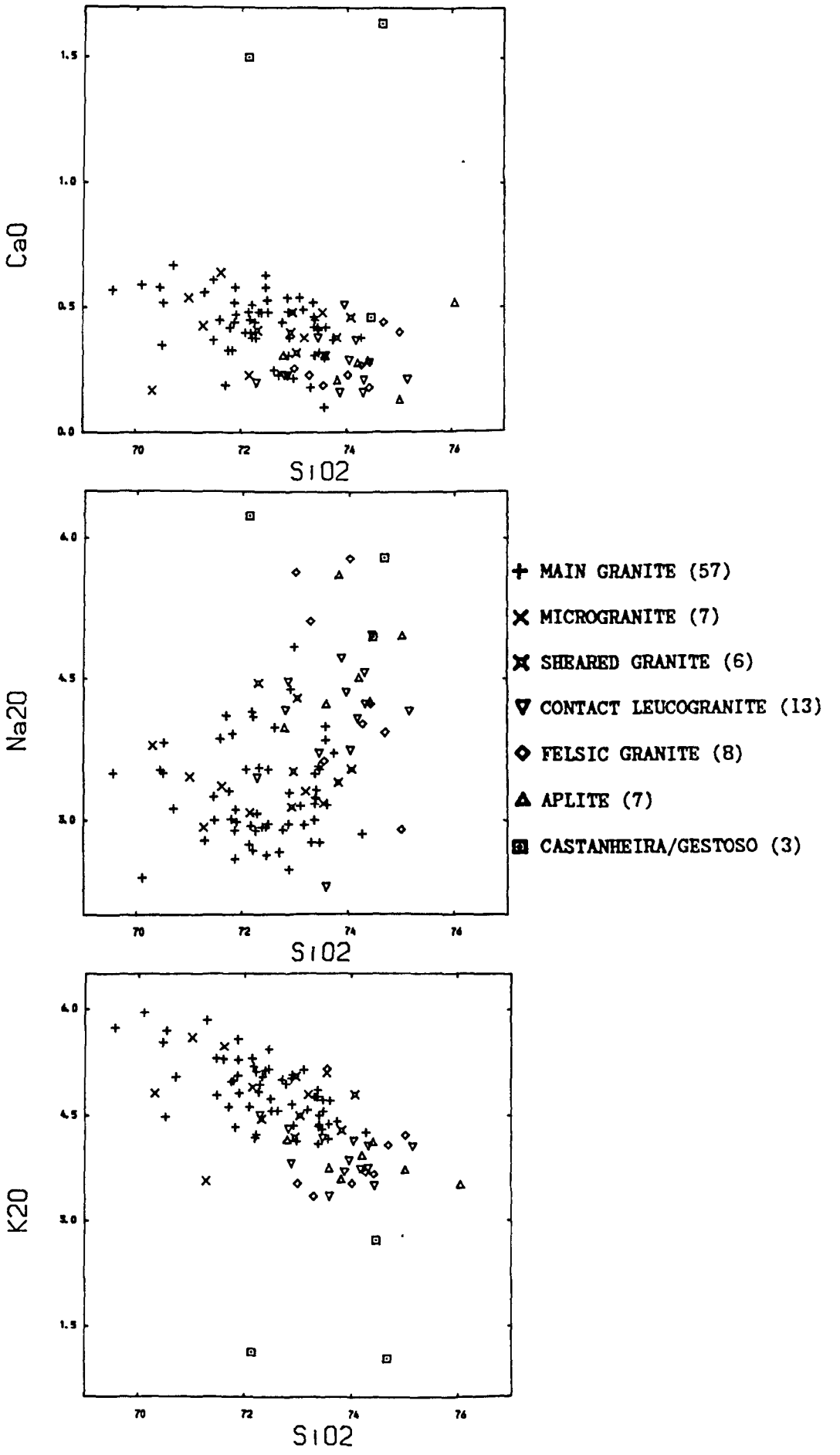

Figure 7.1 - j, k, l

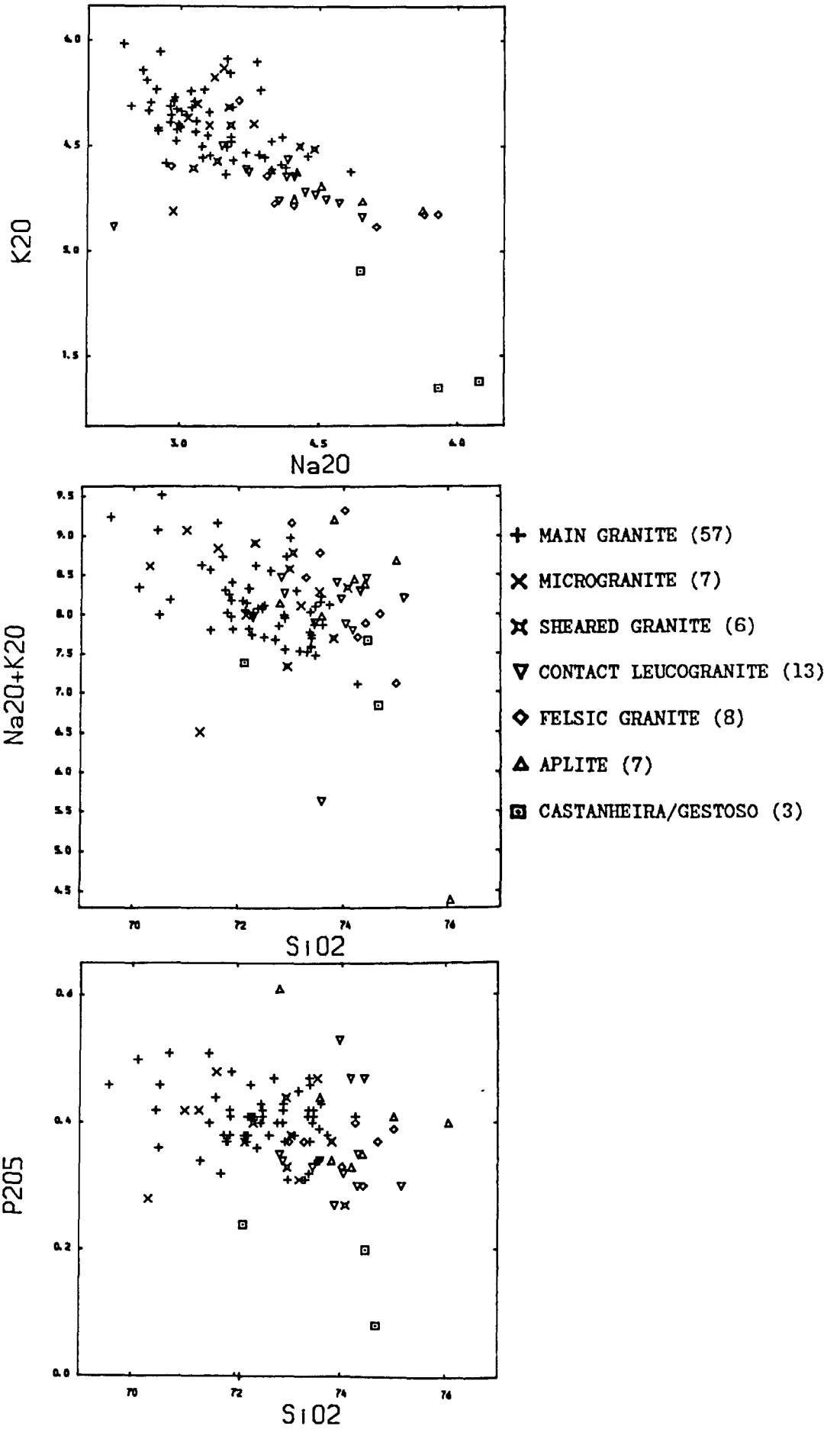

in K2O and P2O5. The CaO enrichment and K2O depletion are most noticeable and the samples plot well away from the other groups for these oxides.

The Na2O enrichment through the muscovite granites to the nodular granites is reflected on a Q-Or-Ab diagram by an increase in normative albite (Figure 7.2a). An AFM plot confirms the overall low values for Fe and Mg and the trend towards Fe and Mg depletion in the muscovite granites (Figure 7.2b).

All the granites are strongly peraluminous (Clarke, 1981) with A/CNK > 1.1 (Figure 7.3a-b), however the K2O/Na2O plot shows that few of the granites fall in the Lachlan S-type field (White and Chappell, 1983); although K2O values are comparable (most have K2O between 3% and 6%), Na2O is much higher in the Serra da Freita granites typically between 2.5% and 6% (Figure 7.3c). The nature of peraluminous and S-type granites will be discussed later.

TRACE ELEMENTS

Little variation is seen in Nb, La, Ni, Cu, Zn, and Pb (Figure 7.4a-f).

Rb, Sr

Rb contents are generally high, most falling between 200 and 400 ppm. Within this range, there is a lot of scatter and no clear trend. The contact leucogranite shows distinct enrichment with two samples > 500 ppm. The nodular granites (F313G and F457G) are severely Rb depleted with values of 19 ppm and 49 ppm respectively. The leucocratic roof zone of Castanheira shows mild depletion, falling just below the main group (Figure 7.4g).

Most granites have < 100 ppm Sr. As with Rb, no correlation is apparent

Figure 7.2 - a, b

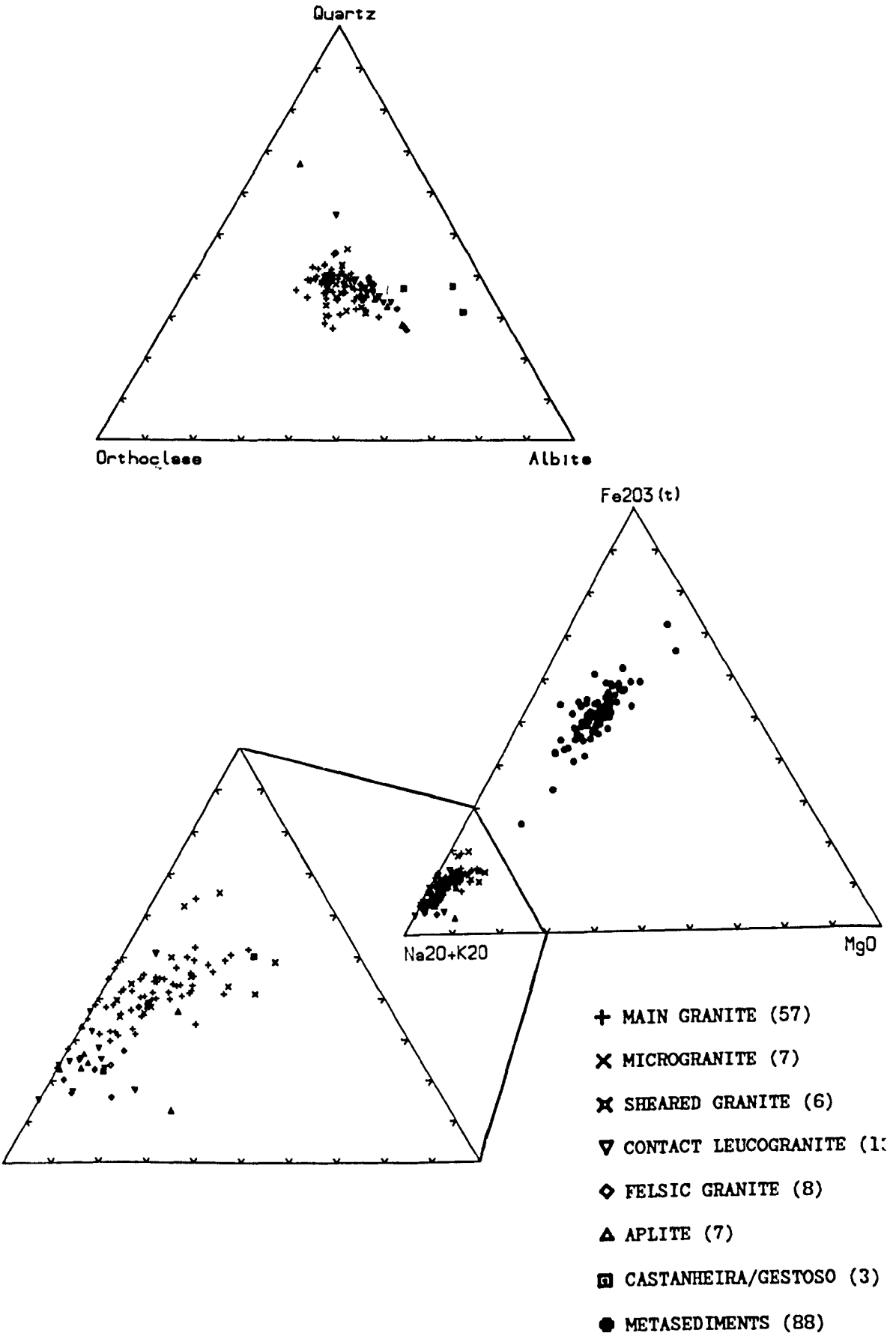
Quartz
Orthoclase
Albite
Fe203(t)
Na20+K20
MgO
+ MAIN GRANITE (57)
× MICROGRANITE (7)
⊠ SHEARED GRANITE (6)
▽ CONTACT LEUCOGRANITE (1
◇ FELSIC GRANITE (8)
△ APLITE (7)
▣ CASTANHEIRA/GESTOSO (3)
● METASEDIMENTS (88)

Figure 7.3 - a, b, c

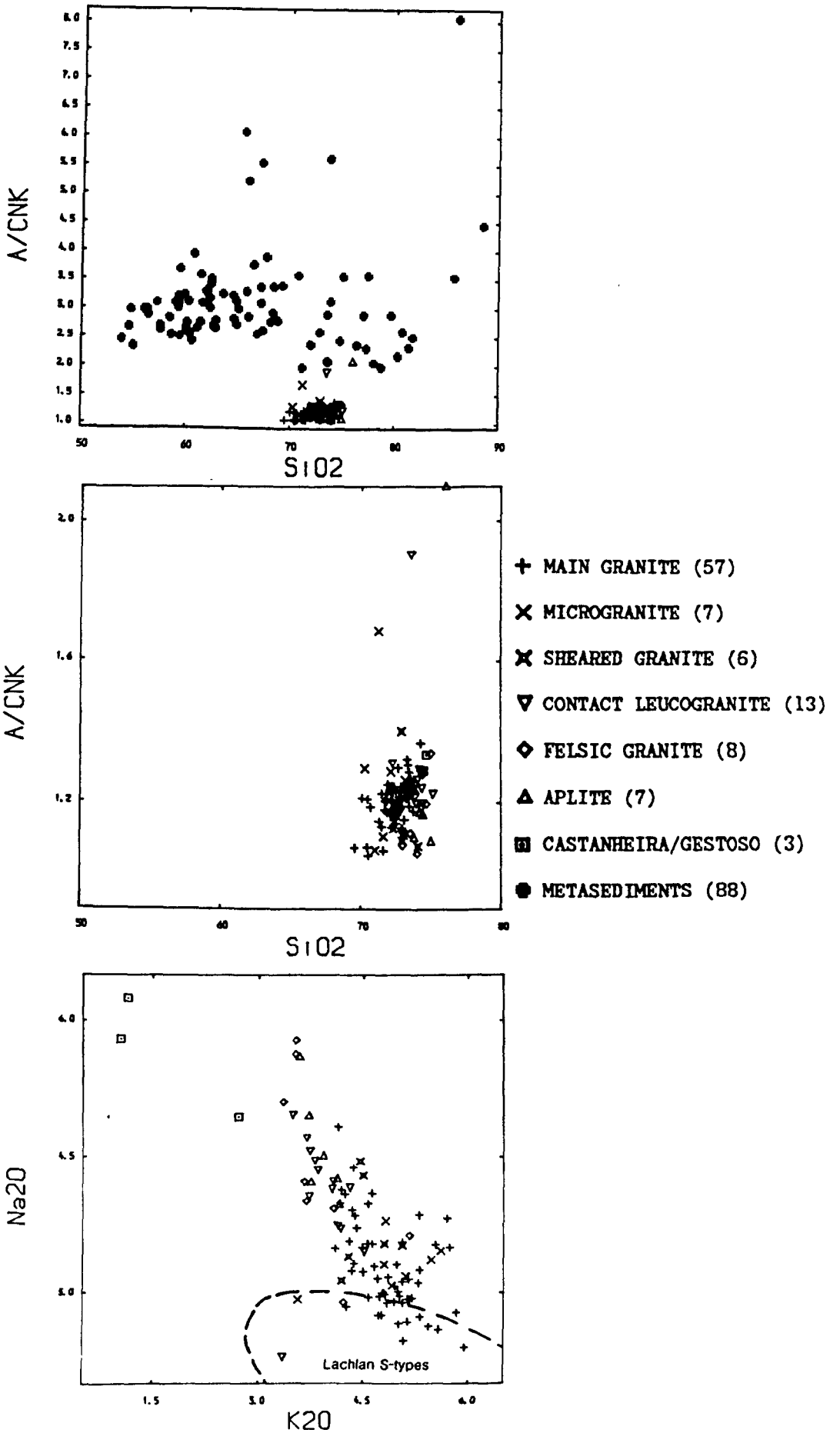

Figure 7.4 - a, b, c

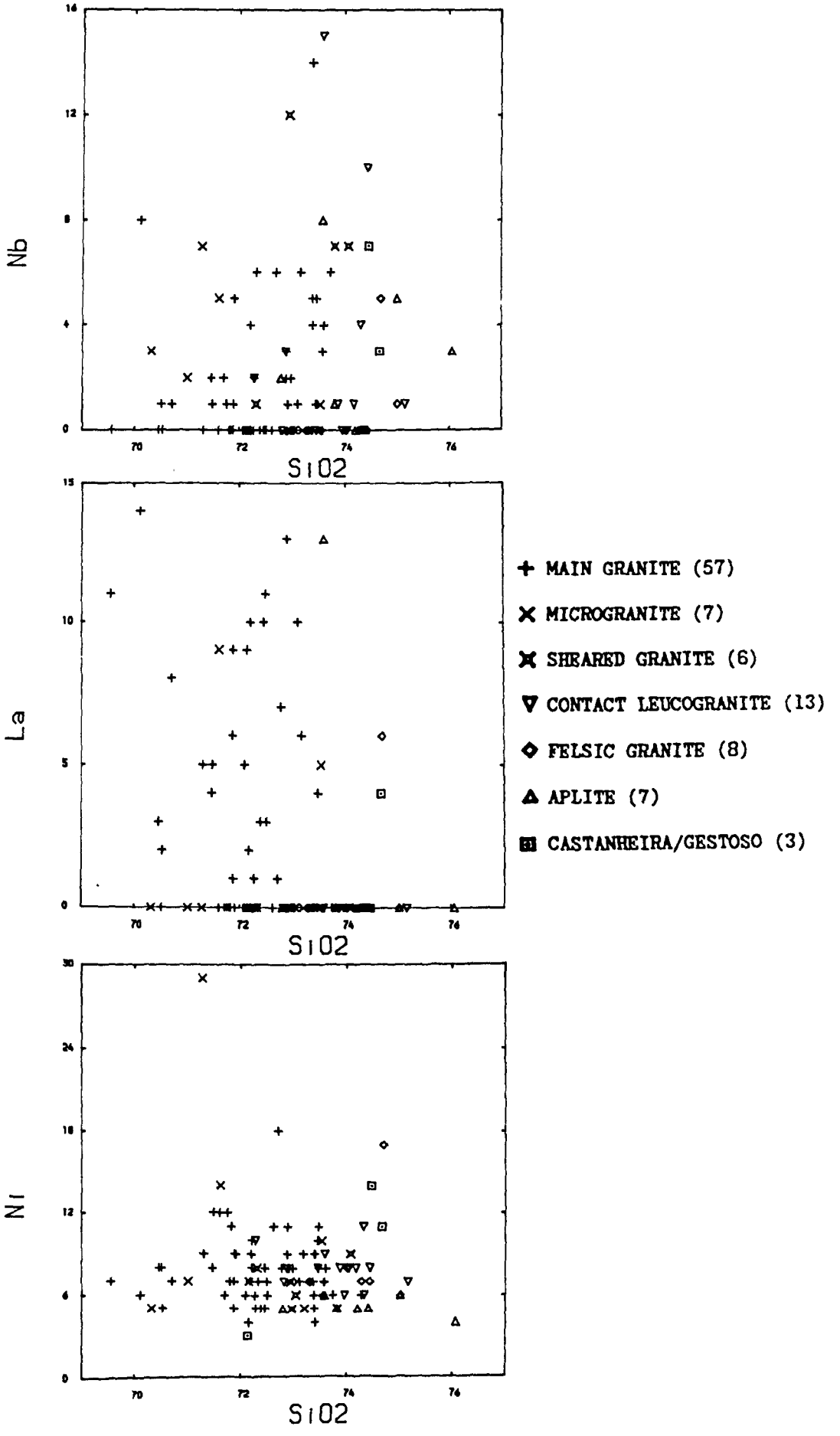

Figure 7.4 - d, e, f

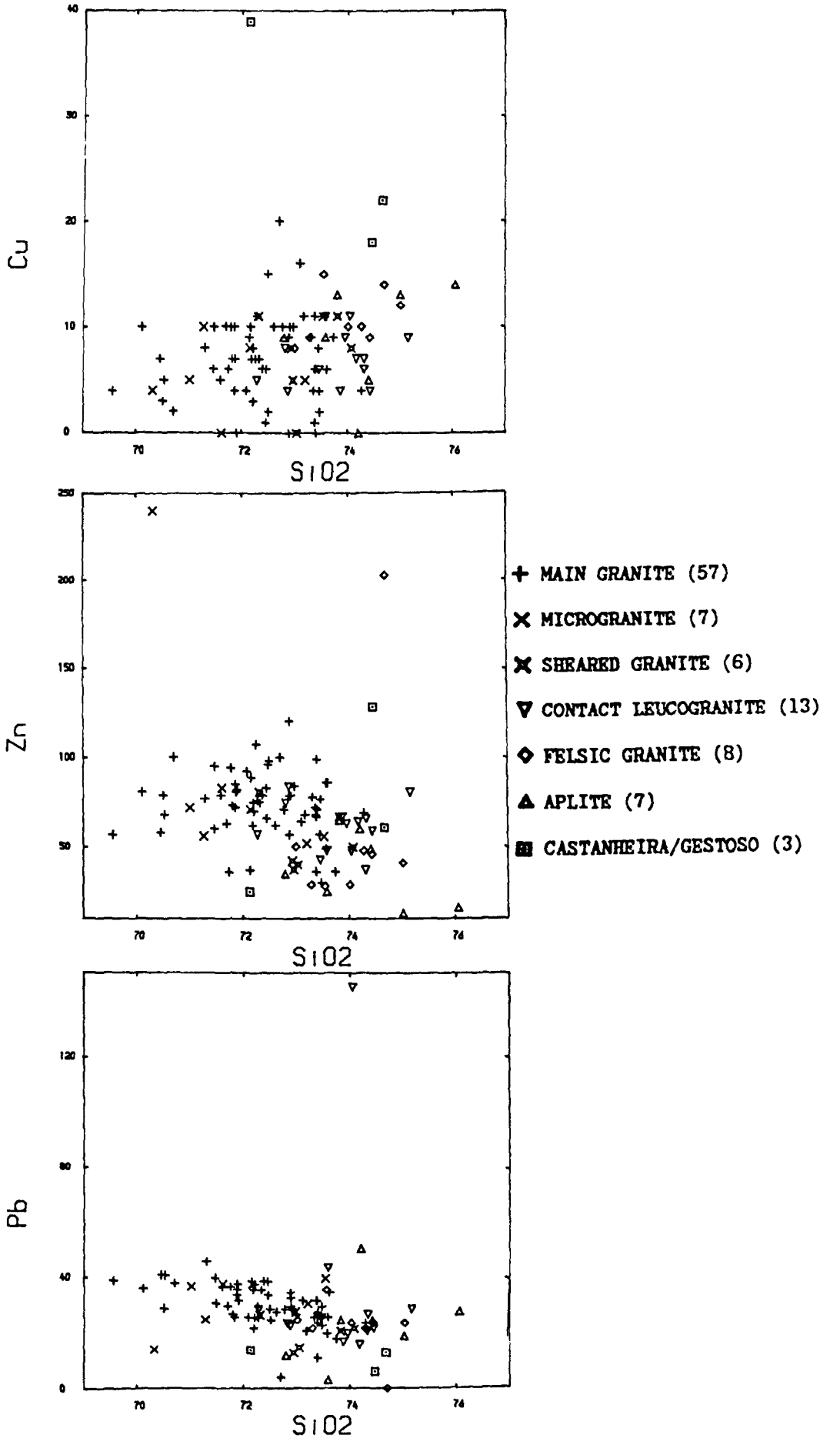

Figure 7.4 - g, h, i

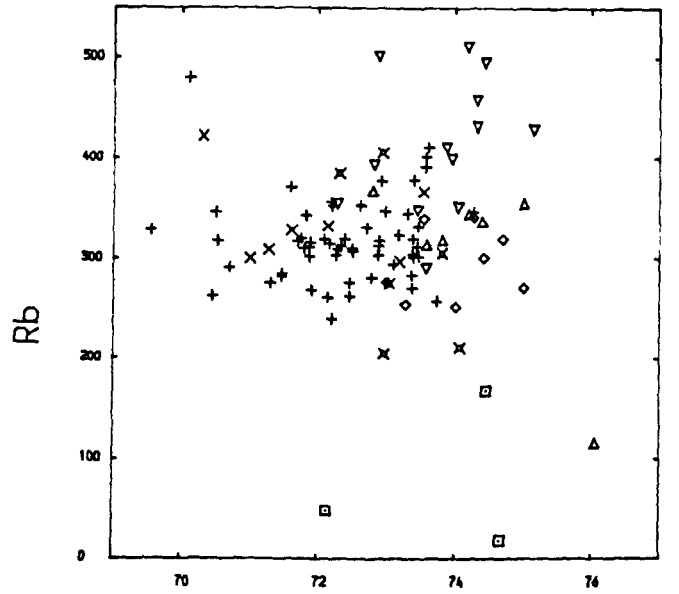

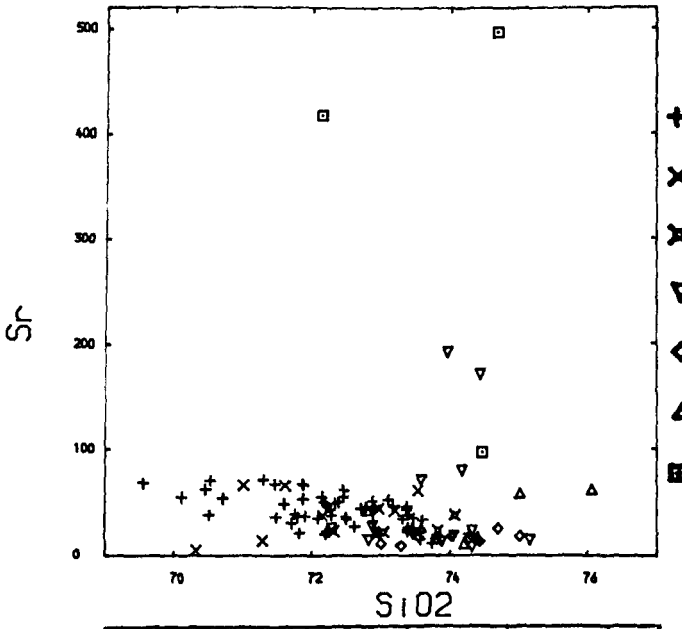

+ MAIN GRANITE (57)
× MICROGRANITE (7)
⊠ SHEARED GRANITE (6)
▽ CONTACT LEUCOGRANITE (13)
◇ FELSIC GRANITE (8)
△ APLITE (7)
⊡ CASTANHEIRA/GESTOSO (3)

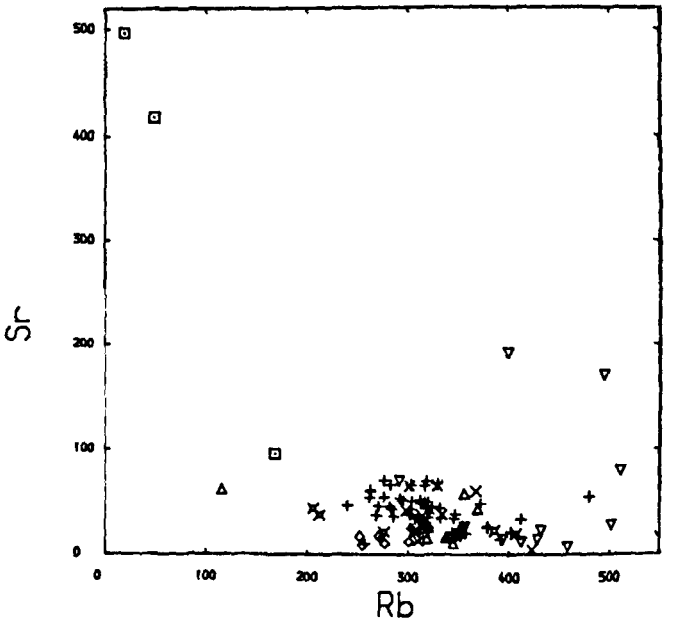

with SiO2. The two nodular granites which were depleted in Rb show extreme Sr enrichment to almost 500 ppm. The Castanheira roof sample (F522G) and some contact leucogranites also show some enrichment (Figure 7.4h). The contact leucogranites generally have the highest Rb/Sr and the 2-mica nodular granites, the lowest (Figure 7.4i).

Ba, Zr, Ce

These elements show a broad negative correlation with SiO2. Ba levels are widely scattered, ranging from 0 - > 500 ppm. Almost all the muscovite granites have very low or negligible Ba concentrations, the 2-mica granites show much greater variation. Both facies of the Castanheira granite are Ba enriched, and the Gestoso granite plots near the top of the range of the 2-mica granites (Figure 7.4j).

Zr falls with increasing SiO2, most of the muscovite granites have < 40 ppm, the 2-mica granites range from > 120 ppm to < 20 ppm (Figure 7.4k).

Ce - the internodular granites and most of the muscovite granites have no detectable Ce, the other samples show a wide scatter (Figure 7.4l).

V, Th, Y

These show general negative correlations with SiO2, but there is much more overlap between the 2-mica and muscovite granites. The sheared granite displays some enrichment in Y (Figure 7.4m-o).

Bulk geochemical differences, attributible mainly to the presence or absence of biotite, have enabled distinction to be made between the 2-mica granites and the muscovite granites. The contact leucogranite and the biotite nodular granites merit special discussion.

Figure 7.4 - j, k, l

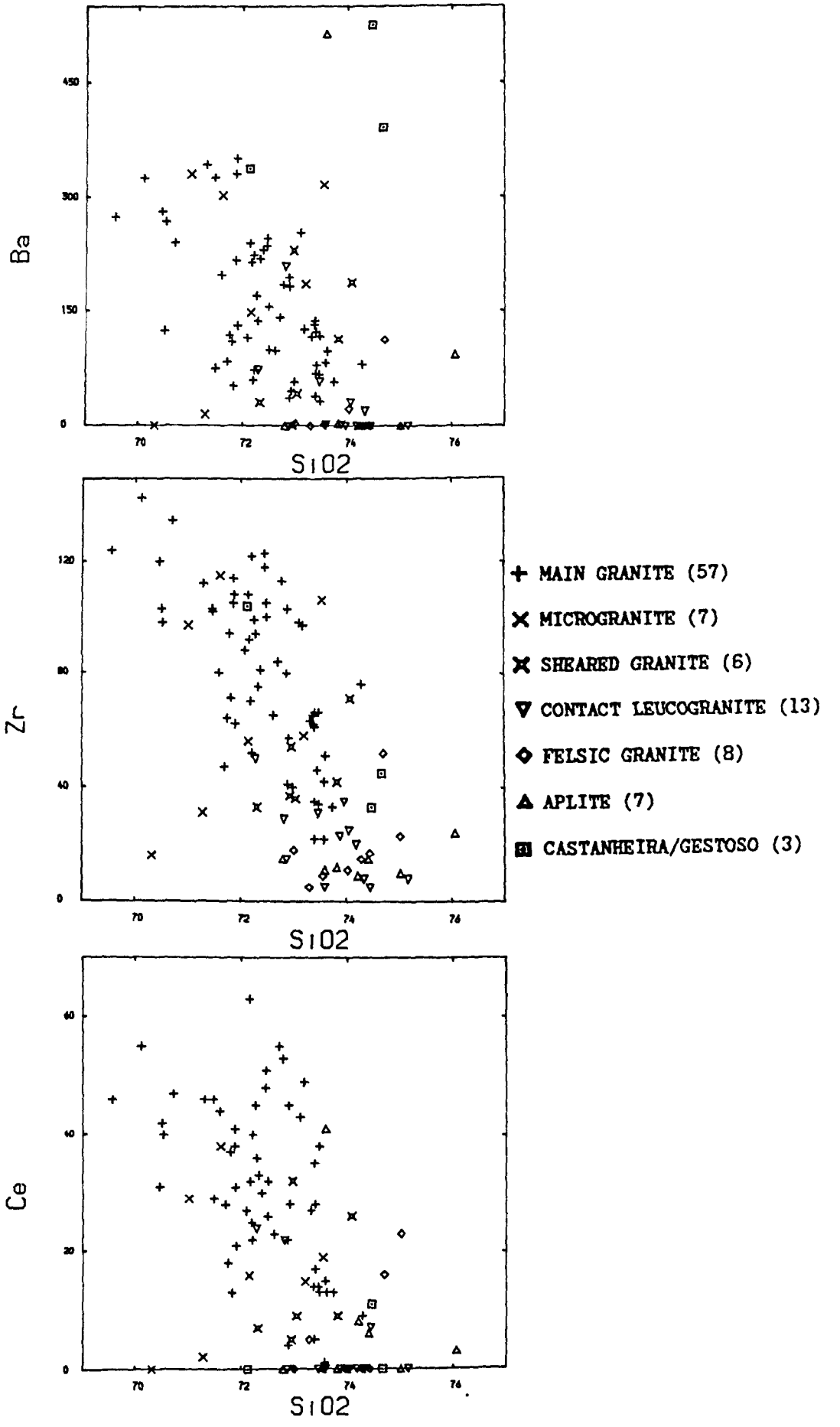

Figure 7.4 - m, n, o

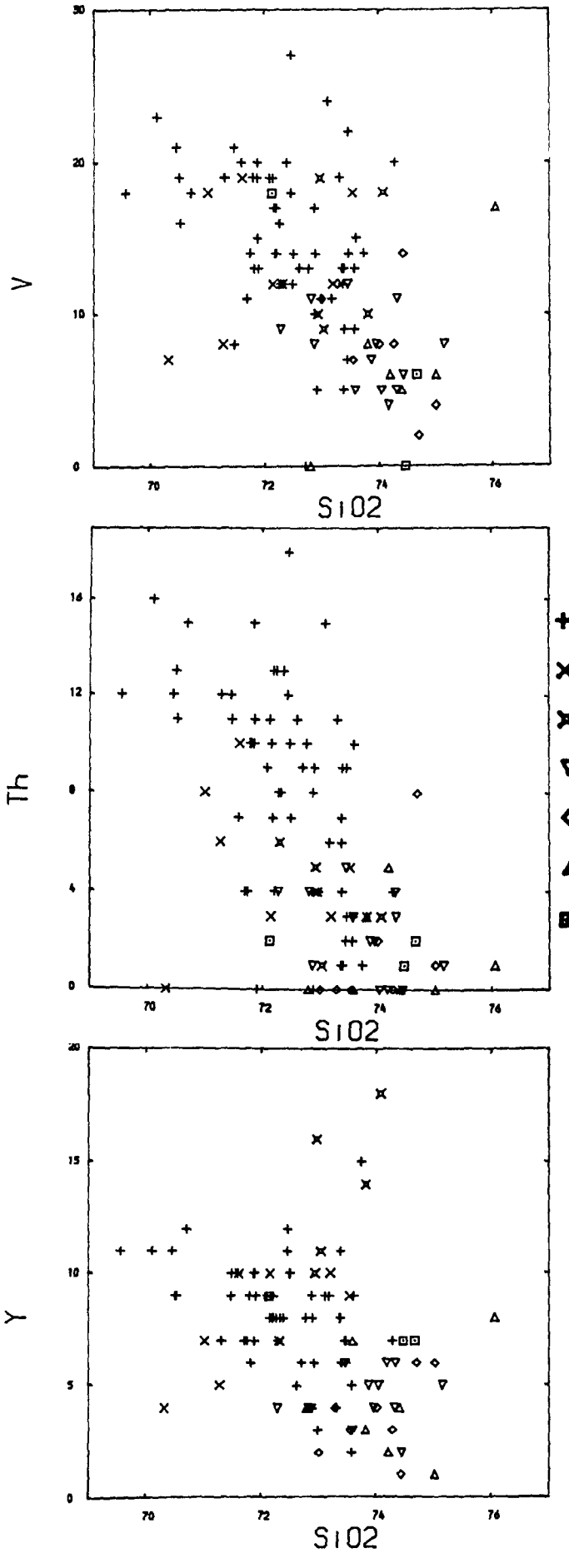

Contact Leucogranite

Conclusions from field evidence and petrographic studies are:

(i) This facies is found only along the northern and southern contacts of the main granite.

(ii) It is gradational into the main granite over 10-20 m.

(iii) No contacts and no grain size variations exist between the two facies.

(iv) There is no petrographic evidence that biotite was ever present.

These observations suggest that, at the time of emplacement, conditions prevailing at the margins of the intrusion not only prevented biotite from nucleating, but must have buffered elements such as Fe, Ti and Mg normally present in biotite. This explains, in terms of major elements, why the contact leucogranite falls in the muscovite granite field for these elements.

This facies displays a distinct Rb enrichment, and to a lesser extent some Sr enrichment as well. The former is surprising as biotite, a major Rb bearing phase, is absent; Rb must in this case be incorporated in muscovite and to a lesser extent K-feldspar.

A more general point is worth mentioning here; the granites as a group have higher Rb concentrations than do the metasediments, implying that the granites are likely to have higher Rb values than any similar pelitic source. Rb levels must be raised by some external means such as a fluid phase to explain the data. Although not considered at all in this study the Serra da Freita granite has late quartz veins associated with Sn-W mineralization. Tin bearing granites display enrichment in a suite of characteristic trace elements such as Sn, F, B, and Rb (Lehmann, 1987).

The possibility that these magmas were rich in halogens and boron has been mentioned, so the presence of Rb-rich magmatic fluids during intrusion seems feasible and could usefully explain the enhanced Rb levels in the granites. Following this argument, fluids could be concentrated along the intrusion's contacts and enhance Rb levels even further in the magma closest to the wall, giving rise to the characteristic chemistry of the contact leucogranite. Under such conditions, the activities of Fe, Mg and Ti may have been buffered by low O2 fugacitites, thus preventing biotite crystallization.

Biotite-nodular Granites

There is considerable evidence, presented earlier, that the Castanheira pluton represents a volatile-rich part of the intrusion's roof which has ballooned upwards. A model similar to that of Van Diver (1970) has been discussed in which the biotite nodules represent the products of flocculation around possible gas bubbles in a fluidized melt. The presence of granite cores to the nodules strongly suggests a magmatic rather than a restitic/xenolithic origin for these bodies. Depletion in Rb and K in the internodular granites provides powerful evidence for the former process, as this accords with crystal-liquid equilibria for partition coefficients of Rb in biotite of about 2-4 (Nash & Creecraft, 1985). Widespread biotite fractionation would therefore remove much of the available K and Rb from the melt.

The abundance of tourmaline in the schists immediately above the intrusion points to B-rich fluids circulating within and above the cupola. If the Castanheira granite is involved in fluid movement on the scale proposed to account for the contact leucogranite, then the effects of any

associated Rb · enrichment so caused has been removed by biotite crystallization.

The enrichments in Na, Ca, Sr, and Ba are more problematical. Na enrichment is reflected by an increase in normative plagioclase. Ca and Sr enrichment implies plagioclase with a higher An content than is generally present. Normative An is much higher (ca. 7%) compared with negligible values in the rest of the 2-mica granites. In thin section, the cores of the feldspars are generally andesine compared to oligoclase or albite in the rest of the granites. It is unlikely that the Castanheira granite is more basic or "primitive" than the other facies, indeed the opposite is the case. The higher An content requires an alternative explanation. It is possible that higher H_2O pressure shifted the melt composition towards higher An content, or that the crystallization path had left the Or field and entered the Q-Ab-An system.

7.4 - Geochemical Characteristics of Metasedimentary rocks

The metasedimentary rocks define a much broader SiO2 field (50% - 90%), which reflects all lithologies present in the area. They are enriched relative to the granites in Mg, Fe, Ti (Figure 7.5 a-d)., depleted in K and Na (Figure 7.5e-f), and overlap in Al, Ca and P (Figure 7.5g-i). The negative correlations between K, Al, Mg, and Ti, and to a lesser extent Fe, with increasing SiO2 reflect control by aluminous phases especially biotite and muscovite, which are obviously lacking in the quartz rich samples.

Abundances of Pb, Ni, Zn, Nb, Th, Hf and Sr overlap those of the granites (Figure 7.6a-g); Ba, La, Cu and Ce have some overlap but tend towards enrichment in the metasediments (Figure 7.6h-k). Zr, V, and Y in the metasediments are markedly higher than in the granites with no overlap in values (Figure 7.6 l-n) and Rb concentrations are higher in the granites with limited overlap (Figure 7.6o).

Figure 7.5 - a, b, c

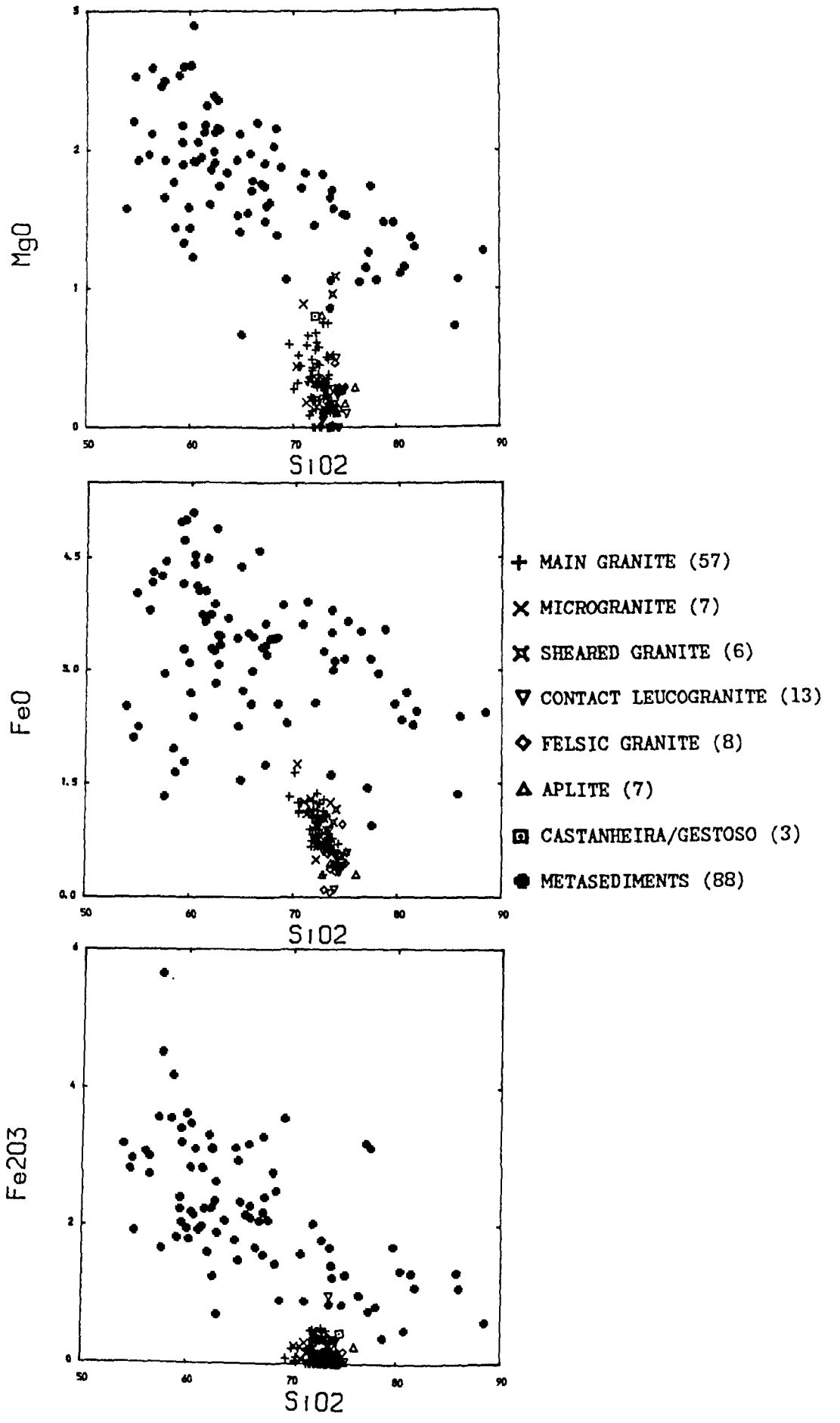

Figure 7.5 - d, e, f

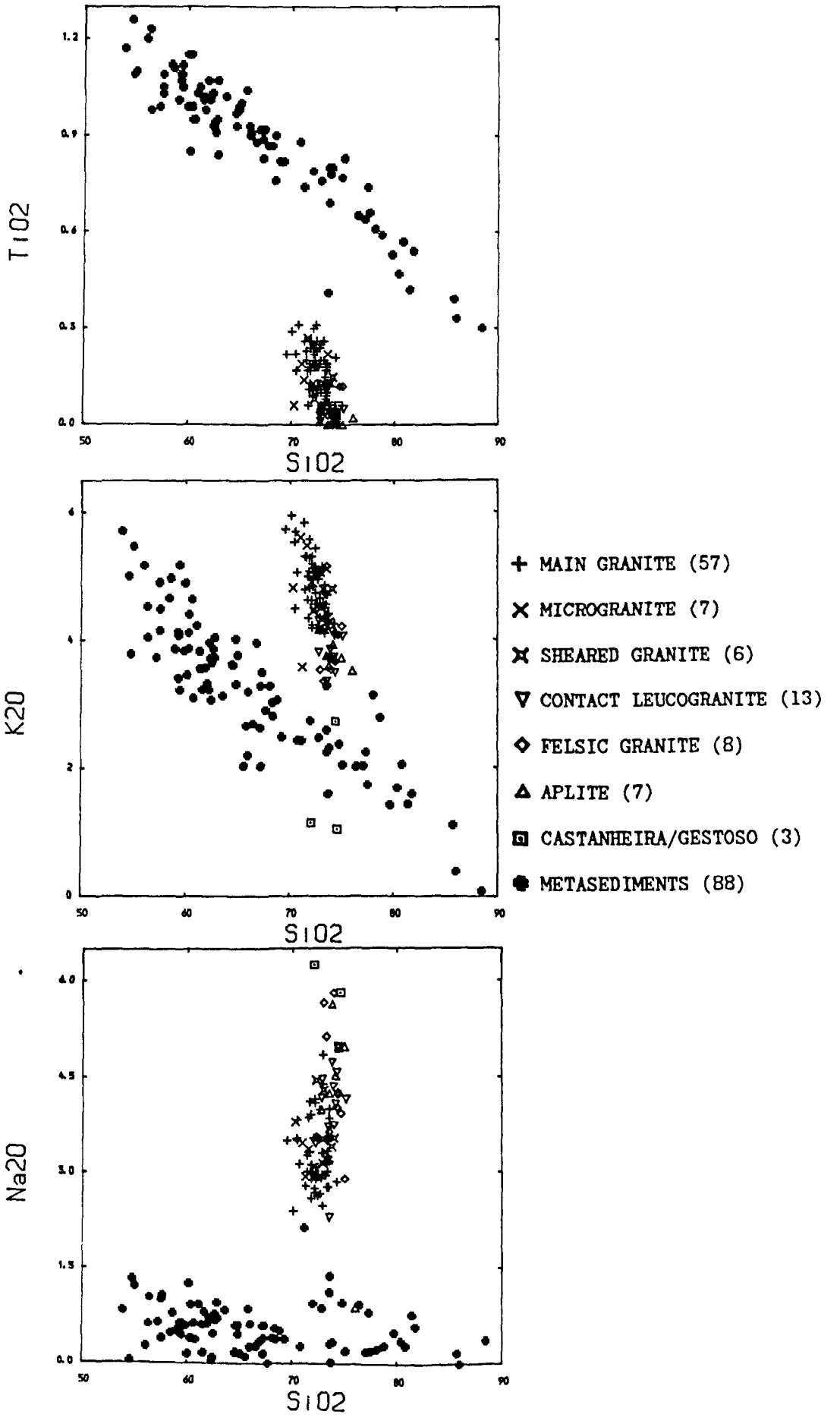

Figure 7.5 - g, h, i

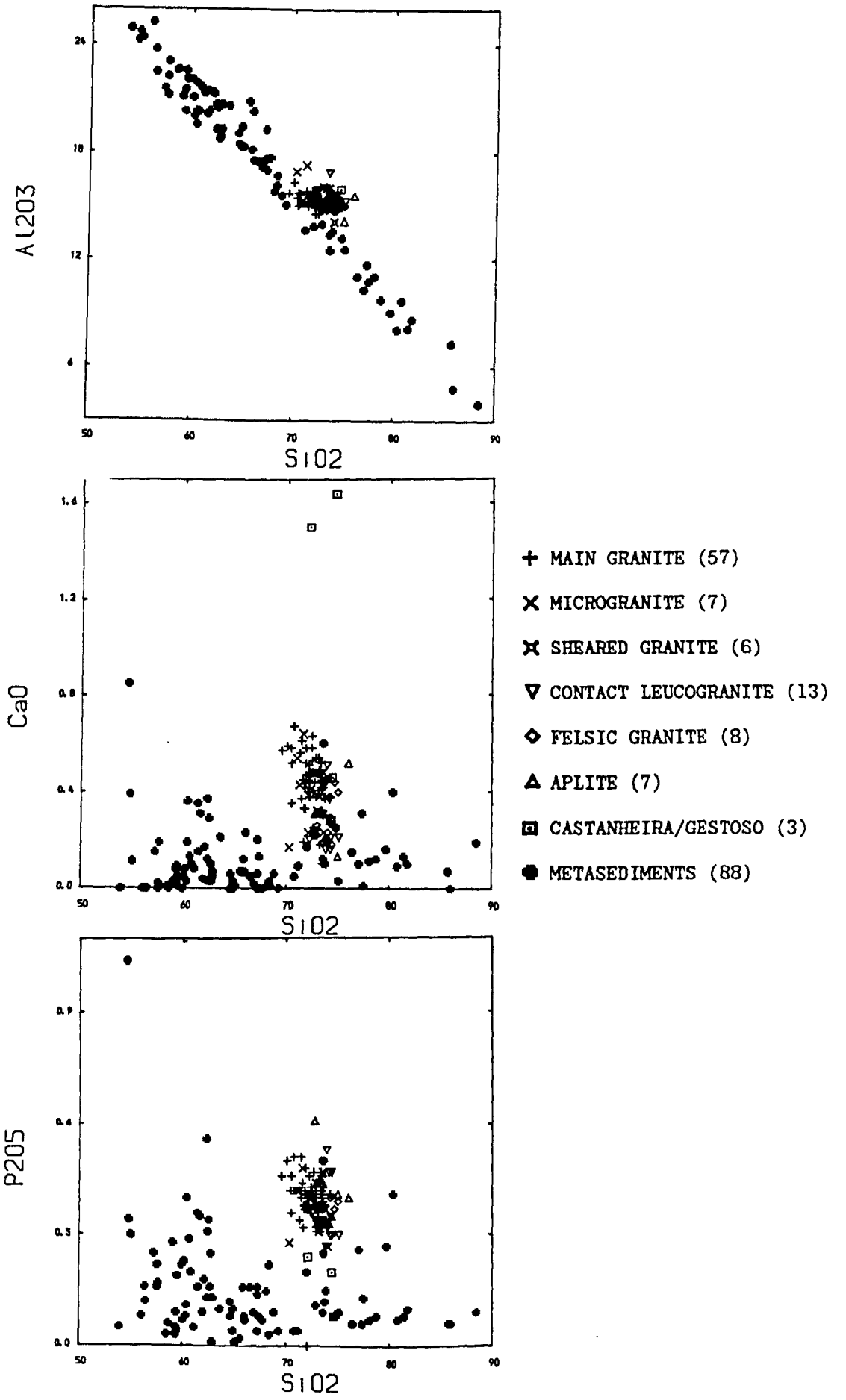

Figure 7.6 - a, b, c

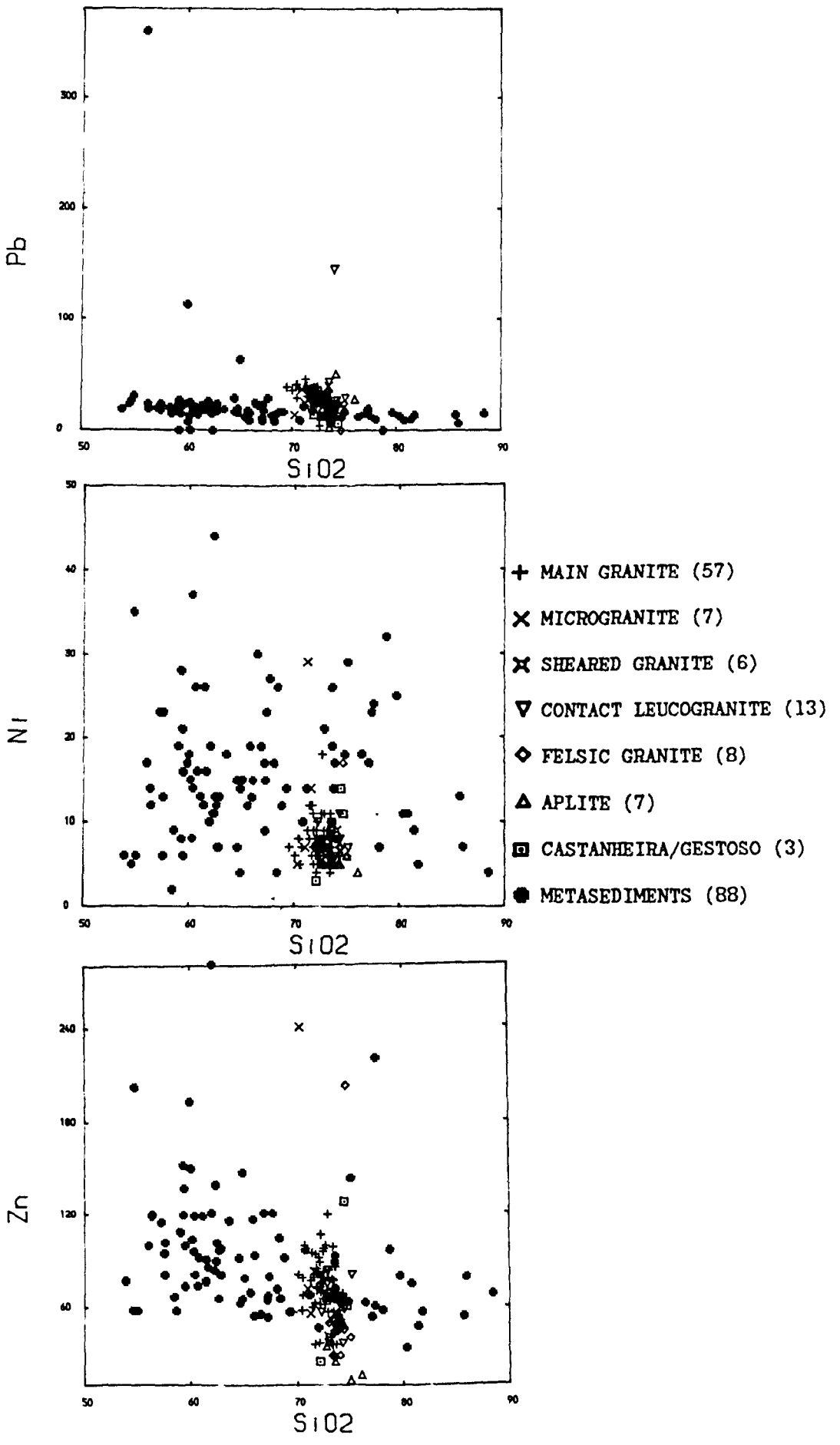

Figure 7.6 - d, e, f

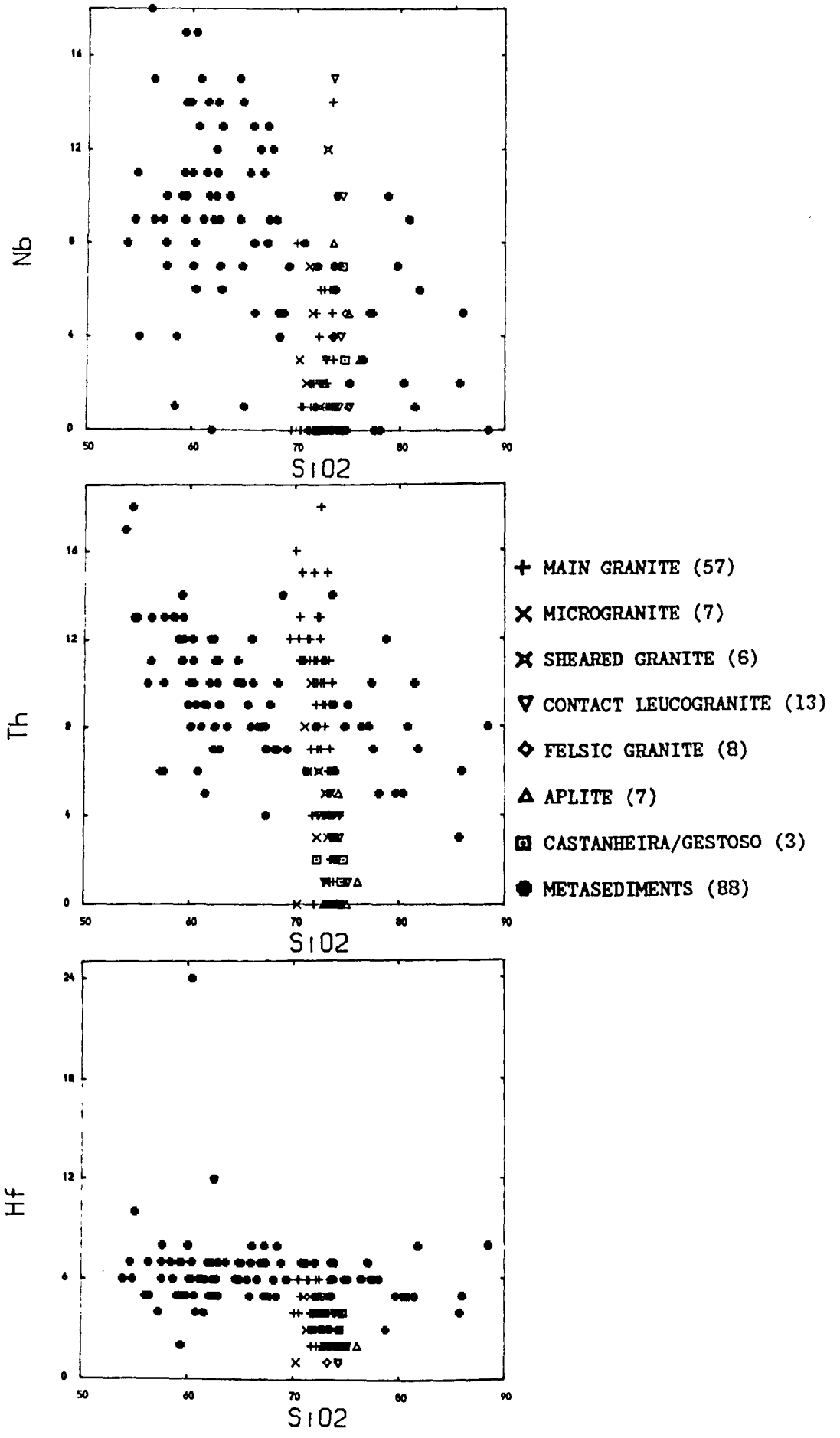

Figure 7.6 - g, h, i

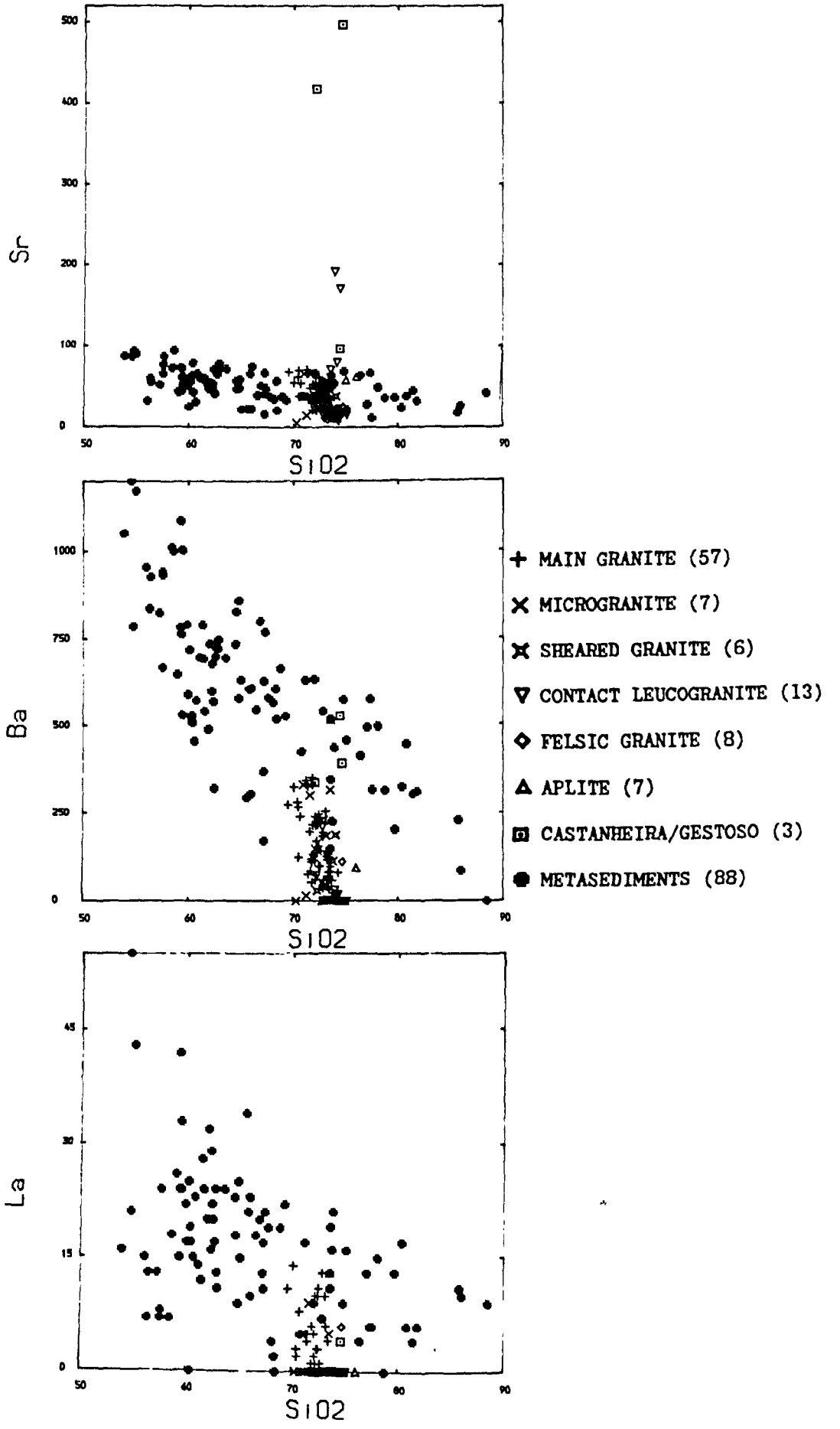

Figure 7.6 - j, k, l

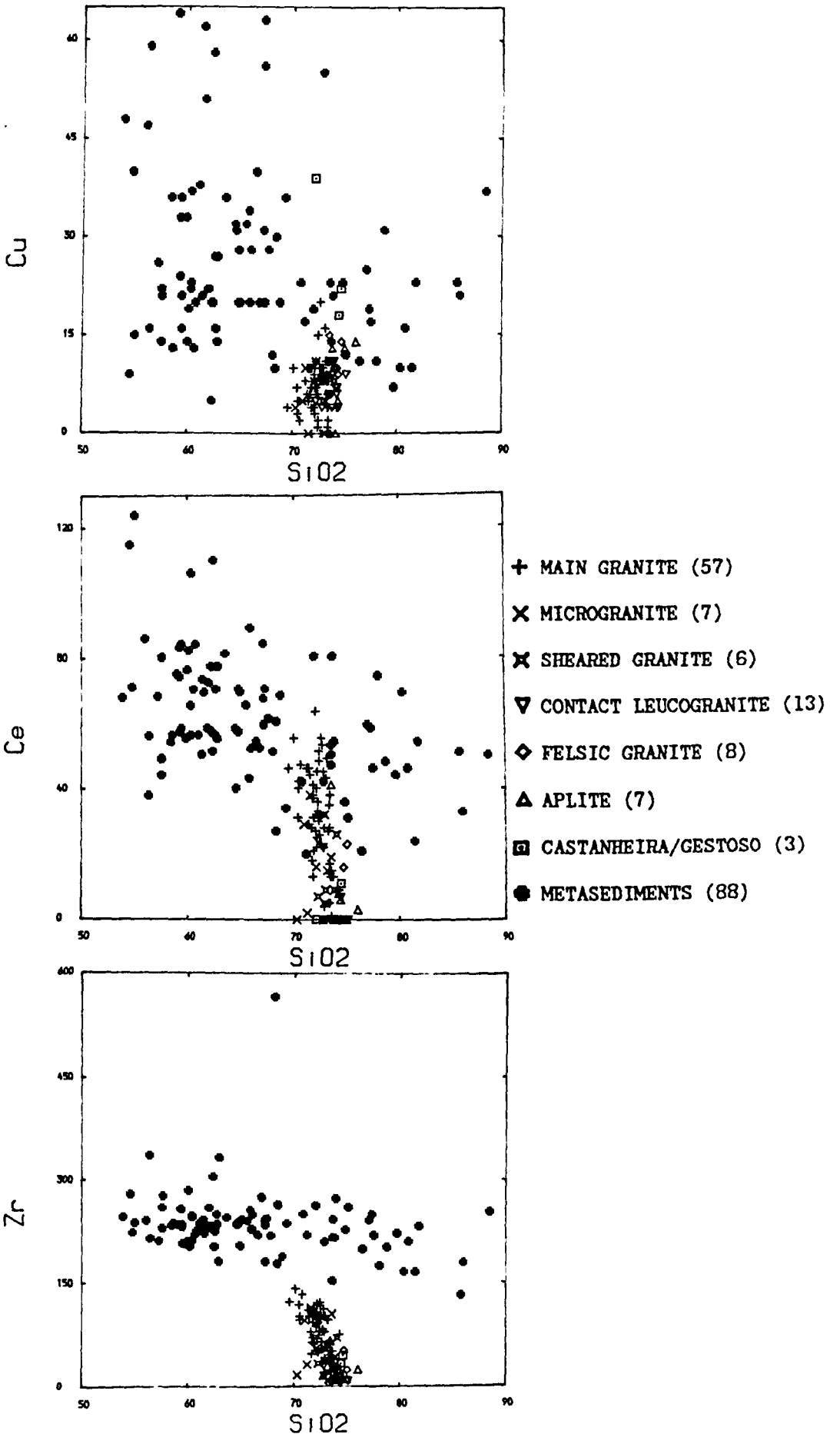

Figure 7.6 - m, n, o

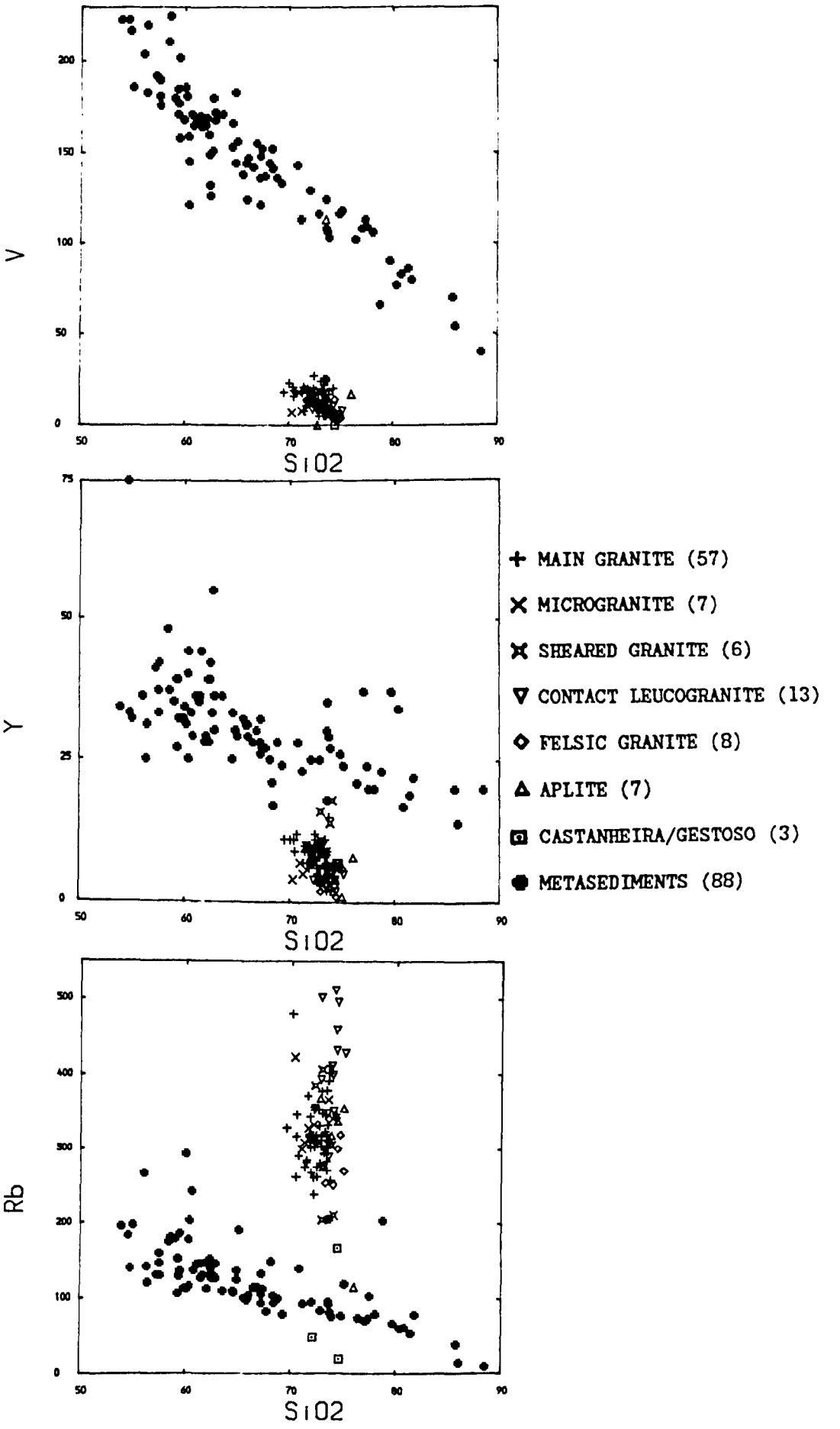

7.5 - Discussion

Harker diagrams have usefully illustrated variations within the facies of the granite, in particular making possible distinctions between the 2-mica granites, muscovite granites and biotite nodular granites. They clearly show that, relative to the metasediments, the granites as a group lie in a more restricted field for most major and trace elements.

Element - element plots are more powerful tools in considering element behaviour. In this case the main considerations are as follows.(i) Do variations within the granites suggest a simple fractionation sequence or do they represent a series of several successive partial melts? (ii) Could the granites be produced by anatexis of the metasediments?

A major problem with any interpretation of the data is that all the granites lie in a restricted range with little internal variation in contrast to that described for the calc-alkaline association by e.g. Fourcade and Allegre (1981), Perfit et al. (1980), and Tarney and Saunders (1979). Although a trend similar to the extreme end of a calc-alkaline fractionation sequence is apparent on an AFM plot, certain other features discussed below mitigate against this interpretation. Tarney and Saunders (1979) warn that the portrayal of major element relationships on such diagrams convey too simple a picture and are of limited value in elucidating petrogenetic processes. Much of the following discussion is therefore based on interpretations of trace element behaviour.

Zr and Ba both fall as K decreases, suggesting that Ba and Zr are mobilized by early alkali-rich melts (Figure 7.7a-d). The fall in K with SiO2 suggests that the muscovite granites are not simply the products of fractionational crystallization in which K values should normally

Figure 7.7 - a, b, c

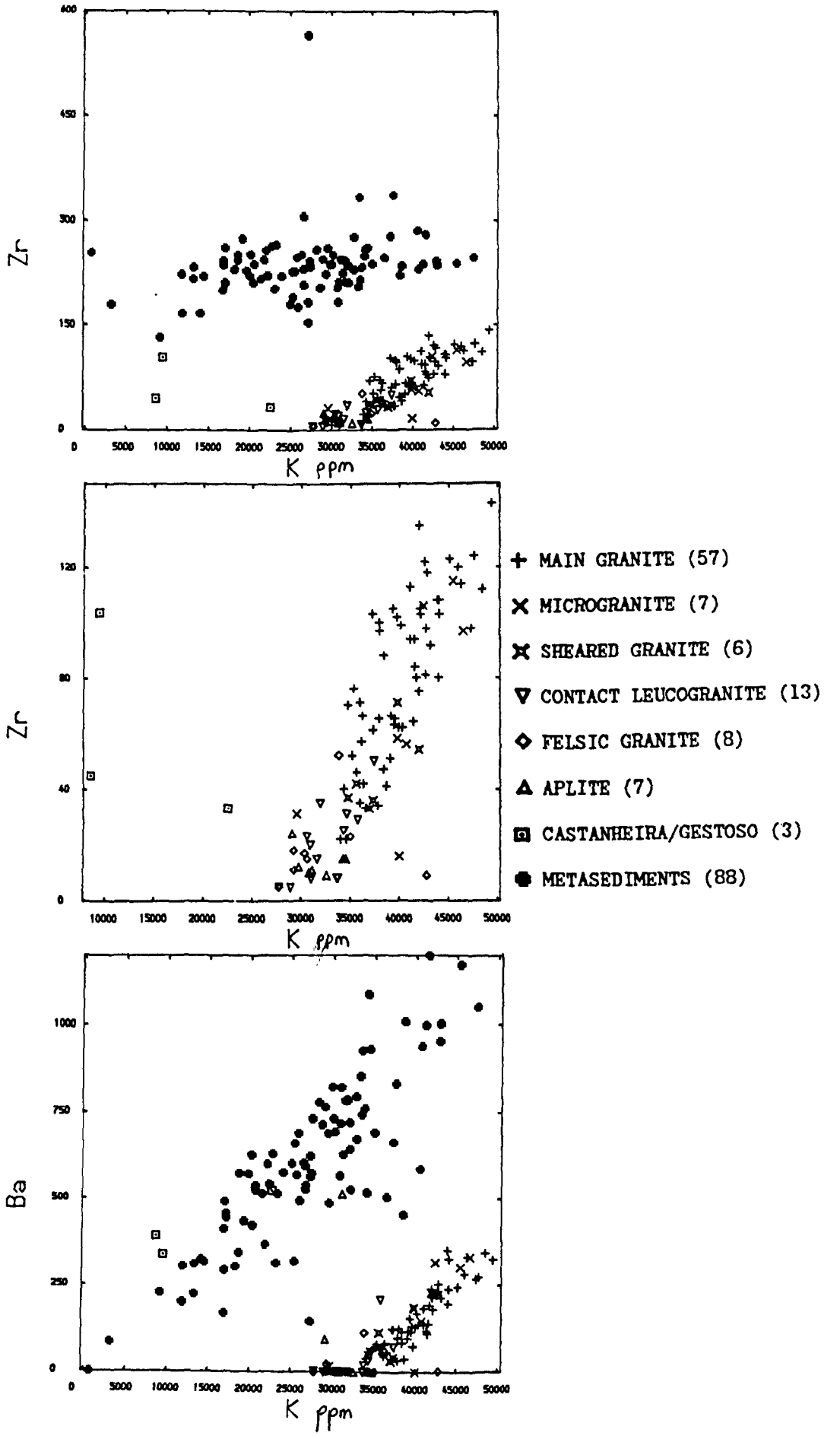

Figure 7.7 - d, e, f

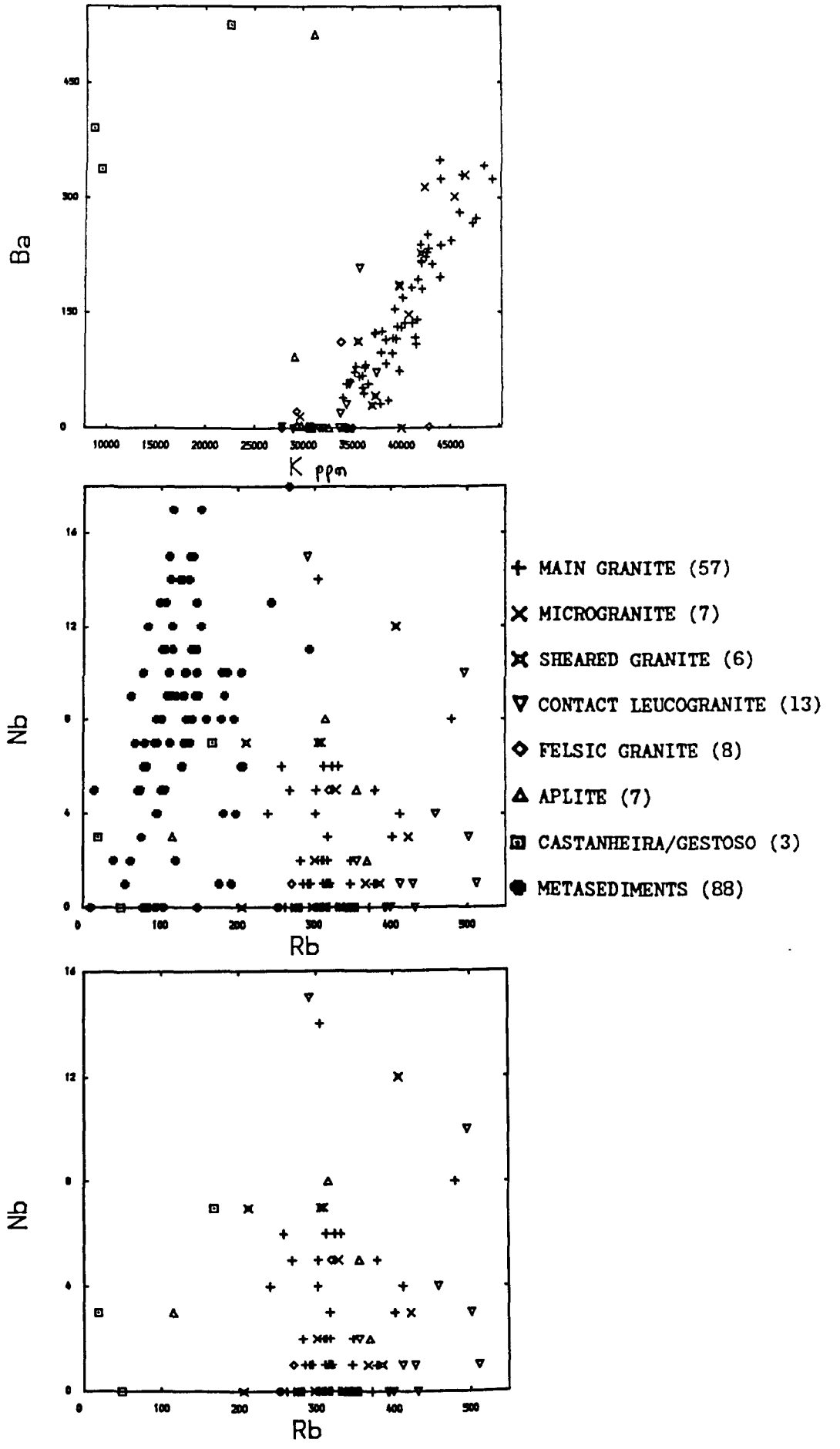

increase. (Tarney and Saunders, 1979).

A Rb-Nb plot provides more striking evidence that simple fractionation alone was not operating. Nb and Rb are two of the most incompatible trace elements (Tarney and Saunders, 1979), however there is no trend of enrichment in either element in the later granites (Figure 7.7 e-f). Tarney and Saunders concluded that "such trace element relationships caution against too readily accepting fractional crystallization as the main mechanism relating rock types." An alternative explanation is that trace element characteristics are "determined by partial melting conditions".

The absence of Rb depletion suggests that the Ba and Rb concentrations are being influenced more by alkali feldspar than by biotite (Figure 7.7g). However a positive correlation between K-Rb (Figure 7.7g) and K-Ba (Figure 7.7c) in the metasediments is probably biotite controlled. A progressive fall in K/Rb is due to decreasing K (Figure 7.7h-i), as Rb values remain fairly constant. K/Rb falls with fractionation (Atherton et al., 1979), but Ba should rise (Tarney and Saunders, 1979) until alkali feldspar fractionation becomes dominant. In evolved granitic compositions, Ba levels should then decrease as Ba becomes compatible. A Ba-K/Rb plot shows that Ba levels are very low in most of the 2-mica granites (Figure 7.7h-i). Although this plot could be explained by fractionation, other element behaviour discussed above argues against this.

Moorhouse et al. (1983) show that a gneiss which has lost the least anatectic melt will have higher Ba and higher K/Rb than one which has lost more anatectic melt. Therefore a sequence of gneisses (or other metamorphic rocks liable to lose melt fractions) will show positive

Figure 7.7 - g, h, i

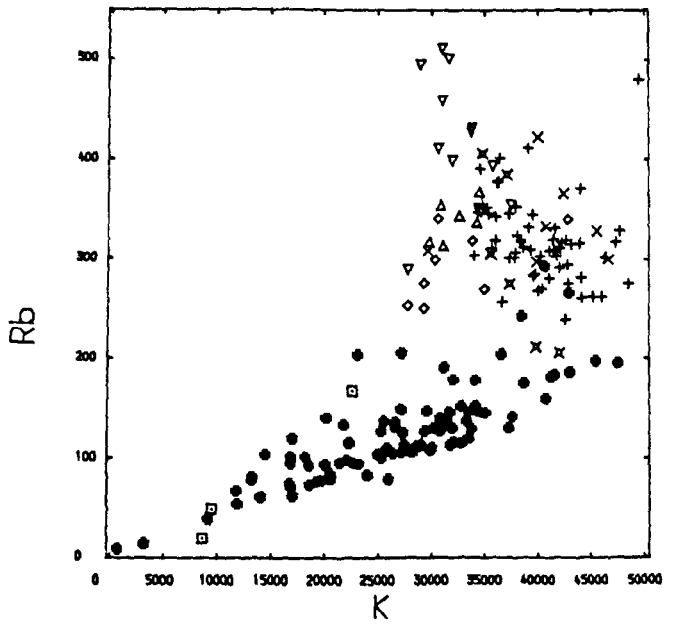

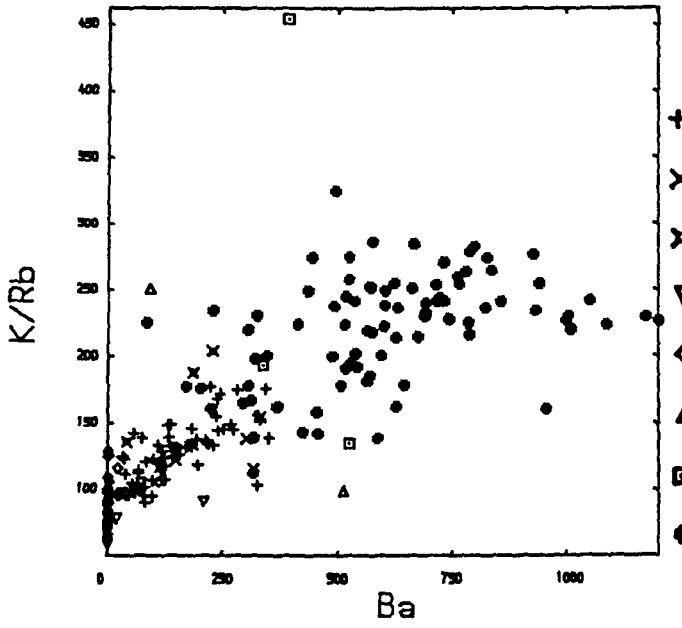

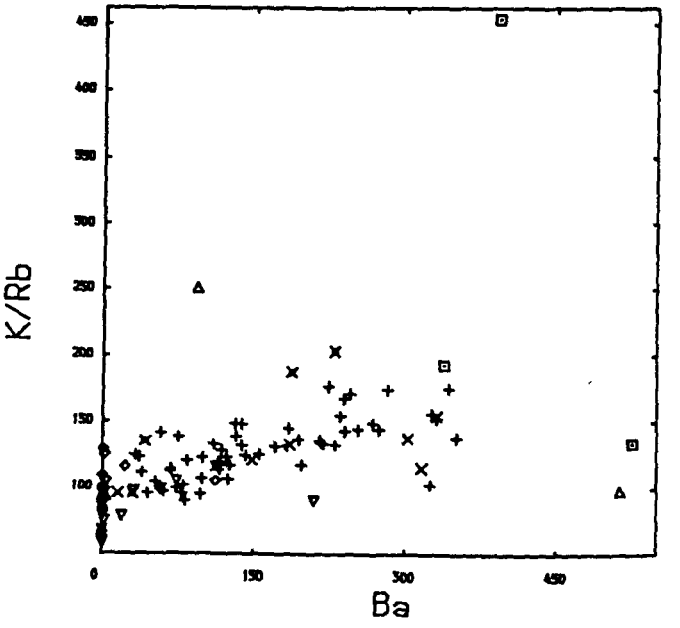

+ MAIN GRANITE (57)
× MICROGRANITE (7)
× SHEARED GRANITE (6)
▽ CONTACT LEUCOGRANITE (13)
◇ FELSIC GRANITE (8)
△ APLITE (7)
⊡ CASTANHEIRA/GESTOSO (3)
● METASEDIMENTS (88)

correlations between Ba and K/Rb. This can be explained by Rb being held in biotite in the restite in preference to Ba and K which will be lost to the melt. This trend is therefore consistent with a spectrum of anatectic magmas which reflect different degrees of melting from a heterogeneous source.

On a La-Ce-Y triangular plot, those granites which do not have 0 ppm La, possess similar La values to the schists (Figure 7.8a). Y and Ce show a wide spread in the granites whereas the schists form a distinct field. The fact that the granites have lower Y and higher Ce values than the schists on this diagram, suggests that if they are related this is by varying degrees of melting. If total melting had taken place the two fields would coincide. In a partial melting situation, Ce would be more incompatible than Y which would be retained in refractory phases such as garnet, apatite and biotite. Small degree partial melts would therefore have lower Y and higher Ce than the parent. The sheared granite shows apparent Y enrichment, and on a Ce-Y plot it forms a distinct trend away from the main group of granites (Figure 7.8 b-c). Field data point to this granite being an early pulse of 2-mica granite and enrichment in Y suggests an initially higher degree of melting. A Ce/Y-SiO2 plot leads to a similar conclusion. Most of the schists have Ce/Y ratios between 1 and 3 (Figure 7.8d), this is in marked contrast to the wide range shown by the granites (0-9) (Figure 7.8e). This highly variable pattern in Ce/Y, which reflects the light/heavy REE ratio, could be explained by varying degrees of partial melting. The sheared granites cluster towards the lower end of the 2-mica granite field, whilst no detectable Ce in many of the muscovite granites accounts for the quoted zero values.

Figure 7.8 - a, b, c

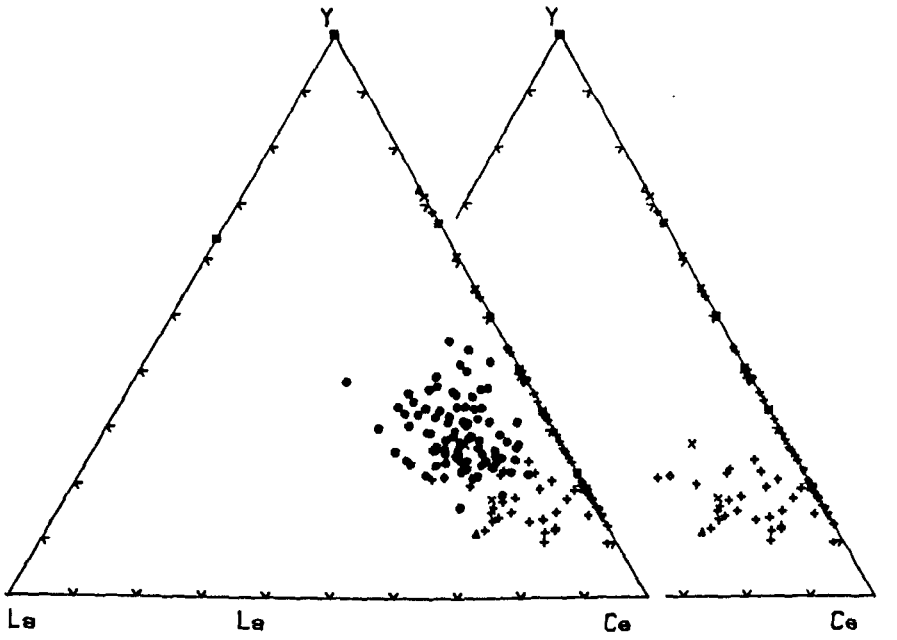

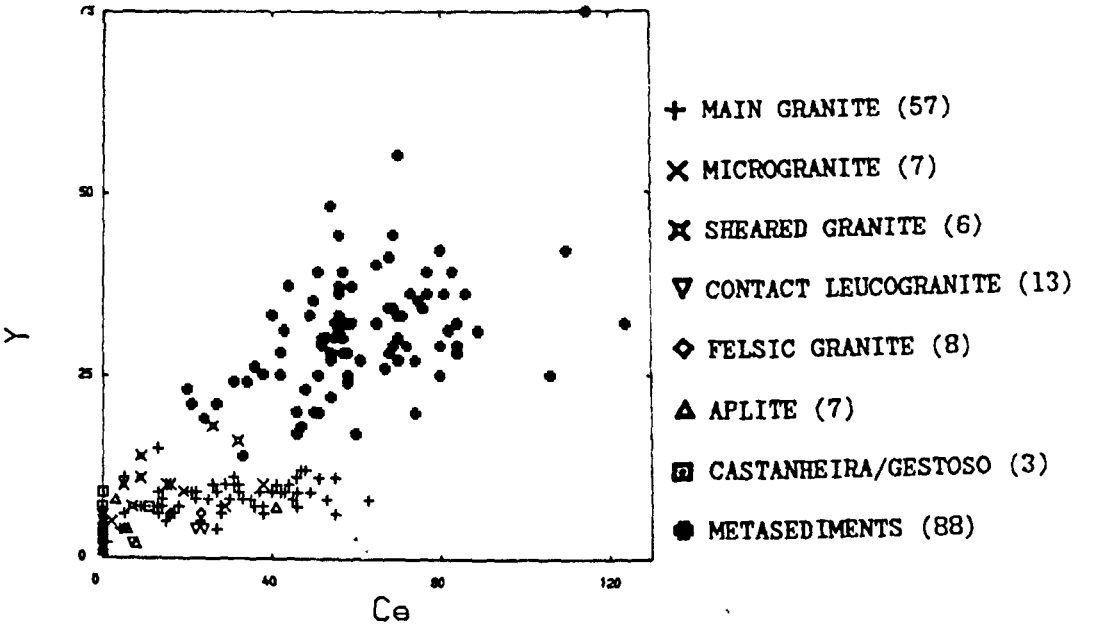

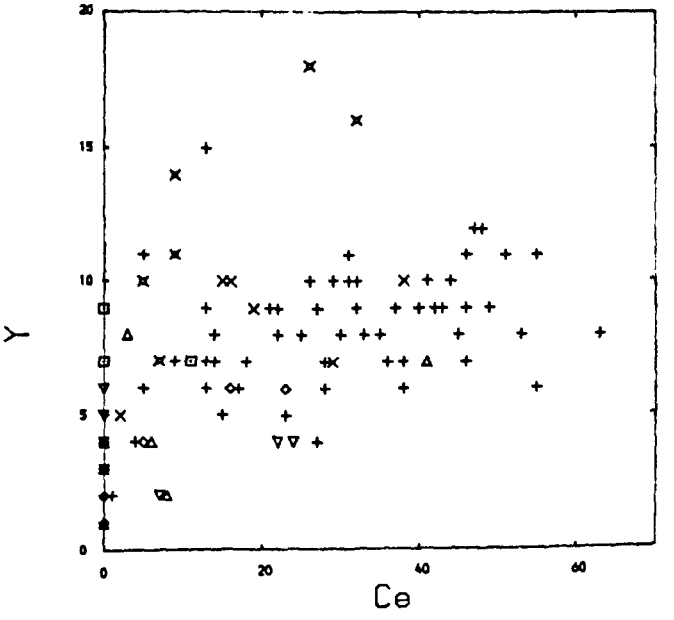

Figure 7.8 - d, e, f

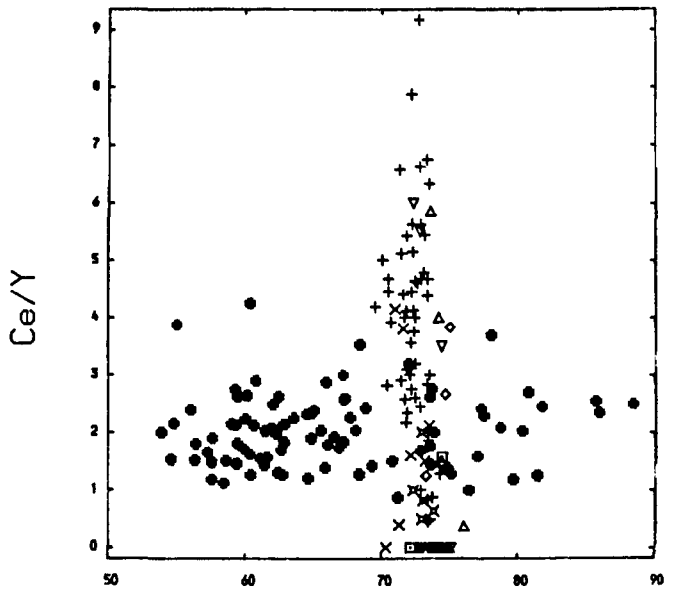

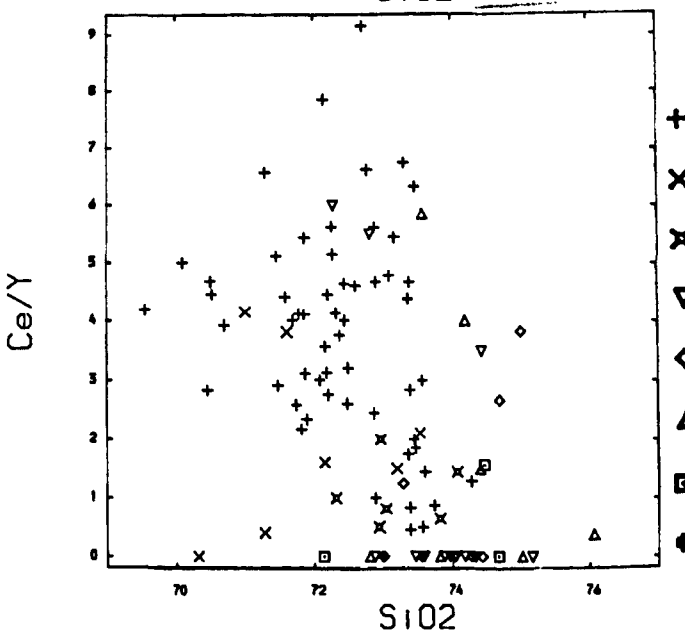

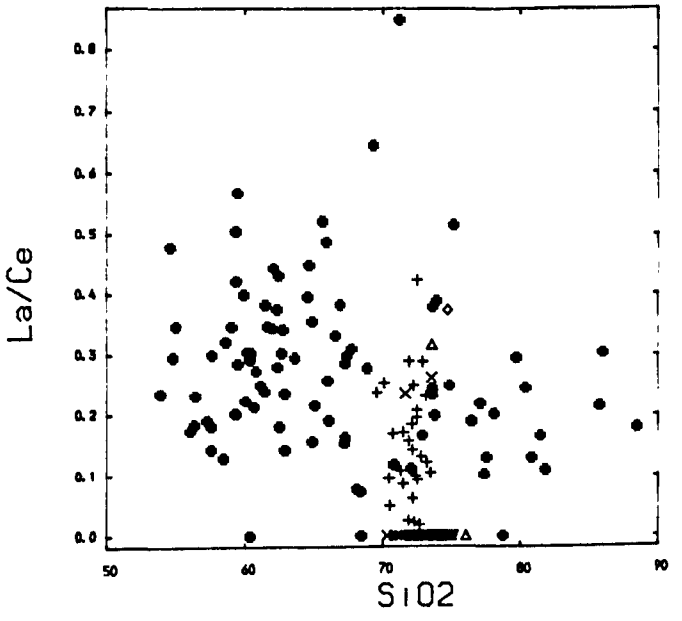

La and Ce would behave similarly during melting, therefore the La/Ce ratio should not change with melting. To some extent this is reflected in the broad overlap in values on the La/Ce-SiO2 diagram (Figure 7.8f). However if these schists actually represented a depleted parent which had lost some melt, then absolute values of Ce and La should be depleted in the restite. This is not the case as seen on the La-SiO2 and Ce-SiO2 diagrams (Figure 7.6i, 7.6k). However the similarity in La/Ce ratio between granites and country rocks means that the granites could have been derived from metasediments with similar La/Ce values as those into which it has been intruded. In summary, the metasediments sampled around the Serra da Freita pluton could be parental to a granite with such a La/Ce ratio, but do not themselves represent the restite in this case.

7.6 - Conclusions

The behaviour of certain elements suggests that trends within the granites cannot be explained by simple fractionation. A model of derivation of successive melts by continual anatexis of a heterogeneous source is suggested. Such a process can easily be envisaged in terms of the emplacement model for the pluton already proposed; repeated melting is succeeded by continual emplacement of batches of magma into the shear zone leading to the narrow wedges and thin sheets which characterize the later intrusions within the main mass.

CHAPTER VIII--ISOTOPE GEOCHEMISTRY

8.1 - Introduction

Isotopes are powerful tools in evaluating hypotheses on magma sources and their subsequent modifications. This chapter considers the implications of isotopic measurements of the Serra da Freita pluton and its country rocks for models of S-type magma generation. All analyses were carried out at the Scottish Universities Research and Reactor Centre, East Kilbride. Details of the analytical techniques are documented in Appendix 4. The samples selected and tha analyses performed are shown in Table 8.1.

8.2 - Stable Isotopes - Oxygen

Whole rock oxygen isotope values for 4 metasediments and 10 granitoids were obtained, in addition, mineral analyses were determined for one main granite. The results are listed in Table 8.2. The 10 granite samples represent all the facies of the Serra da Freita pluton, and the metasediments are representative of all grades of metamorphism in the regional belt. The total data cluster between values of 10.64 $\pm$ 0.2 - 14.15 $\pm$ 0.4; it is impossible to discriminate between the schists and the granites on $\delta^{18}O$ alone as the two groups have ranges of 12.38 $\pm$ 0.24 - 14.15 $\pm$ 0.4 and 10.64 $\pm$ 0.24 - 13.00 $\pm$ 0.12 respectively.

8.2.1 - Granites

The values obtained for the granites fall entirely within the HH division of Taylor (1968) i.e. $\delta^{18}O > 10.3$. Most granites in the world are H group (7.8 - 10.2), the latter could be partial melts of 18O rich metasediments

Sample	Facies	Grid Reference	Rb-Sr WR	O_2WR	O_2Mineral
F334G	Main granite	6195 2340	+	+	
F441G	Sheared granite	6527 2383	+	+	
F458G	Main granite	6380 2360	+	+	+
F474G	Sheared granite	6570 2430	+	+	
F485G	Main granite	5859 2555	+	+	
F488G	Main granite	6070 2536	+	+	
F4103G	Contact leucogranite	6290 2470	+	+	
F4126G	Aplite	6464 2444	+	+	
F4130G	Aplite	6467 2448	+		
F4138G	Microgranite	6370 2280	+		
F4143G	Microgranite	6330 2310	+	+	
F4150G	Felsic granite	6320 2270	+	+	
F327S	Metasediments	6188 2190	+	+	
F337S	"	6225 2495	+	+	
F343S	"	5963 2433		+	
F460S	"	6730 2610	+	+	
F478S	"	6595 2470	+		
F4108S	"	6203 2400	+		
F4125S	"	6462 2442	+		

+ = Analyses obtained.

Table 8.1

Table 8.2

OXYGEN ISOTOPE DATA (WR)

Sample	Facies	$\delta^{18}O‰$	Mean value
F334G	Main granite	12.88 13.13	13.00 ± .12
F441G	Sheared granite	12.90 12.64	12.77 ± .13
F458G	Main granite	12.30 12.24	12.27 ± .03
F474G	Sheared granite	10.88 10.40	10.64 ± .24
F485G	Main granite	12.43 12.29	12.36 ± .07
F488G	Main granite	12.74 13.04	12.89 ± .15
F4103G	Contact leucogranite	12.31 12.06	12.18 ± .12
F4126G	Aplite	12.65 12.87	12.76 ± .11
F4143G	Microgranite	12.78 12.33	12.55 ± .22
F4150G	Felsic granite	12.38 12.01	12.19 ± .18
F327S	Metasediments	12.87 13.01	12.94 ± .07
F337S	"	12.14 12.62	12.38 ± .24
F343S	"	14.19 14.11	14.15 ± .4
F450S	"	14.14 13.86	14.00 ± .14

Mineral Data

F458G	Main Granite	$\delta^{18}O$ Mean values
	Quartz	13.68
	K-feldspar	12.42
	Muscovite	6.69
	Biotite	6.13
	Δ(Q-Kf)	1.26
	Δ(Q-Mu)	6.99
	Δ(Q-Bi)	7.55

but would require mixing and homogenizaton at depth. However granites in the HH group do not present this problem and these values could simply represent melting of δ180 rich metasediments (Taylor, 1968).

O'Neil & Chappell (1977) showed that granites with mineralogical and geochemical characteristics indicative of sources which had undergone surface weathering had higher δ180 than those with igneous parentage. These two groups can be conveniently be divided at δ180 of 10. O'Neil et al. (1977) suggest that bulk rock δ180 may provide the "single most diagnostic criterion for recognizing S- and I-type granites".

All the values from the Serra da Freita granites fall within the S-type range (O'Neil & Chappell, 1977) and the HH field (Taylor, 1968). It can therefore be concluded from δ180 values that the Serra da Freita could represent a metasedimentary sourced magma with no requirement for the involvement of other sources.

8.2.2 - Metasediments

It has been widely recorded that bulk rock δ180 is reduced by fluid loss during metamorphism, e.g. (Shieh & Taylor, 1969; Shieh & Schwarcz, 1974). Values of 18-20 in low grade rocks are likely to be reduced to 12-15 in high grade assemblages.

Wickham & Taylor (1985) showed that a heterogeneous sedimentary sequence of pelites and carbonates could have original variations in δ180 homogenized at metamorphic grades above the andalusite isograd by pervasive flushing with an O-bearing fluid. Pelites originally at 15 and carbonates with values as high as 25 were transformed by exchange with a lower δ180 reservoir to lie in a limited range of 11-15.

The metasediments analysed from the Serra da Freita do not show evidence of high grade homogenization as F460S from the chlorite zone on the NE traverse has similar δ18O to higher grade schists. However it has been argued elsewhere that B-rich fluids were actively present during anatexis and emplacement, so the possibility exists that fluid induced homogenization has occurred on a scale which involves metasediments of all grades around the pluton.

8.2.3 - Relationships between the granites and the metasediments

δ18O values in a granite depend on the degree of partial melting of the source, the fractionation of 18O/16O between the melt and the minerals in the refractory residue, and the effects of fractional crystallization. As 18O fractionation decreases with increasing temperature, this effect will be more marked in lower temperature wet S-type melts. O'Neil et al. (1977) argue that the residue in S-type melting would be rich in quartz and Al-rich phases such as sillimanite and biotite. As quartz is the most 18O rich mineral in a rock, its presence as a refractory phase may more than offset a tendency for the partial melt to develop δ18O values greater than the protolith. The resulting magma would therefore have an 18O content approximately equal to or slightly less than the source rocks. However Wickham and Taylor (1985) maintain that leucogranites, being richer in quartzo-feldspathic constituents than the pelites from which they are derived, would tend to be slightly more 18O rich than the parent.

The exact relationship between an S-type granite and its pelitic parent seems largely to be a function of the proportion of quartz-rich material which remains in the restite. The important point is that almost

identical δ180 values for the granites and metasediments is consistent with the derivation of the granites from high grade Beira Schists.

8.2.4 - Mineral Separates

δ180 values can be lowered or raised by various processes. Some of the most important are low temperature deuteric alteration which tends to raise values and interaction and exchange with meteoric waters which decrease δ180. A study of δ180 content of individual minerals for F458G was undertaken to try and quantify any such effects (Table 8.2).

The order of decreasing δ180 agrees with that of Taylor (1968). Equilibrium values of Δ(Q-Kf) should be in the range 0.8 - 2.0 (Taylor & Epstein, 1962; O'Neil & Taylor, 1967). A value of 1.26 is therefore acceptable for equilibrium oxygen isotope distributions and it seems unlikely that post-magmatic exchange processes to which feldspars are susceptible have taken place.

A Δ(Q-Kf) temperature of 360° C probably reflects feldspar exsolution, i.e. the system remained open until sub-solidus reactions had ceased. The data are also consistent with the common observation that the 180 K-feldspar value is close to the that of the whole rock.

Values of Δ(Q-Bi) between 3 & 5 are expected if magmatic equilibration has been achieved. A value of 7.55 requires an alternative explanation. Several workers have reported high Δ(Q-Bi) values (O'Neil & Chappell, 1977; O'Neil et al., 1977). This could indicate that oxygen isotopes continued to equilibrate below the solidus, i.e., biotite may in part be post-magmatic. Alternatively, meteoric fluids could have selectively lowered the δ180 content of the biotite. As the Δ(Q-Kf) value is

unaffected, biotite would have to be more susceptible than feldspar. This conclusion is supported by O'Neil et al. (1977). The relative exchange rates of biotite and feldspar depend markedly on the chemical compositions of the fluid (O'Neil & Taylor, 1967), and it has been demonstrated (Cole & Ohmoto, 1976) that biotite exchanged more rapidly than feldspar in an experiment with granite gneiss and a 0.1M NaCl solution at 200°C.

Temperatures of 340°C and 200° C were obtained from Δ(Q-Bi) and Δ(Q-Mu) respectively, probably reflecting post-crystallization growth of micas.

8.2.5 - Conclusions

(1) Similar values of δ18O in the local Beira Schists of all metamorphic grades suggests that some homogenization of oxygen isotopes has taken place, possibly by fluid fluxing through the sediments at an early stage.

(2) The whole rock values for the schists and granites overlap at values between 10 and 14; the data are consistent with a model involving anatexis of high grade pelitic schists to produce an S-type granitic magma.

(3) Mineral analyses show that the rocks have not undergone large scale deuteric or hydrothermal alteration. Some muscovite and biotite growth is likely to have been post-magmatic.

8.3 - Radiogenic Isotopes - Rb-Sr

The Rb-Sr system was used to test the hypothesis of anatexis of the Beira Schists as source of the Serra da Freita granites.

8.3.1 - Introduction

Rb-Sr measurements were made to find (i) the age of the intrusion, and (ii) the initial 87Sr/86Sr ratio of the granite magma.

The samples shown in Table 8.3 were selected to be representative and to provide a reasonable spread in Rb/Sr ratios.

8.3.2 - Age Dating of the Serra da Freita Pluton

Seven samples (main granite, 4; microgranite, 2; felsic granite, 1) define a 324 $\pm$ 4 Ma WR isochron with an initial ratio of 0.7136 $\pm$ 0.0008 (MSWD = 3.2) using the decay constant of 1.42×10^{-11}, (Steiger & Jager, 1977) (Figure 8.1).

Analyses of the sheared granite, contact leucogranite and aplite depart from the isochron, possible explanations are discussed below.

The age of Portuguese granitoids has been discussed in Section 1.2.2. This study completes the dating of granites in northern central Portugal, and place the Serra da Freita pluton within the Pre-older (Pinto, 1979) or Namurian (Pinto, 1983, 1985) group of granites.

Page & Bell (1986) have shown that Rb-Sr systematics can be disturbed by deformation, and conclude that primary whole rock ages cannot be expected even in weakly deformed granites, unless emplacement is syntectonic. Field data show that the Serra da Freita pluton was syntectonic, and this age is therefore proposed as an intrusion age, contemporaneous with movements on

Table 8.3

Rb-Sr Isotope Data

Sample	Facies	Rb ppm	Sr ppm	Rb/Sr	$^{87}Rb/^{86}Sr$	$^{87}Sr/^{86}Sr$
F334G	Main granite	304	42	7.23	20.8085	.8091
F441G	Sheared granite	292	22	13.27	39.6248	.9548
F458G	Main granite	287	50	5.74	16.5735	.7907
F474G	Sheared granite	373	18	20.72	62.6816	1.1157
F485G	Main granite	330	19	17.36	50.5584	.9490
F488G	Main granite	326	34	9.58	28.3472	.8428
F4103G	Contact Leucogranite	392	13	30.15	93.6289	1.1347
F4126G	Aplite	100	58	1.72	5.0088	.7534
F4130G	Aplite	330	11	30	93.2356	1.1480
F4138G	Microgranite	401	4	100.25	354.5852	2.3486
F4143G	Microgranite	275	39	7.05	20.5629	.8092
F4150G	Felsic granite	278	11	25.27	74.1857	1.0575
F327S	Metasediments	113	37	3.05	8.8518	.7548
F337S	"	130	62	2.09	6.1111	.7451
F460S	"	197	89	2.21	6.4357	.7499
F478S	"	108	71	1.52	4.4165	.7389
F4108S	"	292	34	8.58	25.4456	.8678
F4125S	"	239	29	8.24	24.0428	.8432

Figure 8.1 - Rb-Sr data for the Serra da Freita granites
(a)- Isochron samples
(b)- Samples analysed, not on isochron

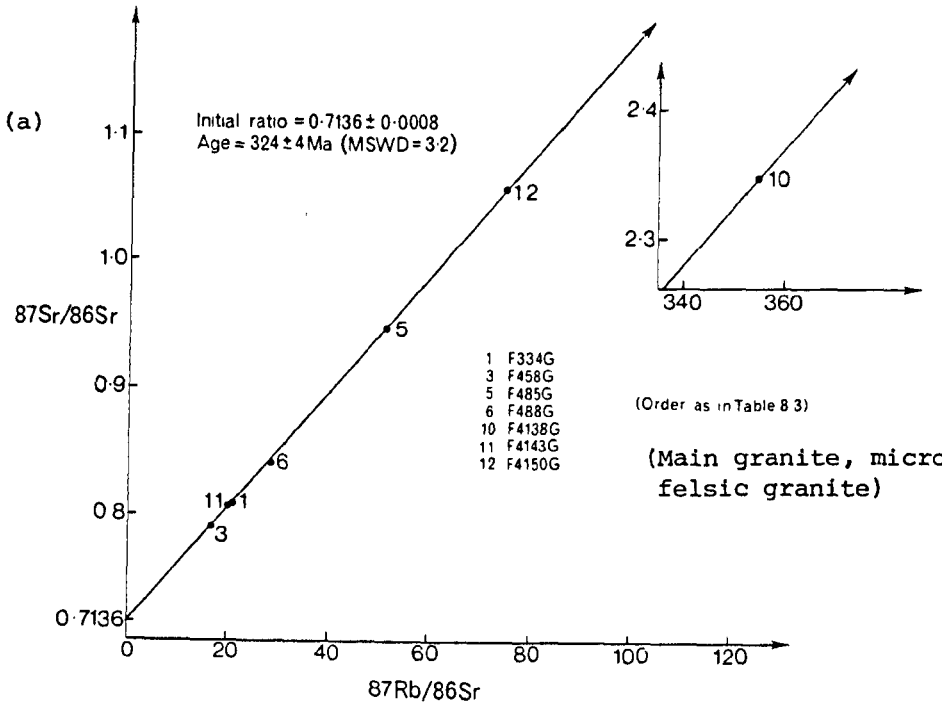

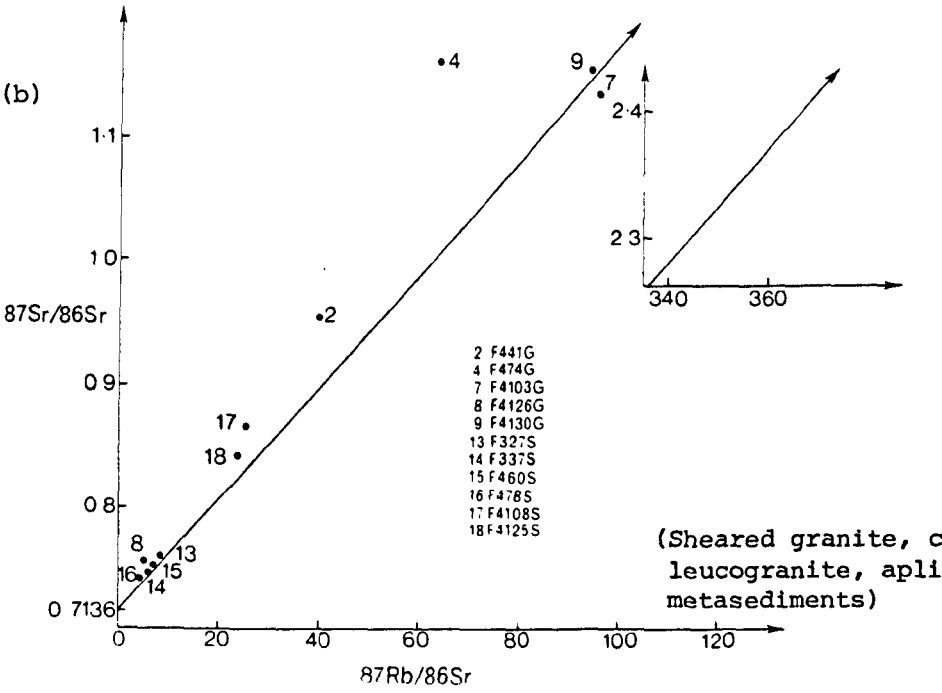

the Serra da Freita shear zone.

It has been shown that intrusion of the microgranite and felsic granite took place while the main granite was still behaving plastically, e.g. lobate contacts between the main granite and the felsic granite, and the general lack of chilled margins in the later minor intrusions. This idea is therefore supported by these samples plotting on the isochron with the main granite, i.e. intrusion of these facies was not substantially later than the main facies of the pluton, and occurred before the overall system closed.

Other facies are displaced from the isochron and some possible explanations are proposed below.

It has already been noted that the contact leucogranite is extremely Rb-enriched, possibly by fluids concentrated along the contact zone; enhanced Rb levels could account for this facies plotting to the right of the isochron, i.e. with an increased Rb/Sr ratio.

The sheared granite shows evidence of Rb/Sr reduction. This facies is (i) coarser grained and (ii) lies completely in the zone where shear bands are developed as a response to continued sinistral transpression in the shear zone. It is likely that this coarse-grained facies which, from Y enrichment, represents an early pulse and is therefore older, is more susceptible to grain boundary deformation than the main granite to the south. Page & Bell (1986) point out that resetting of the Rb-Sr system can be induced even by weak deformation, and it is not suprising that this facies provides some evidence of tectonic disturbance. An attempt to date any resetting is obviously impossible as only two samples were analysed in this preliminary study, however it can be speculated that Rb loss has

taken place possibly by cataclasis and recrystallization of Rb-bearing phases such as biotite or K-feldspar.

The aplites analysed lie close to the isochron on the Rb-poor side. A reason for this is not immediately apparent, the aplites may be much later and the source rock may be Rb-depleted.

The explanations offered above for these facies of the pluton departing from the isochron are not necessarily the only valid ones, however the isochron obtained is thought to represent the true emplacement age of the syn-tectonic granite and the intial ratio of the magma, the petrogenetic significance of which is discussed in the next section.

8.3.3 - Petrogenetic Implications of the Initial Ratio

Sediments normally have enhanced levels of radiogenic Sr due to high levels of Rb in clay minerals, therefore an S-type granite magma would normally have a higher initial ratio than an I-type granite magma. Chappell & White (1974) proposed that S-types should have initial $^{87}Sr/^{86}Sr$ ratios > 0.708.

For pelitic parentage, a value of > 0.71 is suggested (Miller, 1985). The Serra da Freita pluton has an initial $^{87}Sr/^{86}Sr$ ratio of 0.7136 ± 0.0008, and therefore fulfils the criteria to be S-type (Chappell & White, 1974) and pelite-derived (Miller, 1985). Six metasediments were analysed for comparison with the granites. All plot to the left of the isochron and give a $^{87}Sr/^{86}Sr$ ratio at 324 Ma of 0.7117 ± 0.0034. Little significance can be attached to such a value as the Rb-Sr system is likely to be severely disrupted by sillimanite grade metamorphism.

8.4 - Discussion

A Sr isotope initial ratio alone can be ambiguous; Pitcher (1982) cites extreme cases where apparent S-types have low initial ratios (Flood & Shaw, 1977), and I-types with high 87Sr/86Sr initial ratios (Richards, 1980). A more powerful technique is to consider the Rb-Sr system in conjunction with other systems such as 18O-16O. Oxygen isotope data are sparse for Iberian granitoids, so it is useful to compare these results with those obtained for the French Hercynian plutons. These have been divided into three major associations: calkalkaline, subalkaline and aluminopotassic (Stussi &de la Roche, 1984). The third group appears to be chemically similar to the Portuguese "Older Granites", and as they are found in the South Armorican shear system, part of the Ibero-Armorican Arc, they are directly comparable with the Serra da Freita pluton in terms of chemistry and tectonic setting. The aluminopotassic granites, the most abundant type in the Massif Central and SW England as well as in Armorica, can be characterized as forming an 18O-rich province; δ18O ranges from 9-13.5 with most values > 10. The oxygen isotope data exclude involvement of mixing of widely distinct source rocks such as felsic and mafic components and are considered to have been derived from a metasedimentary source, probably pelitic (Sheppard, 1977; Bernard-Griffiths et al., 1985). An initial 87Sr/86Sr ratio - δ18O plot characterizes Hercynian granites in France, England and Germany as high δ18O and high initial 87Sr/86Sr types. The analyses of the Serra da Freita granites overlap the S. Armorican field (Bernard-Griffiths et al., 1985) (Figure 8.2), and shows for the first time that isotopic data for Portuguese granites are comparable with other parts of the European Hercynian belt. The aquisition

Figure 8.2 - Isotopic characteristics of the Serra da Freita granites compared with those of the South Armorican granites

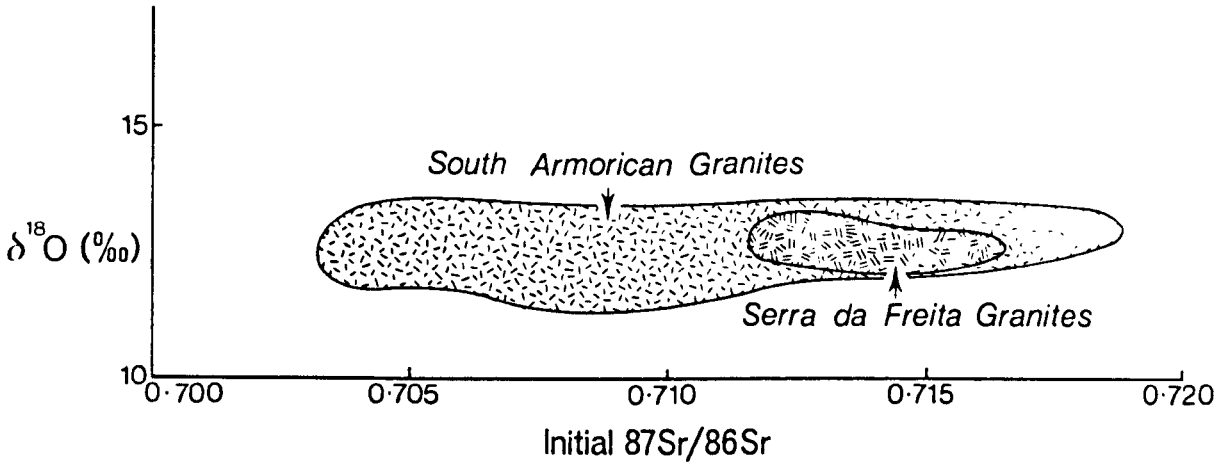

of such data is necessary before Hercynian magmatism can be fully described and characterized.

8.5 - Conclusions

Figure 8.3, adapted from Taylor (1980), shows the isotopic characteristics of some of the major source reservoirs which might be melted to give rise to magmas. The Serra da Freita granites and metasediments fall within the high $\delta^{18}O$, high initial $^{87}Sr/^{86}Sr$ range of the diagram which fully supports earlier isotopic conclusions concerning the origin of the Serra da Freita granite magmas; the results of 180-160 and Rb-Sr, considered independantly and then together, all point to the Beira Schists as being the principal source-rock for the pluton.

Figure 8.3 - Isotopic characteristics of various crustal and mantle source reservoirs
from Taylor (1980)

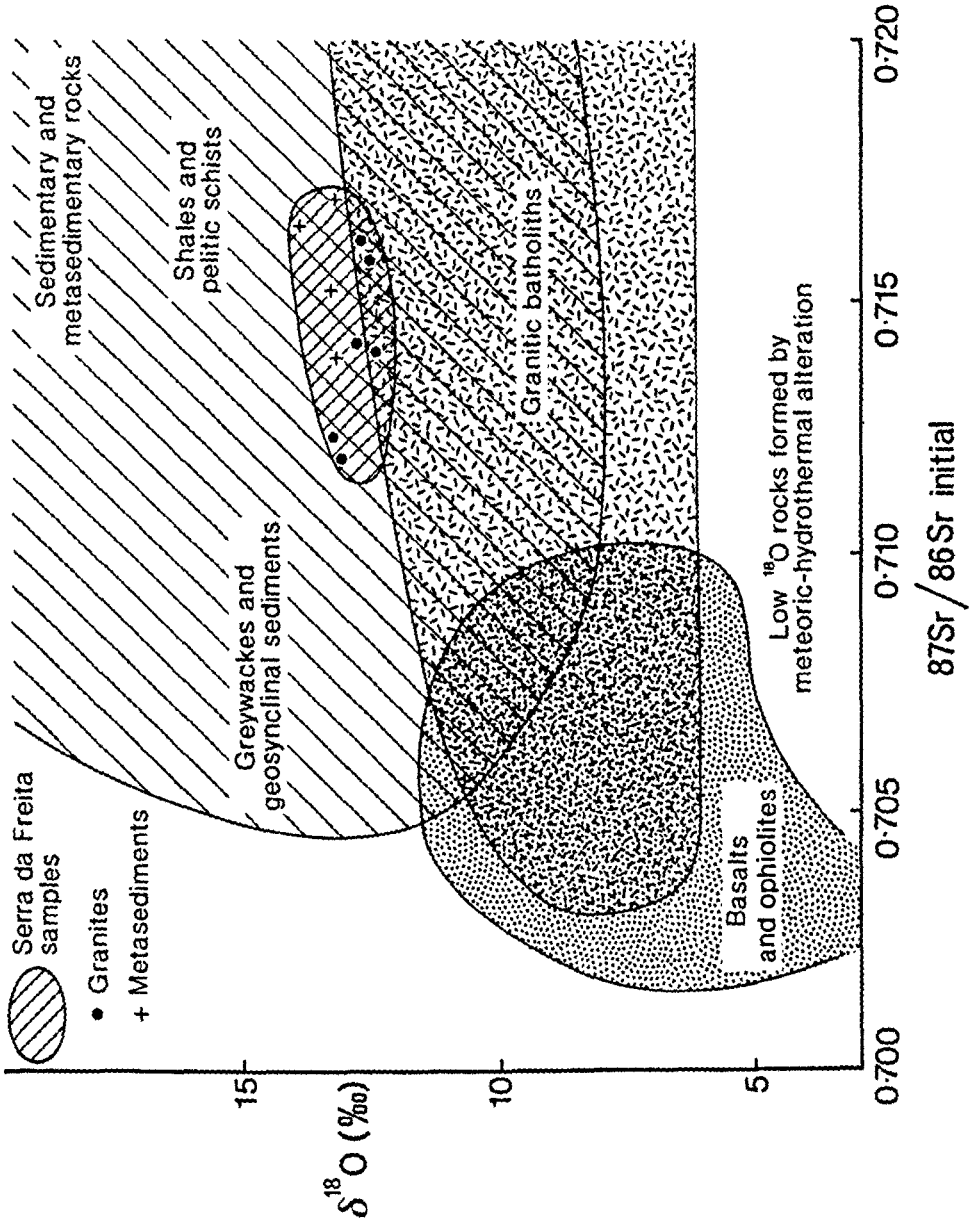

PART IV -- DISCUSSION AND CONCLUSIONS

CHAPTER IX

The aims of this final chapter are to: (i) bring together various themes which have been developed in the preceding chapters, (ii) place the findings in a regional context, (iii) state the main conclusions, and (iv) outline problems which are still outstanding which merit further research.

9.1 - The Petrogenesis of the Serra da Freita Pluton

Section 1.3.1. demonstrates that some confusion has arisen over the terminology of peraluminous granites which has led to their being widely regarded as being synomonous with S-type granites. There are two main reasons for this.

(1) The original definition (Chappell & White, 1974) applied only to the Lachlan Fold belt of SE Australia for granites derived from a source which had been through a weathering cycle. As the geochemistry of granites reflects features inherited from their source region, S-types in their type locality will be characteristic of that source whereas S-types in e.g. Iberia will correspondingly differ as conditions in source regions change. "It can only be a first order subdivision of granite types based on source rock characteristics, further differences will arise due to varying degrees of partial melting" (Pitcher, 1982). The main point therefore is that although the S- and I-type classification is extremely useful as a guideline, as granite chemistry is generally source-controlled, the classification should not be applied too simplistically. The original classification has now been revised and extended to a more

global application, summarized by Pitcher (1982).

(2) The other problem is that several processes can give rise to peraluminous magmas. All S-types are normally peraluminous, as pelites are largely composed of Al-rich phyllosilicates, however peraluminous compositions represent a point of convergence of diverse evolutionary processes (Clarke, 1981) such as: fractional crystallization from metaluminous magma (Cawthorne et al., 1976), the removal of alkalis as complexes soluble in a volatile phase from Al-saturated magma, anatexis of pelitic source material (White & Chappell, 1977), and contamination of metaluminous melts by pelitic country rocks.

Many workers have stated that S-types, as originally defined, represent granites with pelitic parentage. Miller (1985) defined a Ps (strongly peraluminous) granite as those with a phase more aluminous than biotite, and in addition to the original definition for S-type granites (Chappell & White, 1974) (Table 9.1), establishes new criteria for pelitic parentage which few Ps granites satisfy. These are set out in Table 9.2 and the facies of the Serra da Freita granites are shown for comparison (Table 9.3).

However, White et al., (1986) believe that "the dominant source rocks for the Lachlan Fold Belt S-types were not meta-shales, but quartzofeldspathic greywackes with a minor shale component." This refutes publications by e.g. Flood & Shaw, 1975; Green, 1976, 1977; Miller & Bradfish, 1980; Barker, 1981; Lee et al., 1981; Thompson, 1982; and Todd & Shaw, 1985.

It appears therefore that the original definitions have recently been re-emphasized in the light of inaccuracies concerning the exact usage of the classification.

Table 9.1

CRITERIA FOR IDENTIFYING S-TYPE GRANITES

Na_2O:	<3.2 wt% (felsic rocks, K_2O=5%)
	<2.2 wt% (less felsic rocks, K_2O=2%)
Al_2O_3:	mol. A/CNK>1.1; normative corundum >1 wt%
SiO_2:	restricted - relatively high (>65 wt%)
Variation:	oxide variation diagrams irregular
Initial	
($^{87}Sr/^{86}Sr$):	most >0.708
$\delta O18$:	>10‰
Mineralogy:	biotite + muscovite, garnet, cordierite, sillimanite, andalusite, NO hornblende
Accessories:	+ ilmenite, monazite, apatite, zircon, NO sphene, magnetite uncommon
Enclaves:	pelitic dominant

from Miller (1985)

(after Chappell & White, 1974; O'Neil & Chappell, 1977; Didier et al., 1982)

Table 9.2

CRITERIA FOR IDENTIFYING PELITC PARENTAGE OF IGNEOUS ROCKS

Major Element Chemistry/Phase Equilibria

Na_2O:	Relatively high in minimum melt leucogranite, (=3.5-4 wt%), but falling rapidly in less felsic (<2 wt% @65 wt% SiO_2)
CaO:	Low, even in less felsic rocks (<2 wt%)
Al_2O_3:	Normative corundum >5 wt%, rising in less felsic rocks
SiO_2:	Restricted - relatively high (>65 wt%)
Paragenesis:	Quartz and aluminous minerals (probably Al_2SiO_5 minerals + muscovite, garnet, cordierite) as early liquidus phases

Trace Elements

Rb: >100ppm Sr: <300-400ppm Ba: <600-1000ppm Rb/Ba: >0.25

Isotopic Compositions

Initial ($^{87}Sr/^{86}Sr$): >0.71 (generally >>0.71)

$\delta^{18}O$: >11-12‰

from Miller (1985)

Table 9.3

THE SERRA DA FREITA GRANITES

Major Element Chemistry/Phase Equilibria

Na_2O:	Most between 2.5 wt% and 4.5 wt%
CaO:	All granites <0.7 wt% except biotite nodular granites which have values around 1.5 wt%
Al_2O_3:	Normative corundum mean value of 4.7% Mol. A/CNK between 1.1 and 1.5
SiO_2:	Relatively restricted and high (Between 69.5 wt% and 76 wt%)
Paragenesis:	Quartz, orthoclase, albite/sodic oligoclase, biotite, muscovite, sillimanite (rare)

Trace Elements

Rb: most between 200-500ppm (biotite nodular granites <200ppm)

Sr: most <200ppm (biotite nodular granites 400-500ppm)

Ba: most between 0-300ppm

Rb/Ba: 1-9

Isotopic Compositions

Initial ($^{87}Sr/^{86}Sr$): 0.7136 ± 0.0008

$\delta^{18}O$: Average of 12 granites = 12.33‰

Range = 10.58‰ - 13.00‰

The Serra da Freita granites fit well with Miller's (1985) criteria for pelitic parentage, however they are slightly higher in Na2O than originally allowed by Chappell & White (1974).

It can therefore be concluded that the Serra da Freita pluton

(1) is strongly peraluminous (Miller, 1985),

(2) has geochemical and isotopic characteristics which point to a metapelitic source,

(3) fulfils Chappell & White's criteria (1974) for S-types, albeit Na2O values are higher in the Serra da Freita granites than in the granites of the Lachlan Fold Belt.

In general, the Hercynian aluminopotassic granites have many characteristics in common with Australian S-types. However, Pichavant and Stussi (1986) have suggested that the source rocks for the Australian S-types were dominated by greywackes, but the Hercynian aluminopotassic suite were derived from more pelitic-rich material. Conclusion (2) above provides strong evidence to support this view.

Placing the discussion back in the context of local geology, the main conclusion concerning the origin of the Serra da Freita pluton is that the geochemical and especially the isotopic data presented earlier strongly support the Beira Schists as the principal source rocks for the magma (see Conclusions Section).

9.2 - Tectonothermal Considerations

The Porto-Viseu metamorphic belt has been characterized as being of biotite, andalusite/staurolite, sillimanite type (Chapter V); this linear high temperature, low pressure belt represents an exceptionally steep thermal gradient, estimated by Godhino (1974) at $49^{\circ} \pm 6^{\circ}$ /km leading to anatexis at a possible shallow depth of 12-15 km.

As discussed in Section 1.2.3, this style of metamorphism typifies much of the Hercynian metamorphism in Spain and Portugal, therefore its representation by a tectonothermal model would be a major advance in understanding of the development of the Hercynian orogen.

Wickham & Oxburgh (1985) described a very similar situation from the Pyrenees where, within 4 km, a traverse is possible from unmetamorphosed Silurian shales through andalusite and sillimanite schists to migmatites and S-type granitoids. However they pointed out that this is unlikely to represent a true crustal gradient as conditions corresponding to points on such a P/T array may have been attained at different times. Dismissing burial, Wickham & Oxburgh (1985) proposed several possibilities by which these temperatures could have been attained in the upper crust. A large body of mafic magma emplaced at 15 km would be capable of maintaining such conditions, however such an intrusion would need to be in the order of 10 km thick. Alternatively, if an increase in crustal conductive heat flow caused by a perturbation at the base of the crust was sufficient to produce this thermal structure in the upper crust, temperatures would be high enough to melt the lower crust and heat would advect by ascending granitoids. Maximum perturbations of crustal temperature are likely to occur where the lithosphere is thinnest, therefore a rifting environment

was proposed as the most plausible setting in which an attenuated lower crust was heated by hot upwelling asthenosphere, with metamorphism and anatexis occurring at ca. 12 km. Wickham & Oxburgh (1985) concluded that in the Pyrenees, Hercynian orogenesis was a rifting event and they speculate that a zone of continental rifting may be the possible tectonic setting of all high temperature low pressure metamorphic belts.

The metamorphic parageneses and the thermal gradients in the Porto-Viseu metamorphic belt are similar to the Pyrenees, however the explanations offered for that region are not applicable to northern Portugal. A mafic body of the size postulated by Wickham & Oxburgh (1985) might be expected to impart some isotopic signature into any subsequent crustal melt. It is being argued here that the Serra da Freita granite has no recognizable mantle component. Neither is severe alteration in lower crustal heat flow produced by rifting feasible in this setting. The Ibero-Armorican Arc represents oblique strike-slip continental collision (Section 1.3.3), and whereas Wickham & Oxburgh (1985) admitted the possibility of strike-slip comonents in a rifting environment, the movements associated with the Coimbra-Cordoba shear system are dominated by strike-slip collision and strike-slip thrusting in Galicia and Asturias (Figure 1.5a). Pitcher (1982) regarded the Hercynian in Europe as a continental collisional mobile belt, involving strong compression with the production of penetrative cleavages, upright folds and steep thrust faults. The 2-mica granites are "the most characteristic rock type of the Iberian Hercynian" (Pitcher, 1982) and it is therefore appropriate to use trace element data from the Serra da Freita granite on diagrams which may distinguish between tectonic settings of various granitoid types.

Pearce et al. (1984) presented an Y+Nb-Rb plot to distinguish syn-collision granites from other types, and the Serra da Freita samples clearly fall in the syn-collision field (Figure 9.1). The analyses obtained fit well into the syn-collision peraluminous group (Group II) of Harris et al. (1986), which are characterized by high Rb/Zr and low K/Rb ratios. The group II analyses presented by Harris et al. (1986) are taken from Galicia, the French Pyrenees and Cornwall, no previous trace elements of this group of Portuguese granitoids have been utilized in this way, although the data of Albuquerque (1971, 1978) for later post-tectonic intrusions have been used.

Group II granites are syn-orogenic collision granites and if these plots are good discriminators, they show that a collision setting must be invoked for the most abundant plutonic type in western Iberia. As with the isotopic analyses, these results provide the first Portuguese contribution to the existing geochemical database on French and Spanish Hercynian granitoids.

Regional tectonics, local structural studies and trace element plots of syn-tectonic granites all show that the tectonic environment in north central Portugal during Hercynian orogenesis was dominated by collision tectonics involving shear zone systems. Although the metamorphism in the Pyrenees may have been produced in a zone of continental rifting, the assertion that all belts characterized by high temperature low pressure metamorphism with steep thermal gradients lie in such zones (Wickham & Oxburgh, 1985) is clearly far too sweeping a generalization. Wickham & Oxburgh (1985) stated that there is "no evidence for continental collision" in their area of study in the Pyrenees. However similar

Figure 9.1 - Discrimination diagrams for the tectonic settings of granites

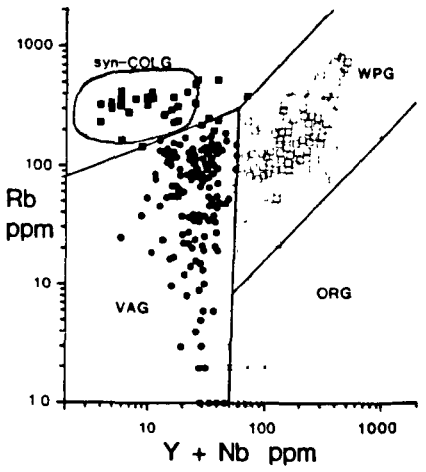

from Pearce et al. (1984)

Field of 'main' granite

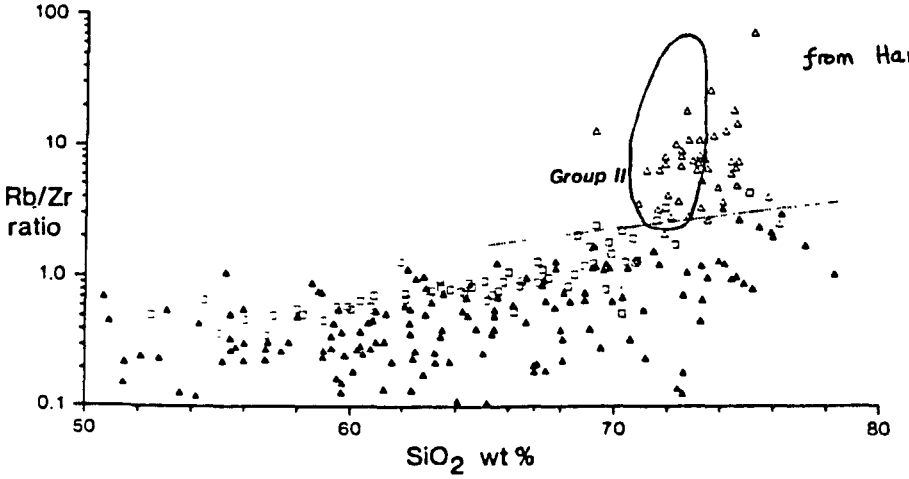

from Harris et al. (1986)

metamorphic environments are present within the Ibero-Armorican Arc in what is demonstrably a collision setting.

Having established a collision setting for the metamorphism and magmatism, the major outstanding problem is the source of sufficient heat energy to cause this type of metamorphism and the subsequent anatexis of the high grade schists. This leads onto controversial ground where models are simple and poorly constrained.

As quoted in Section 1.3.3, Pitcher (1979) believed that "large faults acting at depth would have imposed special pressure and temperature conditions in their vicinity, especially a decrease in pressure, favouring the formation and migration of anatectic melts. These melts would rise and be emplaced at high crustal levels under the structural control imposed by the same deep-seated shearing event which helped produce the melts in the first place".

It seems reasonable that the shear strain concentrated along this belt must, in some way, be related to the thermal events in the region. The subsequent discussion focusses on two regions in France at the northern end of the Ibero-Armorican Arc.

Nicholas et al. (1977) described a situation east of Brittany where the metamorphic isograds present a zonation symmetrical with respect to the axial zone of a major lineament. They proposed a model in which shear heating in the axial zone reaches anatexis temperatures of ca. 650°C. Once partial melting has occurred, viscous heating decreases considerably and the temperature can stabilize. The metamorphic isograds should correspond to the maximum temperature attained.

Along strike in southern Brittany Hercynian muscovite biotite leucogranites intrude the South Armorican shear zone. Strong & Hanmer (1981) invoked models involving fractional melting in fault zones either

by increasing the temperature by frictional heating or by lowering the melting temperatures by hydrous fluxing through the fault zone. They regarded the relationship between strike-slip faulting and the production of leucogranites to be so intimate as to imply a genetic relationship. A model involving a frictional temperature increase of 100° C above an ambient 30°C/km geotherm allows water-deficient melting at the upper stability field of muscovite. Repeated fractional melting by intermittent seismic shearing or continuous aseismic shearing could initiate lubrication of the fault zone by a melt, causing a decrease in frictional heat. After this melt moved upward and crystallized, further frictional heating could take place. It has been suggested that B, Li and F can, if present, substantially reduce the temperatures required for melting. Manning & Pichavant (1983) have shown experimentally that the presence of B and F in addition to H2O can cause a reduction in solidus temperatures from 715°C (H2O only) to 600°C (15% B2O3) at 1 kbar. They concluded that: (i) F- or B-bearing rocks will begin to melt at lower temperatures than similar F-or B-free rocks; (ii) F- or B- bearing fluids will allow melting at lower temperatures than would be expected for the system. Strong & Hanmer (1981) argued that such factors could have substantially lowered the melting temperature in the Brittany situation by more than 100°C.

In a discussion of the role of fluids in their model, Strong & Hanmer (1981) stressed the importance of H2O in fault systems. Melting along a 30 °C/km geotherm at 6 kbar could result from lowering of the melting temperature from the upper stability of muscovite to the water saturated granite solidus. As in the first model, fractional melting could be initiated by seismic pumping causing variations in water pressure. Wickham

& Taylor (1985) argued that in the Pyrenees, anatexis of pelite occurred at depths of 10-12 km and that deep penetration of surface waters was important in promoting major anatexis. It was a direct consequence of the availability of an external water source that shallow melts were produced at relatively low temperatures over a restricted temperature interval. Wickham (1987) stated that the "formation of kilometre-sized granitic plutons by large scale anatexis of the continental crust will be more easily achieved in those regions which are infiltrated by externally derived aqueous fluid".

Much theoretical criticism of models of frictional heating has been put forward. Brun & Cobbold (1980) proposed several models and concluded that no physically-valid model, except those involving thermal runaway, predicts temperatures high enough to cause partial melting. However they admitted that thermal runaway could occur in seismic situations involving narrow zones and high stresses, and that all such models are by nature very simplistic, e.g. the assumption that material in shear zones is homogeneous. Strong & Hanmer (1981) and Brun & Cobbold (1980) both drew attention to the work of Fleitout & Froidevaux (1980) who suggested that in a stratified (inhomogeneous) sequence, the temperature in the less ductile layers can increase sufficiently to melt the neighbouring more ductile material. The Beira Schists in the Serra da Freita region, comprised of interbedded greywackes and pelitic schists, certainly fulfil this condition of inhomogeneity.

In conclusion, it appears that frictional heating in shear zones being responsible for anatexis may be geologically feasible and that theoretical physical models which are critical of the process may be oversimplified.

Further work on the modelling is required but the coincidence of such plutons with major shear zones cannot be ignored.

The thermal effects of crustal thickening in collision zones must be considered as well. England & Thompson (1986) maintained that crustal thickening can lead to widespread crustal melting without the involvement of material from the mantle. It is therefore suggested that several favourable factors combine to allow melting at the depths and temperatures discussed. The initiation of shearing associated with collision may dictate the site of a heat flow anomaly in which frictional heating may operate to some extent. However other factors, such as the presence of fluids fluxing through the shear zone and the heterogeneous nature of the rocks involved, may be equally or more important. The lack of tourmaline or fluorite in the Serra da Freita granites may initially suggest that B or F were absent from any circulating fluids, however as mentioned in Part II, tourmaline is a common accessory in the metasediments and the occurrence of "tourmalinite" above the Castanheira intrusion strongly supports a model in which B-rich fluids migrated from the granites into the schists. There is no direct or indirect evidence for the presence of F, however it is possible that this element could be accommodated in biotite.

A simple model can be envisaged in which some frictional heating coupled with the effects on melting temperatures induced by fluxing of aqueous fluids, possibly enriched in B and/or F, could promote anatexis of the heterogeneous Beira Schists in a narrow linear zone, possibly at depths of 12-15 km as envisaged by Godhino (1974) and Wickham & Oxburgh (1985). These melts could rise and be responsible for the "plutonometamorphic"

zones of the Porto-Viseu metamorphic belt, although the resulting plutons are not presently exposed. This model accounts for the linear and symmetrical nature of the highest grade metamorphic zones, coincident with the locus of the shear zone. The Serra da Freita pluton exposed today could represent later batches of metasedimentary melt intruded into the shear system within the metamorphic zonation already developed. The fact that the contacts of the Serra da Freita pluton cross the sillimanite isograd could be explained if the actual intrusive units presently exposed were much smaller by volume and therefore had a lower heat capacity than the proposed deep level intrusions responsible for the high grade metamorphism. The ability of a small body of magma emplaced at high crustal levels to induce any local metamorphism would be limited if the rocks of the envelope at the time of intrusion were still at temperatures not far below that of the magma itself.

In conclusion, the close spatial and temporal association of high grade metamorphism and locally derived S-type magmas may be explained by models involving some frictional heating along a major crustal discontinuity, aided by a general lowering of melting temperatures by aqueous fluids fluxing through a heterogeneous metasedimentary protolith. In this model, the concentration of high strains in a narow zone can help explain the steep thermal gradients encountered; and the close genetic links between deformation, metamorphism and plutonism are emphasized.

9.3 - Regional Petrogenetic Considerations

Finally it is appropriate to consider the geochemical data in conjunction with other more general ideas about petrogenesis of Portuguese Hercynian

granitoids.

As documented in Section 1.2.2, published geochemical analyses of Portuguese granites are sparse compared with other segments of the European Hercynian belt. Most recent work e.g. Barr & Areias (1980), Pinto (1979, 1980, 1985) has largely been concerned with attempting to solve the complex age relations between intrusions. The work of Pinto (1983, 1985) is the most rigorous treatment of this complex issue. Petrogenetic interpretations are generally lacking, where trace element data are available much of the work is purely descriptive. However Pinto (1979) and Barr & Areias (1980) discussed geochemical characteristics in terms of S- and I-types and the resulting implications for source material. Pinto (1979) concluded that in north central Portugal, granitoids of various age and contrasting geochemical affinities exhibit characteristics best explained by processes such as crustal contamination of mantle derived melts, crustal anatexis, and varying degrees of fractional crystallization. There has however been no attempt to use geochemical data for the syn-tectonic 2-mica granites in a systematic way. The present study includes major and trace element analyses of the Beira Schists, and stable isotope data of Portuguese Hercynian granites, not previously available. Albuquerque (1978) presented REE data for some post-tectonic granitoids from northern Portugal and it is significant that his REE modelling indicated derivation of granite magmas from the greywackes and pelites of the orogenic belt.

Schermerhorn (1987) presented a completely new model for Hercynian magmatism in Portugal, claiming that the granites were the products of fractionation of mantle derived basic magmas. As Schermerhorn has studied

Portuguese granites for several decades, this work merits a thorough discussion.

(i) It claims to be a summary of all available age data for Portuguese granitoids, however the recent high-precision work of Pinto (1979, 1983, 1985) is not referenced.

(ii) Trace element data are presented for granites, tonalites and gabbros with no reference to the relative ages of the samples concerned. In an area where the character of magmatism changes with time, such an omission renders variation diagrams virtually meaningless.

(iii) It is widely accepted that most of the 2-mica leucogranites are "Older" and syn-tectonic, whilst the "Younger" granites are post-tectonic and more variable in composition e.g. tonalite, granodiorite etc. Schermerhorn (1987) claimed that the "Older" granites are pre-tectonic and comprise granites, granodiorites and tonalites, whilst the later granites belong to a gabbro - tonalite - leucogranite suite. This completely reverses all generally accepted relationships between tectonics and granitoid types known in northern Portugal.

(iv) It was claimed that any crustal contaminatiom could only occur when magma chambers existed in the lower to middle crust, not at higher crustal levels, and that leucogranites derived from granite magmas in the upper crust are uncontaminated fractionates, however no basis for this theory was presented.

Several attempts have been made to estimate the depth of emplacement of granitoid magmas in the region. Miller et al. (1981) showed that the presence of primary muscovite need not limit depth of crystallization to 11 km (3 kbar), the commonly considered minimum pressure at which magmatic

muscovite can crystallize. Primary muscovite may occur at surprisingly shallow depths due to factors such as: departures from ideal end member compositions, increased stability resulting from impurities, and the point of intersection (i.e. the minimum pressure for primary muscovite) of the muscovite breakdown and the H2O-saturated granite solidus curves being lowered by B-rich fluids.

Albuquerque (1971) proposed crystallization of the granites studied as approximating to a ternary minimum melt at PH2O = 3 kbar, (11 km). The granite sampled by Barr & Areias (1980) inferred a PH2O of about 2 kbar (<10 km), implying shallow emplacement. The Serra da Freita samples plot near the ternary minimum and could represent crystallization at around 2-4 kbar, which seems to correspond well with estimates of anatexis depths of 12-15 km, at temperatures in the range of 650°C - 700°C.

This brief review shows that major problems still exist in the interpretation of the petrogenesis of Portuguese granitoids. The data presented in this thesis represent an attempt to analyse Portuguese magmatism in a systematic way with the aim of constraining models for granite petrogenesis. Similar work carried out in the rest of Portugal and indeed Iberia should allow a clearer regional picture of granite magmatism to emerge. This should help to clarify any problems which presently exist regarding the ages of intrusion and the relationships between granites and their source.

9.4 - Conclusions from Laboratory Studies (Part III)

The main conclusions from the mapping and field interpretations were stated at the end of Part II. It is now appropriate to draw the various

ideas presented in Part III together and integrate them with those of Part II. As in any study, there is always scope for more detailed investigation of specific aspects, some of which are suggested in the final section.

9.4.1. - Geochemical and Isotopic Conclusions

(1) Major and trace element data suggest that the facies of the Serra da Freita pluton cannot be explained by a simple fractionation sequence; a model is proposed in which successive melts are derived by continual anatexis of a heterogeneous source.

(2) Oxygen isotopic data are consistent with a model involving anatexis of high grade pelitic schists to produce a granite magma.

(3) Radiogenic isotopes show that the granite can be regarded as a true metasedimentary crustal melt with no requirement to involve a mantle component - the Serra da Freita pluton is a true S-type.

9.5 - Integrated Model

In view of the discussion presented (Chapter IX), the following model is proposed.

Collisional movements along the Ibero-Armorican Arc in the upper Palaeozoic were accommodated on strike-slip ductile faults and shear zone systems. The Serra da Freita shear zone in north central Portugal is a typical sinistral transpressive shear zone associated with this overall NW sense of displacement.

Continental collision on this scale must have had profound effects on the thickness and consequently on the heat flow patterns in the continental

crust. In the Serra da Freita shear zone, it is argued that heat flow increased sufficiently to allow anatexis of the Beira Schists at depths of 12-15 km. This was achieved by a combination of (i) the increased heat flow mentioned above, (ii) the lowering of melting temperatures caused by fluxing of hydrous fluids, and (iii) a heterogeneous assemblage of greywackes and pelites which would encourage local high ductility contrasts. These melts rose in the restricted narrow belt controlled by the shear zone to cause the high temperature low pressure metamorphism of the Porto-Viseu belt, characterized by a paragenesis of biotite, andalusite/staurolite and sillimanite. It was into these zones that successive batches of melt, carrying isotopic signatures of a metasedimentary protolith, were periodically generated and emplaced as sheets and wedges at a high crustal level to form the Serra da Freita pluton. Petrographic evidence suggests that the minor intrusions began crystallizing before final emplacement into the body of the pluton. At high levels, existing structural anisotropies in the country rocks affected the final geometry of the intrusion, producing a folded nearly flat sheet where magma reached areas of lower strain.

Finally the dominant role played by the Serra da Freita shear zone throughout the evolution of the region must be emphasized, as all metamorphic, plutonic and tectonic features are in some way controlled by this structure which was active during metamorphism, anatexis, and emplacement and consolidation of the pluton. It seems likely that the marked concordance between metamorphic and plutonic styles over much of Hercynian Iberia could be explained by the existence of similar, but as yet unrecognized shear zones.

9.6 - Suggestions for Further Research

Based on an integrated field mapping, petrographical, geochemical, stable and radiogenic isotope study, an insight into the geological evolution of a small complex structural-igneous-metamorphic terrain has been gained. Whether the model and conclusions presented are of wider application elsewhere in the Iberian Hercynian belt is not yet known as few such integrated studies have been attempted. Such an approach in other areas should provide more detailed information which could gradually be integrated into a regional evolutionary history. Within the Serra da Freita area itself, the use of the following techniques would greatly augment the results presented here.

(1) A detailed microprobe study of mineral phases present in both granite and schist could throw light on problems such as the mineralogical relationships between the various facies of the granite and the evolution of the metamorphic belt. The general lack of garnet in this belt is unfortunate as it precludes any geothermometry, however other similar high temperature low pressure "plutonometamorphic" belts in northern Portugal may have suitable parageneses where such an approach might be successful.

(2) Research into these metamorphic belts would yield valuable data about crustal evolution in the region. As two crystals of kyanite were observed in this study, the P-T history of these belts is probably more complex than is presently apparent. It is stressed that the interpretation of metamorphic history presented here is only preliminary and should provide a basis for more detailed study. In particular, the use of fission track and 40Ar-39Ar dating might be very valuable in understanding the P-T

evolution of the whole belt.

(3) Modern research, in particular the use of stable isotopes, is required to elucidate the conditions responsible for Sn-W mineralization which is widespread in and around Iberian Hercynian granites.

(4) Magnetic and gravity surveys of the region would greatly assist in the formulation of regional tectonic models.

Finally, it should now be apparent that further work is required before the complexities of the geology of northern central Portugal, including the granite/schist relationships, are fully understood. Various types of research are required to be integrated and it is hoped that the ideas presented in this thesis provide at least a first insight into the intriguing geology of a beautiful region.

APPENDIX I -- SAMPLES ANALYSED AND LOCALITIES OF COLLECTION

All grid references are based on the national Portuguese grid and taken from the 1:25000 scale Sheet 155 (AROUCA). The national designation for the area shown on this sheet is 29TNF**** ****. The samples are coded as either FXABG or FXABS where F = Freita; X = year of collection (3 = 1983, 4 = 1984, 5 = 1985); AB is the sample number; G = granite, S = metasediment. Sa Da Mo was collected from the mountain top of Senhora da Mo which overlooks Arouca.

SAMPLE	TYPE	GRID REFERENCE
F334G	MAIN GRANITE	6195 2340
F336G	"	6220 2480
F345G	"	6035 2520
F346G	"	6250 2190
F348G	"	6597 1865
F349G	"	6635 2000
F351G	"	6743 2160
F354G	"	6738 2370
F43G	"	6018 2433
F49G	"	5975 2482
F415G	"	6048 2565
F416G	"	6020 2540
F417G	"	6030 2571
F418G	"	6018 2581
F436G	"	6415 2330
F437G	"	6475 2330
F438G	"	6480 2356
F443G	"	6430 2395
F444G	"	6390 2380
F445G	"	6335 2540
F446G	"	6235 2315
F448G	"	6260 2320
F449AG	"	6300 2310
F453G	"	6325 2285
F454G	"	6460 2255
F458G	"	6380 2360
F482G	"	6315 2350
F484G	"	5815 2604
F485G	"	5859 2555

F487G	MAIN GRANITE	5970 2540
F488G	"	6070 2536
F490G	"	6025 2495
F492G	"	6045 2480
F494G	"	6110 2490
F496G	"	6135 2500
F497G	"	6140 2470
F498G	"	6165 2505
F4101G	"	6195 2460
F4104G	"	6270 2455
F4105G	"	6240 2430
F4106G	"	6205 2433
F4107G	"	6200 2420
F4109G	"	6220 2370
F4115G	"	6170 2350
F4116G	"	6190 2370
F4117G	"	6150 2360
F4118G	"	6100 2380
F4119G	"	6130 2410
F4120G	"	6090 2430
F4122G	"	6320 2445
F4133G	"	6170 2450
F4140G	"	5900 2570
F4142G	"	6310 2290
F4146G	"	6430 2270
F4147G	"	6510 2265
F4148G	"	6360 2250
F512G	"	Not on Scale
F347G	MICROGRANITE	6615 2130
F414G	"	6060 2570
F435G	"	6405 2330
F483G	"	6315 2350
F4138G	"	6370 2280
F4143G	"	6330 2310
F4144G	"	6360 2330
F440G	SHEARED GRANITE	6530 2343
F441G	"	6527 2383
F442G	"	6455 2425
F474G	"	6570 2430
F4151G	"	6589 2331
F4152G	"	6589 2371
F332G	CONTACT LEUCOGRANITE	6200 2262
F333G	"	6200 2262
F338G	"	6225 2495
F486G	"	5863 2545
F489G	"	6090 2550
F495G	"	6120 2540
F499G	"	6160 2520
F4100G	"	6200 2500
F4102G	"	6250 2480
F4103G	"	6290 2470

F4110G	CONTACT LEUCOGRANITE	6200	2280
F4123G	"	6360	2440
F4139G	"	6230	2330
F447G	FELSIC GRANITE	6235	2310
F449BG	"	6300	2310
F451G	"	6325	2285
F452G	"	6326	2286
F4141G	"	6310	2290
F4149G	"	6350	2240
F4150G	"	6320	2270
F525G	"	6474	2250
F411G	APLITE	5955	2474
F439G	"	6528	2323
F450G	"	6300	2310
F4124G	"	6461	2442
F4126G	"	6462	2444
F4128G	"	6463	2444
F4130G	"	6466	2446
F313G	CASTANHEIRA	6100	2240
F457G	GESTOSO	6455	2248
F522G	CASTANHEIRA	6140	2235
F325S	METASEDIMENTS	6150	2190
F326S	"	6133	2170
F327S	"	6188	2190
F328S	"	6196	2225
F329S	"	6200	2262
F330S	"	6200	2262
F331S	"	6201	2263
F335S	"	6204	2385
F337S	"	6225	2495
F339S	"	6210	2545
F340S	"	6205	2585
F341S	"	6195	2618
F342S	"	6200	2642
F342AS	"	6200	2642
F343S	"	5963	2433
F344S	"	6035	2420
F350S	"	6714	2094
F352S	"	6713	2395
F355S	"	6595	1852
F41S	"	6031	2421
F42S	"	6015	2433
F46S	"	5980	2440
F47S	"	5970	2440
F48S	"	5973	2429
F410S	"	5960	2480
F412S	"	5951	2471
F413S	"	5949	2476
F419S	"	6019	2589
F420S	"	6080	2570

F421S	METASEDIMENTS	6081	2581
F423S	"	6103	2574
F424S	"	6125	2587
F425S	"	6120	2590
F426S	"	6123	2591
F427S	"	6127	2595
F428S	"	6140	2590
F429S	"	6145	2588
F430S	"	6160	2586
F431S	"	6169	2612
F432S	"	6181	2625
F433S	"	6190	2635
F434S	"	6284	2436
F455S	"	6455	2255
F459S	"	6744	2628
F460S	"	6730	2610
F461S	"	6705	2596
F462S	"	6705	2596
F463S	"	6689	2590
F464S	"	6669	2581
F465S	"	6651	2570
F466S	"	6631	2559
F467S	"	6628	2540
F468S	"	6627	2532
F469S	"	6627	2532
F470AS	"	6625	2520
F470BS	"	6625	2520
F471S	"	6621	2511
F472S	"	6615	2509
F473S	"	6618	2500
F475S	"	6572	2439
F476AS	"	6580	2447
F476BS	"	6580	2447
F477AS	"	6593	2459
F477BS	"	6593	2459
F478S	"	6595	2470
F479S	"	6594	2481
F481S	"	6604	2492
F491S	"	6025	2495
F493S	"	6035	2485
F4108S	"	6203	2400
F4111S	"	6135	2300
F4112S	"	6140	2310
F4113S	"	6150	2315
F4114S	"	6160	2320
F4121S	"	5960	2515
F4125S	"	6467	2444
F4129S	"	6463	2448
F4132S	"	6145	2432
F4135S	"	6144	2433
F4137S	"	6370	2280

F4145S	METASEDIMENTS	6410 2350
F4153S	"	6405 2490
F4154S	"	6405 2505
F4155S	"	6410 2520
SaDaMo	"	6465 3150
F521AS	"	6145 2235
F528S	"	6285 2710
F530S	"	6265 2678

APPENDIX II -- WHOLE ROCK GEOCHEMICAL ANALYSIS - TECHNIQUES

(Much of the technical details in Appendices II and IV are based on the work of Zaleski (1982)).

2.1 - Introduction

X-ray fluorescence spectrometry (XRF) analysis was carried out at St Andrews on a Phillips PW 1212 automatic x-ray spectrometer linked to an Apple II microcomputer for on-line data processing. Computer software was designed for all aspects of XRF calibration, resolution monitoring and analysis (Stephens, 1982).

The PW 1212 accomodates 4 specimens in pots within the sample chamber, allowing processing of 3 samples plus the pot 1 monitor per run. Fifteen front panel channels corresponding to selected goniometer settings and various chosen parameters allow automatic counting on 15 sequential angular positions.

2.2 - Instrument Conditions

Major and trace elements were grouped according to compatibility of optimum conditions and the constraint of 15 automatically available goniometer positions. The conditions of Norrish & Chappell (1977) were adhered to for major oxide analysis of SiO_2, Al_2O_3, TiO_2, Fe_2O_3, MgO, CaO, Na_2O, K_2O, and P_2O_5.

Trace element conditions were adapted from Norrish & Chappell (1977), Leake et al. (1970), and those used by the Grant Institute of Geology, University of Edinburgh. MnO was grouped with trace elements Au-A due to

interference from the Cr tube used for major oxide analysis. For analysis of Zr, Y, Sr, Rb, Nb, and Th, backgrounds were generally measured on each side of the peak to allow for the sloped background of the "high on the continuum" position of most of these analytical lines. In traces Au-A, the Ti KB+1 line was also counted for use in an interference corrected multiple regression calibration of V.

2.3 - Major Oxide Analysis: Sample Preparation

Analyses were performed on fused beads which were prepared after the method of Harvey et al. (1973) adapted by Batchelor to St Andrews specifications. Lanthanum oxide, lithium tetraborate, lithium carbonate mixture "Spectroflux", used as flux, was ignited and the weight loss recorded. NH4NO3 as an oxidant and 0.5 g of sample powder were added to the flux; the mixture was devolatilized and homogenized by heating for 20 minutes over a Meker burner at full heat. Weight change was recorded prior to casting the bead on an aluminium disc. Beads were protected by a silica cover during 30 minutes of annealing on a hot plate. The weight change difference between flux and sample mixture for each specimen and the monitor bead was used in subsequent correction adjusting to a constant dilution. Problems due to quench crystal growth or bead cracking were alleviated by refusing or recasting.

2.4 - Trace Element Analysis: Sample Preparation

Analysis were performed on powder pellets. Six grams of sample powder was finely ground in a mortar and pestle to ensure homogeneity and to crush any persistent mineral fragments. The fine powder was mixed with

approximately 12 drops of moviol and subjected for 1 minute to 12 tons pressure between tungsten carbide dies. The pellet was dried in an oven and the sample name was written on the edge in pencil.

2.5 - Ferrous Iron (FeO) Determination

This was performed on all samples using the titration method of Wilson (1955) as adapted by Batchelor (pers. comm.). The digested sample was oxidized by addition of ammonium metavanadate, the excess of which was subsequently reduced by addition of excess ferrous ammonium sulphate. Excess Fe^{2+} was titrated with potassium dichromate using a sodium diphenylamine sulphonate indicator solution. Samples and blanks of chemicals alone were jointly titrated, with Fe^{2+} content of the sample determined by subtraction. Two-sigma error is $\pm$ 0.24 wt% FeO, with a coefficient of variation of 4.7%.

2.6 - Data Processing

The calculation of CIPW normative mineralogy, geochemical parameters and element ratios, and all plotting routines were carried out on the St Andrews VAX-11/780 computer system, using programs prepared by W.E.Stephens.

APPENDIX III -- WHOLE ROCK GEOCHEMICAL ANALYSIS - RESULTS

The analyses are in the order used in Appendix I, i.e. the granites are listed by facies in the order, Main Granite, Microgranite, Sheared Granite, Contact Leucogranite, Felsic Granite, Aplite, and Castanheira/Gestoso, followed by the metasediments.

Sample	F334G	F336G	F345G	F346G	F348G	F349G	F351G	F354G
SiO2	72.89	73.61	73.47	73.40	71.90	72.21	72.33	73.39
TiO2	0.25	0.13	0.09	0.18	0.17	0.30	0.20	0.08
Al2O3	15.06	15.27	14.94	15.04	15.50	15.11	15.67	14.85
Fe2O3	0.10	0.22	0.10	0.16	0.00	0.00	0.17	0.23
FeO	1.29	0.74	0.68	0.84	1.15	1.37	0.96	0.80
MnO	0.02	0.01	0.01	0.01	0.02	0.01	0.01	0.03
MgO	0.76	0.11	0.13	0.24	0.19	0.68	0.29	0.17
CaO	0.48	0.42	0.32	0.31	0.47	0.51	0.48	0.42
Na2O	2.47	3.16	3.54	3.32	2.98	2.68	3.56	3.49
K2O	5.08	4.71	4.56	4.37	4.82	5.13	5.06	4.10
P2O5	0.43	0.43	0.42	0.37	0.48	0.38	0.41	0.47
Loss	1.40	1.20	1.80	1.40	1.80	1.60	0.20	1.20
TOTAL	100.32	100.09	100.11	99.71	99.55	100.07	99.43	99.28
Nb	3	4	5	5	5	4	6	14
Zr	103	51	34	66	62	122	75	22
Y	8	9	7	6	9	9	8	11
Sr	44	33	25	26	37	47	49	24
Rb	318	412	303	379	269	240	313	305
Th	8	10	3	9	0	13	8	6
Pb	33	35	30	27	32	38	36	11
Zn	120	86	30	99	82	75	75	36
Cu	0	6	2	0	0	3	7	11
Ni	11	8	11	9	9	10	7	9
Cr	0	0	0	0	0	0	0	0
V	14	15	14	13	13	17	12	13
Ba	182	97	32	79	131	223	218	39
Hf	4	3	3	5	3	5	4	3
Ce	45	13	13	17	21	40	33	5
La	13	0	0	0	0	10	0	0

Sample	F43G	F49G	F415G	F416G	F417G	F418G	F436G	F437G
SiO2	72.89	71.59	73.58	72.28	72.92	73.57	72.78	72.49
TiO2	0.11	0.17	0.12	0.18	0.10	0.07	0.24	0.23
Al2O3	15.22	15.28	15.98	15.20	15.23	15.55	15.16	15.22
Fe2O3	0.53	0.19	0.22	0.07	0.36	0.01	0.34	0.05
FeO	0.30	0.90	0.68	1.08	0.64	0.66	0.84	1.23
MnO	0.00	0.01	0.00	0.01	0.01	0.00	0.00	0.00
MgO	0.21	0.09	0.01	0.46	0.75	0.00	0.33	0.45
CaO	0.31	0.45	0.30	0.38	0.38	0.10	0.44	0.53
Na2O	3.29	3.86	3.85	3.07	4.38	3.99	2.90	2.96
K2O	4.66	5.30	4.38	4.95	4.36	4.17	4.95	4.74
P2O5	0.42	0.44	0.39	0.41	0.37	0.34	0.40	0.42
Loss	1.40	1.20	0.60	2.00	1.00	2.00	1.80	1.80
TOTAL	99.39	99.57	100.18	100.17	100.57	100.51	100.26	100.20
Nb	2	0	3	2	1	0	0	0
Zr	41	80	42	94	57	22	113	105
Y	4	10	5	7	6	2	8	10
Sr	32	48	22	38	25	15	46	36
Rb	313	372	402	310	378	392	282	311
Th	0	7	3	8	9	2	10	10
Pb	30	37	26	26	29	20	29	29
Zn	57	79	66	76	79	49	71	96
Cu	9	5	11	11	10	11	10	15
Ni	8	12	7	5	8	7	8	7
Cr	0	0	0	0	0	0	0	0
V	10	20	13	12	5	9	13	12
Ba	36	197	82	137	45	0	184	155
Hf	3	4	2	4	2	2	3	4
Ce	4	44	15	36	28	1	53	26
La	0	0	0	0	0	0	7	11

Sample	F438G	F443G	F444G	F445G	F446G	F448G	F449AG	F453G
SiO2	72.21	73.74	71.79	71.70	73.11	73.40	70.11	71.88
TiO2	0.11	0.07	0.19	0.06	0.26	0.19	0.29	0.24
Al2O3	15.27	14.85	15.51	15.66	15.25	15.34	16.37	15.79
Fe2O3	0.13	0.15	0.16	0.20	0.13	0.32	0.22	0.04
FeO	0.82	0.78	1.09	0.67	1.10	0.79	1.65	1.16
MnO	0.01	0.00	0.01	0.01	0.00	0.00	0.01	0.00
MgO	0.33	0.19	0.49	0.37	0.29	0.75	0.28	0.43
CaO	0.38	0.37	0.42	0.19	0.54	0.45	0.59	0.58
Na2O	4.09	3.71	3.01	4.10	3.15	3.23	2.39	3.11
K2O	4.24	4.41	5.00	4.63	5.15	4.50	5.95	5.29
P2O5	0.41	0.38	0.37	0.32	0.38	0.46	0.50	0.41
Loss	1.20	1.00	1.40	1.40	0.20	0.80	1.60	1.20
TOTAL	99.27	99.70	99.52	99.37	99.65	100.30	100.09	100.24
Nb	0	6	0	2	1	4	8	1
Zr	52	33	94	47	98	61	143	108
Y	8	15	9	7	9	6	11	10
Sr	23	11	36	30	52	38	55	66
Rb	353	258	311	318	295	302	480	317
Th	4	1	10	4	15	1	16	11
Pb	26	18	27	30	32	28	36	38
Zn	70	36	94	63	64	71	81	81
Cu	8	9	10	10	16	6	10	7
Ni	8	6	7	6	7	4	6	9
Cr	0	0	0	0	0	0	0	0
V	14	14	19	11	24	9	23	15
Ba	73	57	110	84	253	123	325	351
Hf	2	2	4	2	4	3	4	4
Ce	22	13	37	28	43	28	55	31
La	0	0	0	0	10	0	14	9

Sample	F454G	F458G	F482G	F484G	F485G	F487G	F488G	F490G
SiO2	72.98	72.88	73.18	71.82	72.19	70.71	73.32	72.46
TiO2	0.06	0.20	0.20	0.13	0.12	0.31	0.15	0.31
Al2O3	15.25	15.20	14.85	15.34	14.61	15.70	15.31	15.14
Fe2O3	0.17	0.00	0.01	0.03	0.12	0.22	0.13	0.09
FeO	0.70	1.14	1.07	1.05	1.00	1.25	0.76	1.24
MnO	0.01	0.00	0.00	0.01	0.01	0.00	0.00	0.00
MgO	0.27	0.30	0.51	0.12	0.13	0.44	0.22	0.58
CaO	0.22	0.54	0.49	0.33	0.40	0.67	0.18	0.63
Na2O	4.84	2.96	2.95	3.91	4.14	3.12	2.76	2.63
K2O	4.14	5.03	4.58	4.34	4.19	5.06	4.76	5.44
P2O5	0.31	0.40	0.45	0.37	0.37	0.51	0.31	0.43
Loss	1.60	1.60	1.80	2.80	1.80	1.80	1.80	1.00
TOTAL	100.61	100.33	100.17	100.32	99.15	99.89	99.77	100.04
Nb	2	0	6	0	0	1	0	0
Zr	40	80	97	71	70	135	63	123
Y	3	9	9	6	8	12	4	11
Sr	19	51	46	21	20	54	34	61
Rb	348	304	324	344	357	292	346	263
Th	4	4	6	10	7	15	11	18
Pb	27	35	21	26	22	38	26	39
Zn	84	79	68	73	62	100	78	66
Cu	10	9	11	7	7	2	9	1
Ni	8	9	9	11	9	7	7	5
Cr	0	0	0	0	0	0	0	0
V	11	17	11	13	14	18	19	27
Ba	57	194	126	52	60	240	116	245
Hf	2	4	5	4	3	5	2	6
Ce	0	22	49	13	25	47	27	51
La	0	0	6	0	0	8	0	10

Sample	F492G	F494G	F496G	F497G	F498G	F4101G	F4104G	F4105G
SiO2	71.30	72.26	71.75	71.48	73.45	70.51	73.39	71.87
TiO2	0.26	0.24	0.11	0.20	0.10	0.17	0.11	0.26
Al2O3	15.86	15.09	15.58	15.00	15.05	15.04	15.37	15.42
Fe2O3	0.05	0.08	0.00	0.19	0.00	0.02	0.01	0.07
FeO	1.13	1.15	0.75	1.15	0.77	1.11	0.76	1.27
MnO	0.00	0.00	0.00	0.01	0.00	0.02	0.00	0.00
MgO	0.59	0.61	0.22	0.66	0.18	0.44	0.29	0.41
CaO	0.56	0.44	0.33	0.37	0.42	0.35	0.31	0.52
Na2O	2.78	2.89	3.31	3.00	3.57	3.50	3.24	2.89
K2O	5.84	4.84	4.99	4.79	4.30	4.49	4.34	5.07
P2O5	0.34	0.46	0.38	0.40	0.40	0.36	0.32	0.42
Loss	1.40	1.40	2.00	2.20	1.20	1.60	2.00	2.00
TOTAL	100.21	99.55	99.49	99.52	99.50	97.69	100.20	100.29
Nb	0	0	1	1	1	1	0	0
Zr	112	99	64	102	46	103	35	105
Y	7	8	7	10	7	9	6	10
Sr	71	43	39	36	25	38	22	53
Rb	276	304	321	286	312	347	320	312
Th	12	13	4	11	2	13	4	10
Pb	46	30	37	31	26	29	24	34
Zn	77	107	36	95	57	79	67	72
Cu	8	7	6	10	8	3	1	4
Ni	9	6	12	12	10	8	5	5
Cr	0	0	0	0	0	0	0	0
V	19	16	14	8	7	19	5	19
Ba	343	170	118	75	67	124	68	216
Hf	6	4	3	3	2	6	2	5
Ce	46	45	18	29	14	42	5	41
La	5	1	0	5	0	0	0	1

Sample	F4106G	F4107G	F4109G	F4115G	F4116G	F4117G	F4118G	F4119G
SiO2	70.46	72.46	71.47	73.38	70.53	74.28	73.37	72.09
TiO2	0.22	0.26	0.23	0.17	0.17	0.21	0.19	0.19
Al2O3	15.50	15.06	15.53	15.54	15.78	15.30	15.36	14.96
Fe2O3	0.05	0.41	0.00	0.40	0.10	0.38	0.48	0.50
FeO	1.25	0.90	1.14	0.67	1.14	0.70	0.60	0.77
MnO	0.01	0.00	0.00	0.00	0.01	0.00	0.00	0.01
MgO	0.32	0.38	0.33	0.35	0.52	0.27	0.49	0.00
CaO	0.58	0.58	0.61	0.46	0.52	0.38	0.52	0.40
Na2O	3.53	2.93	3.25	3.17	3.82	2.85	3.00	3.54
K2O	5.54	5.16	5.31	4.86	5.70	4.26	4.77	4.63
P2O5	0.42	0.40	0.51	0.42	0.46	0.41	0.41	0.00
Loss	1.60	1.40	0.40	1.20	1.40	1.40	1.20	2.20
TOTAL	99.57	100.03	98.88	100.69	100.25	100.51	100.46	99.37
Nb	0	0	2	0	0	0	0	0
Zr	120	118	103	62	98	76	65	88
Y	11	12	9	8	9	7	8	9
Sr	62	55	67	46	70	20	43	35
Rb	263	276	283	271	318	347	284	320
Th	12	12	12	7	11	4	1	9
Pb	41	34	40	32	41	24	32	26
Zn	58	83	60	68	68	69	72	92
Cu	7	6	6	6	5	4	4	4
Ni	8	8	8	6	5	6	7	6
Cr	0	0	0	8	0	0	0	0
V	21	18	21	12	16	20	13	19
Ba	282	235	326	137	268	80	132	115
Hf	6	5	6	3	4	3	4	5
Ce	31	48	46	35	40	9	14	27
La	3	10	4	0	2	0	0	5

Sample	F4120G	F4122G	F4133G	F4140G	F4142G	F4146G	F4147G	F4148G
SiO2	72.38	73.47	72.14	72.50	69.56	72.17	72.62	71.87
TiO2	0.19	0.17	0.25	0.18	0.22	0.22	0.12	0.26
Al2O3	15.40	15.22	15.09	14.61	15.75	15.89	15.36	15.70
Fe2O3	0.35	0.29	0.26	0.47	0.08	0.39	0.01	0.48
FeO	0.71	0.75	0.92	0.83	1.33	0.78	1.00	0.83
MnO	0.00	0.00	0.00	0.01	0.02	0.00	0.01	0.00
MgO	0.33	0.38	0.19	0.00	0.60	0.56	0.01	0.00
CaO	0.48	0.41	0.48	0.48	0.57	0.45	0.25	0.44
Na2O	2.93	2.76	2.74	3.54	3.50	2.94	3.98	2.59
K2O	5.14	4.72	5.31	4.57	5.74	5.20	4.57	5.58
P2O5	0.36	0.41	0.38	0.41	0.46	0.38	0.38	0.38
Loss	1.80	1.40	2.40	1.60	2.20	1.40	2.00	1.60
TOTAL	100.16	100.05	100.25	99.27	100.13	100.47	100.38	99.83
Nb	0	0	0	0	0	0	0	0
Zr	81	66	108	100	124	92	65	114
Y	8	6	8	10	11	9	5	7
Sr	50	35	55	34	68	50	27	67
Rb	320	333	262	308	329	316	354	303
Th	13	9	11	7	12	10	11	15
Pb	39	23	39	25	39	36	28	36
Zn	79	77	37	98	57	89	62	85
Cu	6	4	9	2	4	10	10	10
Ni	5	8	4	6	7	7	11	7
Cr	0	0	0	0	0	0	0	0
V	20	22	19	14	18	17	13	20
Ba	230	117	239	99	274	214	98	331
Hf	4	6	6	5	6	4	4	4
Ce	30	38	63	32	46	32	23	38
La	3	4	9	3	11	2	0	6

Sample	F512G	F347G	F414C	F435C	F483G	F4138G	F4143G	F4144G
SiO2	72.71	71.61	71.28	71.01	73.54	70.32	73.20	72.15
TiO2	0.18	0.27	0.14	0.19	0.22	0.06	0.13	0.13
Al2O3	15.45	15.67	17.32	15.35	16.05	16.98	16.04	15.89
Fe2O3	0.05	0.18	0.31	0.08	0.00	0.26	0.10	0.48
FeO	1.03	1.30	1.10	1.26	1.25	1.76	0.89	0.49
MnO	0.01	0.02	0.01	0.01	0.00	0.00	0.00	0.00
MgO	0.00	0.34	0.18	0.89	0.52	0.44	0.35	0.32
CaO	0.23	0.64	0.43	0.54	0.48	0.17	0.38	0.23
Na2O	2.66	3.36	2.93	3.46	3.18	3.79	3.31	3.08
K2O	5.01	5.48	3.57	5.61	5.11	4.82	4.80	4.91
P2O5	0.47	0.48	0.42	0.42	0.47	0.28	0.31	0.37
Loss	2.40	0.60	2.00	1.80	2.00	0.60	1.00	2.20
TOTAL	100.28	100.05	99.74	100.72	102.92	99.55	100.58	100.32
Nb	6	5	7	2	1	3	0	0
Zr	84	115	31	97	106	16	58	56
Y	6	10	5	7	9	4	10	10
Sr	44	66	14	66	61	5	42	38
Rb	332	329	310	301	367	423	298	334
Th	9	10	6	8	5	0	3	3
Pb	4	38	25	37	40	14	31	38
Zn	100	83	56	72	56	240	52	71
Cu	20	0	10	5	11	4	5	8
Ni	18	14	29	7	10	5	5	7
Cr	0	0	0	0	0	0	0	0
V	0	19	8	18	18	7	12	12
Ba	141	302	15	331	316	0	185	148
Hf	5	5	3	5	4	1	5	3
Ce	55	38	2	29	19	0	15	16
La	1	9	0	0	5	0	0	0

Sample	F440G	F441G	F442G	F474G	F4151G	F4152G	F332G	F333G
SiO2	74.08	73.82	72.31	72.94	72.97	73.04	73.59	74.44
TiO2	0.15	0.13	0.08	0.06	0.13	0.04	0.05	0.00
Al2O3	14.15	14.94	15.56	16.13	14.80	14.99	16.90	15.39
Fe2O3	0.33	0.12	0.35	0.35	0.00	0.37	0.99	0.03
FeO	1.16	0.99	0.67	0.70	1.04	0.75	0.05	0.34
MnO	0.02	0.01	0.01	0.03	0.00	0.03	0.01	0.01
MgO	1.09	0.96	0.21	0.14	0.34	0.13	0.14	0.00
CaO	0.46	0.38	0.41	0.40	0.48	0.32	0.31	0.28
Na2O	3.54	3.40	4.45	3.14	3.52	4.29	2.29	4.97
K2O	4.80	4.29	4.46	4.19	5.06	4.50	3.35	3.49
P2O5	0.27	0.37	0.40	0.44	0.33	0.38	0.34	0.47
Loss	0.60	1.00	0.80	1.80	1.20	1.60	2.40	1.20
TOTAL	100.72	100.47	99.77	100.38	99.94	100.49	100.47	100.70
Nb	7	7	1	12	0	0	15	10
Zr	71	42	33	37	54	36	5	5
Y	18	14	7	10	16	11	3	2
Sr	38	23	23	20	44	22	71	171
Rb	212	306	386	407	206	276	291	496
Th	3	3	6	5	4	1	3	0
Pb	22	21	27	13	28	15	44	22
Zn	50	67	81	42	37	40	48	59
Cu	8	11	11	8	5	0	11	4
Ni	9	5	8	7	5	6	9	8
Cr	0	0	0	0	0	0	0	0
V	18	10	12	10	19	9	5	6
Ba	187	113	30	0	229	42	2	0
Hf	4	3	3	3	2	2	2	3
Ce	26	9	7	5	32	9	0	7
La	0	0	0	0	0	0	0	0

Sample	F338G	F486G	F489G	F495G	F499G	F4100G	F4102G	F4103G
SiO2	74.32	73.46	75.16	74.33	74.05	72.28	72.88	73.88
TiO2	0.02	0.11	0.05	0.04	0.05	0.10	0.01	0.03
Al2O3	14.80	14.96	15.30	15.67	15.37	15.97	15.12	15.38
Fe2O3	0.04	0.00	0.03	0.33	0.05	0.00	0.00	0.00
FeO	0.54	0.89	0.58	0.33	0.55	0.67	0.60	0.58
MnO	0.01	0.00	0.00	0.00	0.00	0.00	0.00	0.00
MgO	0.00	0.00	0.10	0.23	0.10	0.17	0.05	0.28
CaO	0.16	0.38	0.21	0.21	0.29	0.20	0.23	0.16
Na2O	4.57	3.71	4.15	4.23	3.74	3.45	4.46	4.72
K2O	3.74	4.18	4.06	4.07	4.14	4.51	3.81	3.69
P2O5	0.30	0.33	0.30	0.35	0.32	0.41	0.34	0.27
Loss	1.60	1.80	0.60	0.40	1.40	2.20	1.00	0.60
TOTAL	100.16	99.88	100.60	100.25	100.13	100.03	98.57	99.65
Nb	4	0	1	0	0	2	3	1
Zr	8	31	8	8	25	50	15	23
Y	4	6	5	6	5	4	4	5
Sr	8	20	15	23	18	26	27	13
Rb	459	349	429	432	352	356	502	412
Th	4	5	1	3	0	4	1	2
Pb	21	26	29	27	145	29	23	17
Zn	37	43	81	66	48	57	84	67
Cu	6	6	9	7	11	5	4	4
Ni	11	8	7	6	8	10	8	8
Cr	0	0	0	0	0	0	0	0
V	5	12	8	11	5	9	8	7
Ba	0	58	0	19	31	73	0	2
Hf	1	2	2	2	2	5	3	2
Ce	0	0	0	0	0	24	0	0
La	0	0	0	0	0	0	0	0

Sample	F4110G	F4123G	F4139G	F447G	F449BG	F451G	F452G	F4141G
SiO2	73.96	72.82	74.18	75.02	73.55	73.29	74.02	74.28
TiO2	0.04	0.03	0.02	0.12	0.03	0.04	0.00	0.04
Al2O3	15.38	15.18	15.60	15.04	14.98	15.46	14.78	15.24
Fe2O3	0.35	0.15	0.02	0.17	0.07	0.00	0.11	0.13
FeO	0.10	0.69	0.40	0.44	0.37	0.57	0.34	0.40
MnO	0.00	0.01	0.00	0.00	0.00	0.00	0.01	0.00
MgO	0.16	0.08	0.50	0.29	0.17	0.23	0.46	0.00
CaO	0.51	0.23	0.37	0.40	0.19	0.23	0.23	0.27
Na2O	4.35	4.16	4.07	2.90	3.63	5.12	5.79	4.02
K2O	3.85	4.31	3.73	4.22	5.16	3.35	3.53	3.69
P2O5	0.53	0.35	0.47	0.39	0.34	0.37	0.33	0.40
Loss	1.20	1.60	0.10	1.20	1.20	1.40	1.00	1.40
TOTAL	100.50	99.69	99.53	100.23	99.74	100.10	100.64	99.92
Nb	0	0	1	1	0	0	0	0
Zr	35	29	20	23	9	5	11	15
Y	4	4	6	6	3	4	4	3
Sr	192	15	80	18	17	9	18	16
Rb	400	394	512	271	341	255	252	342
Th	2	4	0	1	0	0	2	0
Pb	20	24	16	24	36	22	24	22
Zn	63	75	64	41	28	29	29	48
Cu	9	8	7	12	15	9	10	10
Ni	6	7	8	6	6	7	8	7
Cr	0	0	0	0	0	0	0	0
V	8	11	4	4	7	12	8	8
Ba	0	209	0	0	2	0	22	0
Hf	4	3	2	2	2	1	2	1
Ce	0	22	0	23	0	5	0	0
La	0	0	0	0	0	0	0	0

Sample	F4149G	F4150G	F525G	F411G	F439G	F450G	F4124G	F4126G
SiO2	73.00	74.43	74.70	75.02	74.41	72.80	73.59	76.06
TiO2	0.05	0.04	0.12	0.00	0.04	0.01	0.00	0.02
Al2O3	14.91	15.27	14.98	14.19	15.02	15.00	15.40	15.64
Fe2O3	0.49	0.18	0.00	0.03	0.00	0.02	0.39	0.25
FeO	0.10	0.40	0.96	0.60	0.57	0.30	0.45	0.30
MnO	0.00	0.00	0.01	0.01	0.00	0.00	0.02	0.00
MgO	0.08	0.29	0.27	0.17	0.14	0.81	0.00	0.29
CaO	0.26	0.18	0.44	0.13	0.29	0.31	0.31	0.52
Na2O	5.64	4.23	3.93	4.97	4.26	3.98	4.23	0.88
K2O	3.53	3.66	4.08	3.72	4.13	4.16	3.75	3.51
P2O5	0.37	0.30	0.37	0.41	0.35	0.61	0.44	0.40
Loss	1.40	0.80	0.40	1.60	1.40	1.80	1.40	2.80
TOTAL	99.87	99.82	100.34	100.90	100.66	99.85	100.09	100.71
Nb	0	0	5	5	0	2	8	3
Zr	18	17	52	10	15	15	11	24
Y	2	1	6	1	4	4	7	8
Sr	11	13	25	58	17	43	26	62
Rb	277	301	320	356	338	369	315	116
Th	0	0	8	0	0	0	0	1
Pb	25	24	0	19	25	12	3	28
Zn	50	46	203	13	49	35	25	16
Cu	8	9	14	13	5	9	9	14
Ni	7	7	17	6	5	5	6	4
Cr	0	0	0	0	0	0	0	0
V	11	14	2	6	5	0	113	17
Ba	3	0	112	0	1	0	514	93
Hf	3	3	4	2	3	2	6	2
Ce	0	0	16	0	6	0	41	3
La	0	0	6	0	0	0	13	0

Sample	F4128G	F4130G	F313G	F457G	F522G	F325S	F326S	F327S
SiO2	73.82	74.21	74.67	72.13	74.47	64.55	64.87	66.53
TiO2	0.00	0.01	0.06	0.10	0.03	0.97	0.98	0.88
Al2O3	15.23	15.15	16.00	15.67	15.28	19.08	18.32	17.51
Fe2O3	0.19	0.24	0.44	0.31	0.11	1.80	1.51	1.69
FeO	0.44	0.45	0.45	1.03	0.41	3.42	4.38	4.59
MnO	0.01	0.02	0.02	0.02	0.06	0.03	0.05	0.05
MgO	0.02	0.11	0.27	0.80	0.26	1.93	2.12	2.20
CaO	0.21	0.28	1.64	1.50	0.46	0.00	0.03	0.05
Na2O	5.62	4.52	5.80	6.24	4.95	0.18	0.46	0.27
K2O	3.59	3.93	1.04	1.14	2.72	3.62	3.30	2.68
P2O5	0.34	0.33	0.08	0.24	0.20	0.12	0.10	0.16
Loss	1.20	0.80	0.40	1.20	0.80	4.20	3.40	3.40
TOTAL	100.72	100.10	100.98	100.48	99.85	100.07	99.68	100.16
Nb	1	0	3	0	7	15	14	12
Zr	12	9	45	104	33	237	242	222
Y	3	2	7	9	7	25	30	28
Sr	16	11	497	418	97	57	48	39
Rb	319	345	19	49	168	111	126	116
Th	3	5	2	2	1	10	10	8
Pb	25	51	13	14	6	29	20	25
Zn	65	60	61	25	128	92	147	56
Cu	13	0	22	39	18	32	20	40
Ni	5	5	11	3	14	15	14	30
Cr	0	0	0	0	0	140	137	126
V	8	6	6	18	0	153	144	142
Ba	3	0	392	338	526	732	575	543
Hf	2	2	4	4	2	6	6	6
Ce	0	8	0	0	11	58	57	54
La	0	0	4	0	0	23	9	18

Sample	F328S	F329S	F330S	F331S	F335S	F337S	F339S	F340S
SiO2	56.34	65.85	59.89	62.35	73.58	61.49	73.90	62.42
TiO2	1.23	0.93	0.99	0.93	0.41	1.02	0.80	0.93
Al2O3	23.74	18.19	22.09	19.32	15.83	21.46	13.63	20.55
Fe2O3	2.75	3.19	3.64	3.13	0.04	2.84	1.26	3.11
FeO	4.17	2.54	3.10	3.25	1.62	4.05	3.12	2.82
MnO	0.05	0.03	0.04	0.05	0.02	0.06	0.05	0.04
MgO	2.12	1.98	1.59	1.99	0.86	2.18	1.58	1.91
CaO	0.00	0.12	0.00	0.12	0.60	0.15	0.20	0.03
Na2O	0.62	0.86	0.59	0.05	1.12	0.17	0.33	0.10
K2O	4.53	2.65	3.83	3.95	3.28	3.54	2.31	3.71
P2O5	0.16	0.16	0.22	0.13	0.50	0.16	0.15	0.31
Loss	4.40	3.20	4.40	4.40	2.00	3.00	2.40	4.20
TOTAL	100.32	99.86	100.57	99.84	99.94	100.30	99.86	100.29
Nb	15	13	14	12	6	14	10	11
Zr	337	258	212	230	154	224	274	204
Y	25	31	32	28	18	36	27	39
Sr	60	66	51	47	50	61	54	71
Rb	142	99	114	153	207	128	77	141
Th	11	8	9	12	14	5	6	8
Pb	24	18	24	19	19	19	12	15
Zn	119	117	193	139	89	91	54	90
Cu	59	34	33	5	0	62	21	58
Ni	14	19	17	44	10	26	17	11
Cr	196	136	156	137	0	149	101	150
V	183	144	168	149	25	166	103	132
Ba	835	602	789	675	147	690	436	566
Hf	7	5	5	6	5	4	7	5
Ce	38	43	55	57	47	73	54	51
La	7	21	22	16	11	28	21	22

Sample	F341S	F342S	F342AS	F343S	F344S	F350S	F352S	F355S
SiO2	62.87	67.24	59.49	60.81	80.81	56.06	67.72	79.71
TiO2	1.07	0.83	1.05	1.03	0.57	1.20	0.87	0.53
Al2O3	20.67	17.66	22.08	21.64	9.72	25.25	17.72	9.06
Fe2O3	0.71	3.30	2.05	3.12	0.49	3.08	2.09	1.70
FeO	3.33	1.75	5.00	4.06	2.70	3.80	3.41	2.55
MnO	0.03	0.02	0.07	0.04	0.03	0.04	0.05	0.03
MgO	1.74	1.49	2.60	2.06	1.16	1.97	1.62	1.48
CaO	0.07	0.00	0.05	0.10	0.09	0.00	0.00	0.16
Na2O	0.72	0.40	0.63	0.37	0.28	0.27	0.01	0.49
K2O	4.03	3.28	3.21	3.08	2.05	5.17	2.89	1.42
P2O5	0.13	0.04	0.19	0.20	0.07	0.08	0.07	0.27
Loss	3.80	3.80	3.00	3.40	1.80	3.20	3.00	2.60
TOTAL	99.36	99.97	99.58	100.07	99.88	100.38	99.60	100.09
Nb	13	13	14	15	9	18	12	7
Zr	334	183	208	227	211	242	221	223
Y	36	32	32	29	17	36	27	37
Sr	78	67	53	66	38	32	38	36
Rb	147	107	137	138	62	267	84	67
Th	9	4	12	6	8	10	9	5
Pb	24	23	15	21	9	360	29	16
Zn	81	68	100	92	75	100	121	80
Cu	14	63	21	20	16	47	28	7
Ni	13	15	16	16	11	17	27	25
Cr	162	136	152	155	67	175	124	72
V	168	148	158	165	83	204	137	90
Ba	743	625	528	569	446	954	577	202
Hf	7	5	5	4	5	5	5	5
Ce	77	59	84	84	46	86	61	44
La	11	17	24	23	6	15	19	13

Sample	F41S	F42S	F46S	F47S	F48S	F410S	F412S	F413S
SiO2	73.75	65.96	62.29	65.58	62.08	66.88	80.37	67.22
TiO2	0.78	0.90	1.03	1.04	1.01	0.92	0.47	0.89
Al2O3	14.92	20.30	20.69	20.84	21.29	17.21	8.09	17.61
Fe2O3	1.43	2.29	2.26	2.17	3.32	2.08	1.35	1.59
FeO	3.00	2.98	3.88	3.49	3.28	3.30	2.34	3.62
MnO	0.01	0.02	0.04	0.03	0.04	0.04	0.01	0.03
MgO	1.71	1.71	2.39	1.55	1.86	1.76	1.11	1.74
CaO	0.10	0.07	0.37	0.07	0.17	0.02	0.40	0.20
Na2O	0.02	0.26	0.71	0.11	0.72	0.35	0.36	0.60
K2O	1.59	2.19	3.21	2.03	3.31	3.95	1.69	2.62
P2O5	0.12	0.08	0.56	0.02	0.18	0.09	0.41	0.16
Loss	1.00	3.20	3.00	2.60	3.20	3.80	2.60	3.20
TOTAL	98.53	100.08	100.60	99.65	100.65	100.58	99.29	99.61
Nb	6	8	10	11	9	11	2	8
Zr	217	230	306	242	234	277	167	244
Y	29	31	39	32	29	30	34	28
Sr	11	23	53	23	55	51	24	41
Rb	82	102	133	102	114	116	61	134
Th	9	12	7	9	12	8	5	8
Pb	7	9	21	12	26	23	13	11
Zn	45	55	84	70	281	121	34	65
Cu	14	20	20	32	22	20	10	56
Ni	14	13	11	12	19	19	11	17
Cr	109	127	141	131	133	99	48	113
V	106	124	160	138	169	155	77	136
Ba	225	305	595	294	733	798	325	369
Hf	6	7	7	6	5	7	5	7
Ce	80	89	77	65	72	52	69	84
La	16	23	29	34	32	20	17	13

Sample	F419S	F420S	F421S	F423S	F424S	F425S	F426S	F427S
SiO2	67.39	69.30	59.38	85.74	73.64	61.63	61.09	59.04
TiO2	0.92	0.82	1.09	0.39	0.69	0.98	1.05	1.01
Al2O3	17.03	15.09	22.54	7.32	12.55	20.33	21.30	21.12
Fe2O3	2.42	3.57	3.42	1.32	1.69	2.25	1.94	1.83
FeO	3.20	2.30	3.28	1.36	3.50	4.48	3.74	4.97
MnO	0.03	0.03	0.04	0.00	0.06	0.04	0.04	0.05
MgO	1.60	1.07	1.90	0.73	1.06	2.32	1.95	2.54
CaO	0.13	0.00	0.09	0.07	0.44	0.31	0.08	0.03
Na2O	0.60	0.39	0.55	0.17	1.37	0.81	0.93	0.51
K2O	3.49	2.48	4.07	1.10	2.24	3.21	4.22	3.86
P2O5	0.08	0.04	0.09	0.06	0.25	0.35	0.05	0.28
Loss	3.00	4.80	4.00	2.00	2.60	3.00	3.80	4.60
TOTAL	100.06	100.02	100.64	100.33	100.21	99.87	100.36	100.02
Nb	9	7	9	2	7	10	9	10
Zr	245	238	233	133	243	231	238	236
Y	27	24	39	20	35	44	36	35
Sr	48	33	61	18	64	56	60	43
Rb	114	80	130	39	93	132	146	180
Th	7	7	11	3	4	9	8	12
Pb	18	17	25	14	14	18	14	21
Zn	80	57	137	54	93	86	119	109
Cu	20	36	36	23	23	51	38	64
Ni	23	14	21	13	19	16	13	19
Cr	118	108	138	46	87	109	122	126
V	152	133	177	70	108	164	168	180
Ba	767	525	762	229	345	539	693	645
Hf	7	6	2	4	6	6	6	5
Ce	70	34	57	51	50	69	56	75
La	21	22	24	11	19	24	14	26

Sample	F428S	F429S	F430S	F431S	F432S	F433S	F434S	F455S
SiO2	63.59	62.63	64.61	56.42	81.80	72.05	77.36	70.82
TiO2	1.02	0.91	0.93	0.98	0.54	0.79	0.74	0.88
Al2O3	20.59	18.77	18.50	22.46	8.64	13.91	11.74	15.20
Fe2O3	2.08	2.36	3.13	3.01	1.11	2.04	0.76	1.60
FeO	3.69	3.46	2.25	4.30	2.45	2.56	3.15	3.61
MnO	0.04	0.05	0.04	0.05	0.00	0.00	0.02	0.05
MgO	1.84	2.16	1.53	2.59	1.30	1.46	1.26	1.73
CaO	0.21	0.10	0.06	0.00	0.10	0.17	0.31	0.05
Na2O	0.84	0.78	0.60	1.04	0.58	0.95	0.81	0.26
K2O	3.11	3.64	3.60	4.04	1.59	2.73	2.24	2.43
P2O5	0.10	0.16	0.08	0.12	0.10	0.20	0.06	0.04
Loss	2.80	4.60	4.60	5.40	1.80	3.00	1.40	1.40
TOTAL	100.09	99.79	100.10	100.61	100.11	100.01	99.99	98.20
Nb	10	9	9	9	6	7	5	8
Zr	247	251	237	216	233	264	251	252
Y	36	33	33	31	22	25	24	28
Sr	72	68	47	55	32	67	67	38
Rb	111	131	109	121	79	96	74	141
Th	8	10	11	13	7	8	10	11
Pb	19	21	17	19	14	18	19	9
Zn	116	66	63	120	57	47	61	97
Cu	36	27	31	16	23	19	19	23
Ni	18	12	7	12	5	7	23	10
Cr	125	119	127	172	62	97	82	106
V	171	151	166	220	80	129	113	143
Ba	691	695	825	927	311	632	574	425
Hf	7	6	6	5	8	7	6	7
Ce	81	56	40	56	54	80	58	42
La	24	17	18	13	6	9	6	5

Sample	F459S	F460S	F461S	F462S	F463S	F464S	F465S	F466S
SiO2	54.58	55.02	85.99	58.45	59.46	58.63	60.13	68.37
TiO2	1.26	1.10	0.33	1.12	1.12	1.11	0.85	0.76
Al2O3	24.26	24.44	4.81	22.57	22.11	22.61	20.03	16.22
Fe2O3	2.83	1.93	1.10	3.57	3.21	4.19	1.81	1.46
FeO	2.11	2.25	2.38	1.96	1.79	1.65	5.10	3.43
MnO	0.02	0.03	0.03	0.01	0.01	0.03	0.04	0.01
MgO	2.21	1.93	1.07	1.77	1.33	1.44	2.61	2.16
CaO	0.85	0.11	0.00	0.01	0.01	0.00	0.08	0.03
Na2O	0.05	1.22	0.00	0.47	0.45	0.79	1.26	0.56
K2O	5.01	5.47	0.38	4.66	5.18	4.97	3.45	3.01
P2O5	1.04	0.30	0.06	0.03	0.04	0.06	0.23	0.22
Loss	5.40	4.20	2.40	5.80	5.20	4.80	4.60	3.80
TOTAL	99.87	98.23	98.61	100.63	100.12	100.50	100.36	100.17
Nb	9	4	5	1	10	4	7	5
Zr	281	239	180	235	236	238	204	180
Y	75	32	14	48	32	37	31	21
Sr	87	91	26	73	62	95	56	57
Rb	184	198	14	176	187	182	113	105
Th	18	13	6	13	13	13	8	7
Pb	24	31	6	21	21	15	8	8
Zn	58	58	79	67	74	58	104	105
Cu	9	15	21	36	16	13	19	10
Ni	5	6	7	2	6	9	15	4
Cr	172	115	37	157	154	188	145	104
V	223	186	54	211	202	225	181	152
Ba	1201	1173	85	1009	1003	999	716	604
Hf	7	10	5	7	7	6	6	5
Ce	115	124	33	54	58	56	82	27
La	55	43	10	7	33	18	25	2

Sample	F467S	F468S	F469S	F470AS	F470BS	F471S	F472S	F473S
SiO2	68.85	57.56	88.46	62.72	62.85	53.89	64.87	57.57
TiO2	0.82	1.05	0.30	0.95	0.84	1.17	0.99	1.03
Al2O3	15.62	22.24	3.95	18.88	19.30	24.91	19.45	21.22
Fe2O3	0.93	5.65	0.60	2.64	1.90	3.19	2.95	4.53
FeO	3.87	1.33	2.43	3.07	3.45	2.52	1.55	2.95
MnO	0.02	0.04	0.03	0.01	0.01	0.05	0.03	0.05
MgO	1.88	2.50	1.27	2.36	2.15	1.58	1.41	1.66
CaO	0.06	0.00	0.19	0.03	0.05	0.00	0.00	0.02
Na2O	0.52	0.39	0.36	0.69	0.96	0.83	0.60	1.01
K2O	3.05	4.91	0.08	3.85	3.72	5.72	4.01	4.15
P2O5	0.09	0.22	0.09	0.25	0.01	0.05	0.04	0.16
Loss	3.20	4.80	0.80	4.20	4.20	5.60	4.40	5.60
TOTAL	99.06	100.89	98.62	99.83	99.61	99.74	100.48	100.15
Nb	5	8	0	7	6	8	7	10
Zr	190	231	254	237	183	247	206	261
Y	28	37	20	55	30	34	30	33
Sr	38	66	42	65	71	88	59	77
Rb	101	160	9	131	128	196	138	147
Th	14	10	8	11	7	17	10	6
Pb	17	18	15	18	17	19	16	23
Zn	92	95	68	97	98	77	66	81
Cu	20	14	37	16	27	48	28	22
Ni	12	6	4	7	7	6	4	13
Cr	105	163	48	129	145	176	128	154
V	135	190	40	180	172	223	183	181
Ba	662	940	0	722	718	1051	856	932
Hf	7	6	8	5	5	6	7	7
Ce	68	44	50	70	55	68	70	49
La	19	8	9	24	13	16	25	7

Sample	F475S	F476AS	F476BS	F477AS	F477BS	F478S	F479S	F481S
SiO2	73.61	78.06	81.43	76.42	57.63	66.05	60.38	60.33
TiO2	0.80	0.61	0.42	0.65	1.09	0.91	0.95	1.15
Al2O3	13.44	11.10	8.15	11.10	23.07	17.60	20.33	21.88
Fe2O3	0.87	0.83	1.31	1.00	1.67	2.12	2.21	3.50
FeO	3.60	2.95	2.27	3.52	4.45	3.44	4.42	2.38
MnO	0.02	0.02	0.04	0.05	0.06	0.03	0.06	0.05
MgO	1.66	1.06	1.37	1.05	1.93	1.78	1.92	1.23
CaO	0.12	0.11	0.13	0.15	0.19	0.23	0.36	0.03
Na2O	0.30	0.23	0.77	0.93	1.08	0.62	0.39	0.39
K2O	2.58	3.13	1.43	2.02	4.49	3.18	4.40	4.11
P2O5	0.09	0.07	0.08	0.06	0.17	0.07	0.40	0.08
Loss	2.80	2.40	2.60	2.60	2.60	3.80	3.60	4.40
TOTAL	100.22	100.69	100.09	99.66	98.61	99.99	99.57	99.69
Nb	4	0	1	3	7	5	6	8
Zr	217	176	167	200	278	251	247	249
Y	30	20	19	21	42	29	44	40
Sr	56	49	45	64	87	75	43	64
Rb	96	80	54	75	131	106	205	179
Th	6	5	10	8	13	10	10	12
Pb	14	10	10	12	24	16	14	25
Zn	72	58	48	63	102	94	81	96
Cu	6	11	10	11	21	28	23	22
Ni	26	7	9	18	23	15	14	8
Cr	97	79	54	82	149	121	120	146
V	124	106	86	102	176	147	121	159
Ba	516	496	305	413	666	605	506	518
Hf	7	6	5	6	8	8	7	6
Ce	53	74	24	21	80	52	56	65
La	13	15	4	4	24	10	17	19

Sample	F491S	F493S	F4108S	F4111S	F4112S	F4113S	F4114S	F4121S
SiO2	77.52	68.44	60.01	57.26	54.78	61.41	67.24	77.07
TiO2	0.66	0.90	1.15	0.99	1.09	1.01	0.92	0.64
Al2O3	10.81	16.75	21.08	21.57	24.73	20.15	19.31	10.36
Fe2O3	3.13	2.51	1.96	3.58	2.98	1.99	2.20	3.20
FeO	0.94	2.55	2.69	4.25	4.03	3.65	3.32	1.44
MnO	0.01	0.01	0.02	0.05	0.04	0.03	0.03	0.03
MgO	1.74	1.39	1.44	2.46	2.53	2.13	1.91	1.15
CaO	0.01	0.01	0.05	0.15	0.39	0.35	0.06	0.10
Na2O	0.20	0.39	0.15	0.65	1.33	0.61	0.16	0.19
K2O	1.74	2.80	4.89	3.73	3.79	3.82	2.03	2.03
P2O5	0.13	0.03	0.07	0.25	0.34	0.36	0.14	0.26
Loss	3.20	4.60	4.60	3.80	3.80	4.40	3.20	3.20
TOTAL	100.21	100.52	98.31	98.93	100.04	100.09	100.62	99.80
Nb	0	4	11	9	11	11	8	5
Zr	220	266	286	212	225	243	236	242
Y	20	17	34	41	33	35	26	37
Sr	11	21	25	52	94	61	16	28
Rb	104	95	294	131	140	147	95	71
Th	7	10	10	6	13	9	7	8
Pb	13	14	113	20	27	22	9	15
Zn	220	66	150	115	203	77	54	54
Cu	17	30	14	26	40	21	31	25
Ni	24	26	18	23	35	12	9	17
Cr	74	106	152	144	159	137	125	74
V	109	141	186	192	217	170	121	108
Ba	317	517	587	823	785	788	170	493
Hf	6	8	8	4	6	6	8	7
Ce	46	60	76	68	71	50	67	59
La	6	0	17	13	21	12	11	13

Sample	F4125S	F4129S	F4132S	F4135S	F4137S	F4145S	F4153S	F4154S
SiO2	60.63	68.12	59.32	75.13	65.03	74.83	72.87	61.96
TiO2	0.95	0.87	1.09	0.83	1.00	0.77	0.76	1.07
Al2O3	20.28	15.87	20.29	12.60	18.34	13.23	14.02	21.38
Fe2O3	2.17	2.78	2.41	1.29	2.35	0.86	1.80	1.62
FeO	4.12	3.42	4.73	3.65	2.72	3.15	3.25	3.74
MnO	0.04	0.05	0.04	0.04	0.01	0.02	0.04	0.03
MgO	1.92	2.03	2.18	1.53	0.67	1.54	1.83	1.61
CaO	0.13	0.01	0.08	0.03	0.01	0.25	0.22	0.04
Na2O	0.63	0.41	0.63	0.20	0.16	0.96	0.87	0.62
K2O	4.64	3.28	3.40	2.05	3.76	2.37	2.47	3.56
P2O5	0.29	0.15	0.05	0.09	0.01	0.08	0.11	0.09
Loss	4.20	3.20	4.80	2.80	5.80	2.80	1.60	4.20
TOTAL	100.15	100.37	99.21	100.38	100.03	101.00	99.97	100.07
Nb	13	9	11	2	1	0	0	0
Zr	222	566	259	261	244	228	211	261
Y	33	25	27	24	29	26	25	28
Sr	31	35	45	22	22	69	55	47
Rb	244	150	107	120	192	78	85	148
Th	9	7	11	9	10	8	11	10
Pb	19	13	27	17	64	12	12	18
Zn	74	72	152	143	79	64	67	121
Cu	13	12	24	12	20	23	55	22
Ni	26	17	28	29	15	18	21	10
Cr	130	115	132	99	123	86	85	135
V	171	144	171	118	156	116	116	165
Ba	454	564	781	457	629	572	538	488
Hf	5	6	7	6	7	6	4	7
Ce	70	51	74	31	69	36	42	58
La	15	4	15	16	15	9	7	20

Sample	F4155S	SaDaMo	F521AS	F528S	F530S
SiO2	71.20	59.30	78.74	60.37	62.47
TiO2	0.74	1.07	0.59	0.99	0.94
Al2O3	13.68	21.53	9.77	19.59	20.48
Fe2O3	0.92	2.25	0.37	2.85	1.27
FeO	3.91	4.15	3.55	4.53	4.88
MnO	0.04	0.06	0.02	0.06	0.06
MgO	1.84	2.06	1.48	2.90	2.13
CaO	0.09	0.03	0.12	0.19	0.29
Na2O	2.13	0.47	0.28	0.92	0.47
K2O	2.42	4.12	2.78	3.87	3.05
P2O5	0.04	0.03	0.08	0.11	0.34
Loss	1.80	5.20	1.40	3.00	3.20
TOTAL	98.95	100.50	99.29	99.54	99.71
Nb	0	17	10	17	14
Zr	221	259	203	212	227
Y	23	39	23	25	42
Sr	38	73	36	79	41
Rb	94	153	205	117	128
Th	6	14	12	11	11
Pb	22	0	0	0	0
Zn	68	120	97	119	102
Cu	17	33	31	37	20
Ni	14	8	32	37	13
Cr	78	139	38	117	101
V	113	185	66	145	126
Ba	628	1087	316	527	320
Hf	7	5	3	24	12
Ce	20	83	48	106	110
La	17	42	0	0	20

APPENDIX IV -- ISOTOPIC ANALYSIS

Isotopic analyses were carried out at the Scottish Universities Research and Reactor Centre (SURRC), East Kilbride under the supervision of A.N. Halliday (Rb-Sr) and A.E.Fallick (O2). The help of J.Hutchinson and F.McLaren was invaluable.

4.1 - Rb-Sr Determination

4.1.1 - Sample Selection

Whole rock powders prepared for XRF analysis (Appendix II) were used in all isotopic work. The samples selected were checked petrographically for any evidence of alteration, in particular chloritized biotite. Rb and Sr abundances determined by XRF were used to give smaples with as wide a range of Rb/Sr as possible and to ensure accurate spiking.

4.1.2 - Sample Preparation

Chemical extraction of Rb and Sr closely followed methods described by Blaxland et al. (1978) and Halliday et al. (1979). Approximately 0.1 g of powder was precisely weighed into teflon beakers and spiked with 87Rb and 84Sr enriched solutions respectively. Digestion and homogenization were achieved with the addition of "Merck Suprapur" HF; further preparation proceeded in the presence of HNO3 and HCl. The dissolved samples were eluted through Bio-Rod AG 50W-X8 200-400 mesh resin in ion exchange columns, and Rb and Sr "fractions" were collected separately at appropriate volumes of drained liquid. These Rb and Sr concentrates were

dried to a solid residue prior to loading onto Ta filaments. Sr was loaded as a phosphate onto single filament beads and Rb was loaded as a chloride onto the side filament of triple filament beads.

4.1.3 - Instrumentation and Data Processing

Isotope ratios were measured on a VG Micromass 30B mass spectrometer linked to a Data General Nova minicomputer for on-line data processing. All regression analyses were based on the method of York (1969). The decay constant used for 87Rb is 1.42×10^{-11} (Steiger & Jager, 1977).

4.2 - Oxygen Isotopic Analysis

The techniques employed were those of Clayton & Mayeda (1963) as modified by Borthwick & Harmon (1982) and Fallick (pers.comm.).

4.2.1 - Equipment

The system was in two major parts.

(i) The glass high-vacuum line comprised a mercury 3-stage diffusion pump filled with a liquid nitrogen Dewar-type cold trap and connected to a rotary vacuum pump filled with regular pump oil. The remainder of the glass line was a system of interconnected traps separated by grease-sealed high vacuum taps and connected to the main vacuum pumps by a glass manifold.

(ii) The metal system was constructed of "MONEL" and stainless steel, and consists of five interconnected sub-systems. These were (i) the ClF3 bulk cylinder, (ii) Kel-F storage tubes, (iii) an interconnection system, (iv) a waste removal system and (v) a reaction manifold. This manifold

comprised six valve, flange and nickel tube sets.

4.2.2 - Procedure

Before loading of samples could take place the entire system was evacuated to 10^{-5} - 10^{-6} mbar and excess reagent was frozen down and isolated. The nickel tubes were removed individually and loaded with 15-25 mg of sample. After evacuation and degassing, the nickel tubes were cooled to -196°C and charged with ClF3 by freezing reagent into each vessel in turn. The vessels were allowed to return to ambient temperature, and electrical resistance furnaces were put on to raise the vessels to 650°C for 14 hours (overnight). Next morning the furnaces were removed and liquid nitrogen baths used to cool the tubes to -196°C. The oxygen gas was passed through two more traps at -196° C and converted to CO2 using a heated graphite rod. The yield was measured and the gas transferred to a sample tube and removed from the line. After extraction of all six vessels, the metal line was isolated from the glass system and the vessels allowed to return to ambient temperature. The gaseous wastes were passed through the Kbar vessel to convert the fluorine compounds to KF and bromine compounds, the bromine compounds being frozen at -196°C in the second vessel. After evacuation of the system, the next set of samples were loaded.

4.2.3 - Instrumentation

180/160 ratios were measured in the CO2 gas using an AWRE Aldermaston McKinney-Nier type mass spectrometer. 180/160 ratios are reported in the familiar "δ" notation relative to standard mean ocean water (SMOW) as

defined from the Snowbird Quartz (+16.20‰) and African Glass Sand (+9.60‰) standards.

REFERENCES

Assunção, C.T. & Teixeira, C., 1954, Un remarkable phénomène de granitisation: la roche granitique a nodules biotiques de la Serra da Freita, Arouca (Portugal). Bol. Mus. Lab. Min. Geol. Fac. Cienc. Univ. Lisboa, 22.

Albuquerque, C.R., 1971, Petrochemistry of a series of Granitic Rocks from Northern Portugal. Bull. Geol. Soc. America, 82, 2783-2798.

Albuquerque, C.R., 1978, Rare earth elements in "Younger" Granites, Northern Portugal. Lithos, 11, 219-229.

Atherton, M.P., Atkin, B.P., Naggar, M.H., 1974, Kyanite in the Hercynian metamorphic rocks of the Oporto-Viseu belt, north Portugal. Geol. Mijnb., 53, 189-192.

Atherton, M.P, McCourt, W.J., Sanderson, L.M. and Taylor, W.P., 1979, The geochemical character of the segmented Peruvian Coastal Batholith and associated volcanics. In Atherton, M.P. & Tarney, J., (eds), "Origin of granite batholiths: Geochemical Evidence", 45-64, Shiva.

Barker, F.,1981, Introduction to special issue on granites and rhyolites: A commentary for the nonspecialist. J. Geophysical Research, 86, 10131-10135.

Barr, S.M. & Areias, L, 1980, Petrology and geochemistry of granitic intrusions in the Viana do Castelo area, northern Portugal. Geol. Mijnb, 59, 273-281.

Bernard-Griffiths, J., Peucat, J.J., Sheppard, S. and Vidal, P., 1985, Petrogenesis of Hercynian leucogranites from the Southern Armorican massif: contribution of REE and isotopic (Sr, Nd, Pb and O) geochemical data to the study of source rock characteristics and ages. Earth Plan. Sci. Lett.,74, 2/3, 235-250.

Berthe, D., Chroukroune, P. and Jegouzo, P., 1979, Orthogneiss, mylonite and non-coaxial deformation of granites: the example of the South Armorican Shear Zone. J. Struct. Geol., 1, 31-42.

Blaxland, A.B., van Breemen, O., Emeleus, C.H. and Anderson, J.G., 1978, age and origin of the major syenite centres in the Gardar Province of south Greenland. Bull. Geol. Soc. Am., 89, 231-244.

Boorder, N. de., 1965, Petrological investigations in the Aguiar da Beira Granite Area, Northern Portugal. Unpubl. Ph.D. Thesis, University of Amsterdam.

Borthwick, J. & Harmon, R.S., 1982, A note regarding ClF3 as an alternative to BrF5 for oxygen isotope analysis. Geochim. Cc mochim. Acta, 46, 1665-1668.

Brun, J.P. & Cobbold, P.R., 1980, Strain heating and thermal softening in continental shear zones: a review. J. Struct. Geol., 2, 149-158.

Burg, J.P., Iglesias, M., Laurent, P., Matte, P. and Ribeiro, A., 1981, Variscan Intracontinental Deformation: The Coimbra-Cordoba Shear Zone (SW Iberian Peninsula). Tectonophysics, 78, 161-177.

Castro, A., 1985, The Central Extremadura Batholith: Geotectonic Implications (European Hercynian Belt)- An Outline. Tectonophysics, 120, 57-68.

Castro, A., 1986, Structural pattern and ascent model in the Central Extremadura Batholith, Hercynian belt, Spain. J. Struct. Geol., 8, 633-645.

Cawthorne, R.G., Strong, D.F. and Brown, P.G., 1976, Origin of corundum-normative intrusive and extrusive magmas. Nature, 259, 102-104.

Chappell, B.W. & White, A.J.R., 1974, Two Contrasting Granite Types. Pacific Geology, 8, 173-174.

Clarke, D.B., 1981, The Mineralogy of Peraluminous Granites: A Review. Can. Mineral., 19, 3-17.

Clayton, R.N. & Mayeda, T.K., 1963, The use of bromine pentafluoride in the extraction of oxygen from oxides and silicates for isotopic analysis. Geochim. Cosmochim. Acta, 27, 43-52.

Cole, D.R. & Ohmoto, H., 1976, Effect of NaCl on the rate of O isotopic exchange reactions between rocks and water. Geol. Soc. Am. Abstr. Progms., 8, 817.

Conde, L.N., 1971, Existencia em Portugal de Uma Serie Superior a Formacao Xistosa Da Beira e Inferior ao Ordovicico. Studia Geol., 2, 25-26.

Costa, C.V., Pereira, L.G. and Ferreira, M.P., 1971, Distribuicao de Oligoelementos Nas Roches e Solas do Fundao. Mem. Noticias, 71, 1-35.

Didier, J., Duthou, J.L. and Lameyre, J., 1982, Mantle and crustal granites: genetic classification of orogenic granites and the nature of their enclaves. Jour. Volcanol. Geoth. Res., 14, 125-132.

England, P.C. & Thompson, A., 1986, Some thermal and tectonic models for crustal melting in continental collision zones. In Coward, M.P. & Ries, A.C., (eds), "Collision Tectonics", Geol. Soc. Spec. Publ., 19, 83-94.

Fernandes, A., 1970, Contribuicao Para o Estudo da regiao dos Granitos Radioactivos de S. Pedro do Sul. Publ. Junta En. Nuclear.

Ferreira, M.P., 1972, Rochas Metamorficas. Coimbra.

Fleitout, L. & Froidevaux, C., 1980, Thermal and mechanical evolution of shear zones. J. Struct. Geol, 2, 159-164.

Fleury, E., 1922, Plissements Les Hercyniens au Portugal. (Ridéments Caledoniques et Dislocations Atlantiques). Com. Serv. Geol. Portugal, 13, 65-83.

Flood, R.H. & Shaw, S.E., 1975, A cordierite-bearing granite suite from the New England Batholith, N.S.W., Australia. Contrib. Mineral. Petrol., 52, 157-164.

Flood, R.H. & Shaw, S.E., 1977, Two S-type granite suites with low initial 87Sr/86Sr ratios from the New England Batholith, Australia. Contrib. Mineral. Petrol., 61, 163-173.

Fourcade, S. & Allegre, C.J., 1981, Trace element behaviour in granite genesis: a case study - the calc-alkaline plutonic association from the Quernigut complex (Pyrenees, France). Contrib. Mineral. Petrol., 76, 177-195.

Gil Ibarguchi, J.I. & Martinez, F.J., 1982, Petrology of Garnet - Cordierite - Sillimanite Gneisses from the El Tormes Thermal Dome, Iberian Hercynian Foldbelt (W Spain). Contrib. Mineral. Petrol., 80, 14-24.

Godhino, M.M., 1974, Sobre o Plutonometamorfismo da Regiao de Guardao (Caramulo, Portugal). Mem. Noticias, 78, 37-77.

Godhino, M.M. & Silva, F.G., 1974, Litio em Granitoides da regiao de Guardao (Caramulo - Portugal). Mem. Noticias, 78, 79-104.

Goncalves, L., 1974, Geologie und Petrologie des Gebietes von Oliveira de Azemeis und Albergaria-A Velha (Portugal). Unpubl. Ph.D. Thesis, Free University of Berlin.

Green, T.H., 1976, Experimental generation of cordierite- or garnet-bearing granitic liquids from a pelitic composition. Geology, 4, 85-88.

Green, T.H., 1977, Garnet in silicic liquids and its possible use as a P-T indicator. Contrib. Mineral. Petrol., 65, 59-67.

Halliday, A.N., Aftalion, M., van Breemen, O. and Jocelyn, J., 1979, Petrogenetic significance of Rb-Sr and U-Pb isotope systems in the c.400 Ma old British granitoids and their hosts. In Harris, A.L., Holland, C.H. and Leake, B.E., (eds), "The Caledonides of the British Isles - reviewed", Geol. Soc. Spec. Publ., 8, 653-661.

Harland, W.B., Cox, A.V., LLewellyn, P.G., Pickton, C.A.G., Smith, A.G. and Walters, R., 1982, A geological time scale, 131 pp. Cambridge University Press, Cambridge.

Harris, N.B.W., Pearce, J.A. and Tindle, A.G. 1986, Geochemical characteristics of collision zone magmatism. In Coward, M.P. & Ries, A.C., (eds), "Collision Tectonics", Geol. Soc. Spec. Publ., 19, 67-81.

Harvey, P.K., Taylor, D.M., Hendry, R.D. and Bancroft, F., 1973, An accurate fusion method for the analysis of rocks and chemically related materials by X-ray fluorescencs spectrometry. X-ray Spectrometry, 2, 33-44.

Hutton, D.H.W., 1982, A tectonic model for the emplacement of the Main Donegal Granite. J. Geol. Soc. Lond., 139, 615-633.

Iglesias, M. & Choukroune, P., 1980, Shear Zones in the Iberian Arc. J. Struct. Geol., 2, 63-68.

Julivert, M., Fontbote, J.M., Ribeiro, A. and Conde, L.E., 1972, Mapa tectonico de la Peninsula Iberica y Baleares, escala 1:1000000. Inst. Geol. Min de Espanha (memoria explicativa): 1-13.

Julivert, M., Fontbote, J.M., Ribeiro, A. and Conde, L.E., 1974, Mapa tectonico de la Peninsula Iberica y Baleares, escala 1:1000000. Inst. Geol. Min. Espana, Madrid.

Julivert, M., Martinez, F.J. and Ribeiro, A., 1980, The Iberian segment of the European Hercynian foldbelt. In Cogne, J., (coordinator), "Geology of Europe from Pre-Cambrian to the post-Hercynian sedimentary basins", Fr. Bur. Rech. Geol. Minieres. Mem., 108, 132-158.

Leake, B.E., Hendry, G.L., Kemp, A., Plant, A.G., Harry, P.K., Wilson, J.R., Coats, J.S., Ancott, J.W. and Howarth, R.J., 1970, The chemical analysis of rock powders by automatic X-ray fluorescence. Chem. Geol., 5, 7-86.

Lee, D.E., Kistler, R.W., Friedman, I. and Van Loenan, R.E., 1981, The two-mica granites of northeastern Nevada. J. Geophysical Research, 86, 10607-10616.

Lehmann, B., 1987, Tin granites, geochemical heritage, magmatic differentiation. Geol. Runds., 76/1, 177-185.

Lister, G.S. & Snoke, A.W., 1984, S-C Mylonites. J. Struct. Geol., 6, 617-638.

Manning, D.A.C. & Pichavant, M., 1983, The role of fluorine and boron in the generation of granitic melts. In Atherton, M.P. & Gribble, C.D., (eds), "Migmatites, melting and metamorphism", 94-109, Shiva.

Martinez-Catalan, J.R. & Diez-Balda, M.A., 1987, Structural pattern and ascent model in the Central Extremadura Batholith, Hercynian Belt, Spain: Discussion. J. Struct. Geol., 9, 381-382.

Matte, P. & Ribeiro, A., 1975, Forme et orientation de l'ellipsoide de deformation dans le virgation hercynienne de Galice, relations avec le plissement et hypotheses sur la génese de l'arc Ibero-Armoricain. C.R. Acad. Sci. Paris, 280 D: 2825-2828.

Mendes, F., 1967, Contribution à l'Etude Géochronologique par la methode du Stontium des Formations Cristallines du Portugal. Bol. Mus. Lab. Min. Geol. Fac. Cienc. Un. Lisboa, 11, 3-157.

Moorhouse, V.E. & Moorhouse, S.J., 1983, The geology and geochemistry of the Strathy complex of north-east Sutherland, Scotland. Min. Mag., 47, 123-137.

Miller, C.F., 1985, Are strongly peraluminous magmas derived from pelitic sedimentary sources? J. Geol, 93, 673-689.

Miller, C.F. & Bradfish, L.J., 1980, An inner Cordilleran belt of muscovite-bearing plutons. Geology, 8, 412-416.

Miller, C.F., Stodard, E.F., Bradfish, L.J. and Dollase, W.A., 1981, Composition of Plutonic Muscovite: Genetic Implications. Can. Mineral., 19, 25-34.

Nash, W.P. & Creecraft, H.R., 1985, Partition coefficients for trace elements in silicic magmas. Geochim. Cosmochim. Acta, 49 (11), 2307-2322.

Neiva, A.M.R., 1973, Geochemistry of the Granites and their Minerals from the Central Area of Northern Portugal. Mem. Noticias, 76, 1-43.

Neiva, J.C., 1943, Contribuicao Para o estudo dos Granitos Portugueses. Com. Serv. Geol. Portugal, 24, 29-42.

Neiva, J.C., 1953, Granitos da Urgeirica. Mem. Noticias, 34, 47-53.

Neiva, J.C., 1955, Contribuicao Para o Estudo dos Granitos das Beiras e do Sul do Douro Litoral. Com. Serv. Geol. Portugal, 36, 69-82.

Neiva, J.C. & Faria, F., 1952, Rochas eruptivas de entre Murca e Freixo de numao e a ocurrencia de minerais das terras raras.

Nicholas, A., Bouchez, J.L., Blaise, J. and Poirier, J.P., 1977, Geological aspects of deformation in continental shear zones. Tectonophysics, 42, 55-73.

Norrish, K. & Chappell, B.W., 1977, X-ray fluorescence spectrography. In Zussman, J., (ed), "Physical Methods of Determinative Mineralogy", 201-272, Academic Press, London.

Oen, I.S., 1958, The geology, petrology and ore deposits of the Viseu region, northern Portugal. Com. Serv. Geol. Portugal, 41.

Oen, I.S., 1970, Granite intrusion, folding and metamorphism in central northern Portugal. Bol. Geol. Minero., 81, 2/3, 157-184.

Oliviera, J.S., 1970, Geoquimica de alguns Granitos do Norte de Portugal e Suas Relacoes com Mineralizacoes estanifiras. Est. Notas. Trabalhos, 19, 3-4, 227-231.

O'Neil, J.R. & Chappell, B.W., 1977, Oxygen and hydrogen isotope relations in the Berridale batholith. J. Geol. Soc. Lond., 133, 559-571.

O'Neil, J.R., Shaw, S.E. and Flood, R.H., 1977, Oxygen and hydrogen isotope compositions as indicators of granite genesis in the New England batholith. Contrib. Mineral. Petrol., 62, 313-328.

O'Neil, J.R. & Taylor, H.P., 1967, The oxygen isotope and cation exchange chemistry of feldspars. Am. Mineral., 52, 1414-1437.

Page, R.W. & Bell, T.H., 1986, Isotopic and structural responses of granite to successive deformation and metamorphism. J. Geol., 94, 365-397.

Pearce, J.A., Harris, N.B.W. and Tindle, A.G., 1984, Trace element diagrams for the tectonic interpretations of granitic rocks. J. Petrol., 25, 956-983.

Pereira, J.S., 1959, Algumas rochas eruptivas portuguesas. Fenomenos de hidrotermalizacao manifestados em varias rochas sieniticas, colhidas em Aregos (Viseu). Publ. Mus. Lab. Minero. Geol. Faculdade Ciencias Porto, 4, 77.

Pereira, E.L., Goncalves, S.M. and Moreira, A., 1980, Carta Geologica de Portugal, 1:50000, Folha 13-D, Noticia Explicativa. Serv. Geol. Portugal, Lisboa.

Perfit, M.R., Bruekner, H., Lawrence, J.R. and Kay, R.W., 1980, Trace element and isotopic variations in a zoned pluton and associated volcanic rocks, Unalaska Island, Alaska: A model for fractionation in the Aleution calcalkaline suite. Contrib. Mineral. Petrol., 73, 69-87.

Pichavant, M. & Stussi, J.M., 1986, Leucogranites à deux micas et granites "S"- deux types de magmatisme crustal. Réunion des Sciènces de la Terre, Clermont-Ferrand, 147.

Pinto, M.S., 1979, Geochemistry and Geochronology of granitic rocks from the Aveiro and Viseu district (Northern Portugal). Unpubl. Ph.D Thesis, University of Leeds.

Pinto, M.S., 1983, Geochronology of Portuguese Granitoids: a contribution. Stvd. Geol. Salamanticensia, 18: 277-306. (VIII Reun. Geol. Oeste Penins., Salamanca, Coimbra).

Pinto, M.S., 1985, Carboniferous Granitoids of Portugal: Some Geochemical and Geochronological Aspects. An. Fac. Cienc., Porto, 64, 15-33.

Pitcher, W.S., 1979, The nature, ascent and emplacement of granitic magmas. J. Geol. Soc. Lond., 136, 627-622.

Pitcher, W.S., 1982, Granite type and tectonic environment. In Hsu, K.J., (ed), "Mountain Building Processes", 19-40, Academic Press.

Poirier, J.P., Bouchez, J.L. and Jonas, J.J., 1979, A dynamic model for aseismic ductile shear zones. Earth. Plan. Sci. Lett., 45, 441-453.

Priem, H.A., Boelrijk, N.M., Vershure, R., Hebeda, E. and Verdumen, E.T., 1970, Dating events of acid plutonism throughout the Palaeozoic of the Western Iberian Peninsula. Ecologae Geol. Helv., 63/1, 255-274.

Ribeiro, A., 1974, Contribution a l'étude tectonique de Tras-os-Montes oriental. Mem. Serv. geol. Portugal, 24.

Richards, D.N.G., 1980, Palaeozoic Granitoids of Northeastern Australia. In Henderson, R.A. & Stephenson, D.J., (eds), "Geology and Geophysics of NE Australia", Geol. Soc. Aust. Qd. Div. Brisbane, 229-246.

Schermerhorn, L.G., 1956, Igneous, metamorphic and ore geology of the Castro Daire-S. Pedro do Sul-Satao region (Northern Portugal). Com. Serv. Geol. Portugal, 37.

Schermerhorn, L.G., 1981, Framework and evolution of Hercynian mineralization in the Iberian Meseta. Leidse Geol. Medecel., 52, 1, 23-56.

Schermerhorn, L.G., 1987, The Hercynian gabbro - tonalite - granite - leucogranite suite of Iberia: geochemistry and fractionation. Geol. Runds. 76/1, 137-145.

Sheppard, S.M.F., 1977, The Cornubian batholith, SW England: D/H - 180/160 studies of kaolinite and other alteration minerals. J. Geol. Soc. Lond., 133, 573-591.

Shieh, Y.N. & Schwarcz, H.P., 1974, Oxygen isotope studies of granite and migmatite, Grenville province of Ontario, Canada. Geochim. Cosmochim. Acta, 38, 21-45.

Shieh, Y.N. & Taylor, H.P., 1969, Oxygen and hydrogen isotope studies of contact metamorphism in the Santa Rosa Range, Nevada, and other areas. Contrib. Mineral. Petrol., 20, 306-356.

Sluijk, D., 1963, Geology and tin-tungsten deposits of the Regoufe area, Northern Portugal. Unpubl. Ph.D. Thesis, University of Amsterdam.

Steiger, R. & Jager, E., 1977, Subcommision on Geochronology: Convention on the use of decay constants in geo- and cosmochronology. Earth Plan. Sci. Lett., 36, 359-362.

Stephens, W.E., 1982, XRFSS - X-ray fluorescence software system. Unpubl. University of St Andrews.

Streckeisen, A., 1976, To each plutonic rock its proper name. Earth Sci. Rev., 12, 1-33.

Strong, D.F. & Hanmer, S.K., 1981, The leucogranites of southern Brittany: origin by faulting, frictional heating, fluid flux and fractional melting. Can. Mineral., 19, 163-176.

Stussi, J.M. & de la Roche, H., 1984, Le magmatisme orogénque granitique de la châine varisque française. Typologie chimique et répartition spatiale. C.R. Acad. Sci. Paris, 298, Serie II, 43-48.

Tarney, J. & Saunders, A.D., 1979, Trace element constraints on the origin of Cordilleran batholiths. In Atherton, M.P. & Tarney, J., (eds), "Origin of granite batholiths: Geochemical Evidence", 90-105, Shiva.

Taylor, H.P., 1968, The oxygen isotope geochemistry of igneous rocks. Contrib. Mineral. Petrol., 19, 1-71.

Taylor, H.P., 1980, The effects of assimilation of country rocks by magmas on 180/160 and 87Sr/86Sr systematics in igneous rocks. Earth Plan. Sci. Lett., 47, 243-254.

Taylor, H.P. & Epstein, S., 1962a, Relationships between 180/160 ratios in coexisting minerals of igneous and metamorphic rocks. I: Principles and experimental results. Bull. Geol. Soc. Am., 73, 461-480.

Taylor, H.P. & Epstein, S., 1962b, Relationships between 180/160 ratios in coexisting minerals of igneous and metamorphic rocks. II: Applications to petrological problems. Bull. Geol. Soc. Am., 73, 675-694.

Teixeira, C., 1947, Posicao Geologica dos Granitos Portugueses. Tecnica, 147, 369-374.

Teixeira, C., 1955, Notas Sobre a Geologia de Portugal - Formacoes Ante-Mesozoicas. Lisboa.

Teixeira, C., 1970, Aspectos Geologicos da Orls Litoral do Porto e de V.N. de Gaia. Naturalia, 10, 1, 13-29.

Thompson, A.B., 1982, Dehydration melting of pelitic rocks and the generation of H2O-undersaturated granitic liquids. Am. J. Sci., 282, 1567-1595.

Todd, V.R. & Shaw, S.E., 1985, S-type granitoids and an I-S line in the Peninsular Ranges batholith, southern California. Geology, 13, 231-233.

Van Diver, B.B., 1970, Origin of Biotite Orbicules in "Bullseye Granite" of Craftsbury, Vermont. Am. J. Sci., 268, 322-340.

Westerfeld, J., Schermerhorn, L.G., Kluiving, R., Sluijk, D., Oen, I.S., Welter, C.C. and Cohen, C.D., 1956, Roches eruptives, gites metalliferas et metamorphisme entre Mangualde et le Douro dans le Nord de Portugal. Bol. Soc. Geol. Portugal, 12, 1-2, 101-127.

White, A.J.R. & Chappell, B.W., 1977, Ultrametamorphism and granitoid genesis. Tectonophysics, 43, 7-22.

White, A.J.R. & Chappell, B.W., 1983, Granitoid types and their distribution in the Lachlan Fold Belt, SE Australia. Geol. Soc. Am. Mem., 159, 21-34.

White, A.J.R, Chappell, B.W and Wall, V.J., 1986, S-type granites and their probable absence in southwestern N. America. Geology, 14, 115-118.

Wickham, S.M., 1987, Segregation and Emplacement of Granitic Magmas. J. Geol. Soc. Lond., 144, 281-297.

Wickham, S.M. & Oxburgh, E.R., 1985, Continental rifts as a setting for regional metamorphism. Nature, 318, 330-333.

Wickham, S.M. & Taylor, H.P., 1985, Stable isotope evidence for large scale sea water infiltration in a regional metamorphic terrane; the Trois Seigneurs Massif, Pyrenees, France. Contrib. Mineral. Petrol., 91, 122-139.

Wilson, A.D., 1955, A new method for determination of ferrous iron in rocks and minerals. Gt. Brit. Geol. Surv. Bull., 9, 56-58.

Wones, D.R. & Eugster, H.P., 1965, Stability of biotite: Experiment, theory and application. Am. Mineral., 50, 1228-1272.

York, D., 1969, Least squares fitting of a straight line with correlated errors. Earth Plan. Sci. Lett., 5, 230-234.

Zaleski, E., 1982, The geology of Speyside and Lower Findhorn granitoids. Unpubl. M.Sc. Thesis, University of St Andrews.

The Geology of the Serra da Freita Plateau, North Central Portugal

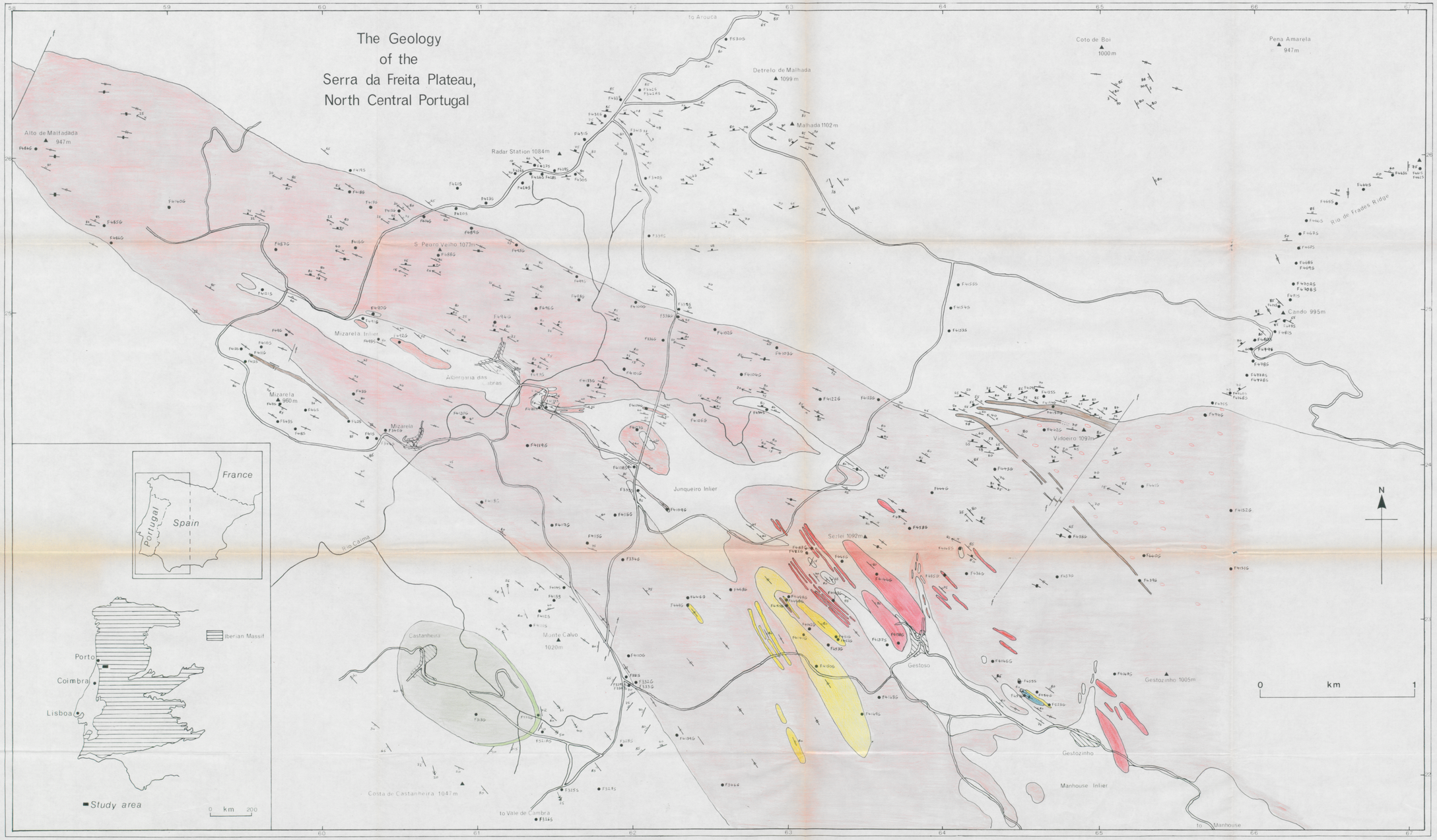

- Main Granite
- Microgranite
- Sheared Granite
- Felsic Granite
- Aplite
- Castanheira Nodular Granite
- Castanheira Roof Facies
- Gestoso Nodular Granite
- Beira Schists
- S2 (vertical)
- S2a (")
- S3 (")
- Folds above Castanheira
- F_3
- Extension lineation
- f Fault
- Sample locality
- Summit
- Road
- Village
- River